Activating senescence in p16-positive Basal-like breast cancer

Madeleine Moore

A thesis presented for the degree of Doctor of Philosophy

2015

Supervisors:

Dr. Cleo L. Bishop

Prof. Mike P. Philpott

Centre for Cell Biology and Cutaneous Research

The Blizard Institute

Barts and the London School of Medicine and Dentistry

Queen Mary, University of London

Statement of originality

I, Madeleine Moore, confirm that the research included within this thesis is my own work or that where it has been carried out in collaboration with, or supported by others, that this is duly acknowledged below and my contribution indicated.

I attest that I have exercised reasonable care to ensure that the work is original, and does not to the best of my knowledge break any UK law, infringe any third party's copyright or other Intellectual Property Right, or contain any confidential material.

I accept that the College has the right to use plagiarism detection software to check the electronic version of the thesis.

I confirm that this thesis has not been previously submitted for the award of a degree by this or any other university.

Signature: Madeleine Moore

Date: 22.10.15

Abstract

Breast cancer is the most common cancer in the UK and Basal-like breast cancer (a highly aggressive subtype) accounts for approximately 8-22% of all cases depending on ethnicity. Unlike most human malignancies and indeed other PAM50 breast cancer subtypes, the vast majority of Basal-like tumours are positive for wild type p16. This p16 signature is associated with a particularly poor prognosis and p16-positive Basal-like breast cancer remains the most clinically challenging subtype and is the focus of this project. Pro-senescence therapies are gaining momentum as attractive strategies for the treatment of those breast cancers with current unmet clinical need. To identify targets for pro-senescence therapy in p16-positive Basal-like breast cancer, a genome-wide siRNA screen and two subsequent validation screens using two p16-positive cancer cell lines were performed. Screening revealed 20 siRNAs that induced senescence within both cancer cell lines. Strikingly, 11 of these 20 siRNAs targeted ribosomal proteins, implicating disrupted ribosomal biosynthesis in senescence activation in p16-positive Basal-like breast cancer. Importantly, subsequent experiments in normal human mammary epithelial cells established that specific ribosomal protein knockdown is well tolerated by normal cells. Analysis of the METABRIC data set showed a high degree of ribosomal dysregulation in Basal-like tumours and revealed that all 11 ribosomal hits identified were frequently overexpressed in p16-positive Basal-like breast cancers. Kaplan Meier analysis confirmed that elevated expression of six of the 11 ribosomal proteins correlates with a reduced overall survival in these women, further supporting a role for these proteins as drivers of disease. These six ribosomal hits, associated with the poorest patient survival, were prioritised for further validation. Senescence induction was found to be highly stable, and associated with dramatic changes to nucleolar morphology, reminiscent of the nucleolar signature observed upon premature senescence induction in normal human mammary epithelial cells. In addition, siRNA rescue experiments indicated that senescence initiation is dependent on p16 and p21 expression and is accompanied by p16 nuclear translocation and p21 degradation. Further, ribosomal protein silencing in MDA-MB-231 cells (p16-null Basal-like breast cancer cell line) resulted in a ‘death-like’ phenotype, partially dependent on p21 expression suggesting that, within a cancer context, ribosomal protein silencing may induce a differential response depending on the status of p16. In conclusion, it is proposed that these six ribosomal candidates may form the basis of a novel pro-senescence therapy for p16-positive Basal-like breast cancer. They may also represent novel prognostic biomarkers for this disease subset and may help to improve disease stratification and future directed personalised therapies.

Acknowledgements

This work was supported by a Medical Research Council PhD Studentship (Grant number: RGJZZY4).

I'd like to thank my supervisors Mike Philpott and Cleo Bishop for their continued knowledge, guidance and support throughout my time at the Blizard. Mike, thank you very much for your invaluable help with presentations and written work as well as your generous support towards laboratory consumables.

Cleo, you have been brilliant. Thank you for your incredible dedication and encouragement throughout the project. You have been instrumental in helping me to gain in confidence, keep focussed and push through the hectic times. Thank you.

I'd also like to thank the members of the Bishop Lab., past and present for all your help and for making work fun and enjoyable. A special thanks to Elly for your friendship and wonderful support. It has meant a lot.

A big thank you to all my friends at the Blizard and especially George and Fiona for keeping me going. A special thanks to Anke, especially during the writing! Thank you for checking in on me and helping me push through! I'd also like to thank Mat for his invaluable advice and guidance in the lab. and Luke for his technical help with the IN Cell.

Finally, I'd like to thank my friends, Cat and Sophie, and my family, Mum, Dad and Abby. Thank you for all your support and encouragement. Abby, thank you for your words of 'wisdom' and for always being first to provide me with a good distraction in the form of a museum night at your work! James, I couldn't have done this without you! I don't think I cooked a single meal whilst writing up so thank you for all your delicious cooking and organising! Thank you for listening, taking care of me, keeping me calm and getting me through.

Contents

List of Figures

List of Tables

List of Abbreviations

Due to the nature of this work, abbreviated gene names are not listed here but are outlined in the main text where appropriate.

Full name	Abbreviation
Angstrom	Å
Basal-like breast cancer	BLBC
β-galactosidase	β-gal
Caenorhabditis elegans	*C. elegans*
Carbon dioxide	CO_2
Central nervous system	CNS
Chromsome	chr
Cyclin Dependent Kinases	CDK
Decoding site	DCS
Dense Fibrillar Centre	DFC
Deoxynucleotide	dNTP
Deoxyribonucleic acid	DNA
Dimethyl sulfoxide	DMSO
Dithiothreitol	DTT
DNA damage response	DDR
Double strand break	DSB
Dulbecco's Modified Eagles Medium	DMEM
Enhanced-Chemiluminescence	ECL
Epstein-Barr virus	EBV
Estrogen receptor	ER
Ethanol	EtOH
Ethylenediaminetetraacetic acid	EDTA
Extracellular matrix	ECM
Fibrillar Centre	FC
Foetal bovine serum	FBS
Genome-wide association studies	GWAS
Gram	g
Granular Component	GC

Hazard Risk	HR
Hepatitis B virus	HBV
HiPerFect Transfection Reagent	HiPerFect
Hoechst 33342	Hoechst
Hours	hr
Human epidermal growth factor receptor	HER2
Human mammary epithelial cells	HMEC
Human papilloma virus	HPV
Hyaluronic acid	HA
Litre	L
Loss of heterozygosity	LOH
Mammary Epithelial Basal Medium	MEBM
Microgram	µg
Microlitre	µL
Micromolar	µM
Milliamps	mA
Millilitre	mL
Millimolar	mM
Minutes	mins
Mitochondrial ribosomal protein	MRP
Molar	M
Molecular Taxonomy of Breast Cancer International Consortium	METABRIC
Mouse embryonic fibroblasts	MEF
Nanogram	ng
Nanomolar	nM
Natural Killer cells	NK cells
Nucleolin	NCL
Off-target effect	OTE
Oncogene-induced senescence	OIS
Passage 4	P4
Passage 6	P6
PBS supplemented with 0.25% Bovine serum albumin	PBS/BSA
Pentose phosphate pathway	PPP
Phosphate-buffered saline	PBS

Polycomb repressive complex	PRC
Prediction Analysis of Microarrays	PAM50
Progesterone receptor	PR
PTEN-loss-induced cellular senescence	PICS
Reactive oxygen species	ROS
Real-Time Quantitative Reverse Transcription PCR	qRTPCR
Revolutions per minute	rpm
Ribonucleic acid	RNA
Ribosomal DNA	rDNA
Ribosomal protein	RP
Ribosomal RNA	rRNA
RNA interference	RNAi
RNA Polymerase I	RNA Pol I
RNA Polymerase II	RNA Pol II
RNA Polymerase III	RNA Pol III
RNA-induced silencing complex	RISC
RNA-sequencing	RNA-seq
Room temperature	RT
Saccharomyces cerevisiae	*S. cerevisiae*
Second	sec
Senescence-associated heterochromatin foci	SAHF
Senescence-associated secretory phenotype	SASP
Small hairpin RNA	shRNA
Small interfering RNA	siRNA
Small Subunit Processome	SSP
Sodium dodecyl sulphate	SDS
Sodium dodecyl sulphate polyacrylamide gel electrophoresis	SDS PAGE
Standard deviation	SD
SYTOXGreen nucleic acid stain	SYTOX
Terminal deoxynucleotidyl transferase dUTP nick end labeling	TUNEL
The Cancer Genome Altas	TCGA
Therapy-induced senescence	TIS
Tissue microarray	TMA
Transfer RNA	tRNA

Transmission Electron Microscopy	TEM
Triple negative	TN
Volume/volume	v/v
Weight/volume	w/v
Wild-type	WT
0.05% Tween-20 in PBS	PBS-T
0.05% Tween-20, 5% Marvel semi-skimmed milk in PBS	PBS-T-M
4',6-diamidino-2-phenylindole	DAPI
5-Bromo-2'-deoxyuridine	BrdU
5-bromo-4-chloro-3-indolyl-beta-D-galacto-pyranoside	X-gal

Chapter 1
Introduction

1.1 *The Cell Cycle*

1.1.1 *Cell cycle checkpoints and regulation*

The vast majority of cells present within most adult human tissues are kept in a reversible state of cell cycle arrest, termed quiescence (G0). However, to enable adequate tissue maintenance and repair, those cells with proliferative capacity may be stimulated to re-enter the cell cycle in response to coordinated mitotic signalling. The eukaryotic cell cycle is comprised of four phases (G1, S phase, G2 and M phase) and three critical checkpoints (G1-S phase, G2-M phase and the Spindle checkpoint which controls entry into anaphase). Cell cycle progression is tightly controlled and is dictated primarily by the activity of Cyclin Dependent Kinases (CDKs)/Cyclin complexes (reviewed in Asghar et al., 2015, also see Figure 1.1). The role of CDK/Cyclin complexes within cell cycle control is well established and many of the core concepts of CDK biology were described over 20 years ago by Nobel laureates, Leland H. Hartwell, Tim Hunt and Sir Paul Nurse (Nurse, 2002, Hunt, 2002). In addition to the evidence demonstrating that the phosphorylation of specific substrates by CDK/Cyclin complexes is critical for correct cell cycle progression, it has also been suggested that global CDK/Cyclin levels may also play an important role within cell cycle control (Coudreuse and Nurse, 2010). For example in *Schizosaccharomyces pombe*, it appears that steadily increasing levels of a single CDK/Cyclin complex from G1-M phase may be sufficient to drive cell cycle progression, however, evidence for this phenomenon within mammalian cells is currently lacking (Coudreuse and Nurse, 2010, and reviewed in Harashima et al., 2013).

Key cell fate decisions, such as the initiation of cell cycle re-entry or the decision to commit to cell division (progression through the Restriction point), are mediated by the E2F family of transcription factors, often described as 'Master regulators' of the cell cycle (reviewed in Dyson, 1998). The E2F gene family encodes six individual proteins (E2F-1–E2F-6) that form heterodimers with two differentiation regulated transcription factor proteins (DP-1 and DP-2) and act to orchestrate transcription of key cell cycle mediators via both activation and repression at specific promotor regions (reviewed in Dyson, 1998). Critical E2F transcriptional targets include Cyclins A and E (required for cell cycle re-entry and S phase initiation), polo-like kinase 1 (PLK1) (required for correct mitotic progression) and the mitotic spindle checkpoint protein (MAD2) (Dalton, 1992, Schulze et al., 1995, Ohtani et al., 1995, and reviewed in Dyson, 1998). regulation of E2F-mediated transcription occurs through the binding of specific Retinoblastoma protein (RB) family members including RB, p130 and p107 (Hiebert et al., 1992, Schwarz et al., 1993, Helin et al., 1993, and reviewed in Dyson, 1998). The RB family proteins are differentially

expressed throughout the cell cycle and form stable multi-protein complexes with E2F-1–E2F-5, resulting in stringent transcriptional repression due to the recruitment of transcriptional co-repressors (Brehm et al., 1998, and reviewed in Dyson, 1998). Importantly, E2F-1–E2F-3 bind preferentially to RB and these complexes are most evident in cells poised at the Restriction point (reviewed in Dyson, 1998).

Cell cycle re-entry (from G0-S phase) and progression through the Restriction Point (from G1-S phase) in response to mitogenic stimuli, such as activated RAS or mitogen-activated protein kinase (MAPK), is mediated by CDK4/6/Cyclin D complex activity (Baldin et al., 1993, and reviewed in Ortega et al., 2002). Once formed, CDK4/6/Cyclin D complexes phosphorylate RB resulting in the disassociation of RB from E2F proteins thereby enabling the E2F-mediated transcription of target genes such as Cyclin A and E (Knudsen and Wang, 1997, and reviewed in Dyson, 1998, and Ortega et al., 2002). CDK2/Cyclin E/A complexes drive S phase progression and amplify initial mitotic signals through additional RB phosphorylation (Ortega et al., 2002). Once Deoxyribonucleic acid (DNA) replication is completed, CDK1/Cyclin A/B complexes drive progression from G2-M phase and subsequent degradation of Cyclin B enables correct anaphase completion followed by cell cycle exit and RB de-phosphorylation (reviewed in in Ortega et al., 2002, and Harashima et al., 2013, and see also Figure 1.1).

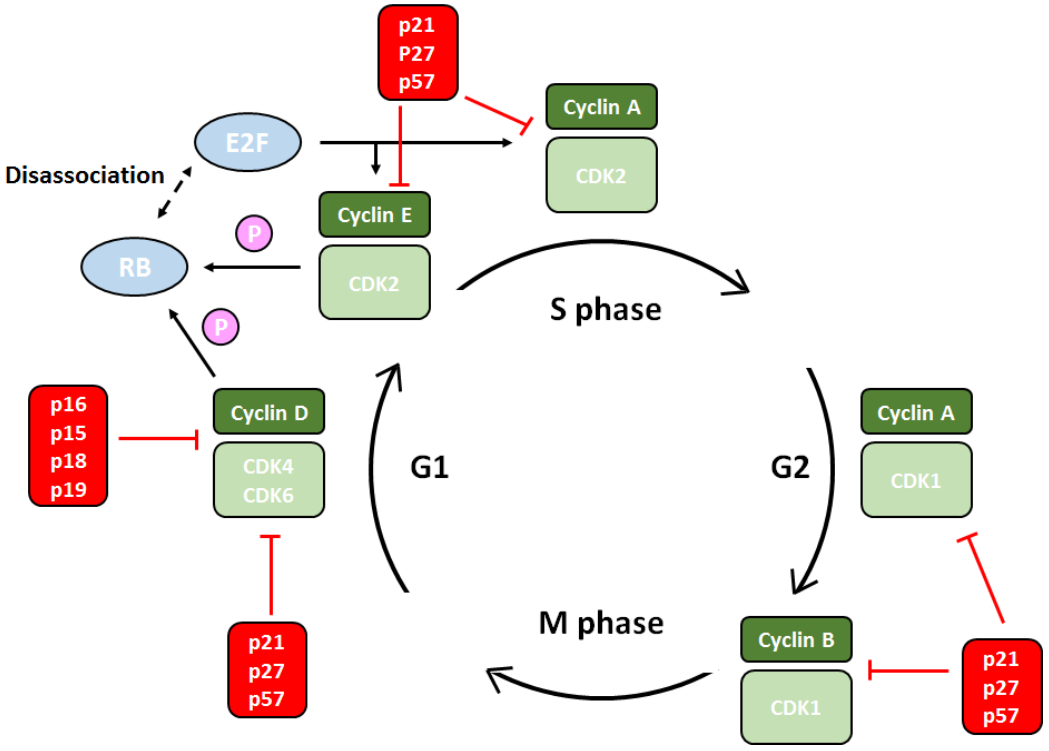

Figure 1.1: Schematic summarising the stages of the cell cycle. Cell cycle progression is mediated by CDK/Cyclin complexes. The CDK4/6/Cyclin D/RB/E2F signalling axis modulates cell cycle entry and progression through G1. CDK inhibitors are shown in red.

The transcriptional regulator, Forkhead box M1 (FOXM1) was recently identified as a critical phosphorylation target of CDK4/6/Cyclin D complexes (Anders et al., 2011) and functions to promote cell cycle progression by mediating the transcription of a whole host of critical G2 and M phase regulators, such as cell division cycle 25B (Cdc25B), PLK1, Cyclin A2, Cyclin B, Aurora B kinase, Aurora A kinase and Survivin (reviewed in Bella et al., 2014, and Lam et al., 2013). Additionally, downstream FOXM1 targets include S-phase kinase-associated protein 2, E3 ubiquitin protein ligase (SKP2) and cyclin-dependent protein kinase regulatory subunit (CKS1) (components of the Skp1-Cullin 1 F-box (SCF) ubiquitin ligase complex). The SCF complex controls the degradation of cyclin-dependent kinase inhibitor (CDKI) proteins (discussed below) during the G1-S transition, thereby promoting cell cycle progression (Westbrook et al., 2007, and reviewed in Bella et al., 2014).

In human cells, the INK4 family members $p16^{INK4a}$ (p16), $p15^{INK4b}$ (p15) on chromosome 9p21 (chr 9p21), $p18^{INK4c}$ (chr 1p32) and $p19^{INK4d}$ (chr 19p13) function to directly inhibit CDK4/6/Cyclin D complex formation and high p16 protein expression is a well-established marker of senescence induction in normal cells (Serrano et al., 1993, Alcorta et al., 1996, and reviewed in Asghar et al., 2015). In addition, CDK-interacting protein/kinase inhibitory proteins, including $p27^{KIP1}$ (p27), $p57^{KIP2}$ (p57) and $p21^{CIP1/WAF1}$ (p21, downstream of p53), also function to halt cell cycle progression by repressing CDK/Cyclin complexes containing Cyclins A, B, D and E (Polyak et al., 1994, Eldeiry et al., 1993, and reviewed in Sherr and Roberts, 1999). Furthermore, numerous studies have shown that in response to cellular stress, such as DNA damage, p53 and p21 activation may drive senescence initiation in normal cells (see Section 1.2.1).

1.1.2 *The INK4b-ARF-INK4a locus and p16 regulation*

The INK4b-ARF-INK4a locus is located on chromosome 9p21 within the human genome and encodes three individual tumour suppressor proteins termed p15, p16 and $p14^{ARF}$ (p14, p19 in mice) (Serrano et al., 1993). As described above, p15 and p16 function to inhibit CDK/Cyclin D complex formation while p14 (a distinct protein, translated from an alternate reading frame) functions to stabilise p53 via inhibition of the proto-oncogene, E3 ubiquitin protein ligase (MDM2) (Stott et al., 1998, and reviewed in Gil and Peters, 2006, and see also Section 1.7.6).

Activation of the INK4b-ARF-INK4a locus occurs in response to cellular stress, such as the overexpression of an oncogene (such as oncogenic harvey rat sarcoma viral oncogene homolog, $H\text{-}RAS^{V12}$ or B-Raf proto-oncogene, serine/threonine kinase, $BRAF^{V600E}$) (Serrano et al., 1997, Zhu et al., 1998) and increased protein levels of all three tumour suppressors has been associated with senescence activation in normal cells (see Section 1.5.1). Additional activators of the locus

include members of the Activator-protein 1 (AP1) family of transcription factors, such as JUNB and C-JUN, melanocyte-inducing transcription factor (MITF), chromatin-remodelling factor, SWI/SNF related, matrix associated, actin dependent regulator of chromatin, subfamily b, member 1 (SNF5) and the master regulator, E2F (reviewed in Gil and Peters, 2006). These transcription factors exert differential regulatory effects on the three genes within the INK4b-ARF-INK4a locus in a context dependent manner. For example, the transcription factor, JUNB was found to activate p16 expression and growth arrest in mouse embryonic fibroblasts (MEFs), whereas a second AP1 family member, JUN-C is associated with p16 repression and p19 activation in MEFs (Passegue and Wagner, 2000). Additionally, MITF is proposed as a p16-activator during melanocyte differentiation (Loercher et al., 2005) and similarly SNF5 loss has been associated with reduced p16 expression in rhabdoid tumour cells. Further, ectopic SNF5 expression in rhabdoid tumour cells resulted in increased p16 expression together with cell cycle arrest (Betz et al., 2002). Supra-physiological levels of E2F-1–E2F-3 proteins have been shown to activate p14 expression, however, at present, evidence demonstrating p16 expression is mediated by E2F activity is lacking (Berkovich et al., 2003, and reviewed in Gil and Peters, 2006).

Given its role within senescence initiation and cell cycle arrest, it is critical that expression of the INK4b-ARF-INK4a locus is tightly controlled during normal cell division. There is now evidence to suggest that Polycomb repressor group proteins (PcG) (first identified in *Drosophila melanogaster*) (Paro and Hogness, 1991) function to repress the INK4b-ARF-INK4a locus via specific epigenetic modifications (Gil et al., 2004, Jacobs et al., 1999, Aguilo et al., 2011). In mammals, highly conserved PcG proteins form two large multi-protein complexes termed Polycomb repressive complex-1 and 2 (PRC1 and PRC2) that work in a co-ordinated manner to achieve transcriptional silencing. The PRC2 complex functions to methylate histone H3 on lysine 27 and recruit PRC1 complexes to specific promotor regions, resulting in further epigenetic modifications and transcriptional silencing (reviewed in Aguilo et al., 2011). Importantly, the PRC1 components, BMI1 proto-oncogene, polycomb ring finger (BMI1) protein and Chromobox homolog 7 (CBX7) have been found to be associated with INK4b-ARF-INK4a repression and senescence bypass *in vitro* (Jacobs et al., 1999, Gil et al., 2004). Furthermore, small hairpin ribonucleic acid (shRNA) silencing of CBX7 in MEFs resulted in premature senescence induction (Gil et al., 2004) and data presented within this thesis demonstrates that CBX7 small interfering RNA (siRNA) knockdown in normal HMECs results in potent senescence activation accompanied with increased nuclear p16 protein levels (see Section 4.4).

1.2 *Classifying the senescence phenotype*

1.2.1 *Replicative senescence*

Senescence (stable G1 growth arrest) was first formally described in 1961 by Leonard Hayflick, who observed the limited ability of fibroblasts to continually proliferate in culture (Hayflick and Moorhead, 1961, Hayflick, 1965). Hayflick cultured normal human fibroblasts over many doublings, during which he observed a gradual decline in the rate of cellular proliferation across the culture (Figure 1.2). Eventually, every cell within the culture lost the ability to divide despite ample space, nutrients and growth factors. This phenotype, initially termed the 'Hayflick limit', is now known as replicative senescence and is thought to be driven primarily by telomere shortening (Hemann et al., 2001, Martens et al., 2000).

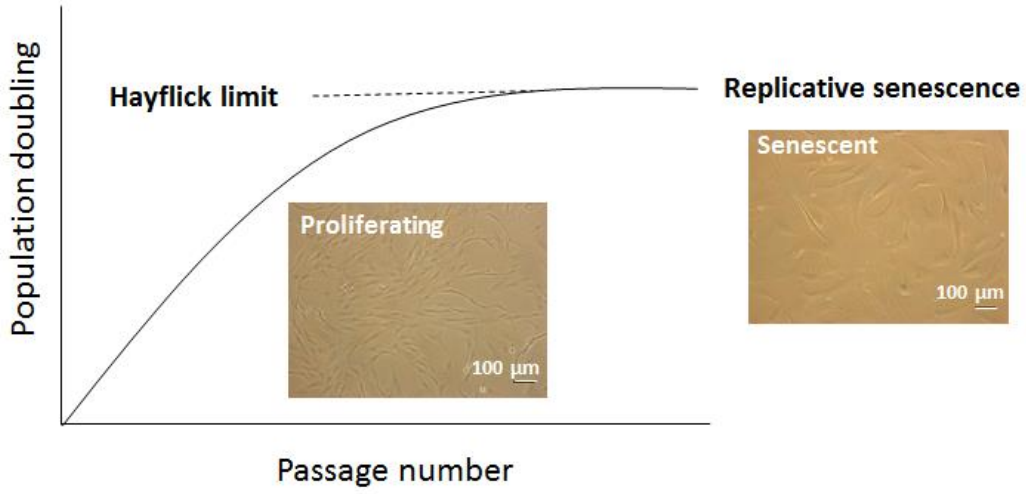

Figure 1.2: Cartoon depicting the Hayflick limit in cultured fibroblasts. Bright field images are of proliferating (passage 14) and senescent (passage 29+3) normal human mammary fibroblasts. Cells were cultured and imaged by Eleanor Tyler. Images are at 10X magnification and size bar denotes 100 µm.

Telomeres are made up of protective regions of repetitive DNA (5'- TTAGGG - 3' in vertebrates), typically 10-15 kilobases in length in humans, and telomeric repeat-binding factors that cap the ends of linear chromosomes (Griffith et al., 1999). The inability of standard polymerases to fully replicate DNA ends results in a phenomenon known as the end-replication problem, which means every completed cycle of cell division results in the loss of 50-200 base pairs of telomeric DNA (Harley et al., 1990). After a pre-defined number of cell divisions, telomeres eventually become critically short and dysfunctional, triggering a classical DNA damage response (DDR) mediated by p53 (d'Adda di Fagagna et al., 2003, Takai et al., 2003, Herbig et al., 2004). Currently, the mechanism by which a cell choses to elicit a transient or a persistent DDR are

unknown, however, DNA damage severity is likely to be an important factor (reviewed in Campisi and di Fagagna, 2007). A transient DDR often leads to a pause in cell division to allow for DNA repair, however, if DNA repair is not possible and the severity of the DNA damage is too great, a persistent DDR may develop and trigger the induction of replicative senescence or apoptosis (reviewed in Campisi and di Fagagna, 2007). The mechanisms by which a cell decides to initiate apoptosis or induce senescence in response to sustained p53 signalling are currently unknown, however, it is likely that the cell type and the nature of the damage are important (reviewed in Campisi and di Fagagna, 2007). For example, DNA damage in lymphocytes tends to induce apoptosis; conversely, in fibroblasts or epithelial cells a senescence response is more likely (reviewed in Campisi and di Fagagna, 2007).

Many proteins are involved in the DDR including the adaptor protein p53-binding protein 1 (53BP1) and the chromatin modifier phosphorylated gamma histone variant 2AX (ϒH2AX) (d'Adda di Fagagna et al., 2003, Takai et al., 2003). These two proteins are widely accepted markers of replicative senescence and localise to DNA damage foci present within senescent cells (d'Adda di Fagagna et al., 2003, Takai et al., 2003, and reviewed in Campisi and di Fagagna, 2007). As well as a stable growth arrest, replicative senescence in fibroblasts is often accompanied with an increase in cellular and nuclear size, an irregular nuclear morphology, the presence of vacuoles, positive staining for β-galactosidase (β-gal), critically short telomeres, a DDR and staining for p53 and/or p16 (reviewed in Sikora et al., 2011, and see Table 1.1). In fibroblasts, replicative senescence induction depends strongly on p53 and p21 signalling (Herbig et al., 2004), however, the p16/RB pathway may also be activated as a late response to severe DNA damage such as double strand breaks (DSBs) or telomeric dysfunction (Jacobs and de Lange, 2004). As such, a senescent fibroblast culture may be positive for both p53 and p16 as cells may express either p53, p16 or both (reviewed in Campisi and di Fagagna, 2007).

As well as global gene expression changes, replicative senescence in fibroblasts is often associated with specific epigenetic changes (Cruickshanks et al., 2013, and reviewed in Sikora et al., 2011). Activation of the p16/RB pathway can lead to the formation of senescence-associated heterochromatin foci (SAHF) that typically contain hypoacetylated histones, histone H3 lysine 9 tri methylation and the heterochromatin protein, Heterochromatin Protein 1 (HP1) (Narita et al., 2003). SAHF silence the expression of pro-proliferative E2F target genes thereby establishing and maintaining cell cycle arrest (Narita et al., 2003).

1.2.2 *Epithelial cellular senescence*

Unlike fibroblasts, epithelial cells have a higher propensity to undergo a p16-dependent senescence phenotype, at least *in vitro*, referred to in this thesis as cellular senescence (Brenner et al., 1998, Huschtscha et al., 1998). Almost all normal epithelial cells will undergo cellular senescence in the absence of telomere shortening, DNA damage and p53 expression in culture (Brenner et al., 1998, Huschtscha et al., 1998). For example, sub-optimal culture conditions (loosely defined as 'culture shock') can induce spontaneous p16 expression and senescence in normal human keratinocytes and mammary epithelial cells (HMECs) with long telomeres (Ramirez et al., 2001).

The exact mechanisms of p16 activation in epithelial cells are currently unknown, however, there is evidence to suggest that oxidative stress may induce p16 expression and drive cellular senescence in epithelial cells (Parrinello et al., 2003). In addition, p16 expression is regulated by the polycomb repressors, BMI1 and CBX7 (Bracken et al., 2007, Gil et al., 2004). Reduced expression of CBX7 in normal human prostate epithelial cells results in an increase of p16 levels together with activation of cellular senescence (Gil et al., 2004).

Cultured HMECs will typically bypass cellular senescence via p16 promoter methylation or gene mutation (Brenner et al., 1998, Huschtscha et al., 1998) and there is now good evidence to show that this also occurs *in vivo* (Holst et al., 2003). Once cellular senescence has been bypassed, cells will continue to divide until telomere-dependent replicative senescence is triggered. Unlike in fibroblasts, replicative senescence in these cells will be mediated solely by p53.

In addition to replicative and cellular senescence, premature senescence may also be triggered by a range of other stimuli such as non-telomeric DNA-damage or chromatin perturbations (Dileonardo et al., 1994, Munro et al., 2004), as well as the overexpression of an oncogene or repression of a tumour suppressor gene (termed oncogene-induced senescence, OIS) (Serrano et al., 1997, and see Section 1.5). More recent studies have also found senescence to be triggered during tissue repair (Krizhanovsky et al., 2008), regeneration (Yun et al., 2015), normal embryogenesis (Storer et al., 2013, Munoz-Espin et al., 2013) and placental maturation (reviewed in Munoz-Espin and Serrano, 2014 and see Section 1.4). In addition to epithelial cells and fibroblasts, senescence has also been observed within a wide range of additional cell types including endothelial cells (Minamino et al., 2002, and reviewed in Munoz-Espin and Serrano, 2014).

1.2.3 *Senescence-associated markers*

It is important to recognise that markers of the senescence phenotype are not specific to senescence induction and that not all senescent cells will feature every possible senescence-associated marker (reviewed in Rodier and Campisi, 2011). As such, a panel of markers is commonly used in order to identify senescence activation (summarised in Table 1.1). The most common hallmarks of senescence activation used to define the phenotype are a stable growth arrest together with an enlarged cellular morphology together with increased β-gal staining (reviewed in Sikora et al., 2011). It is important to note that increased β-gal activity is also associated with contact-inhibition and serum starvation in non-senescent cultures and some normal non-senescent cells *in vivo* (Severino et al., 2000). Further, increased β-gal activity has not been implicated in the p16/RB or p53/p21 senescence-associated signalling pathways and evidence now suggests that those senescence-associated hallmarks with a causal role in senescence activation (such as p16) may be more robust phenotypic markers (reviewed in Sikora et al., 2011). In addition, senescent cells commonly secrete a complex cocktail of inflammatory chemokines, cytokines, growth factors and proteases, termed the senescence-associated secretory phenotype (SASP) (Acosta et al., 2013). Long-term exposure to the SASP is associated with chronic inflammation and perturbed tissue architecture and has been linked with numerous age-associated pathologies such as cancer, Type 2 diabetes and dementia (see Section 1.3.1). More recent evidence has revealed that the SASP may also promote tumour-suppression via senescence reinforcement in neighbouring cells vulnerable to transformation (termed paracrine senescence) (Acosta et al., 2013, Nelson et al., 2012). These opposing effects of the SASP are discussed in more detail in Sections 1.3-1.5 of this Chapter.

At present, many of the senescence-associated markers discussed here need to be fully validated *in vivo*. Further, it is unclear whether this current panel of senescence-associated markers may be used to identify senescence across all tissue types. For example, a robust set of senescence-associated markers applicable to all tissue types may enable pre-malignant lesions, characterised by OIS activation, to be detected regardless of the tissue of origin (reviewed in Sikora et al., 2011). In addition, markers that are able to distinguish premature senescence induction (such as OIS) from replicative or cellular senescence induction *in vivo* are currently lacking. In addition, the nucleoli signature of prematurely senescent cells versus cellular or replicative senescent cells is a key question not yet addressed by the literature. Examination of the nucleoli signature within differentially-induced senescent cells may reveal a novel senescence marker capable of distinguishing between different senescence subtypes.

Preliminary analysis to address this was carried out within this thesis and results are presented in Section 5.5.

Features of the senescence phenotype	Senescence-associated markers	Links to references
Reduced proliferative capacity	• Stable G1 cell cycle arrest, characterised by reduced 5-Bromo-2'-deoxyuridine (BrdU) incorporation or reduced Ki67 (proliferative marker) staining.	Reviewed in (Rodier and Campisi, 2011, Sikora et al., 2011)
Altered cellular, nuclear and nucleoli morphology	• Enlarged and flattened nuclear and cellular morphology. • Cells are often multinucleated and multi-vacuolated. • Irregular nuclear and cellular morphology. • Downregulation of Lamin B1 expression. • Enlarged and rounded nucleoli.	(Freund et al., 2012) (Ugrinova et al., 2007)
Increased lysosomal activity	• Increased β-gal enzymatic activity.	(Dimri et al., 1995)
Telomeric dysfunction/DNA damage/chromosomal instability	• Critically short telomeres. • Persistent DDR foci characterised by 53BP1 or YH2AX. • Oxidative DNA damage characterised by 8-Oxoguanine. • Chromosomal instability and DSBs.	(d'Adda di Fagagna et al., 2003) (Chen et al., 1995) Reviewed in (Rodier and Campisi, 2011, Sikora et al., 2011)
Epigenetic alterations	• Global hypo-methylation. • Hypermethylation at specific CpG-rich DNA regions containing pro-proliferative genes. • SAHF characterised by Histone 3 Lysine 9 (H3K9) tri-methylation and HP1.	(Cruickshanks et al., 2013, Lowe et al., 2015) (Narita et al., 2003)

	• Increased size and number of Premyelocytic leukaemia protein (PML) nuclear bodies.	Reviewed in (Rodier and Campisi, 2011, Sikora et al., 2011)
Expression of tumour suppressor genes	• Increased expression of the tumour suppressors, p15, p14, and p16 and activation of the p16/RB pathway. • Activation of the p53/p21 tumour suppressor pathway.	(Serrano et al., 1997, Ha et al., 2007, Xue et al., 2007, Krimpenfort et al., 2007)
Senescence-associated secretory phenotype (SASP)	• Enhanced secretion of inflammatory cytokines such as interleukin 6 (IL-6) and IL-8, chemokine (C-C motif) ligand 2 (CCL2), matrix metalloproteinases (MMPs), transforming growth factor beta (TGFβ) family ligands and Vascular endothelial growth factor (VEGF). • Stabilisation of inflammasome-associated proteins such as IL-1α, Caspase-1 and NRL family, pyrin domain containing 3 (NLRP3).	(Acosta et al., 2013, Freund et al., 2010) (Acosta et al., 2013)

Table 1.1: Table summarising the most commonly used senescence-associated markers.

1.3 *Senescence, ageing and tissue damage*

1.3.1 *Senescence and ageing*

The world's elderly population is expanding rapidly with the over 85s now the fastest growing cohort in the UK. Age is a major risk factor for a multitude of chronic diseases, such as cancers, Type 2 diabetes and dementias, and is often accompanied by frailty and a loss of independence (reviewed in Tchkonia et al., 2013). An ever increasing elderly population presents an enormous economic and social challenge for governments around the world, and a means of extending healthy lifespan remains the focus of intense research (reviewed in Tchkonia et al., 2013). There is now good evidence showing that senescent cells accumulate with advancing age and are important drivers of age-associated disease in mice (Baker et al., 2011). In addition, a recent

review of over 350 genome-wide association studies (GWAS) revealed that polymorphisms within the p16 gene were associated with multiple age-associated diseases such as cancer, atherosclerosis, glaucoma and Type 2 diabetes (Jeck et al., 2012). However, the exact mechanisms by which senescent cells accumulate and promote the development of chronic disease are yet to be fully resolved (reviewed in Tchkonia et al., 2013).

There are three proposed mechanisms by which senescence is able to drive age-related pathologies (reviewed in Rodier and Campisi, 2011). The first is the ability of senescent cells to deplete stem or progenitor cell populations, compromising tissue repair and regeneration, resulting in tissue dysfunction (Liu et al., 2007). Second, is the ability of senescent cells to modulate surrounding tissue architecture, cell growth, migration, blood vessel formation and differentiation through the secretion of cytokines and (MMPs) resulting in disrupted tissue structure and function (reviewed in Rodier and Campisi, 2011). For example, MMP3, secreted by senescent fibroblasts has been associated with mammary epithelial cell differentiation (Liu and Hornsby, 2007). Third, is the hallmark, low-level chronic inflammation, termed sterile inflammation, often associated with senescence (reviewed in Rodier and Campisi, 2011). Sterile inflammation is initiated and maintained by the secretion of pro-inflammatory cytokines (such as IL-6 and IL-8), Tumour necrosis factor alpha (TNFα), MMPs, monocyte chemoattractant protein-1 (MCP-1) and Insulin-like growth factor (IGF) binding proteins, known collectively as the SASP (reviewed in Tchkonia et al., 2013). Sustained low-level sterile inflammation and the subsequent infiltration of immune cells may result in inflammatory oxidative damage to surrounding tissues, tissue remodelling and the depletion of stem cell niches, driving the development of chronic disease and age-associated mortality (reviewed in Campisi, 2005). Sterile inflammation is the most likely cause of prominent age-associated pathologies and elements of the SASP, such as increased IL-6, TNFα and chemokines, increase in multiple tissues with advancing age and are associated with dementias, cancers and Type 2 diabetes (Bruunsgaard and Pedersen, 2003, Schetter et al., 2010, Pradhan et al., 2001, and reviewed in Tchkonia et al., 2013). The presence of chronic inflammation also correlates with muscle wasting (sarcopenia), fat tissue loss (cachexia) and age-associated frailty, a major risk factor for increased vulnerability to infection, trauma, chronic disease and mortality (reviewed in Tchkonia et al., 2013). Importantly, there is now evidence that p16-positive senescent cells accumulate with increasing age (Wang et al., 2009) and a landmark paper by Baker et al., 2011 provided clear evidence that life-long clearance of p16-positive senescent cells can delay the onset of multiple age-associated pathologies in mice. This study was the first to show that p16-positive senescent

cells are indeed influential drivers of the age-associated phenotype and the development of age-associated pathologies.

In addition, there is now strong evidence that senescent fibroblasts are able to create a cancer permissive microenvironment, fuelled by the SASP, which promotes the growth and malignancy of pre-neoplastic epithelial cells both *in vitro* and *in vivo* (Krtolica et al., 2001, and reviewed in Campisi, 2005). In support of this, the secretory phenotype of senescent fibroblasts closely models that of cancer-associated fibroblasts surrounding ovarian cancer and hepatocellular carcinoma (reviewed in Campisi, 2005). Further, recent studies by Cruickshanks et al., 2013, and Lowe et al., 2015, showed that the senescence associated epigenetic landscape (characterised by global hypomethylation and hypermethylation at specific CpG-rich DNA regions) is retained upon senescence bypass and is similar to that observed within cancer cells. As such, it is proposed that, if bypassed, senescent cells may represent a cellular pool primed to promote human malignancy. Consequently, an ever increasing accumulation of senescent cells (associated with advancing age) is likely to elevate the risk of senescence bypass and tumourigenesis, linking advancing age with an elevated cancer risk.

The notion that multiple chronic diseases may be caused by a few basic processes, such as age-related sterile inflammation (driven, at least, in part by senescence and the SASP) provides an exciting therapeutic opportunity for modulating ageing and extending healthy lifespan (reviewed in Tchkonia et al., 2013). Selective elimination of senescent cells or the SASP may prove to be highly effective at delaying the onset of age-associated pathologies and disrupting the link between age and chronic disease (Baker et al., 2011, reviewed in Tchkonia et al., 2013).

1.4 *Senescence: a paradoxical phenotype*

The studies discussed above implicate senescence induction and the SASP in ageing and age-associated pathologies such as cancer (Krtolica et al., 2001). However, somewhat conversely, there is now mounting evidence to suggest that senescence may be activated in response to an oncogenic event both *in vivo* and *in vitro* and is a crucial tumour suppressor mechanism in cells vulnerable to transformation (Serrano et al., 1997, see Section 1.5). In addition, recent studies have also highlighted the beneficial and potentially instructive role of senescence activation within tissue regeneration and wound healing (Demaria et al., 2014), regeneration (Yun et al., 2015) and normal embryonic development (Storer et al., 2013, Munoz-Espin et al., 2013). Consequently, senescence activation and the SASP is frequently referred to as a ‘paradoxical

phenotype' associated with often opposing and contradictory biological mechanisms (reviewed in Campisi, 2011).

1.4.1 *Senescence and tissue repair*

In contrast with the detrimental effects often associated with senescence induction and chronic exposure to SASP components (discussed above), more recent studies now provide indisputable evidence that senescence is activated during tissue repair and wound healing and may limit tissue fibrosis and drive wound closure. For example, Krizhanovsky et al., 2008 showed that in response to acute liver injury, mouse hepatic stellate cells initially proliferate and secrete extracellular matrix (ECM) components before undergoing a senescence phenotype accompanied by MMP secretion and ECM degradation. Further, acute liver injury in mice whose stellate cells were unable to initiate senescence activation, resulted in severe fibrosis (Krizhanovsky et al., 2008). Similarly, in a mouse model for cutaneous wound healing, tissue repair occurred in conjunction with the accumulation of senescent fibroblasts and wounds that lacked the wild-type (WT) ECM protein cysteine rich protein 61 (Cyr61, also known as CCN1) (binds fibroblasts) were excessively fibrotic (Jun and Lau, 2010). Crucially, topical application of WT CCN1 induced senescence and resolved tissue fibrosis, elegantly demonstrating the essential role of senescence induction in limiting fibrosis and tissue repair (Jun and Lau, 2010). In addition, Demaria et al., 2014 also demonstrated that senescent fibroblasts and endothelial cells accumulated at sites of tissue repair within a mouse model for cutaneous wound healing. In line with the data discussed above, senescence activation at sites of tissue repair appear to mediate myofibroblast differentiation and correct wound healing via the secretion of the novel SASP component, Platelet-derived growth factor AA (PDGF-AA) (Demaria et al., 2014). Further, PDGF-AA treatment of senescence-free wounds (characterised by delayed wound closure) resulted in myofibroblast differentiation and wound closure (Demaria et al., 2014).

1.4.2 *Senescence in limb regeneration and embryogenesis*

In addition to tissue repair, two key studies have shown that tissue remodelling triggered by senescence induction occurs at sites of limb regeneration in salamanders (Yun et al., 2015) and during normal embryonic development in mice (Storer et al., 2013, Munoz-Espin et al., 2013), further implicating senescence induction in normal physiology. Similarly, megakaryocytes and placental syncytiotrophoblasts are also thought to undergo senescence, characterised by increase β-gal activity, during normal maturation (reviewed in Munoz-Espin and Serrano, 2014).

Yun et al., 2015 showed that senescence occurs *in vivo* at sites of recurrent limb regeneration within two species of adult salamanders (*Notophthalmus viridescens* and *Ambystoma*

mexicanum). Upon amputation, β-gal positive senescent cells were transiently observed at the amputation plane and at the blastema (mass of de-differentiated cells that will give rise to the new limb) and it is proposed that this timely activation of senescence is a critical step within normal limb regeneration in salamanders. Implanted senescent cells at sites of regeneration appeared to induce paracrine senescence (see Section 1.5.2) in neighbouring cells and, in line with mammalian data (see Section 1.5.3), were eliminated via macrophage-mediated immune-clearance.

A landmark paper by Storer et al., 2013 elegantly demonstrated that during normal mouse development, transient senescence activation (mediated by p21) occurs throughout the embryo at specific anatomical structures, including the limbs, the tip of the tail and the brain. These senescent cells were non-proliferative, stained positive for β-gal activity, were p21 positive and p16 and p19 negative and were characterised by increased PML bodies and H3K9 tri-methylation. Crucially, qRT-PCR analysis revealed that the gene expression signature associated with developmental senescence closely resembles that expressed by oncogene-induced senescent fibroblasts, indicating that OIS may have evolved from a primordial mechanism for tissue remodelling, still evident during embryogenesis, limb regeneration and tissue repair (Storer et al., 2013).

1.4.3 *Senescence: a double-edged sword*

Although initial studies have focused on the detrimental consequences of senescence activation and the SASP on ageing and age-associated pathologies, more recent have outlined a clear role for senescence induction within normal physiology (see previous Section). Importantly, the senescent phenotype observed within each of these studies was highly transient and senescent cells were efficiently targeted and cleared from tissues via the immune system or via apoptosis (in the case of developmental senescence, Storer et al., 2013). As such, it is proposed that the duration of senescent cell survival and the persistence of the associated SASP may determine the impact of senescence induction on neighbouring cells and tissue function (reviewed in Campisi, 2011, and Tchkonia et al., 2013). Cellular context, senescence stimuli and SASP composition are also likely to impact the opposing consequences of senescence activation *in vivo*. Further, it is unlikely that there is a single SASP universal to all subtypes of senescence. More likely is that the components and potency of the SASP will vary depending on the cell type, senescence trigger and duration (reviewed in Campisi, 2011, and Tchkonia et al., 2013). In addition, it is important to note that much of the work investigating the detrimental effects of the SASP (links with tumour promotion and age-associated disease) was performed in fibroblasts

and a causal relationship between senescent epithelial cells and tumour promotion has yet to be shown.

Given this, it is hypothesised that, at least in early life, the activation of senescence together with a time-restricted localised SASP is critical for correct embryogenesis, effective tissue repair and tumour suppression. However, in later life, senescence induction and a persistent SASP has been shown to associate with chronic inflammation, age-associated disease and the development of a cancer permissive environment (reviewed in van Deursen, 2014). The mechanism by which senescent cells accumulate and persist in aged tissues is unclear, however, it is well-established that the immune system often weakens with advancing age (Arnold et al., 2011, and reviewed in Boraschi and Italiani, 2014). Inefficient clearance of senescent cells together with increased levels of cellular stress may drive age-associated senescent cell accumulation and allow senescent cells to persist within aged tissues and mediate age-associated pathologies (reviewed in Rodier and Campisi, 2011 and van Deursen, 2014).

Given this, the evolutionary theory of antagonistic pleiotropy is often used to explain the origins of senescence (Kirkwood and Austad, 2000). The theory predicts the existence of biological processes beneficial for survival in early life but detrimental in later years. It is hypothesised that senescence is a key physiological mechanism critical for correct embryogenesis and tissue regeneration that is maintained throughout adulthood to protect cells against tumourigenesis in early life at the expense of its age-associated detrimental effects on survival in later years (Kirkwood and Austad, 2000).

Importantly, this thesis is focused on harnessing the beneficial, anti-tumorigenic properties associated with OIS induction, activated in response to an oncogenic event (see Sections 1.5-1.6).

1.5 *Oncogene-induced senescence*

1.5.1 *Oncogene-induced senescence: a critical tumour suppressor mechanism*

There is now a growing body of evidence demonstrating that senescence may also be triggered in response to oncogenic stress independent of telomere attrition, both *in vitro* and *in vivo*. This process is termed OIS and may be activated in both fibroblasts and epithelial cells by the overexpression of an oncogene or the suppression of a tumour suppressor gene. Current literature implicates p16 as a common mediator of OIS in human epithelial cells, however, p53,

p19 and p15 have all been implicated in OIS in mice (Ha et al., 2007, Xue et al., 2007, Krimpenfort et al., 2007).

The first *in vitro* evidence for OIS was published by Serrano et al., 1997 who showed that overexpressing oncogenic H-RAS^{V12} in either normal human or mouse fibroblasts could induce a potent G1 growth arrest, together with p53 and p16 accumulation and increased β-gal activity. Importantly, the senescence response was acute, with cells arresting within days of continued oncogenic exposure, discounting telomeric involvement. Further, senescence induction was not activated in rodent cells deficient for either p53 or p16 (MEFs, p53-null or p16-null) implicating both signalling pathways in the initiation of senescence in this context. In addition, co-expression of H-RAS^{V12} with E1A (viral oncogene) circumvented senescence induction in human fibroblasts (Serrano et al., 1997, and reviewed in Prieur and Peeper, 2008). Since this finding, numerous *in vitro* studies have also demonstrated that OIS is not exclusive to mutant RAS overexpression and that the overexpression of additional oncogenic components of the RAS signalling pathway, such as mitogen-activated protein kinase (MEK) and BRAF^{V600E}, may also elicit a senescence response (Lin et al., 1998, Zhu et al., 1998). Importantly, there is now a wealth of evidence to support the presence of OIS *in vivo* and its physiological role as a crucial tumour suppressor mechanism in cells vulnerable to transformation. The first evidence of this was reported simultaneously by four separate groups in 2005. Collado et al., 2005 showed that mice overexpressing oncogenic H-RAS^{V12} developed multiple benign lung adenomas containing cells with a low proliferative index that stained positive for β-gal activity and p16. These mice also developed malignant adenocarcinomas at a much lower frequency. These lesions did not express the senescence-associated markers present within the benign lesions. Similarly, Braig et al., 2005 showed that OIS was initiated in response to oncogenic RAS using N-RAS transgenic mice and that OIS acted as a barrier to lymphoma development in a histone methyltransferase-dependent manner. Together, these studies indicate that OIS may be activated *in vivo* in response to oncogenic stimulation and that this critical senescence activation acts as a protective mechanism against tumorigenesis (reviewed in Prieur and Peeper, 2008). Further, OIS bypass appears to be an essential step for the development of a malignant lesion and in human epithelial cells bypass is likely to require disruption within the p16/pRB/E2F signalling axis (see Figure 1.3).

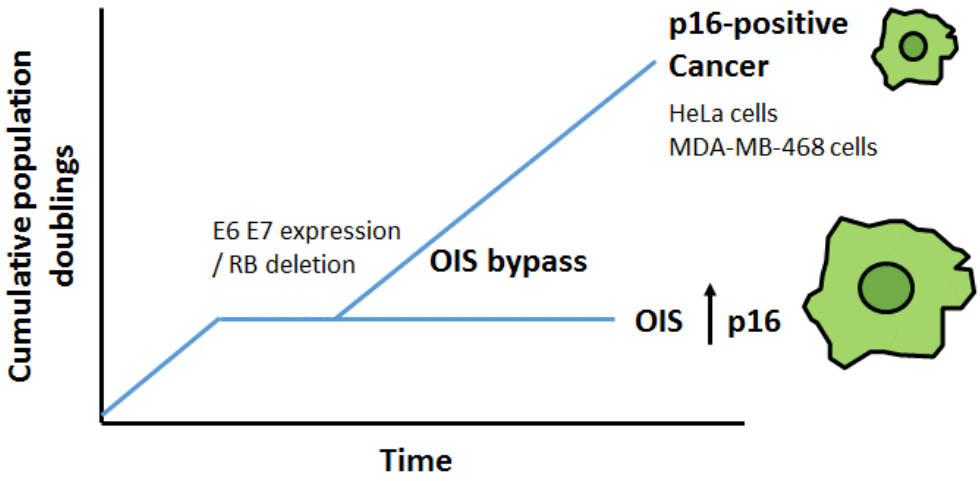

Figure 1.3: Schematic illustrating OIS bypass and p16-positive cancer development in human epithelial cells. It is proposed that OIS bypass is an early event within carcinogenesis and in order for a p16-positive cancer to arise, a pre-malignant cell must first undergo OIS bypass whilst maintaining high p16 protein levels. In this context, OIS bypass may be driven by the expression of viral oncogenes (such as E7 overexpressed within HeLa cells) or mutations to the p16/RB/E2F signalling axis downstream of p16 (such as an RB deletion, present within MDA-MB-468 cells).

A later study by Dankort et al., 2007 showed that mice expressing mutant $BRAF^{V600E}$ also developed numerous benign lung adenomas that were positive for a multitude of senescence-associated markers which rarely progressed to malignant adenocarcinomas. Here, the lesions stained positive for increased p19 (p14 in humans), primarily in the nucleoli, and had reduced Ki67 protein expression. Interestingly, the lesions were negative for β-gal activity, elegantly demonstrating that this widely accepted senescence-associated marker is not specific nor is it always sensitive to senescence induction. It is proposed that the combination of markers present upon senescence induction often depends on the cellular context as well as the oncogenic trigger (reviewed in Rodier and Campisi, 2011).

The first evidence of OIS present within a human pre-malignant lesion was reported by Michaloglou et al., 2005. Initial *in vitro* studies showed that sustained expression of mutant $BRAF^{V600E}$ induced cell cycle arrest accompanied by p16 expression and β-gal activity in human melanocytes. Further, human naevi (benign melanocytic lesions often harbouring mutant $BRAF^{V600E}$ were found to stain positive for β-gal activity together with mosaic p16 activation, strongly suggesting that OIS is a physiologically relevant event that functions in humans as a potent tumour suppressor mechanism. Additional mutations are likely to be required for bypass of the OIS program and melanoma development, and similar findings were reported by (Gray-Schopfer et al., 2006).

As well as the overexpression of an oncogene, such as oncogenic RAS, it has also been demonstrated that PTEN-loss-induced cellular senescence (PICS) may be triggered *in vivo* via the repression of a key tumour suppressor such as phosphatase and tensin homolog (PTEN) (Chen et al., 2005). The loss of PTEN is often associated with a non-lethal prostate cancer that develops after a long latency period. Importantly, Chen et al. demonstrated that PTEN loss within the mouse prostate induces a p53-mediated growth arrest that is rescued by p53 loss. Further, senescence may also be detected within very early stage prostate cancer in humans providing additional evidence for OIS as a tumour suppressor mechanism with physiological relevance.

1.5.2 *Oncogene-induced senescence and the SASP*

As well as activating a potent cell cycle arrest in cells harbouring potentially oncogenic mutations, it is now thought that cells that have undergone OIS are able to trigger a tumour suppressive response in neighbouring cells via the SASP (reviewed in Kuilman and Peeper, 2009). It is proposed that OIS-associated secretory factors may act as 'danger signals' and activate a protective senescence response in surrounding cells, limiting the chance of transformation in damaged cells that may also be vulnerable to malignancy. There is now growing evidence for this both in culture and *in vivo* (Acosta et al., 2013, Nelson et al., 2012). For example, Acosta et al., 2013 showed that soluble SASP components, such as TGFβ and CCL2, are able to induce a paracrine senescence response in neighbouring normal cells both *in vitro* and *in vivo*. In addition, Nelson et al., 2012 showed that senescent fibroblasts induce a DNA damage response (reminiscent of that associated with senescence) and cell cycle arrest in bystander fibroblasts via cell-to-cell contact and increased reactive oxygen species (ROS) production.

Further, components of the SASP produced by cells that have undergone OIS have also been shown to re-enforce the growth arrest of senescent cells by manipulating mitogenic signals from surrounding cells (reviewed in Kuilman and Peeper, 2009). For example, elements of the SASP may dampen the secretion of growth factors that promotes the proliferation of pre-malignant cells. There is also evidence to suggest that components of the SASP may act to block mitogenic signalling by direct interference at the receptor level (Gagnon et al., 1998, Mincione et al., 2003). For example, TGFβ has been shown to inhibit tyrosine phosphorylation and insulin receptor substrate 1 (IRS1) activation (an important mediator of insulin signalling in both mouse fibroblasts and epithelial cells) (Gagnon et al., 1998, Mincione et al., 2003). Finally, senescent cells may also stimulate surrounding stromal cells to secrete proliferation-inhibitory factors that may limit the proliferative potential of nearby pre-malignant cells (reviewed in Kuilman and Peeper, 2009).

1.5.3 *Immunosurveillance of senescent cells*

There is now growing evidence to suggest that as well as triggering a senescence response in potentially vulnerable bystander cells, components of the SASP may also trigger the immune-clearance of senescent pre-malignant cells, limiting the risk of bypass and carcinogenesis (reviewed in Sagiv and Krizhanovsky, 2013). Crucially, the SASP is composed of multiple immune-activating components such as chemokines, activating cytokines, adhesion molecules and the inflammasome (a caspase-1 activating protein complex) (Acosta et al., 2013). The composition of the SASP has been found to vary in a cell type and context-specific manner (reviewed in Freund et al., 2010). As such, depending on the chemokines present within the SASP and the chemokine receptors present on the cells within the microenvironment, it is hypothesised that a distinct subset of immune cells may be recruited to sites of senescence (reviewed in Freund et al., 2010).

Increasing evidence now suggests that as well as immune cell recruitment, senescent cells are targeted and cleared via both the innate and adaptive immune systems (Xue et al., 2007, Krizhanovsky et al., 2008, Kang et al., 2011, Sagiv et al., 2013). For example, chemokines often present within the SASP, including CCL2, chemokine (C-C motif) ligand 5 (CCL5) and IL-8, are known to recruit Natural Killer cells (NK cells, rapidly responding cytotoxic lymphocytes). Importantly, NK cells have a broad specificity to a wide range of chemokines. As such, it is likely that NK cells are recruited to multiple senescent sites including telomere-associated and DNA damage-associated senescence induction (reviewed in Sagiv and Krizhanovsky, 2013). In addition, IL-15 (often present within the SASP) is known to upregulate natural killer group 2D receptor (NKG2D) expression in NK cells (Xue et al., 2007, Krizhanovsky et al., 2008) and NKG2D-activating ligands are often upregulated within senescent cells (Lanier, 2005, Deng et al., 2015). Further, the adhesion molecule, intercellular adhesion molecule 1 (ICAM-1) is also upregulated within senescent cells. ICAM-1 binds to the NK cell receptor, CD58, and, interestingly, the combined function of ICAM-1 and NKG2D ligands results in enhanced NK cell-mediated killing of target cells (Hayakawa and Smyth, 2006).

NKs have been found within the surrounding microenvironment of senescent hepatocytes (Kang et al., 2011) and hepatic stellate cells (Krizhanovsky et al., 2008). NKs have now been found to target and eliminate senescent cells associated with tissue repair (Krizhanovsky et al., 2008, Sagiv et al., 2013) and tumour suppression (Xue et al., 2007). For example, Sagiv et al. demonstrated that granule exocytosis (NK cell directed cell killing) inhibition via perforin (enables granzyme influx into target cells) knockdown prevented senescent cell elimination and

enhanced liver fibrosis *in vivo*. In addition, in a mouse model of liver carcinogenesis induced by p53 depletion, p53 restoration resulted in senescence induction and the clearance of senescent cells mediated by NK cell infiltration (Xue et al., 2007).

As well as eliciting NK cell-mediated immune-clearance, senescent cells have also been shown to recruit and activate macrophages and CD4+ T-cells (Krizhanovsky et al., 2008, Kang et al., 2011). For example, multiple components of the SASP, including macrophage cationic peptide 2, 3 and 4 (MCP-2, MCP-3 and MCP-4) act to recruit inflammatory monocytes (macrophage precursors) and macrophages, neutrophils and dendritic cells are often found within the senescence microenvironment (Krizhanovsky et al., 2008, Xue et al., 2007). In addition, SASP components, colony stimulating factor 2 receptor, beta, low-affinity (granulocyte-macrophage) (GM-CSF) and colony stimulating factor 3 receptor (granulocyte) (G-CSF) are known to drive monocyte production within the bone marrow (Semerad et al., 1999, Semerad et al., 2002). Importantly, Krizhanovsky et al. demonstrated that within a mouse model for liver fibrosis, senescent hepatic stellate cells secreted the SASP components, Interferon ϒ (IFN-ϒ) and IL-6 which drove macrophage polarisation towards M1 (classically activated state associated with anti-tumour activity) and, in turn, eliminated p53-positive senescent cells. Additionally, Kang et al. demonstrated that pre-malignant senescent hepatocytes are cleared by a CD4+ T-cell-dependent adaptive immune response in mice. In line with this finding, benign naevi within human skin expressing multiple senescence-associated markers often gradually regress over many decades supporting the existence of immune-mediated elimination of senescent cells *in vivo* in humans (reviewed in Kuilman and Peeper, 2009).

1.6 *Pro-senescence therapy: an emerging anti-cancer strategy*

1.6.1 *Senescence: a barrier to carcinogenesis*

Increasing evidence now suggests that senescence may be activated *in vivo* in response to an oncogenic event and acts as a crucial protective mechanism against tumourigenesis. Consequently, it is proposed that senescence bypass is an essential, early step on the road towards carcinogenesis. In line with this, the senescence mediators, p53 and p16 are among the most commonly mutated or deleted genes in cancer (Hanahan and Weinberg, 2011). As such, it is hypothesised that loss of either the p53/p21 or p16/RB signalling pathways in pre-malignant cells may enable senescence bypass and tumourigenesis.

Whilst the vast majority of human malignancies harbour p16 mutations or gene deletions, a handful of tumours (including human papilloma virus (HPV)-positive cervical tumours and a

subset of breast tumours) arise whilst maintaining high wild type (WT) p16 protein levels. Within breast cancer, this p16 signature confers a highly malignant phenotype and a poor prognosis for reasons that are currently not fully understood (Hui et al., 2000) (see Section 1.8). Within these tumours it is likely that inactivation of the p16/RB signalling axis render cells insensitive to pro-senescence p16 signalling, enabling uncontrolled cell division despite high p16 protein levels. For example, HPV-positive cervical cancer cells (such as the HeLa cell line) often express the transforming viral oncogenes E6 and E7. Crucially, E6 drives p53 protein degradation whilst E7 competes for binding with active RB, freeing E2F-1 and allowing unchecked cell cycle progression and transformation (reviewed in Yim and Park, 2005) Further, overexpression of the viral oncogene E2 (repressor of E6 and E7) in HeLa cells results in growth arrest, together with an upregulation of p53 and p21 expression (Wells et al., 2000).

1.6.2 *Senescence activation in cancer: an attractive therapeutic strategy*

There is now a growing body of evidence to show that cancer cells from a wide array of human malignancies are able to undergo senescence activation both *in vitro* and *in vivo* (discussed in Section 1.6.3). An elegant example of this was demonstrated by the Lowe laboratory in 2007, who showed that p53 restoration in p53-deficient, H-RAS^{V12} – positive liver carcinomas resulted in senescence induction and complete tumour regression in mice (Xue et al., 2007). Further, MDM2 inhibitors (such as nutlin) that may stabilise p53 are currently under investigation in tumours with WT p53 expression (reviewed in Acosta and Gil, 2012). In addition, it has long been known that senescence may be activated in cancer cells both *in vitro* and *in vivo* in response to specific chemotherapeutic agents (termed Therapy-induced senescence, TIS). *In vitro* studies using the p53 WT human cancer cell lines: MCF-7 (Luminal breast adenocarcinoma), HCT116 (colorectal carcinoma) and A549 (lung adenocarcinoma) have shown that TIS may be induced by cytotoxic agents such as Doxorubicin, Camptothecin and Cisplatin (reviewed in Gonzalez et al., 2015). Further, Han et al., 2002 showed that TIS activated by Camptothecin application was mediated by p53 and p21. Importantly, te Poele et al., 2002 was the first to demonstrate that TIS accompanied by increase β-gal activity and elevated p16 expression may be activated *in vivo* in breast tissue, following chemotherapy.

The effectiveness of radiotherapy and chemotherapeutics have improved greatly since their initial application over 60 years ago. However, these agents are often ineffective against highly aggressive metastatic disease such as p16-positive Basal-like breast cancer (BLBC) where there is a desperate clinical need for more effective alternative treatments (see Section 1.8). Given

this, the activation of senescence in cancer is fast becoming a highly attractive therapeutic strategy and the evolution of novel pro-senescence agents is gaining momentum.

1.6.3 *Current pro-senescence approaches*

Perhaps the most clinically successful pro-senescence anti-cancer agent is the selective CDK4/6 inhibitor, PD0332991 or Palbociclib (Pfizer Inc.) Similarly, Abemaciclib and LEE011 directly inhibit Cyclin D1 interaction with CDK4/6, and Palbociclib has recently been approved by the FDA for use in combination with Letrozole in post-menopausal metastatic hormone receptor-positive human epidermal growth factor receptor (HER2)-negative breast cancer (Harding, 2015). Phase II and III clinical trials are currently ongoing, however, a recent phase three PALOMA-3 clinical trial revealed that Palbociclib in combination with Fulvestrant (Estrogen receptor (ER) antagonist) gave rise to an increase in progression free survival in patients with metastatic hormone receptor-positive HER2-negative breast cancer when compared to Fulvestrant alone (reviewed in Mayer, 2015). *In vitro* studies have also found that monotherapy with Palbociclib results in growth inhibition in HER2-positive breast cancer cell lines and future planned clinical trials will examine the effectiveness of Palbociclib in hormone receptor-positive HER2-positive tumours (reviewed in Mayer, 2015). Importantly, an *in vitro* study that aimed to assess the effectiveness of Palbociclib within 47 individual breast cancer cell lines showed that responsiveness was associated with elevated ER, RB and Cyclin D1 expression and no or low levels of p16 (Finn et al., 2009). Of direct relevance, triple negative (TN) (see Section 1.8) p16-positive BLBC cell lines, such as MDA-MB-468 cells, were highly resistant to Palbociclib-induced cell cycle arrest, suggesting that Palbociclib may prove to be ineffective within highly malignant p16-positive BLBCs that are often characterised by RB mutations or deletions (Finn et al., 2009).

In addition to CDK inhibition, a recent study proposed that progestins (activators of the progesterone receptor, PR) may activate senescence via forkhead box O1 (FOXO1) and p21 activation in PR-positive ovarian cancer (Diep et al., 2013). In line with this, phosphatidylinositol-4,5-bisphosphate 3-kinase (PI3K) (upstream inhibitor of FOXO1) inhibition and PTEN (PI3K inhibitor) overexpression has also been found to induce senescence (reviewed in Acosta and Gil, 2012). Conversely, PTEN inhibition has been found to induce senescence in $PTEN^{+/-}$ tumours, demonstrating that the PTEN/PI3K axis is very finely tuned and modulation of this pathway may prove to be prone to unfavourable consequences (reviewed in Acosta and Gil, 2012).

The inhibition of telomerase (an enzyme acquired by over 90% of human cancers and critical for maintaining telomeric length, see Section 1.2.1) has also been proposed as a pro-senescence anti-cancer strategy. For example, continuous treatment with the telomerase inhibitor,

Imetelstat (GRN163L) has been found to induce both apoptosis and senescence (characterised by β-gal activity and ϒH2AX foci) within ten different pancreatic cancer cell lines (Burchett et al., 2014). In addition, disruption of oncogene-addiction in cancer has also been found to induce senescence both *in vitro* and *in vivo*. For example, C-MYC inhibition via JQ1 (bromodomain inhibitor) in C-MYC-driven medulloblastoma has been found to activate senescence *in vivo* and may represent a novel therapeutic approach in this highly malignant cancer subtype (Venkataraman et al., 2014). Finally, given the findings generated by Acosta et al., 2013 on the paracrine nature of the SASP (see Section 1.2.3), specific SASP pro-senescence components may also have the potential to activate senescence in surrounding cancer cells and may form the basis of a novel anti-cancer strategy (reviewed in Acosta and Gil, 2012).

1.6.4 *The importance of senescent cell clearance and senolytics*

Given the complex and often opposing effects associated with senescence activation, at present it is difficult to estimate the long-term consequences of pro-senescence therapies. It is possible that post-treatment, senescent cancer cells may be quickly eliminated via endogenous immuno-clearance mechanisms (discussed in Section 1.5.3), however, an important study by Sanoff et al., 2014 suggested that TIS activation may induce long-lasting effects and may even accelerate human ageing. Within this study peripheral blood T-cell p16 expression levels were assessed in breast cancer patients prior to and at 12 months post-chemotherapy treatment. Strikingly, chemotherapy was associated with a statistically significant increase in p16 expression levels equivalent to 14.7 years of chronological ageing. Furthermore, this increase in p16 expression appeared to be stable several years after chemotherapy treatment suggesting that therapy-induced senescent cells may remain within the body many years after cytotoxic regimes. This data is in line with the observations that cancer survivors treated with chemotherapy often experience a multitude of age-associated pathologies later in life such as frailty, cognitive impairment and cardiovascular morbidity (Sanoff et al., 2014, Ness et al., 2015).

In addition to the potential detrimental impacts on ageing, if left unchecked, senescent cancer cells may acquire spontaneous mutations, bypass the senescence programme and propagate highly malignant drug-resistant secondary tumours, resulting in disease relapse (reviewed in Gonzalez et al., 2015). Given this, it is proposed that in order for a pro-senescence therapy to be an effective, non-toxic anti-cancer strategy, senescent cancer cells must be rapidly eliminated as part of a two-step therapeutic approach. The field of senescent cell elimination is rapidly expanding and exciting novel mechanisms for inducing senescent cell death are currently being explored. For example, a recent study conducted by Zhu et al., 2015 identified two potential

'senolytic' agents (Dasatinib and Quercetin) that preferentially eliminated irradiated senescent cells both *in vitro* and *in vivo*. Dasatinib disrupts apoptosis suppression while Quercetin is a known inhibitor of PI3K (implicated in pro-survival and anti-apoptotic signalling). The two agents had differential efficacy depending on the cellular context, however, combined application of both senolytics resulted in selective killing across a broader range of senescent cell types (Zhu et al., 2015). Additionally, in an Eμ-myc transgenic mouse lymphoma model, TIS following chemotherapy was associated with enhanced glucose uptake together with increased ATP production. Exploitation of the hypercatabolic nature of the therapy-induced senescent cells through blocking glucose uptake resulted in preferential apoptosis activation within the senescent cells. Crucially, senescent cell clearance was also associated with tumour regression (Doerr et al., 2013). Interestingly, a recent proof-of-concept study also showed that TIS cells may be preferentially targeted by oncolytic viruses (Weiland et al., 2014). Taken together, these studies suggest that strategies harnessing senescence-associated properties, such as apoptosis resistance or altered glucose metabolism, may present novel mechanisms for senescent cell clearance following pro-senescence therapy. However, further studies ought to be completed in order to assess the efficacy of these strategies within senescent cancer cells that have been treated with a specific pro-senescence therapy.

There is now a wealth of evidence to suggest that senescent cells are targeted and eliminated from tissues via stimulation of both the innate and adaptive immune system (see Section 1.5.3). As such, it is hypothesised that immuno-boosting agents administered after an initial pro-senescence therapy may function to enhance immuno-clearance of senescent cancer cells *in vivo*. Interestingly, adjuvants are commonly used within vaccinations in order to enhance their efficacy (reviewed in Boraschi and Italiani, 2014). MF59 (oil in water emulsion) is often used within Influenza vaccinations and functions to enhance monocyte and macrophage recruitment at the vaccination site (O'Hagan et al., 2013). Given this, adjuvants injected directly into senescent tumours may enhance the immuno-clearance of senescent cancer cells.

It is likely that a combination of senolytic and immuno-boosting agents will be required in order to fully eliminate senescent cancer cells following an initial pro-senescence therapy. However, at present, the full impact of widespread senescent cell elimination on human health is unknown and there are currently many unanswered questions in the field. For example, it is unclear how far the tumour suppressive paracrine effects of the SASP may reach *in vivo,* or what the effects of senescent cell clearance may be on pre-malignant cells. Importantly, the work by Baker et al., 2011 suggests that senescent cell clearance may indeed be favourable, however, this study was

performed in a progeroid mouse model and findings may not be directly transferable to the human context.

1.7 *The 80S mammalian ribosome*

1.7.1 *Mammalian ribosomal structure and function*

Ribosomes are ribonucleoprotein translational machines and the primary sites for protein synthesis across all kingdoms of life (Ramakrishnan, 2011). The mammalian 80S structure consists of two distinct subunits: the large 60S ribosomal subunit, composed of three ribosomal RNA (rRNA) molecules (28S, 5S and 5.8S rRNA) and 47 proteins, and the small 40S subunit, formed of just one rRNA molecule (18S rRNA) and 33 proteins (Khatter et al., 2015). The ribosomal core functions to catalyse translation and is highly conserved across all species. Here, located within the small 40S subunit, is the decoding site (DCS), responsible for mRNA reading and decoding. In addition, positioned within the 60S subunit are the catalytic peptidyl transferase and GTPase-associated centres, required for charged-tRNA recruitment and polypeptide chain generation. The nascent amino acid chain is subsequently relocated to the peptidyl (P) site and deacetylated transfer RNA (tRNA) is held at the exit (E) site (both within the 60S subunit) prior to ejection from the ribosome (Khatter et al., 2015, Fatica and Tollervey, 2002). siRNA screening (presented in Chapter 3) identified 11 ribosomal proteins (RPs) as potential senescence evaders within p16-positive cancer cells and six of these (RPL14, RPL18, RPL34, RPL35A, RPS3A and RPS7) were prioritised for further validation. The location of these RPs within the human 80S ribosome is depicted in Figure 1.4A-B.

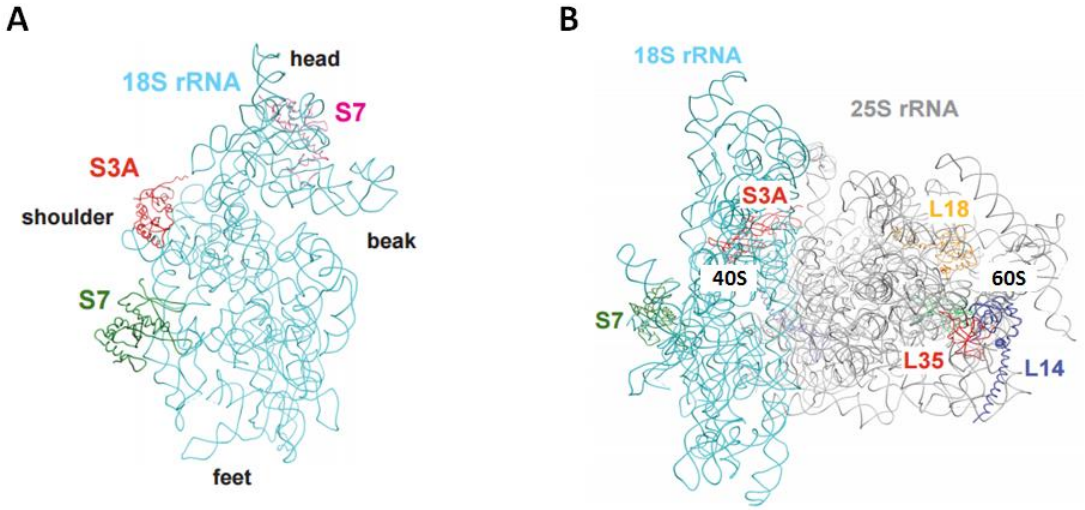

Figure 1.4: Molecular structure of the human 80S ribosome. (A) 40S small ribosomal subunit. **(B)** Human 80S ribosome. The location of five of the top six RP hits identified within the siRNA screens is shown.

Images were generated by Dr. Sander Granneman, Institute of Structural and Molecular Biology, University of Edinburgh.

Recently, a near atomic structure (with an average resolution of 3.6 angstroms, Å) of the human 80S ribosome was published (Khatter et al., 2015). This work revealed the ribosome to be a highly dynamic multiprotein complex capable of subunit rearrangements and widespread conformational changes during translation. For example, during translocation, the 40S subunit is reported to undergo three major movements resulting in dramatic alterations to RP interactions. This analysis by Khatter et al. has identified all potential ligand-binding pockets present within the human ribosome and may facilitate structure-guided *in silico* drug design of compounds designed to target abnormal ribosomal function in diseases such as cancer. Recently, a new system for naming the 40S and 60S RPs was proposed (Ban et al., 2014) and details of the new nomenclature may be found in Table 1.2 (Ban et al., 2014). In order to maintain continuity with the current literature, the old nomenclature is used throughout this thesis.

40S small RPs		**60S large RPs**	
Old name (human)	**New name**	**Old name (human)**	**New name**
SA	uS2	P0	uL10
S2	uS5	P1/P2 (αβ)	P1/P2
S3	uS3	L3	uL3
S3A	eS1	L4	uL4
S4	eS4	L5	uL18
S5	uS7	L6	eL6
S6	eS6	L7	uL30
S7	eS7	L7A	eL8
S8	eS8	L8	uL2
S9	uS4	L9	uL6
S10	eS10	L10	uL16
S11	uS17	L10A	uL1
S12	eS12	L11	uL5
S13	uS15	L12	uL11
S14	uS11	L13	eL13

S15	uS19	L13A	uL13
S15A	uS8	L14	eL14
S16	uS9	L15	eL15
S17	eS17	L17	uL22
S18	uS13	L18	eL18
S19	eS19	L18A	eL20
S20	uS10	L19	eL19
S21	eS21	L21	eL21
S23	uS12	L22	eL22
S24	eS24	L23	uL14
S25	eS25	L23A	uL23
S26	eS26	L24	eL24
S27	eS27	L26	uL24
S27A	eS31	L27	eL27
S28	eS28	L27A	uL15
S29	uS14	L28	eL28
S30	eS30	L29	eL29
RACK1	RACK1	L30	eL30
		L31	eL31
		L32	eL32
		L34	eL34
		L35	uL29
		L35A	eL33
		L36	eL36
		L36A	eL42
		L37	eL37
		L37A	eL43
		L38	eL38
		L39	eL39
		L40	eL40

	L41	eL41

Table 1.2: Table containing the new nomenclature for the small 40S and large 60S RPs. RPs are listed in numerical order according to the old nomenclature. 'u' denotes a RP universal to bacterium, yeast and humans. 'e' denotes those RPs present within eukaryotic ribosomes only. Only those RPs present within the human ribosome are listed. RPs unique to bacterium are not present within this list. Data taken from Ban et al., 2014.

1.7.2 *The nucleolus: the site for ribosomal assembly*

During the early nineteenth century, German physiologists Rodolph Wagner and Gabriel Valentin as well as the Italian pathologist, Giuseppe Pianese were among the first to record their observations of the nucleolus (reviewed in Lam and Trinkle-Mulcahy, 2015), however, it wasn't until the mid-1960s that it was discovered to be the site for rRNA transcription and ribosomal biosynthesis (Brown and Gurdon, 1964, reviewed in Pederson, 2011). It is now accepted that the nucleolus is not simply a feature of the nuclear architecture, but a dynamic non-membrane bound organelle that forms at specific chromosomal loci known as nucleolar organising regions, containing ribosomal DNA (rDNA) (reviewed in Pederson, 2011 and see Figure 1.5A-C). Further, electron microscopy has revealed that the mammalian nucleolus contains three functionally distinct compartments: the Fibrillar Centre (FC); the Dense Fibrillar Centre (DFC); and the Granular Component (GC) (Miller and Beatty, 1969, and reviewed in Pederson, 2011). The FC contains the RNA polymerase I, (RNA Pol I) which is responsible for rRNA transcription. The DFC contains early pre-rRNA processing factors and rRNA transcription occurs at the border between these two regions. Late pre-rRNA processing and ribosomal subunit assembly occurs within the GC region before transportation of the pre-ribosomal subunits into the nucleoplasm (Koberna et al., 2002, and reviewed in Pederson, 2011).

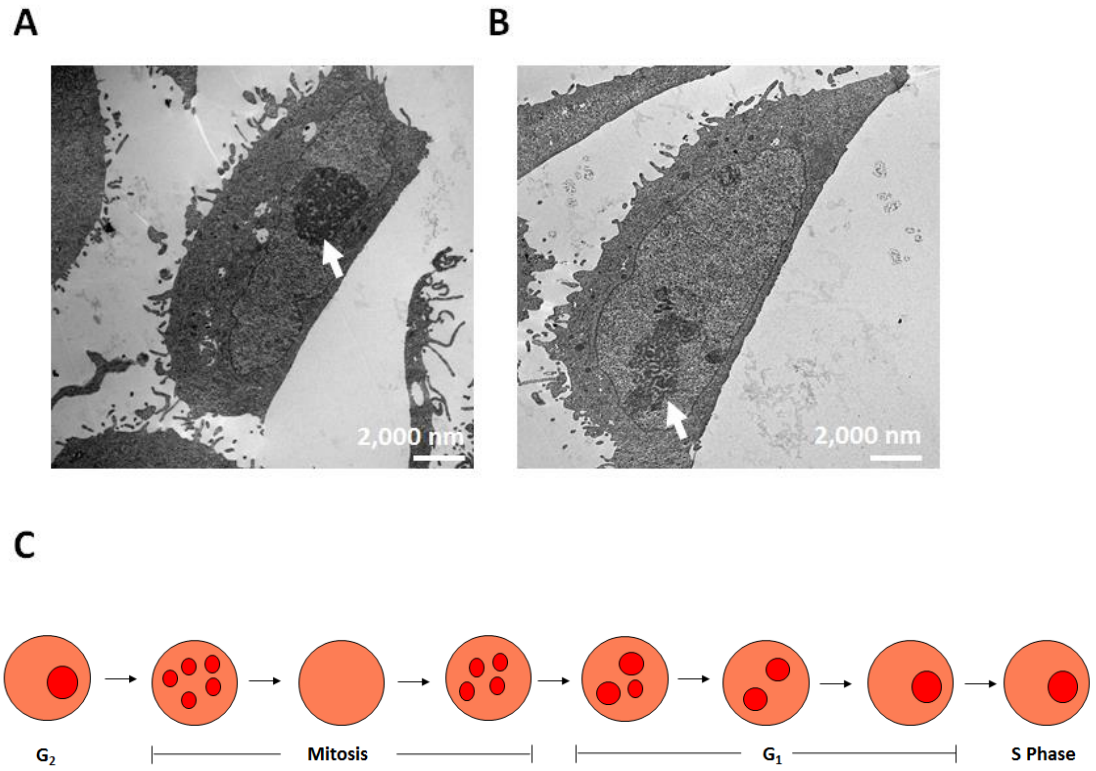

Figure 1.5: Nucleolar disassembly and reassembly during the cell cycle. (A-B) Transmission electron microscopy (TEM) images of proliferating MDA-MB-468 cells. Arrows denote the nucleolus. Images were taken by Guilia Mastroianni, The School of Biological and Chemical sciences, Queen Mary, University of London. **(C)** Cartoon depicting nucleolar disassembly and reassembly during the cell cycle. The nucleolus is highly dynamic and forms at specific chromosomal loci containing actively transcribing rDNA regions. During the early phases of mitosis rDNA transcription is downregulated and the nucleoli disassembles. However, during Telophase and G1 the nucleoli reassembles to coincide with rDNA transcription activation. During S phase and G2 the nucleoli is often enlarged, reflecting an increase in rDNA transcription as the cell prepares to divide once again (Reviewed in Quin et al., 2014). Light red denotes the nucleus, dark red denotes the nucleoli.

Nucleoli purification and mass spectrometry has revealed that the mammalian nucleolus contains approximately 4,500 abundant proteins, the vast majority of which are not components of the mature ribosome (Andersen et al., 2002, Scherl et al., 2002, Ahmad et al., 2009, Pederson, 2011). The function of these non-ribosomal nucleolar-associated proteins is yet to be fully deciphered, however, a recent study using HeLa cells has identified 286 that are required for pre-rRNA processing (Tafforeau et al., 2013). Importantly, 11 of these genes were validated as pre-rRNA processors and many are upregulated in malignancies including breast cancer (Butt et al., 2008). As such, these genes may represent novel potential biomarkers for ribosomal maturation dysfunction within diseases such as cancer or ribosomeopathies (see Section 1.7.5).

1.7.3 *Pre-rRNA processing and eukaryotic ribosomal biosynthesis*

Mammalian ribosomal biosynthesis is complex and tightly regulated, and accounts for approximately 80% of the transcriptional activity of a rapidly dividing cell such as a cancer cell

(Warner, 1999, reviewed in de las Heras-Rubio et al., 2014). For example, it is estimated that a dividing HeLa cells generates approximately 7,500 ribosomal subunits per minute in order to meet its high translational demands (Lewis and Tollervey, 2000, Granneman and Tollervey, 2007, and reviewed in Leary and Huang, 2001). Consequently, the process is extremely 'expensive' and a rate limiting step in the proliferation of a highly transformed cell (reviewed in de las Heras-Rubio et al., 2014). The process spans the nucleolus, nucleoplasm and cytoplasm and requires the synchronised function of RNA pol I, II and III (reviewed in Tschochner and Hurt, 2003). In brief, ribosomal biosynthesis involves two key events: multi-step pre-rRNA processing to form the four mature rRNA molecules, and the assembly of RPs with each other and the structural rRNA to form the final mature ribosome. In order to generate a fully functional 80S mammalian ribosome these two processes must be co-ordinately regulated, however, at present, it is not clear how the pathways interact and details of the order and timings of these events *in vivo* is lacking. It is likely that alterations to the timing or localisation of RP binding to pre-rRNA could severely disrupt the rate of ribosomal biosynthesis, impacting on cell cycle progression and final ribosomal composition (reviewed in Tschochner and Hurt, 2003).

The rate limiting step during ribosomal biosynthesis is the complex process of rRNA maturation reviewed in Lafontaine, 2015). In *Saccharomyces cerevisiae* (*S. cerevisiae)* the process requires over 200 non-ribosomal proteins and approximately 100 small non-coding RNAs (Ferreira-Cerca et al., 2007). In higher eukaryotes, the process of pre-rRNA processing is less-well understood, however, a consensus model for human pre-rRNA processing has been constructed (Figure 1.6). In summary, the mature rRNAs (18S, 5.8S and 28S) are first transcribed as a single ploycistronic transcript (47S pre-rRNA) by RNA Pol I within the nucleolus. The 47S pre-rRNA then undergoes a complex series of cleavage events via two distinct pathways (Pathway A, a minor pathway or Pathway B, see Figure 1.6). Maturation pathways A and B are known to differ in terms of their kinetics and order of pre-rRNA cleavage, however many of the pre-rRNA processing sites are conserved across both pathways. The 5S rRNA is transcribed separately within the cytoplasm by RNA Pol III and is translocated to the nucleolus for assembly. Subsequently, the mature rRNA molecules (18S, 5.8S, 28S and 5S) are folded and assembled together with specific RPs to form the pre-ribosomal 40S and 60S subunits (reviewed in Lafontaine, 2015). Importantly, studies in *S. cerevisiae* have revealed that 5' and 3' cleavage of the 47S pre-rRNA homolog (35S pre-rRNA triggers the formation of the pre-ribosomal subunits and initiates the recruitment of specific non-ribosomal association factors required for subunit biogenesis (Wehner et al., 2002, and reviewed in Tschochner and Hurt, 2003, see Figure 1.7).

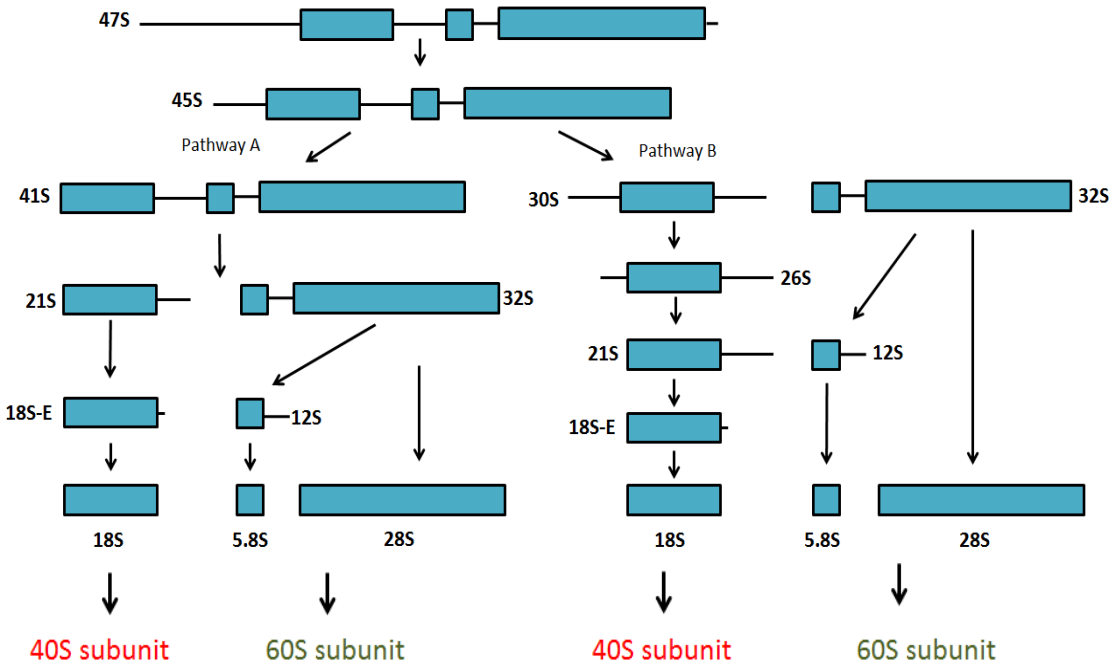

Figure 1.6: Schematic depicting pre-rRNA processing in human cells. 5' and 3' site specific cleavage of the 47S pre-rRNA molecule results in the generation of the 45S pre-rRNA. The 45S pre-rRNA is subsequently processed via two distinct rRNA maturation pathways, Pathway A (minor pathway) or Pathway B (major pathway). Within Pathway A, 41S pre-rRNA undergoes two separate cleavage events to form the pre-rRNA molecules, 21S and 32S. The 32S pre-rRNA is then cleaved to generate the two mature rRNA molecules, 5.8S and 28S for incorporation into the 60S ribosomal subunit. The 21S pre-rRNA molecule is then subsequently cleaved to form the 18S-E intermediate rRNA molecule. The final cleavage event resulting in the generation of the mature 18S rRNA molecule occurs within the cytoplasm. Within Pathway B, a single cleavage event with the 45S pre-rRNA results in the generation of the 30S and 32S pre-rRNA molecules. Subsequently, the 21S and 32S pre-rRNA molecules are processed in the same way as Pathway A (Image adapted from Lafontaine, 2015).

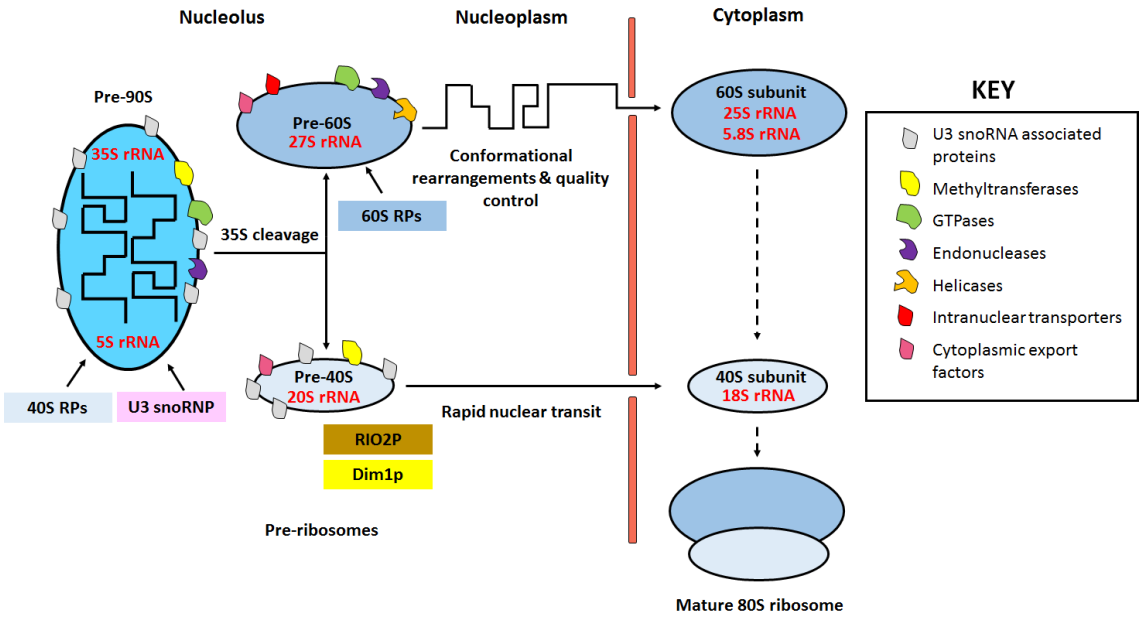

Figure 1.7: Schematic summarising 80S eukaryotic ribosomal biogenesis in *S. cerevisiae*. The 90S pre-ribosomal particle is constructed within the nucleolus at the site of the 35S pre-rRNA and contains structural RPs (predominantly 40S RPs), non-ribosomal association factors and the U3 snoRNP (ribonucleoprotein made up of the U3 snoRNA and 28 U3-associated proteins). Cleavage of the 35S pre-rRNA triggers the generation of two pre-ribosomes (the pre-60S and the pre-40S subunits). 60S RPs and 60S-associated non-ribosomal factors assemble at the 27S pre-rRNA while 40S RPs are assembled at the 20S pre-rRNA. Specific methyltransferases and kinases, such as Dim1p and RIO2P, assemble at the 40S pre-ribosome and are required for 20S pre-rRNA cytoplasmic cleavage. The pre-ribosomes are transported through the nucleus and are exported into the cytoplasm via nuclear pores. Once in the cytoplasm the non-ribosomal association factors disassociate from the pre-ribosomal subunits and the 80S mature ribosome is generated. In yeast the mature 18S rRNA molecule is generated within the cytoplasm prior to 80S formation, however within mammalian cells, this final cleavage event occurs within the nucleus (Schematic adapted from Tschochner and Hurt, 2003).

At present, the best model for RP assembly has evolved from studies conducted in *S. cerevisiae* (Tschochner and Hurt, 2003, see Figure 1.7). Both structural RPs and associated synthesis factors are transcribed and translated in the cytoplasm and are subsequently translocated into the nucleolus (reviewed in Tschochner and Hurt, 2003). Here, an early ribonucleoprotein particle, known as the 90S pre-ribosomal subunit, is constructed at the site of the 47S pre-rRNA homolog, 35S pre-rRNA (Udem and Warner, 1972, Trapman et al., 1975). As well as pre-rRNA, the 90S particle also contains structural RPs (predominately 40S components) and numerous ribosomal synthesis factors, such as endonucleases and methyltransferases, critical for pre-rRNA processing (Nissan et al., 2002, Grandi et al., 2002, and reviewed in Tschochner and Hurt, 2003). Importantly, encompassed within the 90S particle is the Small Subunit Processome (SSP) that assembles co-transcriptionally at the 5' end of the 35S pre-rRNA. The SSP contains pre-rRNA processing factors, including methyltransferases, required for 18S maturation and the small nucleolar RNA, U3 snoRNA, required for guided site specific pre-rRNA cleavage (Dragon et al., 2002, reviewed in Tschochner and Hurt, 2003). Importantly, the SSP mediates a critical early

cleavage event at the 5' and 3' ends (sites A_0 and A_1) of the 35S pre-rRNA molecule (Dragon et al., 2002, reviewed in Tschochner and Hurt, 2003). This cleavage event triggers the recruitment of additional 40S synthesis factors to the 90S particle and the generation of the two pre-ribosomal subunit particles (Wehner et al., 2002, reviewed in Tschochner and Hurt, 2003). Subsequently, 60S structural RPs and synthesis factors are recruited to the 60S pre-ribosomal subunit and assembled on the 27S pre-rRNA (Fatica et al., 2002). 60S synthesis factors include: pre-rRNA modifiers required for 5.8S and 25S rRNA generation (a pre-requisite for nucleolus exit); GTPases and helicases for correct rRNA folding; and transporters essential for subunit translocation to the nucleoplasm (Fatica et al., 2002, reviewed in Tschochner and Hurt, 2003, and Fatica and Tollervey, 2002). Further conformational changes and quality control checks occur within the nucleoplasm before the mature 60S subunit enters the cytoplasm (reviewed in Tschochner and Hurt, 2003). Independent of 60S subunit generation, 35S cleavage also triggers 40S pre-ribosomal subunit processing. Cleavage initiates the majority of the 40S synthesis factors (present within the 90S particle) to disassociate from the pre-ribosomal subunit and the recruitment of specific methyltransferases and protein kinases such as RIO2P to the 20S pre-rRNA (Schafer et al., 2003, reviewed in Tschochner and Hurt, 2003). It is important to note that in mammalian cells, the 21S cleavage event to generate the 18S-E rRNA molecule occurs within the nucleus, unlike in yeast, where 20S cleavage occurs within the cytoplasm (Vanrobays et al., 2001). Interestingly, the 40S pre-ribosomal subunit translocates much faster through the nucleoplasm and undergoes fewer conformational changes than the larger subunit before exiting into the cytoplasm. Within both yeast and mammalian cells, the final 80S ribosome is generated within the cytoplasm and remains in the cytosol or is translocated to the rough endoplasmic reticulum, where it performs its translational function (reviewed in Tschochner and Hurt, 2003, and Fatica and Tollervey, 2002).

At present, the full hierarchy of RP incorporation into the ribosome is unknown. However, a recent study conducted in *S. cerevisiae* identified RPS5 as a potential early 40S component required for pre-rRNA processing and the correct incorporation of eight additional 40S RPs including RPS15 and RPS10 (Ferreira-Cerca et al., 2007). Furthermore, the exact function of each of the RPs is yet to be deciphered, however, a growing body of evidence suggests that many RPs conduct specific functions in addition to their structural role within the mature ribosome. For example, RPL10 has recently been implicated in 60S subunit nuclear exit (Gadal et al., 2001, reviewed in Fromont-Racine et al., 2003) and many proteins, including RPS18 and RPL35A, have been found to play important roles within rRNA processing (Ferreira-Cerca et al., 2005, Babiano and de la Cruz, 2010, Ilin et al., 2011). Additionally, both 60S and 40S components have been

found to harbour extra-ribosomal functions such as cell cycle regulation (Fumagalli et al., 2009, see Section 1.7.6). Together, these studies suggest that each RP component may play a unique biological role either during ribosomal biosynthesis or within a wider cellular pathway and that the loss of key RPs (such as RPL10) may be devastating for the generation of functional ribosomes. Further, it is likely that there are varying degrees of redundancy within the RP population depending on the stage of ribosomal integration (Ferreira-Cerca et al., 2007). As such, the loss of a subset of RPs may not be fatal for the cell, but instead, may result in alterations to ribosomal conformation and translational capacity. Further studies on the hierarchy of RP incorporation may help subcategorise the RPs into 'early' and 'late' components and identify those proteins essential for biogenesis (such as RPS5) and those with greater redundancy.

It is important to note that the majority of the work to fully elucidate the mechanism of ribosomal biogenesis has been performed in the eukaryotic model, *S. cerevisiae*. Until recently, it was assumed that details ascertained using this model could be directly applied to higher eukaryotic organisms, however, this is now considered to be a simplistic view as it is highly likely that mammalian ribosomal biosynthesis is far more complex than the mechanism described here (Tafforeau et al., 2013). For example, the mammalian ribosome is larger and is known to contain additional RPs with no known yeast homologs (Tafforeau et al., 2013). In addition, the mammalian nucleolus contains three distinct compartments as opposed to just two found in yeast and is known to contain at least ten times the amount of abundant proteins (Tafforeau et al., 2013). Together, this indicates that, at the very least, far more ribosomal processing factors are involved in mammalian ribosomal synthesis than in simpler eukaryotic organisms and future work ought to concentrate on fully dissecting ribosomal biogenesis in mammalian cells.

1.7.4 *Regulating eukaryotic ribosomal biosynthesis*

Ribosomal biosynthesis is tightly regulated at multiple stages including: RP synthesis and translocation; rRNA transcription, maturation; and pre-ribosomal subunit assembly (reviewed in Leary and Huang, 2001). Crucially, the rate of ribosomal biosynthesis is altered in order to meet the cell's current translational demands and is closely tied to the cell cycle. For example, biosynthesis is enhanced in response to proliferative stimuli and reduced in response to differentiation, protein synthesis inhibition as well as environmental ques such as nutrient starvation, heat shock or DNA damage (Grummt et al., 1976, and reviewed in Ruggero and Pandolfi, 2003, and Leary and Huang, 2001). A down-regulation of ribosomal biosynthesis is also required during mitosis to ensure correct cell cycle progression (Klein and Grummt, 1999, Ruggero and Pandolfi, 2003). In mouse fibroblasts, serum starvation has been shown to inhibit

ribosomal biosynthesis as well as downregulating mRNA levels of a key assembly protein, Erb1p (Strezoska et al., 2000). Further, heat shock or nutrient depletion in yeast has been shown to reduce the expression of snoRNA-binding rRNA-processing protein IMP4 (IMP4P), a key U3 snoRNP component required for pre-rRNA processing (Planta et al., 1999). In addition, defective cell membrane synthesis in yeast during growth has also been shown to down-regulate pre-rRNA processing and RP assembly (Tsuno et al., 2000, reviewed in Leary and Huang, 2001). However, it is important to note that the mechanisms responsible for mediating such effects in response to environmental cues in mammalian cells *in vivo* remain poorly understood.

The nucleolar phosphoprotein, nucleolin has also been implicated in eukaryotic ribosomal biosynthesis regulation. For example, as well as being required for pre-rRNA processing, the protein has also been found to bind to rDNA and enhance rRNA transcription via chromatin remodelling (reviewed in Leary and Huang, 2001). Furthermore, mitogenic signals, such as v-myc avian myelocytomatosis viral oncogene homolog (MYC) (oncogene) activation, have been found to increase nucleolin and nucleophosmin (required for ribosomal nuclear export) expression (Greasley et al., 2000), and DNA damage in yeast has been reported to induce p53 stabilisation and downregulate nucleolin and fibrillarin (nucleolar protein involved in pre-rRNA processing) expression levels (Jelinsky and Samson, 1999). In addition, MYC has also been shown to activate Pol I, II and III transcription, suggesting that MYC may function as a broad regulator of ribosomal biosynthesis (Gomez-Roman et al., 2006, and reviewed in de las Heras-Rubio et al., 2014).

Importantly, the two key tumour suppressors, RB and p53 are also implicated in mammalian ribosomal biosynthesis regulation (reviewed in de las Heras-Rubio et al., 2014, Leary and Huang, 2001). Importantly, rDNA hypermethylation and histone deacetylation is associated with rDNA silencing (Chen and Pikaard, 1997). RB has been found to bind Pol I and may recruit specific histone deacetylases to rDNA repeats within the nucleolus which, in turn, may act to condense the chromatin and silence rRNA synthesis (reviewed in Leary and Huang, 2001). In addition, RB has also been found to bind UBF (rRNA transcription factor) both *in vitro* and *in vivo* and inhibit rRNA transcription by RNA Pol I (Cavanaugh et al., 1995, Voit et al., 1997). Similarly, p53 has been found to bind SL-1 (rRNA transcriptional complex) preventing interaction of the complex with UBF and suppressing rRNA transcription initiation (Zhai and Comai, 2000).

1.7.5 *The cancer ribosome*

The nucleolus is a dynamic structure that disassembles and reassembles in accordance with RNA Pol I activity and the cell cycle (Figure 1.5). Disassembly occurs early during mitosis and coincides

with the inactivation of rDNA transcription. Reassembly occurs during telophase and G1, and is triggered by the activation of rRNA transcription (reviewed in Quin et al., 2014). Given this, nucleolar number and morphology is often used to indicate the rate of ribosomal biosynthesis as an increase in nucleolar number or size is an indicator of enhanced rRNA transcription (Derenzini et al., 2000). Interestingly, this nucleoli signature has long been associated with cancer by pathologists and is thought to reflect their enhanced rate of ribosome generation required for unchecked proliferation and high translational demands (reviewed in Lam and Trinkle-Mulcahy, 2015). Importantly, a more recent study has identified an enlarged and irregular nucleoli as a poor prognostic biomarker within breast cancer (see Figure 1.8), linking abnormal nucleolar morphology and activity with a highly aggressive cancer phenotype (Derenzini et al., 2009).

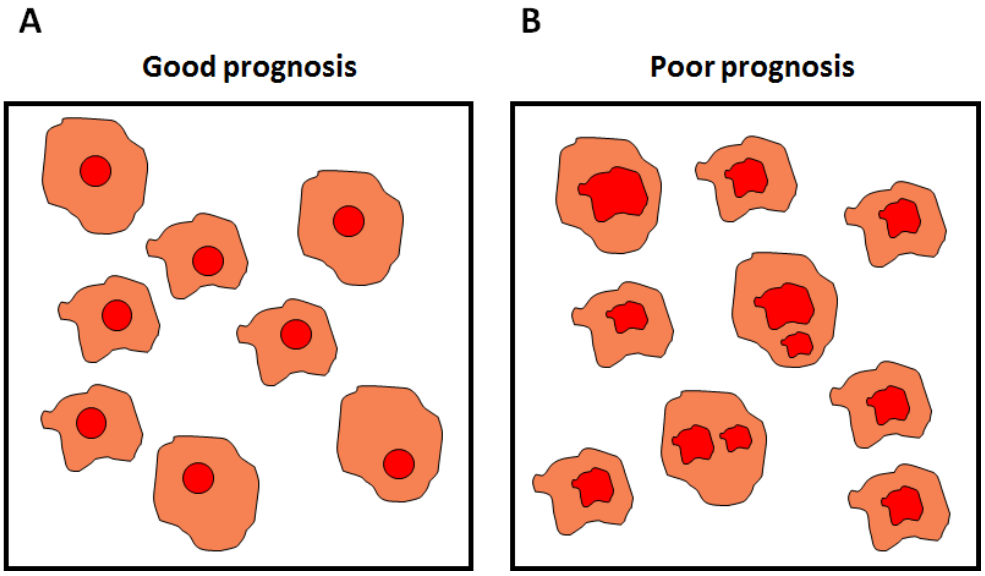

Figure 1.8: Cartoon depicting nucleoli morphology within breast cancer samples associated with either a good or poor prognosis. Cartoon images have been adapted from Derenzini et al., 2009 where breast cancer sections were silver stained to highlight the argyro-philic nucleolar organiser region proteins. **(A)** Cartoon representation of the nucleoli morphology within a breast cancer section taken from a slow growing, p53 WT, RB WT tumour, associated with a good prognosis. **(B)** Cartoon representation of the nucleoli morphology within a breast cancer section taken from a highly mitotic, p53 mutated, RB-null tumour, associated with a poor prognosis. Light red denotes the nucleus, dark red denotes the nucleoli.

As well as an altered nucleolar morphology, enhanced ribosomal biosynthesis is often associated with cancer and multiple RPs have been found to be overexpressed in a wide variety of human malignancies (reviewed in Ruggero and Pandolfi, 2003, de las Heras-Rubio et al., 2014). Further, the collection of rare diseases known as ribosomeopathies, characterised by mutations within RPs, including RPL35A, RPS10 and RPS26, are often associated with an increased cancer risk indicating that disrupted ribosomal biosynthesis may indeed drive cellular transformation (Doherty et al., 2010, Farrar et al., 2008). In addition, studies have shown that ribosomal

biosynthesis is tightly controlled by key tumour suppressor genes to ensure correct cell cycle progression (see Section 1.7.4). As such, cells harbouring deletions or inactivating mutations within these genes (commonly found in BLBC, see Section 1.8) may be highly vulnerable to enhanced ribosomal biosynthesis resulting in unchecked cell cycle progression and transformation. Similarly, constitutive activity of oncogenes, such as MYC and mitogen-activated protein kinase 1 (ERK) (commonly mutated in cancer), may also act to increase the rate of ribosomal biosynthesis and drive transformation (reviewed in de las Heras-Rubio et al., 2014).

Together, this evidence suggests that in cancer the regulatory mechanisms responsible for restricting ribosomal biogenesis are disrupted and the rate of ribosomal biosynthesis is dramatically increased in order to support enhanced proliferation (reviewed in Ruggero, 2012). It is also hypothesised that cancer ribosomes may have an altered RP composition (driven by dysregulated biosynthesis and increased expression of specific RPs) and may direct translation to favour a cancer translatome, driving malignancy (van Sluis and McStay, 2014). Consequently, targeting the cancer ribosome as a novel anti-cancer strategy is highly favourable and may yield effective cancer-specific therapeutic agents. For example, agents that specifically target RNA Pol I and inhibit rDNA transcription, such as CX-3543 and CX-5461, have been shown to be highly effective anti-cancer agents (reviewed in Quin et al., 2014). CX-3543 has been found to induce apoptosis in a panel of cancer cell lines, regardless of p53 status, and to slow tumour growth within breast (MDA-MB-231) and pancreatic cancer xenograft models (Drygin et al., 2009). A more recent Pol I inhibitor, CX-5461, is currently undergoing Phase I trials and has been found to be highly effective in a wide range of human cancers *in vitro*. Importantly, CX-5461 treatment induced senescence in melanoma and pancreatic cancer xenograft models and apoptosis (in a p53-dependent manner) in haematological malignancies *in vivo* (Drygin et al., 2011). Strikingly, these *in vivo* studies showed that CX-5461 functions in a cancer-specific manner, preferentially killing lymphoma and leukemic cells whilst causing no deleterious effects to normal B-cells (Bywater et al., 2012). Crucially, the oncogene and master regulator of ribosomal biosynthesis, MYC is often overexpressed or amplified within these haematological malignancies, resulting in an addiction to enhanced Pol I activity and elevated rDNA transcription (Bywater et al., 2012). Further, MYC-driven Eμ-MYC lymphomas are highly sensitive to CX-5461 treatment (Bywater et al., 2012). As such, it is proposed that this cancer-associated addiction to enhanced ribosomal biosynthesis may enable CX-5461 specificity and can be exploited in order to drive the selective killing of cancer cells. Together, these studies provide the first evidence in support of ribosomal targeting as an anti-cancer therapeutic strategy. Further, this data also shows that in solid

tumours, agents targeting ribosomal biosynthesis may induce senescence, suggesting that this strategy could form the basis of a novel pro-senescence therapeutic approach in cancer.

1.7.6 *Nucleolar-mediated senescence induction*

As well as cancer, the ribosomal machinery is also implicated in cell cycle regulation and senescence induction (Chen et al., 2007, Fumagalli et al., 2009). As well as being the site for ribosomal biosynthesis, the nucleolus is often described as a 'stress sensor' that acts as a critical hub integrating stress signals and co-ordinating the activation and stabilisation of p53 (reviewed in Boulon et al., 2010). Activation or stabilisation of p53 via the nucleolus often results in a halt in cell cycle progression or senescence induction together with a reduction in ribosomal biosynthesis (reviewed in Boulon et al., 2010). As such, altered nucleolar morphology (cancer hallmark) or composition may underlie a cell's ability to induce a p53-mediated cell cycle arrest and enable senescence evasion.

The nucleolus is dynamic and proteins are continually translocated to and from it and the nucleoplasm (reviewed in Quin et al., 2014). Importantly, nucleolar-associated proteins have been found to regulate p53 activity at multiple levels including translation, protein trafficking and MDM2-mediated degradation (reviewed in Boulon et al., 2010). For example, nucleolin and the large subunit RP, RPL26 have been shown to bind directly to the 5' UTR of p53 mRNA and enhance protein translation (Ofir-Rosenfeld et al., 2008). In addition, ubiquitinated p53 is trafficked into the nucleolus. If this translocation occurs in collaboration with components of the ribosome, a downregulation of ribosomal biosynthesis and a subsequent reduction in ribosomal subunit translocation into the cytoplasm may also result in nuclear p53 accumulation and cell cycle arrest (reviewed in Boulon et al., 2010).

Nucleolar-associated proteins have also been found to inhibit the interaction of p53 and the ubiquitin ligase enzyme, MDM2 in response to stress or ribosomal biosynthesis disruption (reviewed in Boulon et al., 2010). For example, the predominantly nucleolar protein, p14 is known to bind MDM2 and inhibit p53 ubiquitination (Llanos et al., 2001). Studies have shown that in response to genotoxic or oncogenic stress, translocation of nucleophosmin (nucleolar protein) to the nucleus results in an upregulation of p14 expression and p53 stabilisation (Chen et al., 2010). Further, more recent studies have shown that the translocation of key RPs, including RPL11; RPL5; RPL23; RPL26; RPL37; RPS7; RPS15; and RPS20, from the nucleolus in response to RP knockdown results in p53-dependent senescence induction (reviewed in Boulon et al., 2010). For example, a landmark paper in 2009 showed that siRNA knockdown of the small ribosomal subunit protein, RPS6 resulted in senescence induction in A549 cells (human lung

adenocarcinoma cell line, $p53^{+/+}$ p16-null) via RPL11-mediated MDM2 inhibition and p53 stabilisation (Fumagalli et al., 2009). Together, these studies indicate that the translocation of specific ribosomal components from the nucleolus may be an important mechanism for p53-mediated senescence induction in response to cellular stress. Moreover, it is proposed that the efficiency of this mechanism may be negatively correlated with transformation, and that within a highly proliferative cell RPs may function to synthesise ribosomes and may be unavailable for nuclear translocation and MDM2 stabilisation. As such, enhanced ribosomal biosynthesis within highly malignant cells may also drive senescence evasion (by disabling the nucleolar stress response pathway) as well as increasing translational capacity (reviewed in Boulon et al., 2010).

1.8 *Breast cancer and Basal-like breast cancer*

1.8.1 *Breast cancer is a collection of highly heterogeneous diseases*

The incidence of breast cancer has risen steadily since the mid-1970s and is now the most common cancer in the UK with approximately 50,000 newly diagnosed cases every year (Cancer Research UK, 2014). Improved adjuvant therapies and earlier diagnoses have dramatically improved patient outcomes within the UK, however, breast cancer remains one of the most common causes of death from cancer in women in the UK, second only to lung cancer (Cancer Research UK, 2014). Breast cancer is a collection of highly heterogeneous diseases and is commonly subcategorised upon diagnosis according to a range clinicopathological criteria including patient age, tumour size, tumour grade, lymph node invasion, hormone receptor status and, more recently, Ki67 staining (reviewed in Harbeck et al., 2014). Molecular profiling has revealed the extent of the disease heterogeneity, identifying at least seven intrinsic breast cancer subtypes including Luminal A, B and C, HER2-enriched, normal-like, Basal-like and Claudin-low/mesenchymal-like tumours (reviewed in Baird and Caldas, 2013). The first of these studies, conducted by Parker and colleagues, developed a '50-gene subtype predictor' known as the Prediction Analysis of Microarrays (PAM50) gene signature and functions as an indicator of intrinsic subtype and patient survival, independent of immunohistochemical staining (Parker et al., 2009). The PAM50 gene signature was subsequently validated within over 2,400 breast tumour samples and NanoString Technologies recently gained FDA approval for its Prosigna™ Breast Cancer Prognostic Gene Signature Assay (based on the PAM50 gene signature) for use as a prognostic indicator within post-menopausal hormone receptor-positive breast cancer (reviewed in Harbeck et al., 2014). A brief outline of each of the intrinsic breast cancer subtypes may be found below.

1.8.2 *Breast cancers may be subcategorised into seven intrinsic subtypes*

Luminal A tumours (account for approximately 40% of all breast cancers) are commonly low grade and are associated with the most favourable prognosis of all the disease subtypes. Tumours within this subtype express genes associated with the Luminal epithelial layer of the mammary gland, such as the ER and PR), and commonly have low levels of Ki67 staining and HER2 expression (reviewed in Kittaneh et al., 2013). Both Luminal A and B tumours are regarded as hormone-sensitive diseases, however, Luminal B tumours (account for approximately 20% of all breast cancers) have a higher incidence of p53 mutations (reviewed in Baird and Caldas, 2013, see Table 1.3), are often associated with a more aggressive phenotype, a greater incidence of lymph node involvement and an elevated risk of disease relapse (Sorlie et al., 2001). Luminal B tumours have varied HER2 expression levels and are associated with a reduced response to ER-targeted therapies (such as Tamoxifen) together with a poorer prognosis compared to Luminal A tumours (Sorlie et al., 2001, and reviewed in Kittaneh et al., 2013). Luminal C tumours (less commonly recognised intrinsic subtype) are less well characterised and are associated with elevated expression of a particular group of genes including transferrin receptor (CD71), nuclear protein p40 and squalene monooxygenase (SQLE) (Sorlie et al., 2001). Interestingly this gene signature is also present within Basal-like and HER2-enriched tumours and Luminal C tumours are associated with the poorest prognosis of all the Luminal subtypes (Sorlie et al., 2001, and reviewed in Kittaneh et al., 2013).

The HER2-enriched subtype (accounts for 20-30% of all breast cancers) is characterised by HER2 oncogene overexpression and tumours are often highly proliferative, contain p53 mutations (reviewed in Baird and Caldas 2013, see Table 1.3), are hormone receptor-negative and non-responsive to endocrine therapies (Perou et al., 2000, Sorlie et al., 2001). Tumours within this subgroup are commonly of a higher grade when compared with Luminal tumours and are often associated with a much poorer prognosis than Luminal tumours (Sorlie et al., 2001, and reviewed in Kittaneh et al., 2013). However, since its approval in 1998, the use of Trastuzumab (Herceptin) (a monoclonal antibody that binds and inhibits HER2) has significantly improved the prognosis of HER2-positive patients (reviewed in Figueroa-Magalhães et al., 2014). Tumours within the recently recognised Claudin-low/mesenchymal-like subgroup are characterised by an epithelial-to-mesenchymal transition gene signature (Prat et al., 2010, reviewed in Kittaneh et al., 2013). Here, tumours commonly overexpress genes associated with cellular communication, cellular matrix formation, cell differentiation, migration, angiogenesis and may express the stem cell-like signature, $CD44^{+}/CD24^{-}$. In addition, tumours are commonly hormone receptor and HER2-negative and until recently, were often categorised within the Basal-like subgroup (Prat et al.,

2010). Tumours within the normal-like subgroup may be ER-positive or negative and are often associated with an intermediate prognosis (Parker et al., 2009). Parker and colleagues estimated that approximately 10% of breast cancers may be classified as normal-like, however they suspected that this subgroup may in fact represent an artefact caused by normal tissue contaminants within the tumour specimens (Parker et al., 2009).

BLBC account for around 8-22% of all breast cancer cases depending on ethnicity and characteristically express genes associated with the normal Basal epithelial layer such as cytokeratins 5, 6, 14 and 17, laminin, fatty-acid binding protein 7 and integrin-β4 (Perou et al., 2000, reviewed in Kittaneh et al., 2013). The subtype frequently affects younger patients (below the age of 50) and tumours are often HER2, ER and PR negative (TN) therefore, targeted treatments such as Trastuzumab or Tamoxifen are not effective within this disease subtype (reviewed in Kittaneh et al., 2013). Histological assessment has shown that Basal-like tumours are commonly high grade and highly mitotic with pushing borders and a central necrotic zone and are often associated with lymphocytic infiltrates (reviewed in Badve et al., 2011). In addition, these tumours often harbour p53 mutations (reviewed in Baird and Caldas 2013, see Table 1.3), have high mRNA levels of p16 and Cyclin E1 and exhibit RB loss of heterozygosity (LOH) together with RB pathway dysregulation (Herschkowitz et al., 2008). Unlike many Luminal tumours, BLBCs do not frequently contain phosphatidylinositol-4,5-bisphosphate 3-kinase, catalytic subunit alpha (PIK3CA) or GATA binding protein 3 (GATA3) mutations and instead, are characterised by a highly heterogeneous mutational landscape (reviewed in Baird and Caldas 2013, see Table 1.3). Critically, Basal-like tumours are highly aggressive and often metastasise (usually to the lungs, liver and central nervous system, CNS) prior to diagnosis and, as a consequence, BLBC patients have a much poorer prognosis than women with any other breast cancer subtype (reviewed in Toft and Cryns, 2011). For example, approximately 46% of patients with metastatic TN BLBC will develop parenchymal CNS metastases, associated with a median survival of less than five months (Lin et al., 2008). Due to the lack of validated molecular targets in BLBC, currently, Basal-like tumours are treated with conventional chemotherapies, such as Doxorubicin (DNA-damaging anthracycline) and Paclitaxel (microtubule-stabilising taxane). However, due to their non-specific nature, these agents and are associated with widespread dose-limiting cytotoxic side effects and a poor patient outcome in BLBC (reviewed in Toft and Cryns, 2011). Consequently, the majority of women with BLBC do not achieve complete pathological response and are at significant risk of disease relapse and death within the first two to five years of diagnosis (Carey et al., 2007). More recently, inhibition of the epidermal growth factor receptor (EGFR) has been explored as a novel targeted treatment strategy in BLBC.

However, phase I and II clinical trials of EGFR inhibitors have failed to improve survival in those patients with pre-treated TN BLBC (Green et al., 2009).

	Approximate mutation frequency (%)			
Gene mutation	**Luminal A**	**Luminal B**	**HER2-enriched**	**Basal-like**
Phosphatidylinositol-4,5-bisphosphate 3-kinase, catalytic subunit alpha **(PIK3CA)**	40-45	29	39	9
Tumor protein p53 **(TP53)**	12	29	72	80
GATA binding protein 3 **(GATA3)**	14	15	2	2
Mitogen-activated protein kinase kinase kinase 1, E3 ubiquitin protein ligase **(MAP3K1)**	13	5	4	0
Lysine (K)-specific methyltransferase 2C **(KMT2C)**	8	6	7	5
Cadherin 1, type 1 **(CDH1)**	9-10	5	5	0

Table 1.3: A summary of the most frequently mutated genes within the four most commonly recognised intrinsic breast cancer subtypes. Adapted from Baird and Caldas, 2013.

1.8.3 *p16-positive BLBC is associated with a poor prognosis*

More recent genetic profiling has highlighted the level of heterogeneity within the intrinsic subtypes commonly used to sub-classify breast cancer. For example, the Cancer Genome Atlas Network (TCGA) (analysis of tumour and germline DNA and RNA from 825 primary breast cancers) confirmed the existence of four broad breast cancer subtypes, concluding that there was considerable heterogeneity within rather than across these molecular subtypes (Koboldt et al., 2012). In addition, Curtis et al., 2012 applied an unbiased approach for the stratification of approximately 2,000 matched breast tumour samples and identified ten novel molecular subtypes (labelled IntClust 1-10), each associated with a distinct clinical outcome. This analysis dissected many of the PAM50 intrinsic subtypes and may prove to be far more effective at guiding personalised therapies and predicting prognosis than current stratification methods. Interestingly, the vast majority of Basal-like tumours were sub-classified within IntClust 10. Tumours within this cluster were associated with the poorest prognosis within the first two to five years post-diagnosis and, interestingly, IntClust 10 tumours were also associated with the highest level of p16 mRNA expression (Curtis et al., 2012). Importantly, this analysis revealed that those tumours with a Basal-like phenotype together with an elevated p16 expression signature (p16-positive BLBC) are associated with the very poorest prognosis and represent the

most clinically challenging breast cancer subtype. Further stratification of this disease subset together with the identification of novel therapeutic targets and cancer-specific targeted therapies may revolutionise the treatment of p16-positive BLBC and dramatically improve patient outcomes.

1.9 *Small interfering RNA (siRNA) technology*

RNA interference (RNAi) is a post-transcriptional silencing mechanism (see Figure 1.9) and was first discovered in 1998 following studies investigating cellular responses to double stranded RNA in *Caenorhabditis elegans* (*C. elegans*) (Fire et al., 1998). Initially, synthetic siRNAs were used to perform small-scale, loss-of-function studies investigating individual gene function. However, following the construction of global siRNA libraries, genome-wide loss-of-function screening has revolutionised functional genomics, and has proven to be an extremely powerful tool in the dissection of biological processes and identification of therapeutic targets in complex disease (reviewed in Boutros and Ahringer, 2008).

Despite its widespread success, siRNA technology has a number of limitations that must be considered. Arguably the biggest consideration when performing siRNA-knockdown is the specificity of synthetic siRNAs and the potential for off-target effects (OTEs). As well as silencing the gene of interest, synthetic siRNAs can induce degradation of additional mRNA transcripts with partial sequence homology and transfection reagents may cause non-specific gene expression changes (OTEs) (reviewed in Pan et al., 2012). Therefore, it is vital that sufficient validation steps are taken to ensure that quantified phenotypic changes are due to the knockdown of the gene of interest and not a consequence of OTEs. siRNA pools (three to four siRNAs with different RNA sequences targeting a single mRNA transcript) are frequently used as they can increase the knockdown efficiency and reduce the time and costs associated with conducting large screening experiments (reviewed in Falschlehner et al., 2010). In addition, this approach is likely to reduce OTEs and identify potent siRNAs with high transfection efficiencies as each siRNA is used at a relatively low concentration (reviewed in Falschlehner et al., 2010). However, deconstructing siRNA pools and transfecting cells with each siRNA individually is a more effective method of controlling for OTEs (reviewed in Falschlehner et al., 2010). If at least two siRNAs from a given pool induce similar phenotypic changes, the likelihood that the changes are a result of an OTE is reduced. Repeating a screen with a second siRNA library purchased from an alternative supplier will also help to control for OTEs (reviewed in Boutros and Ahringer, 2008). It is important that the two libraries are generated using separate algorithms and that the siRNAs they contain are sufficiently different from each other. In addition, multiparameter

analysis may also help to control for OTEs. Increasing the number of parameters used to identify a particular phenotype (such as senescence) will minimise the risk of the quantified phenotype being due to non-specific knockdown.

It is important to note that siRNA-knockdown cannot be used to investigate the function of every gene. For example, genes which encode proteins with long half-lives are very difficult to target using this technique. Furthermore, siRNA-knockdown has a non-heritable, transient effect that may not be appropriate if the resulting phenotype requires a long time to present itself. In addition, siRNA-knockdown is purely a loss-of-function technique. Consequently, a siRNA screen will not identify genes that may induce phenotypic changes upon overexpression. Also, complete gene knockdown is almost impossible to achieve. The level of knockdown depends upon the potency of the siRNA sequence and the transfection conditions. Variability in gene knockdown between experimental repeats is common and reduces the reproducibility of siRNA-knockdown experiments (reviewed in Boutros and Ahringer, 2008), however, adequate optimisation steps are often effective at combatting this issue.

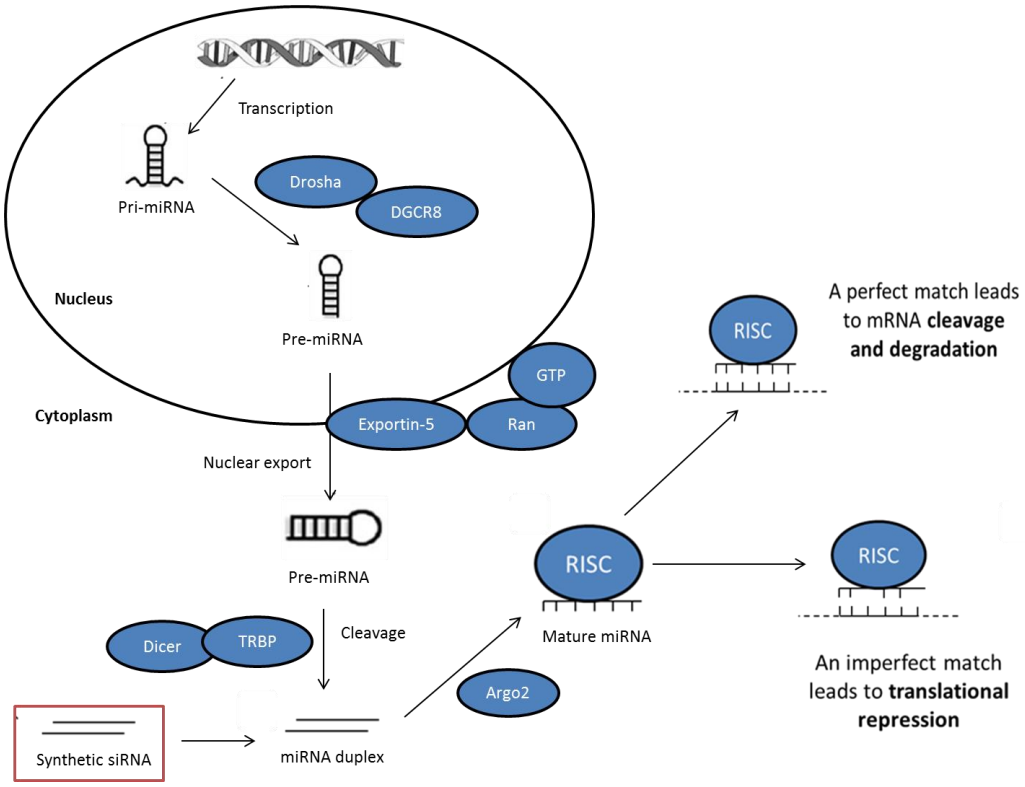

Figure 1.9: A cartoon summarising the RNAi pathway. Endogenous miRNAs are first processed by Drosha (nuclease) to form a pre-miRNA molecule. Once transported to the cytoplasm, the pre-miRNA is processed further by Dicer (ribonuclease enzyme) and is incorporated into the RNA-induced silencing complex (RISC). Synthetic siRNAs mimic endogenous dicer-processed miRNA at this stage. The RNA is unwound and guides the RISC to homologous mRNA substrates. (Adapted from Falschlenhner et al., 2010).

Adopting a high-throughput approach to siRNA screening improves cost effectiveness and increases the number of gene candidates that can be feasibly tested, increasing the chances of pathway dissection and target identification. However, there are many challenges associated with this approach that must be considered. A high-throughput siRNA screen must have a clear objective and sufficient time must be invested in screen optimisation to ensure robustness and reproducibility (reviewed in Boutros and Ahringer, 2008). Large high-throughput siRNA screens are often fraught with false negative and false positive results. For example, sub-optimal transfection conditions and non-functional siRNAs may increase the number of false negative results within a large screen. This number may be reduced by including experimental repeats within a single screen and by repeating the siRNA knockdown with a sub-set of hits using an alternative transfection reagent, if possible (reviewed in Falschlehner et al., 2010). In addition, smaller-scale experiments, such as testing for additional markers of senescence induction, using a sub-set of siRNAs will also help to eliminate false positives. Real-Time Quantitative Reverse Transcription PCR (qRT-PCR) and immunoblotting are key post-siRNA screen validation steps and RNAi rescue experiments may also help to validate a list of the most effective hits.

1.10 *Project aims: pro-senescence therapy in p16-positive BLBC*

The overall aim of this project is to identify genes essential for maintaining senescence evasion in p16-positive cancer ('senescence evaders') with a view to identifying novel therapeutic targets and potential prognostic biomarkers in p16-positive BLBC.

Previously, a genome-wide siRNA screen was performed in HeLa cells (p16-positive cervical cancer cell line, unpublished). A total of 22,010 genes were targeted by pools of three siRNAs and the data generated was compared to a previously published screen in HMECs (Bishop et al., 2010). A significant reduction in cell number, together with a significant increase in cell area was used to define senescence activation. Using these phenotypic criteria, the screen revealed 86 siRNAs that activated senescence in HeLa cells but had no effect on the proliferation or morphology of HMECs (data not published). This project will first aim to re-test these 86 previously identified siRNAs in the HeLa cell line. Second, the most potent activators of senescence (in HeLa cells) will be tested in a p16-positive BLBC cell line (MDA-MB-468 cells) and senescence evaders in these cells will be identified.

Once validated, the proteins implicated have the potential to serve as novel therapeutic targets in p16-positive BLBC and may provide further insight into the mechanisms that regulate senescence evasion in p16-positive cancer.

Chapter 2

Materials and Methods

2.1 *Mammalian Cell culture*

Unless otherwise stated, all reagents and compounds used were purchased from Sigma, UK.

Cells were cultured as monolayers in T75 cm^2 vented flasks (Corning, UK) at 37^oC in the presence of 5% carbon dioxide (CO_2) and 95% relative humidity and were passaged once every 7 days. In order to passage the cells, medium was removed and adherent cells were washed with 15 mL phosphate-buffered saline (PBS) and treated with 3 mL 1X trypsin-ethylenediaminetetraacetic acid (EDTA) (Life Technologies, UK) for 5-8 minutes (mins) at 37^oC. In order to neutralise the trypsin, 15 millilitres (mL) medium with supplements was added and a cell pellet was formed by centrifugation at 1,200 revolutions per minute (rpm) for 5 mins (IEC CL10 centrifuge, Thermo Scientific, UK). The cell pellet was then re-suspended in an appropriate volume of medium with supplements and cells were counted using the Chemometec Nucleocounter System (Sartorius, UK) according to the manufacturer's protocol. Medium was changed every 2-3 days.

2.1.1 *Culture of mammalian cancer cell lines*

MDA-MB-468 cells (ATCC® HTB-132™) (p16-positive human BLBC cell line, derived from a metastatic plural effusion) and MDA-MB-231 cells (ATCC® HTB-26™) (p16-null human BLBC cell line, derived from a metastatic plural effusion) were purchased from ATCC, (USA) while HeLa cells (human cervical cancer cell line) were purchased from CRUK, (UK). MDA-MB-468 and MDA-MB-231 cells were seeded at 10,000 cells/cm^2 and 2,500 cells/cm^2, respectively and were maintained in Dulbecco's Modified Eagles Medium (DMEM) supplemented with 10% volume/volume (v/v) foetal bovine serum (FBS) (Biosera, UK), L-Glutamine (2 mM final concentration) (Life Technologies, UK) and Sodium Pyruvate (1 mM final concentration). HeLa cells were seeded at 3,000 cells/cm^2 and maintained in DMEM supplemented with 5% (v/v) FBS and L-Glutamine (2 mM final concentration).

2.1.2 *Culture of normal human mammary epithelial cells*

Normal HMECs were isolated from reduction mammoplasty tissue and kindly provided by Dr. Martha Stampfer (Lawrence Berkeley National Laboratory, Berkeley, CA, USA). Cells were seeded at 5,000 cells/cm^2 and were maintained in 'M87A' medium composed of 50% (v/v) Mammary Epithelial Basal Medium (MEBM, Lonza, UK) supplemented with MEGM SingleQuot Kit Supplements (excluding gentamycin) (Lonza, UK), 5 micrograms (µg)/mL transferrin, 5 micromolar (µM) isoproterenol and 2 millimolar (mM) L-glutamine, together with 50% (v/v) DMEM Nutrient Mixture F-12 (DMEM/F12) (Life Technologies, UK) supplemented with 10 µg/mL insulin, 5% (v/v) FBS, 100 nanograms (ng)/mL hydrocortisone, 10 nanomolar (nM) 3,3',5-

triiodo-L-thyronine, 10 nM β-estradiol, 5 ng/mL epidermal growth factor (Life Technologies, UK), 0.1% (v/v) AlbuMAXTM I (Life Technolgies, UK) and 0.1 nM oxytocin (Bachem, Switzerland). Cells were cultured from passage 4 (P4) to passage 6 (P6) as described above and siRNA reverse transfections were performed with cells at P6 (see Section 2.3.4).

2.2 *siRNA reverse-transfection optimisation*

Before conducting the siRNA screens, the cell seeding density and volume of HiPerFect Transfection Reagent (HiPerFect, QIAGEN, UK) used to transfect each of the cancer cell lines was optimised in order to produce a high level of transfection efficiency with minimal toxicity.

2.2.1 *Optimisation of cell seeding density in 384-well plate format*

Cells were seeded at range of concentrations in 384-well plate format (Thermo Scientific Nunc, UK) and were incubated at 37°C. Medium was changed after 46 hours (hr) and cells were fixed and stained 72 hr later with 4',6-diamidino-2-phenylindole (DAPI) according to Section 2.4. Cells were then imaged and quantified according to Section 2.5. HeLa cells were seeded at 7,500-15,000 cells/cm^2, MDA-MB-468 cells were seeded at 10,000–36,000 cells/cm^2 and MDA-MB-231 cells were seeded at 4,000–12,000 cells/cm^2 for transfection optimisation.

2.2.2 *Optimisation of transfection reagent dose*

After completion of a cell seeding density test, cells were reverse transfected with 30 nM control siRNAs targeting glyceraldehyde-3-phosphate dehydrogenase (GAPDH) (Ambion, UK) (negative control) or PLK1 (Dharmacon, UK) (Killer control) in 384-well plate format using a range of HiPerFect concentrations. siRNA target sequences are shown in Table 2.1. siRNA/HiPerFect complexes were incubated at room temperature (RT) for 1.5 hr before cells were seeded. Plates were incubated at 37°C and medium was changed after 46 hr. Cells were fixed and stained 72 hr later with DAPI and were subsequently imaged and quantified according to Sections 2.4 and 2.5. HeLa cells were seeded at either 10,000 or 12,000 cells/cm^2 and treated with 0.15 or 0.2 µL/well HiPerFect. MDA-MB-468 cells were seeded at 33,000 cells/cm^2 and were treated with 0.1-0.4 µL/well HiPerFect. MDA-MB-231 cells were seeded at 8,000 cells/cm^2 and were treated with 0.1-0.5 µL/well (including 0.025, 0.05 or 0.075 µL/well) HiPerFect.

siRNA name	siRNA target	Accession Number	Supplier	siRNA target sequence (5'-3')
GAPDH	GAPDH	NM_002046.4	Ambion, UK	GUGGAUAUUGUUGCCAUCAtt
p16	Cyclin-dependent kinase inhibitor 2A (CDKN2A) (p16)	NM_000077	QIAGEN, UK	TACCGTAAATGTCCATTTATA
p21	cyclin-dependent kinase inhibitor 1A (CDKN1A) (p21)	NM_078467 NM_000389 NM_001220778 NM_001220777 NM_001291549	GE, UK	CTACCTTGAAGCTGAAACA CGCTACCTTGAAGCTGAAA GCTACCTTGAAGCTGAAAC GCTGACACTACGCGATTAC
PLK1	PLK1	NM_005030	Dharmacon, UK	Proprietary pool
CBX7	Chromobox homolog 7 (CBX7)	NM_175709	Ambion, UK	GGGTAACACACACCAAGAGT
siGLO	Cyclophilin B (PPIB)	NM_000942	Dharmacon, UK	GAGCCCAGAUCAACCUUUA

Table 2.1: siRNA target sequences for control siRNAs.

2.3 *siRNA reverse transfections*

2.3.1 *siRNA screening in HeLa and MDA-MB-468 cells in 384-well plate format*

Pools of three siRNAs (Ambion, UK) (at a 1:1:1 ratio, final concentration 30 nM) were used to target each gene within the screens together with control siRNAs targeting GAPDH, PLK1, Cyclin-dependent kinase inhibitor 2A (CDKN2A) (p16) (QIAGEN, UK) or (CBX7) (Ambion, UK). Target sequences for control siRNAs are displayed in Table 2.1. HeLa cells were seeded at 12,000 cells/cm^2 and reverse transfected with 30 nM siRNA in 384-well plate format using 0.15 µL/well HiPerFect. MDA-MB-468 cells were seeded at 33,000 cells/cm^2 and reverse transfected with 30 nM siRNA in 384-well plate format using 0.2 µL/well HiPerFect. siRNA/HiPerFect complexes were incubated at RT for 1.5 hr before cells were seeded. Plates were incubated at 37^{o}C and medium changed after 46 hr. Unless otherwise stated, cells were fixed and stained 72 hr later with mouse anti-p16 JC2 (Prof. James Koh, Duke Cancer Institute), goat Alexa Fluor-488 conjugated anti-

mouse (Life Technologies, UK), DAPI and Cell Mask (Invitrogen, UK) according to Section 2.4. Cells were then imaged and quantified according to Section 2.5. Two independent screens were performed using each cell type and each screen was performed in triplicate. Significant hits were identified according to Section 2.5.2.

2.3.2 *Phenotypic validation of each of the top six RP hits in MDA-MB-468 cells*

Unless otherwise stated, MDA-MB-468 cells were reverse transfected with a pool of three siRNAs (Ambion, UK) (each used within the siRNA screens. at a 1:1:1 ratio, final concentration 30 nM) together with three individual siRNAs (Ambion, UK) (each at 30 nM) targeting each of the top ribosomal hits according to Section 2.3.1. Control siRNAs (30 nM final concentration) targeting GAPDH, p16, CBX7 and PLK1 were also used. siRNA target sequences for each of the ribosomal siRNAs are listed in Table 2.2.

siRNA name (siRNA ID)	siRNA target	Accession Number	siRNA target sequence (5'-3')
RPL14_1 (137435)	RPL14	NM_001034996.2 & NM_003973.4	CCUUGCACUCAAGUGAGGAtt
RPL14_2 (13949)	RPL14	NM_001034996.2 & NM_003973.4	GGAAAGCCAAGAUGACAGAtt
RPL14_3 (13857)	RPL14	NM_001034996.2 & NM_003973.4	GGCAGACAUCAAUACAAAAtt
RPL18_1 (217192)	RPL18	NM_000979.3 & NM_001270490.1	CCCUGGAUCCUACUCUCUUtt
RPL18_2 (142176)	RPL18	NM_000979.3 & NM_001270490.1	GCCGAGGCUACAAAAACUAtt
RPL18_3 (9171)	RPL18	NM_000979.3	GGCUGUUGGUCAAGUUAUAtt
RPL34_1 (9365)	RPL34	NM_000995.3 & NM_033625.2	GGAGCUCUGAUAUAUAUCUtt
RPL34_2 (142194)	RPL34	NM_000995.3 & NM_033625.2	GGUUAAAUACUACCAGCACtt
RPL34_3 (9278)	RPL34	NM_000995.3 & NM_033625.2	GGCACAAGCACAGAGUCAGtt
RPL35A_1 (45958)	RPL35A	NM_000996.2	GCACACAGCUCUUCUUAAAtt
RPL35A_2 (9187)	RPL35A	NM_000996.2	GGGAGCACACAGCUCUUCUtt
RPL35A_3 (9279)	RPL35A	NM_000996.2	GGUGUUUACGCCCGAGAUGtt
RPS3A_1 (142201)	RPS3A	NM_001006.4	CGAGACAGGUGCUAAAGUUtt
RPS3A_2 (142200)	RPS3A	NM_001006.4	GCUCAUGGAGCUUCAUGGUtt
RPS3A_3 (142199)	RPS3A	NM_001006.4 & NM_001267699.1	GCACCUGCUAUGUUCAAUAtt
RPS7_1 (142206)	RPS7	NM_001011.3	GCAUGUCGUCUUUAUCGCUtt
RPS7_2 (142207)	RPS7	NM_001011.3	CGGGCAAGGAUGUUAAUUUtt

RPS7_3 (45963)	RPS7	NM_001011.3	GAUGAACUCGGACCUCAAGtt
PGD_1 (11865)	Phosphogluconate dehydrogenase (PGD)	NM_002631.2	ACCCACCACUUUGGUUCCCtt
PGD_2 (112952)	PGD	NM_002631.2	UUUCAUCAGUGGUAUGCCtc
PGD_3 (11961)	PGD	NM_002631.2	CACUUUGGUUCCCUUUGCCtc

Table 2.2: siRNA target sequences used to target the top senescence evaders identified within the siRNA screens. All siRNAs were purchased from Ambion, UK.

2.3.3 *siRNA reverse transfection of MDA-MB-231 cells in 384-well plate format*

Unless otherwise stated, MDA-MB-231 cells were seeded at 8,000 cells/cm^2 in 384-well plate format and were reverse transfected with 30 nM siRNA using 0.075 µL/well HiPerFect. Control siRNAs (30 nM final concentration) targeting GAPDH, CBX7 and PLK1 were also used. siRNA/HiPerFect complexes were incubated at RT for 1.5 hr before cells were seeded. Plates were incubated at 37^{o}C and medium changed after 46 hr. Cells were fixed and stained 72 hr later with DAPI and Cell Mask according to Section 2.4. Cells were then imaged and quantified according to Section 2.5.

2.3.4 *siRNA reverse transfection in HMECs in 384-well plate format*

HMECs at P6 were seeded at 5,000 cells/cm^2 in 384-well plate format and were reverse transfected with 30 nM siRNA using 0.2 µL/well HiPerFect. Control siRNAs included siGLO (targeting PPIB), p16 and CBX7 siRNA (30 nM final concentration). siRNA/HiPerFect complexes were incubated at RT for 1.5 hr before cells were seeded. Plates were incubated at 37^{o}C and medium changed after 46 hr. Cells were fixed and stained 72 hr later with mouse anti-p16 JC2, goat Alexa Fluor-488 conjugated anti-mouse, DAPI and Cell Mask according to Section 2.4. Cells were then imaged and quantified according to Section 2.5.

2.3.5 *siRNA reverse transfection of MDA-MB-468 cells in 6-well plate format*

MDA-MB-468 cells were seeded at 7,500 cells/cm^2 in 6-well plate format (Corning, UK) and were reverse transfected with 30 nM siRNA using 6.9 µL/well HiPerFect. Before adding the siRNA/HiPerFect solution to the plate, each well was washed with 1 mL DMEM with supplements. siRNA/HiPerFect complexes were incubated at RT for 2 hr before cells were

seeded. Cells were harvested for western blotting or RNA extraction according to Sections 2.6 and 2.7.

2.4 *Immunofluorescence staining*

Cells cultured on 384-well plates were washed with PBS and fixed using 3.7% weight/volume (w/v) paraformaldehyde with 5% (w/v) sucrose in PBS for 15 mins at RT. Cells were then washed with PBS and permeabilised with 0.1% (v/v) Triton-X100 for 15 mins at RT. When staining for NCL, cells were permeabilised with 0.1% (v/v) Triton-X100 for 30 mins at RT. Cells were washed with PBS and blocked with PBS supplemented with 0.25% (w/v) Bovine serum albumin (PBS/BSA) for 30 mins before incubation with primary antibody for 2 hr at RT. Cells were incubated with anti-NCL or anti-p21 antibodies overnight at RT. Cells were then washed with PBS/BSA for 30 mins at RT and incubated with secondary antibody, DAPI (1:1,000) and Cell Mask Deep Red (1:20,000 for MDA-MB-468 and MDA-MB-231 cells and 1:10,000 for HMECs) for 2 hr at RT. Cells were washed with PBS/BSA for 30 mins at RT before three final washes with PBS. Cells were then imaged and quantified according to Section 2.5. Details of the antibodies used for immunofluorescence staining and their working dilutions are shown in Table 2.3.

Antibody	Species	Supplier	Working dilution	Conditions
Anti-p16 JC2	Mouse	Prof. James Koh , Duke Cancer Institute, UK	1:1,000	2 hr at RT
Anti-p53	Rabbit	Cell Signalling, USA	1:250	2 hr at RT
Anti-p21	Rabbit	Cell Signalling, USA	1:250	Overnight at RT
Anti-53BP1	Rabbit	Bethyl, USA	1:200	2 hr at RT
Anti-nucleolin	Rabbit	Santa Cruz Biotechnology, USA	1:1,000	Overnight at RT
Alexa Fluor-488 conjugated anti-mouse	Goat	Life Technologies, UK	1:500	2 hr at RT
Alexa Fluor-546 conjugated anti-rabbit	Donkey	Life Technologies, UK	1:500	2 hr at RT
Alexa Fluor-488 conjugated anti-rabbit	Donkey	Life Technologies, UK	1:500	2 hr at RT
Alexa Fluor-546 conjugated anti-mouse	Goat	Life Technologies, UK	1:500	2 hr at RT

Table 2.3: Antibodies used for immunofluorescence staining, their working concentrations and incubation conditions. All antibodies were diluted in 0.25% (w/v) PBS/BSA with the exception of anti-nucleolin which was diluted in PBS supplemented with 1% (w/v) BSA.

2.5 *High content image analysis*

2.5.1 *High content microscopy*

Cells were seeded in 384-well plate format and were fixed and stained according to Section 2.4. Cells were then imaged using the IN Cell 1000 automated microscope (GE, UK) at 10X magnification (nine fields/well) using a triChroic mirror (61003bs*), unless otherwise stated. All excitation and emission filters were from GE, UK. DAPI staining was visualised using a D360_40X excitation filter and a HQ535_50M emission filter (blue), Alexa Fluor-488 staining was visualised using a S475_20X excitation filter and a HQ535_50M emission filter (green), Alexa Fluor-546 staining was visualised using the HQ535_50X excitation filter together with the HQ620_60M emission filter (red) and Cell Mask staining was visualised using a HQ620_60X excitation filter and a HQ700_75M emission filter (far red). Four colours were visualised using the polyChroic

mirror (88100bs*). Image quantitation was then performed using the IN Cell 1000 Developer software version 1.8 (GE, UK).

2.5.2 *Z score generation and hit identification*

Multiparameter analysis was performed using the IN Cell 1000 Developer software version 1.8 and a list of the measures used are displayed in Table 2.4.

Name of parameter (used within heatmaps)	**Name of the IN Cell 1000 Developer software measure**	**Description**
Number	Count	Total number of targets
Area	Area	Target area (μm^2)
Roundness	Form Factor	Target circularity (expressed as a value from 0–1, 1 equals a perfect circle)
Elongation	Major/Minor axis ratio	Major axis length (the longest of two perpendicular axes of symmetry)/Minor axis length (the shortest of two perpendicular axes of symmetry)
Protrusions	End nodes	Total number of end points in a single target
Protein density	Mass/Area	Mass (sum of all pixel values in a target)/target area (μm^2)
Protein Intensity	Dens Levels	Mean grey level of the pixels contained within a target (expressed as a value from 0–4,095 where 0 equals black and 4,095 equals white)

Table 2.4: **A description of each of the parameters used within the multiparameter analysis.** Measures were obtained using the IN Cell 1000 Developer software version 1.8.

Unless otherwise stated, Z scores were generated according to the formula below:

Z score = (mean value of two independent experiments for experimental siRNA **–** mean value (of two independent experiments) for GAPDH siRNA)**/**Standard deviation (SD) for GAPDH siRNA of two independent experiments.

For each of the parameters analysed, significance was defined as three Z scores away from the GAPDH siRNA mean and senescence activation was defined as a significant decrease in cell

number together with a significant increase in cell area. This senescence criteria was used for hit identification within the siRNA screens. Importantly, within the siRNA screens each of the technical repeats across two independent experiments were combined, and mean values and standard deviations were subsequently calculated. This method generated a highly stringent significance threshold, ensuring only the strongest hits were identified.

2.6 *Sodium dodecyl sulphate polyacrylamide gel electrophoresis (SDS-PAGE) and western blotting*

2.6.1 *SDS-PAGE*

Adherent cells were first washed with PBS before being lysed using RIPA buffer supplemented with 4% (w/v) protease cocktail inhibitor (Roche, UK) at 4^{o}C for 5 mins. Cell lysates were stored long-term at -20^{o}C. Protein concentration of the cell lysates was determined using the Bio-Rad Protein Assay kit (Bio-Rad, UK) according to the manufacturer's protocol and an appropriate volume of 2X Laemmli Sample Buffer (0.1 M Tris pH 6.8, 20% (v/v) glycerol, 1% (v/v) β-mercaptoethanol, 1% (w/v) sodium dodecyl sulphate (SDS), 0.01% (v/v) Bromophenol blue) was added. Samples were then heated to 95^{o}C for 5 mins and centrifuged using a bench top centrifuge (Accuspin micro, Fisher Scientific, UK) at 13,000 rpm for 5 mins before being loaded into the stacking gel (5 µg protein per lane). The compositions of the resolving and stacking gels used are shown in Table 2.5. Protein separation was achieved using the Bio-Rad Mini-PROTEAN III system (Bio-Rad, UK) in running buffer (25 mM Tris (Fisher Scientific, UK), 192 mM Glycine, 0.1% (w/v) SDS) at 100 V for 1-2 hr. The Precision Plus Protein all blue standards protein ladder (Bio-Rad, UK) was loaded alongside the samples to indicate protein size.

	5% Stacking gel	12% Resolving gel
Acrylamide (30%)/Bis Acrylamide (0.8%) solution (National Diagnostics, UK)	1.67 mL	4.15 mL
1 M Tris pH 8.8	-	3.7 mL
1 M Tris pH 6.8	1.25 mL	-
20% (w/v) SDS	50 µL	50 µL
20% (w/v) Amps	50 µL	60 µL
Temed (Severn Biotech Ltd, UK)	10 µL	10 µL
dH_2O	7.03 mL	2.05 mL

Table 2.5: Composition of the polyacrylamide gels required for gel electrophoresis.

2.6.2 *Immunoblot analysis*

Proteins were transferred onto Hybond Enhanced-Chemiluminescence (ECL) nitrocellulose membrane (GE, UK) using the western transfer Mini-PROTEAN 3 system (Bio-Rad, UK) in transfer buffer (25 mM Tris, 192 mM Glycine, 20% (v/v) methanol (Fisher Chemical, UK)) at RT for 2 hr at 350 milliamps (mA). The membrane was then blocked in 0.05% (v/v) Tween-20, 5% (w/v) Marvel semi-skimmed milk in PBS (PBS-T-M) for 1 hr at RT. The membrane was then incubated with primary antibody diluted in 0.05% (v/v) Tween-20 in PBS (PBS-T). The membrane was then washed (3X 10 mins) in PBS-T before incubation with an appropriate secondary antibody conjugated to horseradish peroxidase. Details of the antibodies used, their incubation conditions and working dilutions are shown in Table 2.6. The membrane was then washed (3X 10 mins) in PBS-T and bands were visualised using ECL (GE, UK) according to the manufacturer's protocol.

Antibody	Species	Supplier	Working dilution	Conditions
Anti-p16 JC2	Mouse	Prof. James Koh , Duke Cancer Institute, UK	1:5,000	2 hr at RT
Anti-p53	Rabbit	Cell Signalling, USA	1:1,000	Overnight at 4°C
Anti-p21 (C-terminus)	Rabbit	Cell Signalling, USA	1:1,000	Overnight at 4°C
Anti-p21 [CP74] (N-terminus)	Mouse	Abcam, USA	1:500	Overnight at 4°C
Anti-GAPDH	Rabbit	Abcam, UK	1:5,000	Overnight at 4°C
Anti-β tubulin	Mouse	EnoGene, UK	1:20,000	Overnight at 4°C
Anti-cyclophilin B	Rabbit	Abcam, UK	1:1,000	Overnight at 4°C
Anti-RPS3A	Rabbit	Abcam, UK	1:5,000	Overnight at 4°C
Anti-RPS7	Mouse	Abcam, UK	1:500	Overnight at 4°C
Anti-PGD	Rabbit	Abcam, UK	1:1,000	Overnight at 4°C
HRP-conjugated anti-mouse	Goat	Dako, UK	1:5,000	1 hr at RT
HRP-conjugated anti-rabbit	Goat	Invitrogen, UK	1:5,000	1 hr at RT

Table 2.6: Antibodies used for immunoblotting, their working dilutions and conditions. All antibodies were diluted in PBS-T.

2.6.3 *Densitometry*

Protein quantification was performed using Image J software. Density levels were obtained and normalised against an appropriate loading control in order to calculate total protein levels. Protein levels were then normalised to the GAPDH siRNA control and presented as a bar chart +SD of two independent experiments.

2.6.4 *Membrane stripping*

Membranes were stripped for 30 mins at RT in 25 mL stripping buffer (25 mM Glycine with 1% (w/v) SDS) and washed twice for 10 mins with PBS-T at RT before being blocked for 1 hr at RT in PBS-T-M and re-probed with additional antibodies.

2.7 *RNA extraction, cDNA conversion and qRT-PCR*

2.7.1 *RNA extraction and spectrophotometric analysis*

Adherent cells were first washed with PBS before being lysed with 42 µL/cm^2 Qiazol lysis reagent (QIAGEN, UK) for 5 mins at RT. Cell lysates were subsequently 'snap frozen' on dry ice for 5 mins before being stored overnight at -80^{o}C. Cell lysates were then defrosted, homogenised (by pipetting up and down 5X) and transferred to a pre-prepared MaXtract High Density Phase Lock tube (phase lock tube) (QIAGEN, UK). Prior to their use, phase lock tubes were centrifuged using a bench top centrifuge at 13,000 rpm at RT for 2 mins. In order to achieve adequate phase separation, chloroform (200 µL/1 mL Qiazol lysis reagent) was added and the tubes were inverted for 20 seconds (sec). The tubes were then centrifuged using a bench top centrifuge at 13,000 rpm at 4^{o}C for 15 mins. After centrifugation, the aqueous phase was transferred to a RNeasy Mini Spin Column (QIAGEN, UK) and RNA extraction was performed using the miRNeasy Mini Kit (QIAGEN, UK) according to the manufacturer's protocol. RNA was eluted in 30 µL RNase-free water (Invitrogen) and the RNA concentration and purity were determined by spectrophotometric analysis using the Nanodrop ND-1000 before storage at -80^{o}C. Absorbance was analysed at 230 nm (A_{230}), 260 nm (A_{260}) and 280 nm (A_{280}) and the A_{260}/A_{230} and A_{260}/A_{280} ratios were calculated. Pure RNA will have a A_{260}/A_{230} ratio of 2-2.2 and a A_{260}/A_{280} ratio of ~2. RNA precipitation was performed on RNA samples that did not meet this criteria before downstream applications were carried out.

2.7.2 *Ethanol RNA precipitation*

Following spectrophotometric analysis, 3 µL NaOAc, 75 µL 100% (v/v) ethanol (EtOH) and 1 µL glycogen (GlycoBlue) (ThermoFisher Scientific, USA) was added to 30 µL RNA sample in a 1.5 mL Eppendorf microcentrifuge tube (Eppendorf, UK) and incubated overnight at -20^{o}C. RNA was pelleted by centrifugation using a bench top centrifuge at 13,000 rpm at 4^{o}C for 20 mins and the supernatant was removed carefully. 500 µL of 80% (v/v) EtOH was added to the tube and the RNA was pelleted a second time via centrifugation using a bench top centrifuge at 13,000 rpm at 4^{o}C for 10 mins. This step was repeated before the tube was centrifuged for a further 1 min at 4^{o}C using a bench top centrifuge at 13,000 rpm. Once all of the EtOH had been carefully removed, the pellet was left to air dry for 10 mins at RT. The RNA pellet was then re-suspended in 30 µL RNase-free water and spectrophotometric analysis was performed according to Section 2.7.1.

2.7.3 *Reverse transcription of mRNA to cDNA*

1 µL OligodT^{18} (MERK, Millipore, UK) (50 µM) and 1 µL deoxynucleotides (dNTPs) (10 mM each) (ThermoFisher, USA) were combined with 1 µg RNA and topped up with RNase-free water to reach a total of 13 µL before being incubated at 65^{o}C for 5 mins. The mixture was then incubated on ice for a further 5 mins. 4 µL 5X first strand buffer (Invitrogen, UK) 1 µL dithiothreitol (DTT) (0.1 M) (Invitrogen, UK), 1 µL RNase OUT ribonuclease Inhibitor (40 U/µL) (Invitrogen, UK) together with 1 µL Superscript III Reverse Transcriptase (200 U/µL) (Invitrogen, UK) was added to form a 20 µL total reaction volume. The reverse transcription reaction was then performed using the PeQSTAR thermal cycler (PeQlab, UK) according to Table 2.7. Newly generated cDNA was stored long-term at -20^{o}C.

Time	Temperature
45 mins	50^{o}C
15 mins	70^{o}C

Table 2.7: Reverse transcription reaction conditions.

2.7.4 *qRT-PCR*

qRT-PCR was performed using SYBR Green PCR Master Mix (Applied Biosystems, UK) on a 7500 Fast System RealTime PCR cycler (Applied Biosystems, UK). Each reaction was setup according to Table 2.8. Primer sequences were generated using the Harvard Primer Bank (found at: http://pga.mgh.harvard.edu/primerbank/) and were purchased from Eurofins Genomics, UK. A list of the primer sequences used may be found in Table 2.9. Cycling conditions may be found in Table 2.10. CT values were generated using the 7500 software version 2.0.6 (Applied Biosystems, UK) using the 'Auto threshold' function and primer efficiencies were calculated using a standard curve of cDNA diluted from 1:10 – 1:1,000. CT values were normalised to the values generated by the housekeeping control and relative mRNA expression level changes were expressed as a fold change relative to the GAPDH siRNA control.

Reagent	Volume (µL)	Final concentration
Mastermix (2x)	12.5	1x
Forward primer 20 µM	0.2	0.16 µM
Reverse primer 20 µM	0.2	0.16 µM
dH_2O	10.1	-
Template cDNA	2	-
Total volume	**25**	**-**

Table 2.8: qRT-PCR reaction setup for each reaction.

Target gene	Forward primer (5'-3')	Reverse primer (5'-3')
GAPDH	GGCTGCTTTTAACTCTGG	GGAGGGATCTCGCTCC
HPRT1	ACCAGTCAACAGGGGACATAA	CTTCGTGGGGTCCTTTTCACC
PPIA	CCCACCGTGTTCTTCGACATT	GGACCCGTATGCTTTAGGATGA
PPIB	AAGTCACCGTCAAGGTGTATTTT	TGCTGTTTTTGTAGCCAAATCCT
TBP	CCCGAAACGCCGAATATAATCC	AATCAGTGCCGTGGTTCGTG
RPL14	GACCTTGCACTCAAGTGAGGA	CTTGTCGGACATACTTCTGGTG
RPL18	ATGTGCGGGTTCAGGAGGTA	CTGGTCGAAAGTGAGGATCTTG
RPL34	TGGTGGTTCCATGTGTGCTAA	GCTTGTGCCTTCAACACTTTC
RPL35A	TTGAAGGTGTTTACGCCCGAG	TGCTTCGGAATTTGGCACGA
RPS3A	GGCAAGAACAAGCGCCTTAC	CAGGTGCTTTCACATCATACCAA
RPS7	GTGAAGCCCAATGGCGAGAA	TGAGGTCCGAGTTCATCTCCA

Table 2.9: A list of the forward and reverse primer sequences used.

Stage	Temperature	Time	Number of cycles
Initial denaturation	95°C	10 mins	1
Denaturation Annealing / Extension	95°C 60°C	15 sec 1 min	40
Hold	72°C	5 mins	1
Melt curve	95°C 60°C 95°C 60°C	15 sec 1 min 15 sec 15 sec	1 1 1 1

Table 2.10: qRT-PCR reaction conditions.

2.8 β-*galactosidase activity assay*

Cells seeded in 384-well plate format were washed with PBS and fixed with 0.2% (w/v) glutaraldehyde (in PBS) for 5 mins at RT. Cells were washed a second time with PBS and incubated with 5-bromo-4-chloro-3-indolyl-beta-D-galacto-pyranoside (X-gal) solution (see Table 2.11) for 6 hr at 37°C without additional CO_2. Cells were imaged at 4 and 6 hr using a light microscope (Nikon) at 20X magnification and single representative image of each well was taken.

Reagent	Volume (to make 10 mL)	Working Concentration
X-gal (ThermoFisher, UK) (20 mg/mL)	0.5 mL	1 mg/mL
NaCl (5 M)	0.3 mL	150 mM
$MgCl_2$ (1 M)	20 µL	2 mM
$K_3Fe(CN)_6$ (100 mM)	0.5 mL	5 mM
$K_4Fe(CN)_6$ (100 mM)	0.5 mL	5 mM
NaPi pH 6.0 (100 mM)	4 mL	40 mM
dH_2O	4.18 mL	-

Table 2.11: A table detailing the components of the X-gal solution used.

2.9 *SYTOX assay*

MDA-MB-231 cells were reverse transfected with 30 nM siRNA according to Section 2.3.2. Medium was changed after 46 hr and 120 hr (Day 5). At Day 6 cells were incubated with SYTOXGreen nucleic acid stain (SYTOX) (Invitrogen, UK) (500 nM final concentration) and Hoechst 33342 (Hoechst) (Invitrogen, UK) (1.62 µM final concentration) in DMEM with supplements for 2.5 hr at 37°C. Cells were imaged at 30 mins and 2.5 hr using the IN Cell 1000 automated microscope according to Section 2.5.1. Hoechst was visualised using a D360_40X excitation filter and a HQ535_50M emission filter (blue) and SYTOX staining was visualised using a S475_20X excitation filter and a HQ535_50M emission filter (green). The percentage of SYTOX-positive nuclei was calculated using the IN Cell Developer software version 1.8.

2.10 *Actinomycin D drug treatment*

MDA-MB-468 cells were seeded at 66,000 cells/cm^2 in 384-well plate format and after 12 hr cells were incubated with 0.001 µg/mL-100 µg/mL Actinomycin D in DMSO (VWR, USA) in DMEM with supplements for 8 hr at 37^oC. Cells were then fixed and stained with DAPI, rabbit anti-NCL and donkey Alexa Fluor-546 conjugated anti-rabbit according to Section 2.4. Cells were then image and analysed according to Section 2.5.1.

2.11 *Statistical analysis*

Statistical analysis was performed using the online statistics tool GraphPad Quickcalcs software (found at: http://www.graphpad.com/quickcalcs/ttest1/). In order to compare the means of two groups, an unpaired t-test was performed. A One-way Analysis of Variance (ANOVA) was used to assess western blotting data using GraphPad InStat software. Unless otherwise stated, at least two independent experiments were performed in triplicate.

Chapter 3 **siRNA screening to activate senescence in p16-positive cancer.**

3.1 *Introduction*

OIS is a potent tumour suppressor mechanism in cells at risk of transformation and is triggered by the overexpression of an oncogene or the repression of a tumour suppressor gene (see Section 1.5). OIS bypass and continual senescence evasion are thought to be essential for cancer initiation and survival. As such, the activation of senescence in cancer is a highly attractive therapeutic strategy and one that is gaining momentum (see Section 1.6). In epithelial cells (the primary origin of most human malignancies) OIS can be mediated by the tumour suppressor, p16. p16 is one of the most frequently mutated or deleted genes in cancer (Hanahan and Weinberg, 2011) and disruption to the p16/RB signalling pathway may result in OIS bypass in pre-malignant cells, an early step on the path towards carcinogenesis (see Section 1.5).

Breast cancer is the most common cancer in the UK and BLBC (a highly aggressive subtype) accounts for approximately 8-22% of all cases depending on ethnicity (see Section 1.8). Unlike most human malignancies and indeed other PAM50 breast cancer subtypes, the vast majority of BLBCs are positive for WT p16. This p16 signature in BLBC is associated with a particularly poor prognosis and as discussed earlier, p16-positive BLBC remains the most clinically challenging subtype and is the focus of this project.

The overarching aim of this project is to activate senescence in p16-positive BLBC cells using siRNA screening as a route to identifying those proteins responsible for maintaining senescence evasion (termed 'senescence evaders'). Once validated, the proteins implicated may serve as novel potential therapeutic targets in this disease subtype. The longer-term hope is that the newly identified senescence evaders may also act as suitable prognostic biomarkers in p16-positive BLBC and may help to further stratify the disease subset and inform better personalised therapeutic regimes.

In order to identify siRNAs capable of senescence activation in p16-positive cancer cells, a previously performed genome-wide siRNA screen, conducted in HeLa cells (p16-positive human cervical cancer cell line) was re-mined. Here, 22,010 genes were targeted by pools of three siRNAs. A significant reduction in cell number, together with a significant increase in cell area was used to define senescence activation in these cells. These phenotypic criteria were based on well-established markers of senescence induction (a reduction in proliferation together with an increase in cell size). Here, significance was defined as a change of more than three Z scores from the negative control mean as this level of stringency is an accepted means of defining hits in a screen of this size (see Section 2.5.1). Implementing this relatively high level of stringency when defining the senescence phenotype ensured that only the most potent siRNAs were

classified as hits. This significance threshold was applied to each of the phenotypic parameters analysed within each of the siRNA screens presented within this Chapter.

In order to identify those cancer-specific activators of senescence, the data generated by the HeLa genome-wide siRNA screen was compared to a previously published screen in normal, finite lifespan HMECs. Using the phenotypic criteria for senescence outlined above, this cross-referencing exercise revealed 86 siRNAs that were able to activate senescence in the HeLa cell line but, importantly, had no significant effect on the proliferation or morphology of HMECs (data not shown, see Figure 3.1).

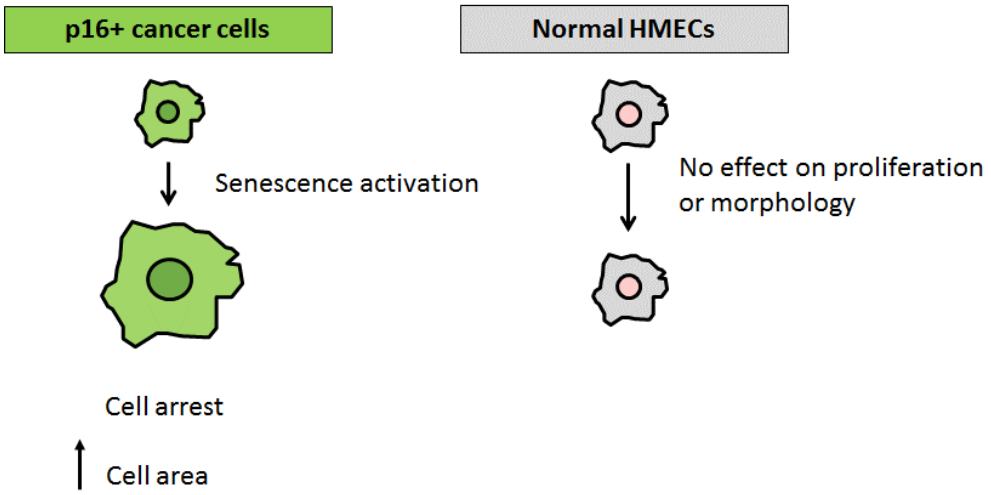

Figure 3.1: Cartoon summarising the criteria used to select the 86 siRNAs to be included in the validation screens presented within this Chapter.

3.1.1 *Chapter aims*

1. To perform a validation siRNA screen in the HeLa cell line that will aim to re-test the 86 siRNAs previously identified within the genome-wide siRNA screen.

2. To test the most potent activators of senescence (within the HeLa cell line) in a second p16-positive cancer cell line, MDA-MB-468 ($p16^{+/+}$, $p53^{R273H}$, RB-null BLBC cell line) in order to identify novel potential senescence evaders in p16-positive BLBC.

3. To conduct multiparameter analysis across both the HeLa and MDA-MB-468 siRNA screens in order to explore the complexities of the senescence phenotype and to enable sub-categorisation of the significant activators of senescence.

4. To investigate whether senescence activation is accompanied by an increase in nuclear p16 levels.

The MDA-MB-468 BLBC cell line will be used to model p16-positve BLBC throughout this thesis. This cell line was isolated from a pleural effusion in a 51 year old woman with metastatic adenocarcinoma of the breast. Despite their metastatic origin, MDA-MB-468 cells contain many of the gene signatures associated with primary BLBC tumours (see Section 1.8). For example the cells are documented to contain the $p53^{R273H}$ gain-of-function mutation, are RB-null and crucially, the cells stain positive for WT p16.

3.2 *Transfection optimisation in 384-well plate format*

3.2.1 *Optimisation of siRNA reverse transfection in HeLa and MDA-MB-468 cells*

Before conducting the siRNA screens, the transfection reagent dose and cell seeding density were first optimised for each cell type in order to produce maximal transfection efficiency with minimal cytotoxicity (see Section 2.2.1). When conducting a siRNA screen to identify activators of senescence, an ideal seeding density is one at which there are enough cells to detect a significant reduction in proliferation (induction of senescence) and one where the control cells remain sub-confluent after 120 h (experimental endpoint) to ensure accurate quantitation. With this in mind, a seeding density of 12,000 cells/cm^2 was selected for the HeLa siRNA screens and cells were seeded at 33,000 cells/cm^2 for the MDA-MB-468 screens to allow the detection of as many significant hits as possible.

GAPDH siRNA was used throughout this thesis as a negative control for the siRNA reverse transfections. The GAPDH siRNA mean was also used as a baseline for Z score generation and significance thresholding (outlined in Section 2.5.2). PLK1 is a Serine-threonine kinase that plays an essential role in numerous aspects of mitosis such as mitosis initiation, centrosome maturation, spindle formation and cytokinesis (reviewed in Archambault et al., 2015) As such, PLK1 is critical for correct mitotic progression and cancer cells transfected with PLK1 siRNA undergo apoptosis as they attempt to enter the cell cycle. Consequently, PLK1 siRNA was used as a 'killer control' during siRNA transfection optimisation. The transfection reagent, HiPerFect, was selected as it was used to conduct the previously performed HeLa (unpublished) and HMEC genome-wide siRNA screens (Bishop et al., 2010).

Using the seeding densities outlined above, reverse transfection with 30 nM siRNA targeting GAPDH or PLK1 was optimised for HeLas (data not shown) and MDA-MB-468 cells (Figure 3.2A-B) such that maximum transfection efficiency with minimal toxicity was achieved (see Section 2.2.2). MDA-MB-468 cells were seeded at 33,000 cells/cm^2 and reverse transfected with 30 nM siRNA targeting GAPDH or PLK1 using 0.1-0.4 µL/well HiPerFect according to Section 2.2.2.

HiPerFect doses 0.15-0.25 µL/well produced a high level of transfection efficiency (as indicated by the PLK1 siRNA) with a relatively low level of cytotoxicity (5.02% +/- 6.41% cytotoxicity at 0.15 µL/well and 14.09% +/- 4.67% cytotoxicity at 0.25 µL/well) (Figure 3.2A-B). In addition, HiPerFect doses above 0.3 µL/well induced an unacceptably high level of cytotoxicity (0.3 µL/well induced cytotoxicity of 27.9% +/- 6.54%) and so an optimal HiperFect dose range of 0.15-0.25 µL/well was identified.

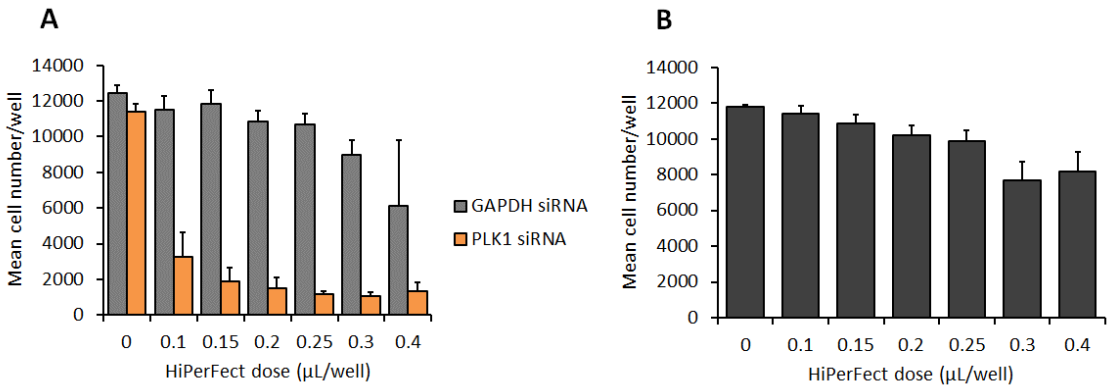

Figure 3.2: Optimisation of HiPerFect dose in MDA-MB-468 cells. MDA-MB-468 cells were seeded at 33,000 cells/cm^2 and transfected with 30 nM siRNA targeting GAPDH or PLK1 using 0.1-0.4 µL/well HiPerFect according to Section 2.2.2. Cells were then fixed and stained with DAPI and imaged and quantified according to Sections 2.4 and 2.5. **(A)** Mean cell number/well of cells transfected with either 30 nM GAPDH siRNA or PLK1 siRNA using 0.1-0.4 µL/well HiPerFect. **(B)** Mean cell number/well of cells treated with 0.1-0.4 µL/well HiPerFect alone. Bars denote mean +SD of a single representative experiment containing five technical repeats.

3.2.2 *Validation of the mouse anti-p16 JC2 antibody and siRNA knockdown of p16 in HeLa and MDA-MB-468 cells*

Protein knockdown following siRNA transfection using p16 siRNA was then assessed at each of the HiPerFect doses within the optimal dose range identified (0.15-0.25 µL/well) for both HeLas and MDA-MB-468 cells. First the mouse anti-p16 JC2 antibody was validated via western blotting. HeLa and MDA-MB-468 cell lysates (p16-positive cancer cell lines) were run alongside MDA-MB-231 cell lysate (p16-null BLBC cell line) and all three samples were probed for p16 according to Section 2.6. Western blot analysis revealed one clean band at approximately 16KDa in the p16-positive cell lines and no band in the MDA-MB-231 cells, confirming that the antibody was suitable for immunofluorescence staining (Appendix, Figure A.1A).

Subsequently, HeLas and MDA-MB-468 cells were reverse transfected with siRNA targeting either GAPDH or p16 at 0.15, 0.2 and 0.25 µL/well HiPerFect and cellular p16 protein levels were quantified via immunofluorescence staining according to Sections 2.4 and 2.5. A HiPerFect dose

of 0.15 µL/well produced a reduction in cellular p16 protein levels together with minimal toxicity in HeLa cells and was selected for future siRNA screening (Figure 3.3A-B). In MDA-MB-468 cells, a HiPerFect dose of 0.2 µL/well produced a greater level of p16 protein knockdown following p16 siRNA transfection when compared to 0.15 µL/well HiPerFect and a dose of 0.25 µL/well was not able to increase the level of p16 protein knockdown any further (Figure 3.3C-D). As such, 0.2 µL/well HiPerFect was selected for the future MDA-MB-468 siRNA screens.

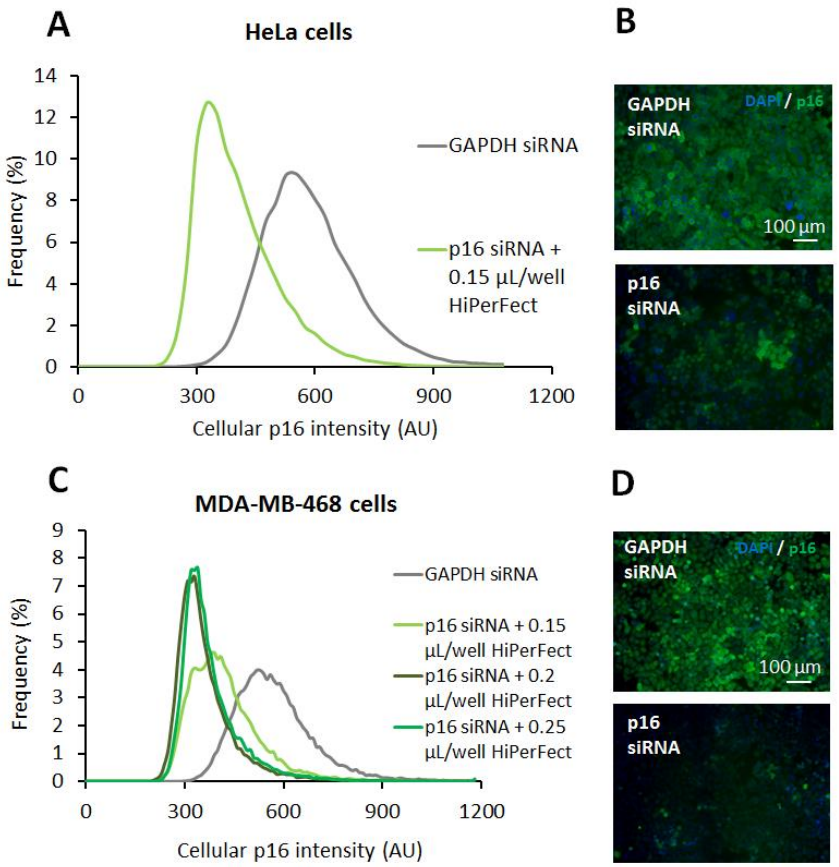

Figure 3.3: siRNA knockdown of p16 in HeLa and MDA-MB-468 cells. (A) Representative frequency distribution of cellular p16 intensity levels following reverse transfection of HeLa cells with 30 nM siRNA targeting either GAPDH or p16. HeLa cells were seeded at 12,000 cells/cm^2 in 384-well plate format and were reverse transfected with 30 nM siRNA using 0.15 µL/well HiPerFect. Cells were fixed and stained with mouse anti-p16 JC2, goat Alexa Fluor-488 conjugated anti-mouse, DAPI and Cell Mask and were then imaged and quantified according to Sections 2.4 and 2.5. **(B)** Representative immunofluorescence images of HeLa cells treated with either GAPDH siRNA or p16 siRNA. DAPI (blue), p16 (green). **(C)** Representative frequency distribution of cellular p16 intensity levels following reverse transfection of MDA-MB-468 cells with 30 nM siRNA targeting either GAPDH or p16. MDA-MB-468 cells were seeded at 33,000 cells/cm^2 in 384-well plate format and were reverse transfected with 30 nM siRNA using 0.15, 0.2 and 0.25 µL/well HiPerFect. Cells were fixed and stained with mouse anti-p16 JC2, goat Alexa Fluor-488 conjugated anti-mouse, DAPI and Cell Mask and were then imaged and quantified according to Sections 2.4 and 2.5. **(D)** Representative immunofluorescence images of MDA-MB-468 cells treated with either GAPDH siRNA or p16 siRNA. DAPI (blue), p16 (green). Images are at 10X magnification and size bar denotes 100 µm.

3.3 *siRNA screening to activate senescence in p16-positive cancer*

3.3.1 *Identification of 28 senescence evaders in HeLa cells*

A previous genome-wide siRNA screen revealed 86 siRNAs (see Appendix, Figure A.2) that activated senescence in HeLa cells (data not shown) but had no effect on the proliferation or morphology of normal, finite lifespan HMECs. Due to the large-scale nature of the genome-wide siRNA screen, each siRNA was tested just once. Therefore, to further validate these 86 siRNAs as activators of senescence, HeLa cells were reverse transfected with the previously identified 86 siRNAs and control siRNAs targeting GAPDH or PLK1 according to Section 2.3.1. Two independent siRNA screens were performed, each in triplicate.

The level of cytotoxicity induced by the transfection protocol was at an acceptable level (15.63% +/- 7.94%) (Figure 3.4A). Further, PLK1 siRNA induced 93.11% +/- 9.29% cell death when compared to cells treated with GAPDH siRNA, indicating that optimal transfection efficiency had been achieved (Figure 3.4A). As such, the data generated by the GAPDH siRNA was used as a baseline for Z score generation (see Section 2.5.2) to determine the effects of each of the 86 siRNAs on proliferation and morphology in the HeLa cells (Figure 3.4A-B). As described in Section 3.1, a significant reduction in cell number, together with a significant increase in cell area was used to define senescence activation and identify a group of reproducible senescence evaders in this p16-positive cancer cell line. According to these phenotypic criteria, the siRNA screens identified 28 siRNAs that were able to activate senescence in the HeLa cell line (Figure 3.4C). In addition, it was further confirmed that GAPDH siRNA was an appropriate negative control as there was no significant change in the proliferation or morphology of HeLa cells treated with GAPDH siRNA when compared with cells treated with HiPerFect alone (Figure 3.4A-B).

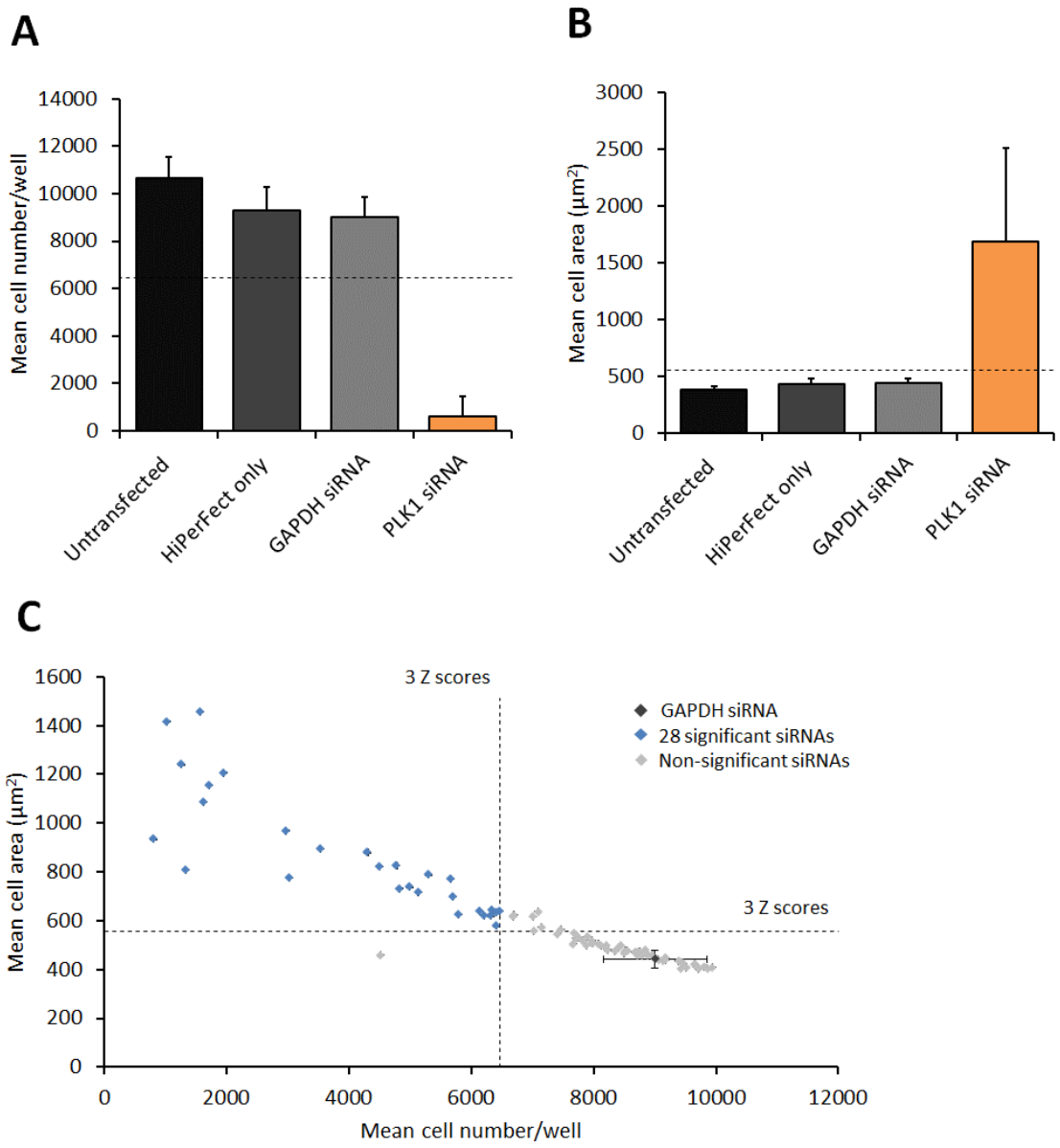

Figure 3.4: Two independent siRNA screens reveal 28 siRNAs that activate senescence in HeLa cells. HeLa cells were seeded at 12,000 cells/cm^2 and transfected with 30 nM siRNA targeting 86 genes together with control siRNAs targeting GAPDH or PLK1 in 384-well plate format according to Section 2.3.1. Cells were fixed and stained with DAPI and Cell Mask and then imaged and quantified according to Sections 2.4 and 2.5. **(A)** Mean cell number/well for the control siRNAs. **(B)** Mean cell area for the control siRNAs. Bars denote mean +SD of two independent screens, each performed in triplicate. **(C)** Scatter plot of mean cell number versus mean cell area generated by each of the 86 siRNAs within the two independent siRNA screens. The mean data generated by the GAPDH siRNA is shown in dark grey. Non-significant siRNAs are shown in light grey and significant siRNAs are depicted in blue. Throughout, the dotted lines denote the significance thresholds at three Z scores away from the GAPDH siRNA negative control mean.

3.3.2 *Identification of 25 senescence evaders in MDA-MB-468 cells*

In order to address the second aim of this Chapter, MDA-MB-468 cells were reverse transfected with the top 50 siRNAs identified within the previously performed HeLa screens according to

Section 2.3.1. So as to be as inclusive as possible, the 86 siRNAs tested in the HeLa cells were ranked according to their Z score for cell number and the 50 siRNAs that produced a reduction in cell number together with an increase in cell area of at least one Z score were selected for screening in the MDA-MB-468 cells.

Interestingly, of the 28 significant hits identified within the HeLa screen, 11 siRNAs targeted genes encoding RPs. These 11 hits were also among the most potent senescence activators to be identified. Furthermore, of the top 50 siRNAs identified within the HeLa screen, two mitochondrial ribosomal proteins (MRPs) were present (MRPL13 and MRPS24). As such, it was hypothesised that siRNA silencing of RPs or MRPs may also activate senescence in the MDA-MB-468 cells. Therefore, the HeLa genome-wide siRNA screen was re-mined for siRNAs targeting RPs or MRPs. In total, 182 ribosomal siRNAs were tested, of which 90 siRNAs induced a reduction in cell number of at least one Z score. Once the 13 RP hits identified above had been excluded, 77 ribosomal siRNAs remained. Next, the HMEC siRNA screen was subsequently re-mined. Only seven out of these 77 ribosomal siRNAs did not induced any significant change to cellular proliferation or morphology in the HMECs (data not shown). Interestingly, all seven of these additional siRNAs targeted genes encoding MRPs. In summary, a total of 57 siRNAs were selected for testing within the MDA-MB-468s (Appendix, Figure A.3). These were significantly enriched for siRNAs targeting either RPs (11 siRNAs) or MRPs (nine siRNAs) (Figure 3.5).

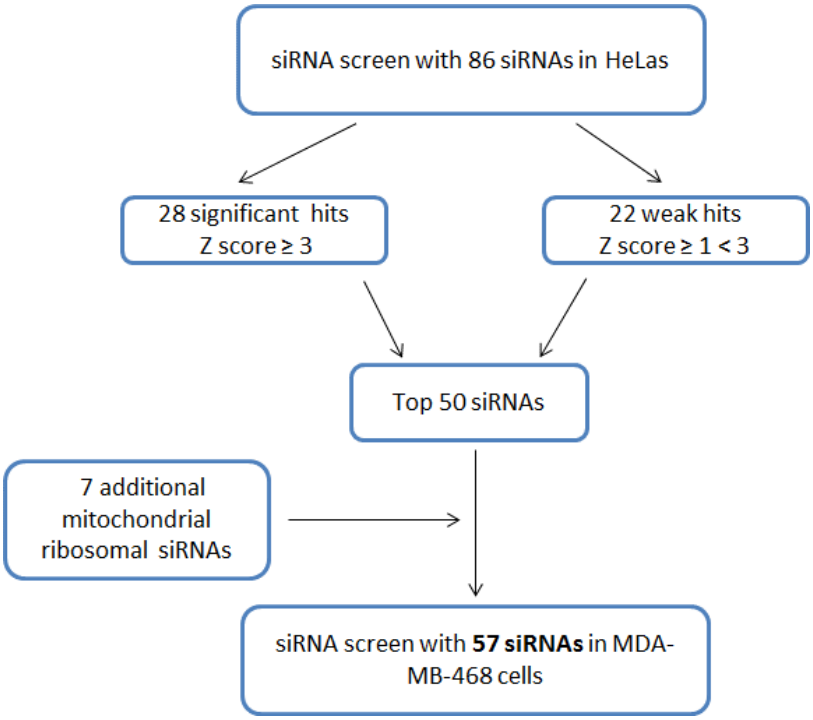

Figure 3.5: A schematic illustrating how the siRNAs were selected for the MDA-MB-468 screens.

Before siRNA screening in the MDA-MB-468s, it was first established whether or not senescence could be activated in these cells. In order to test this, MDA-MB-468 cells were reverse transfected with either GAPDH siRNA or CBX7 siRNA according to Section 2.3.2. CBX7 is a polycomb group repressor of the INK4b-ARF-INK4a locus and the Bishop laboratory has previously demonstrated that siRNA knockdown of CBX7 in HMECs causes an increase in p16 protein levels together with senescence induction (Bishop et al., 2010). Further details on the regulatory function of CBX7 may be found in Section 1.1.2. Interestingly, reverse transfection of MDA-MB-468 cells with CBX7 siRNA resulted in a decrease in cell number together with an increase in both cell and nuclear area suggesting that these cells are vulnerable to senescence activation despite their highly aggressive malignant phenotype (Figure 3.6A-D). As such, CBX7 siRNA was used as a positive control for senescence activation in the MDA-MB-468 siRNA screens.

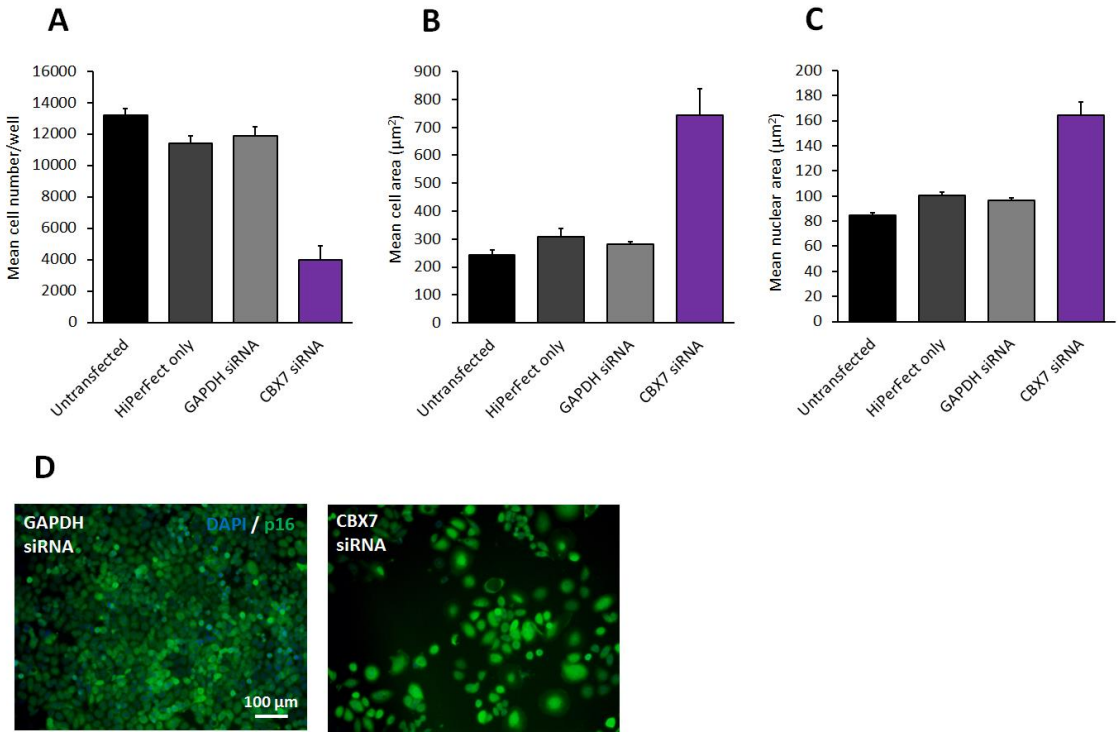

Figure 3.6: Activation of senescence in MDA-MB-468 cells with CBX7 siRNA. MDA-MB-468 cells were transfected with 30 nM siRNA targeting GAPDH or CBX7 according to Section 2.3.2. Cells were fixed and stained with mouse anti-p16 JC2, goat Alexa Fluor-488 conjugated anti-mouse, DAPI and Cell Mask and cells were then imaged and quantified according to Sections 2.4 and 2.5. **(A)** Mean cell number/well. **(B)** Mean cell area. **(C)** Mean nuclear area. Bars denote mean +SD of a single representative experiment containing six technical repeats. **(D)** Representative immunofluorescence images of MDA-MB-468 cells transfected with either 30 nM GAPDH siRNA or CBX7 siRNA and stained for DAPI (blue) and p16 (green). Size bar denotes 100 µm.

Once it had been established that the MDA-MB-468 cells were capable of senescence activation, two independent siRNA screens were performed, each in triplicate. As in the HeLa screens, GAPDH siRNA was used to determine the level of cytotoxicity induced by the transfection protocol and was also used as a baseline for Z score generation (see Section 2.5.2). CBX7 siRNA was used as a positive control for senescence activation and PLK1 siRNA was used as a 'killer control' to determine transfection efficiency.

The cell numbers produced by each of the control siRNAs were in line with previous data and, as in the HeLa screens, the level of cytotoxicity induced by the transfection protocol was at an acceptable level (17.80% +/- 8.55%, see Figure 3.7A). Furthermore, PLK1 siRNA induced 88.65% +/- 13.40% cell death indicating that optimal transfection efficiency had been achieved across the two screens (Figure 3.7A). Therefore, the data generated from the screens was used to determine the effects of each of the 57 siRNAs on the proliferation and morphology of the MDA-MB-468 cells. The same phenotypic criteria (outlined in Section 3.1) used within the HeLa screens for hit detection was applied to define senescence activation in the MDA-MB-468 cells (Figure 3.7A-B). According to these parameters, the siRNA screens revealed 25 siRNAs capable of activating senescence in the MDA-MB-468 cells (Figure 3.7C).

In line with the data generated by the genome-wide siRNA screen in HeLa cells, five of the seven additional MRP siRNAs induced a non-significant reduction in cell number together with a non-significant increase in cell area in the MDA-MB-468 cells (data not shown). However, in contrast to the HeLa cell line, two siRNAs (targeting MRPL10 and MRPS31) caused significant changes in both cell number and cell area in the MDA-MB-468s (Figure 3.8B) These findings suggest a possible cell type-specific role for MRPL10 and MRPS31 in senescence evasion. It is possible that MDA-MB-468s may be more reliant upon MRPL10 and MRPS31 expression for senescence evasion and that siRNA silencing of these genes in MDA-MB-468s may induced a more potent senescence induction when compared to silencing in HeLa cells.

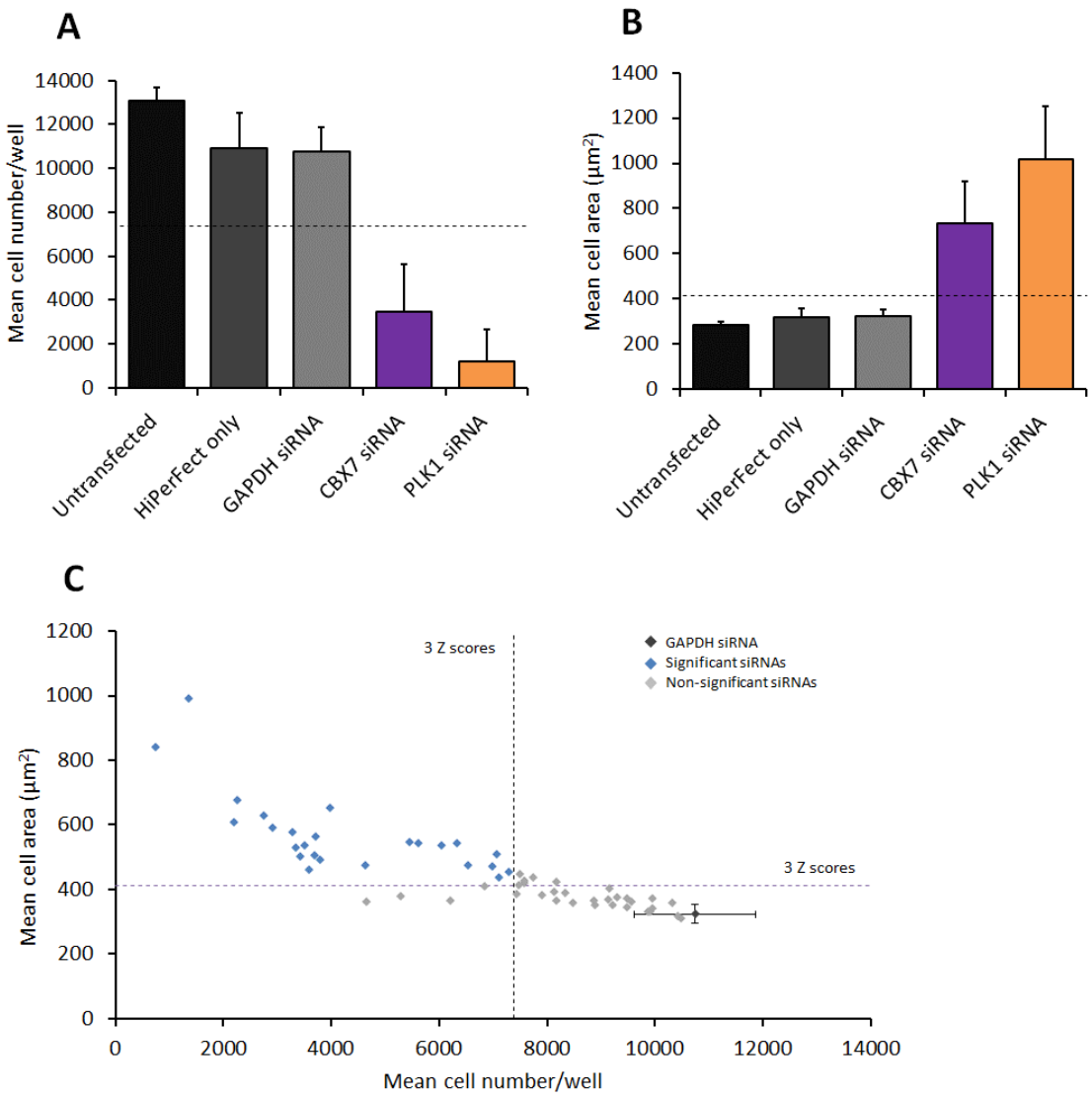

Figure 3.7: Two independent siRNA screens reveal 25 siRNAs that activate senescence in MDA-MB-468 cells. MDA-MB-468 cells were transfected with 30 nM siRNA targeting 57 genes together with control siRNA targeting GAPDH, CBX7 or PLK1 according to Section 2.3.1. Cells were fixed and stained with DAPI and Cell Mask and were then imaged and quantified according to Section 2.4 and 2.5. **(A)** Mean cell number/well for the control siRNAs. **(B)** Mean cell area for the control siRNAs. Bars denote mean +SD of two independent screens, each performed in triplicate. **(C)** Scatter plot of mean cell number and mean cell area generated by each of the 57 siRNAs within two independent siRNA screens, each performed in triplicate. The mean data generated by the GAPDH siRNA is shown in dark grey. Non-significant siRNAs are shown in light grey and significant siRNAs are depicted in blue. Throughout, the dotted lines denote the significance thresholds at three Z scores away from the GAPDH siRNA negative control mean.

3.3.3 *Multiparameter analysis of the top senescence evaders*

Across both siRNA screens, senescence activation was often accompanied by multiple additional morphological changes characteristic of the senescent phenotype. Further, the senescence phenotype induced by each of the top siRNAs appeared to vary depending on the cell type and the siRNA used. In order to quantify these observed morphological changes and to explore the complexities of the activated senescence phenotype, multiparameter analysis was performed across both siRNA screens. Importantly, this approach was also used to assess whether the top siRNAs could be sub-classified according to the morphological changes induced and to determine whether different morphological features had been activated. In addition, it was hypothesised that siRNAs targeting genes encoding proteins of the same biological complex (i.e. the ribosome) would induce similar morphological changes upon senescence activation. It has previously been shown that siRNA silencing of CBX7 in HMECs causes potent senescence induction, together with significant changes to cellular and nuclear morphology (Bishop et al., 2010). Furthermore, siRNA silencing of CBX7 in MDA-MB-468s resulted in senescence activation (Figure 3.6A-D). As such, CBX7 siRNA was used as an initial basis to select additional senescence-associated parameters for quantitation. Multiparameter analysis was then performed across both siRNA screens and results for the significant senescence evaders are displayed in the form of a heatmap in Figure 3.8A-D.

This analysis showed that many of the top siRNAs from both screens induced significant changes in multiple senescence-associated parameters (Figure 3.8A-D). For example, within the HeLa screen all but one (distal-less homeobox 5 (DLX5) siRNA) of the 28 significant siRNAs induced a significant change in at least one additional senescence-associated parameter. Furthermore, ten of the top 11 siRNAs (classified as strong activators of senescence as they caused a reduction in cell number of more than six Z scores from the GAPDH siRNA negative control mean) induced significant changes in at least three additional parameters.

This approach allowed the top siRNAs from each screen to be sub-classified according to the various morphological changes observed and the significant siRNAs were grouped into seven broad categories, suggesting multiple routes to senescence induction had been activated. Many of the siRNAs induced similar morphological changes across both screens (including siRNAs targeting interleukin 13 receptor, alpha 1 (IL13RA1) and sperm adhesion molecule 1 (PH-20 hyaluronidase, zona pellucida binding), SPAM1) and were sub-classified into the same category (Category 2) within each cell type. Further, many of the most potent siRNAs (including siRNAs targeting RPS3A and RPL35A) induced a significant increase in both nuclear area and nuclear

roundness within both cell types. However, two of the strongest hits across both screens (targeting RPLP2 and RPL34) induced opposing changes to nuclear morphology upon senescence induction within the two cell types. These siRNAs induced a significant reduction to nuclear elongation in the MDA-MB-468 cell line (rounded phenotype, Category 1), while inducing a significant increase to nuclear elongation in the HeLa cells (Category 4). Together, these finding suggests that RPLP2 and RPL34 may have cell type-specific roles in senescence evasion and phenotypic changes associated with the activation of senescence in p16-positive cancer cells may also be cell-type specific. In addition, many of the siRNAs that activated senescence in both cell types, including those targeting ubiquitin A-52 residue ribosomal protein fusion product 1 (UBA52) (HeLa: Category 6, MDA-MB-468: no significant change to cellular or nuclear morphology, Category 7), 6-phosphogluconate dehydrogenase (PGD) (HeLa: category 2, MDA-MB-468: Category 7) and Topoisomerase II beta (TOP2B) (HeLa: Category 4, MDA-MB-468: Category 7) induced shifts in more additional senescence-associated parameters in the HeLa cell line when compared to the MDA-MB-468 screen. This data suggests that UBA52, PGD and TOP2B may also play cell type-specific roles in senescence evasion in p16-positive cancer cells and that phenotypic changes associated with senescence activation may differ depending on the cell type.

Notably, in contrast to the senescence phenotype observed in the HeLa cells, senescence activation in the MDA-MB-468 cells was largely associated with a reduction in cellular elongation. Arrested MDA-MB-468 cells developed a more rounded morphology (Category 1), while senescence activation in the HeLa cells by many of the siRNAs caused the cells to become significantly more elongated (Category 5). For example, of the top 28 siRNAs identified within the HeLa screens, nine siRNAs induced a significant increase in cellular elongation, while just one siRNA achieved this in the MDA-MB-468 cells. Again, this data also indicates a possible tissue-specific role for these senescence evaders and suggests, under certain conditions, the senescence phenotype may also be cell-type dependent.

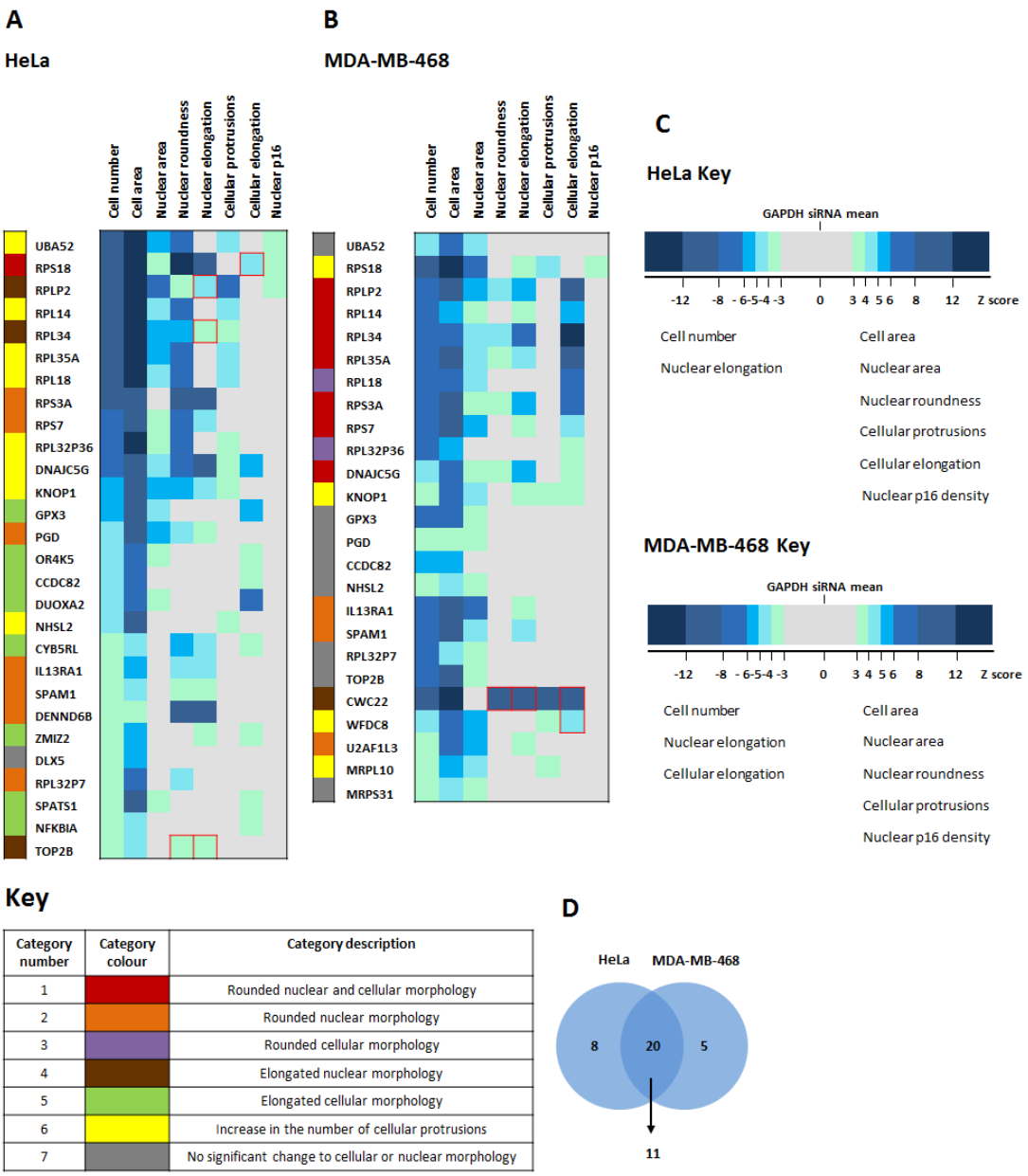

Category number	Category colour	Category description
1		Rounded nuclear and cellular morphology
2		Rounded nuclear morphology
3		Rounded cellular morphology
4		Elongated nuclear morphology
5		Elongated cellular morphology
6		Increase in the number of cellular protrusions
7		No significant change to cellular or nuclear morphology

Figure 3.8: Sub-categorisation of the top siRNAs in HeLa and MDA-MB-468 cells according to multiparameter analysis. Two independent siRNA screens, each in triplicate were performed in HeLa and MDA-MB-468 cells according to Section 2.3.1. Cells were then fixed and stained with mouse anti-p16 JC2, goat Alexa Fluor-488 conjugated anti-mouse, DAPI and Cell Mask according to Section 2.4. Cells were then imaged and quantified according to Section 2.5 and multiparameter analysis was performed on the significant siRNAs using the IN Cell 1000 Developer software version 1.8. Z scores were generated according to Section 2.5.2. **(A-B)** Heatmaps depicting significant changes in each of the senescence-associated parameters selected for quantification for the significant siRNAs from two independent siRNA screens. Scores highlighted in red denote a significant shift in the parameter in the opposite direction to that shown in the **(C)** Key. The top 25 siRNAs were then sub-categorised into seven categories. **(D)** A Venn diagram summarising the results of siRNA screening in the HeLa cell line and the MDA-MB-468 cell line. 50 genes were targeted by pools of three siRNAs in two p16-positive cancer cell lines. 20 genes were classified as senescence evaders in both cell lines.

There was considerable overlap between the senescence evaders identified across the two screens. Of the 50 siRNAs tested in both cell lines, 20 scored significantly in both the HeLa cells and the MDA-MB-468 cells for cell number and cell area. Strikingly, of these 20 siRNAs, 11 target genes that encode for both 40S and 60S RPs and will form the basis of future study (see Chapter 4). Importantly, these 11 ribosomal siRNAs were among the most potent activators of senescence across both screens. Within the HeLa cell line the majority of these siRNAs fell into Category 2 (rounded nuclear morphology) or 6 (rounded nuclear morphology and increased cellular protrusions) with the exception of RPS18 siRNA (Category 1, rounded cellular and nuclear morphology) and siRNAs targeting RPLP2 and RPL34 (Category 4, elongated nuclear morphology). As in the HeLa screen, the majority of these ribosomal siRNAs induced a rounded nuclear morphology in the MDA-MB-468s, however, unlike in the HeLa cells, senescence activation was often associated with a significant increase in cellular roundness with the majority of the ribosomal siRNAs falling into Category 1 or 3. Strikingly, just one siRNA targeting RPS18 gave rise to an increase in the number of cellular protrusions, a defining feature of the activated senescence phenotype in HeLa cells. Together, this data suggests that some morphological changes, such as increased nuclei roundness, may characterise senescence activation via RP silencing in p16-positive cancer regardless of cell type. By contrast, additional senescence-associated features such as increased cellular protrusions or increased cellular roundness may be cell-type specific.

3.3.4 *Activation of senescence in p16-positive cancer cells is associated with increased nuclear p16 protein levels*

In order to address the fourth aim of this Chapter, the original HeLa and MDA-MB-468 siRNA screening plates were stained with p16 antibody according to Sections 2.4 and 2.5 . Within the HeLa screen, p16 staining identified three siRNAs (targeting UBA52, RPS18 and RPLP2) that activated senescence together with a significant increase in nuclear p16 density (Figure 3.8A). In addition, a further four siRNAs (targeting RPL14, RPS7, RPS3A and RPL34) induced an increase in nuclear p16 density of more than two Z scores above the GAPDH siRNA control mean. Interestingly, all seven of these siRNAs were potent activators of senescence and targeted genes that encode RPs. As in the HeLa screen, RPS18 siRNA induced a significant increase in nuclear p16 density (Figure 3.8B) while many other RP siRNAs (including RPLP2) siRNA induced a reproducible, although not significant increase in nuclear p16 protein levels (see Chapter 5). Together, these findings suggest that the knockdown of specific RPs in p16-positive cancer may re-sensitise these cells to p16 signalling, allowing the activation of senescence. The mechanisms

by which silencing of these RPs drives senescence activation in cancer together with the p16-dependency of the senescence induction will be explored in more detail in Chapter 5.

The HeLa cell line expresses the viral oncoprotein E7, which, in turn, acts to inhibit RB. Further, MDA-MB-468 cells are predicted to be RB-null. Given this, together with the p16 and p53 status of these cells and the data that suggests that, under certain circumstances, nuclear p16 levels increase upon senescence activation, it was hypothesised that senescence activation is mediated by p16 signalling independent of RB. Interestingly, the transcriptional regulator, FOXM1 was recently identified as a critical phosphorylation target of CDK4/6–cyclin D complexes (Anders et al., 2011)and is often overexpressed in breast cancer (see Section below). As such, it was hypothesised that the senescence evaders identified above may be novel downstream transcriptional targets of FOXM1 and that aberrant FOXM1 activity may mediate senescence evasion in MDA-MB-468 cells. In order to explore these questions, a collaboration was established with the Lam laboratory (Imperial College, London).

3.4 *FOXM1 knockdown does not activate senescence in MDA-MB-468 cells*

FOXM1 is a key transcription factor that functions to regulate the expression of a plethora of genes involved in embryonic and foetal development as well as adult tissue homeostasis and repair (reviewed in Bella et al., 2014). Although FOXM1 is highly expressed during embryogenesis and plays an essential role in ensuring the correct development of a multitude of tissues, such as the heart, liver, intestines and oesophagus (Ye et al., 1997), during adulthood, FOXM1 is tightly controlled and expression is restricted to proliferating cells, often at sites of tissue damage (liver, heart and spinal cord) (Ye et al., 1999, Bolte et al., 2012, Zhang et al., 2013). Here, FOXM1 expression enhances cellular proliferative capacity to ensure sufficient tissue repair is achieved. Downstream target genes of FOXM1 include a wide array of cell cycle regulators (see Section 1.1.1).

FOXM1 has also been found to be overexpressed in a diverse collection of cancers, including lung, cervical, gastric and pancreatic cancers and the role of FOXM1 within cancer initiation is now well established (reviewed in Lam et al., 2013). In addition, FOXM1 expression in cancer has been linked with epithelial-mesenchymal transition, enhanced tumour growth, cancer angiogenesis and metastasis (Bao et al., 2011, Wang et al., 2007, Huang et al., 2012). Importantly, FOXM1 has also been found to be highly expressed within breast cancers and elevated expression of FOXM1 within these tumours is associated with a reduced prognosis

(Bektas et al., 2008). Crucially, there is now a growing body of evidence to suggest that FOXM1 expression in cancer mediates senescence evasion and promotes genotoxic agent resistance (Tao et al., 2014, Li et al., 2008, Zeng et al., 2009, Liu et al., 2014, Kwok et al., 2010). Although targeting FOXM1 directly would have widespread detrimental effects on normal cells (given its crucial role within the cell cycle), tempering its pro-tumorigenic effects within cancer cells by modulating specific downstream FOXM1 targets may be highly beneficial (reviewed in Bella et al., 2014).

In order to explore the upstream transcriptional regulation of the senescence evaders identified and to further investigate the mechanism of senescence evasion in p16-positive BLBC cancer, a collaboration was established with the Lam laboratory (Imperial College, London). Given the regulatory role of p16 via CDK4/6–cyclin D complexes over FOXM1 activity, it was hypothesised that a sub-group of the senescence evaders identified here may be novel downstream transcriptional targets of FOXM1 and that p16-insensitivity through aberrant FOXM1 activity may drive senescence evasion in MDA-MB-468 cells. It was also proposed that this analysis would allow further sub-classification of the senescence evaders according to whether their transcriptional regulation was under FOXM1 control.

To test this, chromatin immunoprecipitation sequencing (ChIP-seq) for FOXM1 target genes performed by the Lam laboratory (Imperial College, London) identified 1,462 potential FOXM1 targets. In order to select putative FOXM1 targets for further investigation, the genome-wide HeLa and HMEC screens were re-mined. This cross-comparison exercise identified seven siRNAs (including those targeting the MRPs, MRPL13 and MRPS24) that activated senescence in the HeLa cells but, crucially, were non-toxic to the HMECs. Just three of these siRNAs (targeting lysine-rich nucleolar protein 1 (KNOP1), MRPS24 and gem (nuclear organelle) associated protein 6, GEMIN6) gave rise to a reduction in cell number (>1 Z score) within the two HeLa validation screens and were selected for further investigation. Notably, these three putative FOXM1 targets all encode ribosomal biosynthesis-associated proteins. As such, the genome-wide screens were re-mined a second time for ribosomal siRNAs that induced a reduction in cell number (>1 Z score) within the HeLa screens and were non-toxic to the HMECs. Of these, two hits (MRPL13 and MRPL55) were found to be putative FOXM1 targets and therefore a total of five candidates were included in further investigations. In order to test the hypothesis that these five putative FOXM1 transcriptional targets may mediate senescence evasion in p16-positive cancer cells, MDA-MB-468 cells were transfected with siRNA targeting each of these five genes.

These experiments identified just one siRNA, targeting KNOP1, that activated senescence in the MDA-MB-468s accompanied by a subtle non-significant (<1 Z score) increase in nuclear p16-protein levels. Two additional siRNAs targeting MRPs, MRPS24 and MRPL55, also induced small shifts (2 Z scores from the GAPDH siRNA negative control mean) in both cell number and cell area suggesting these putative FOXM1 targets may function as weak senescence evaders in these cells (Figure 3.9).

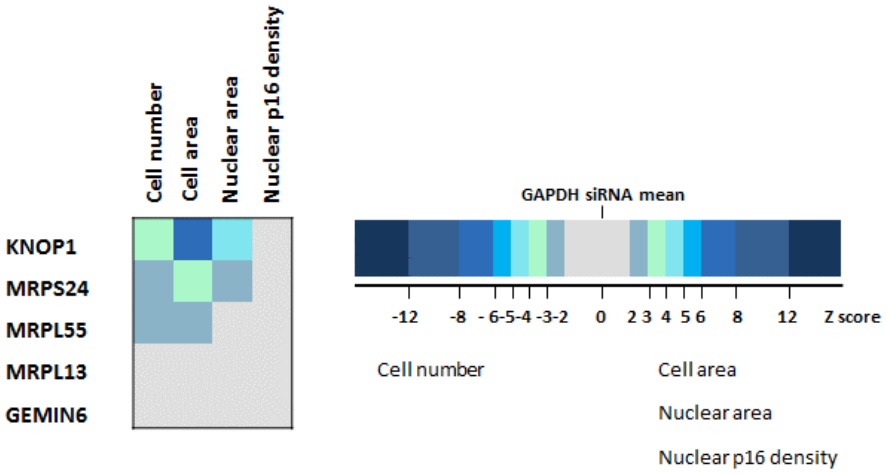

Figure 3.9: siRNA knockdown of five potential FOXM1 target genes in MDA-MB-468 cells. MDA-MB-468 cells were reverse transfected with 30 nM siRNA targeting five potential FOXM1 target genes, GAPDH or CBX7 according to Section 2.3.2. Cells were then fixed and stained with mouse anti-p16 JC2, goat Alexa Fluor-488 conjugated anti-mouse, DAPI and Cell Mask according to Section 2.4. Cells were then imaged and quantified according to Section 2.5.

Together, this data suggests that for the majority of the senescence evaders identified here, transcriptional control is not mediated by FOXM1. However, three putative FOXM1 targets were identified as potential senescence evaders in MDA-MB-468 cells. Given this, it is possible that enhanced FOXM1 activity and increased expression of target genes KNOP1, MRPS24 and MRPL55 may mediate senescence evasion in these cells. As such, it was hypothesised that FOXM1 may also mediate senescence evasion in p16-positive BLBC cells. To test this, MDA-MB-468 cells were subsequently transfected with a previously validated FOXM1 siRNA (kind gift from Prof. Eric Lam, Imperial College London) at 30, 60 or 90 nM in order to achieve maximal knockdown and senescence activation was assessed (Figure 3.10A-C). Interestingly, FOXM1 siRNA transfection did not induce senescence in the MDA-MB-468s at either of the three siRNA concentrations tested, suggesting that FOXM1 does not mediate senescence evasion within these cells. Further, this data suggests that the potential regulatory control of FOXM1 over the putative target genes (KNOP1, MRPS24 and MRPL55) identified above is not present or has been lost within the MDA-MB-468 cells.

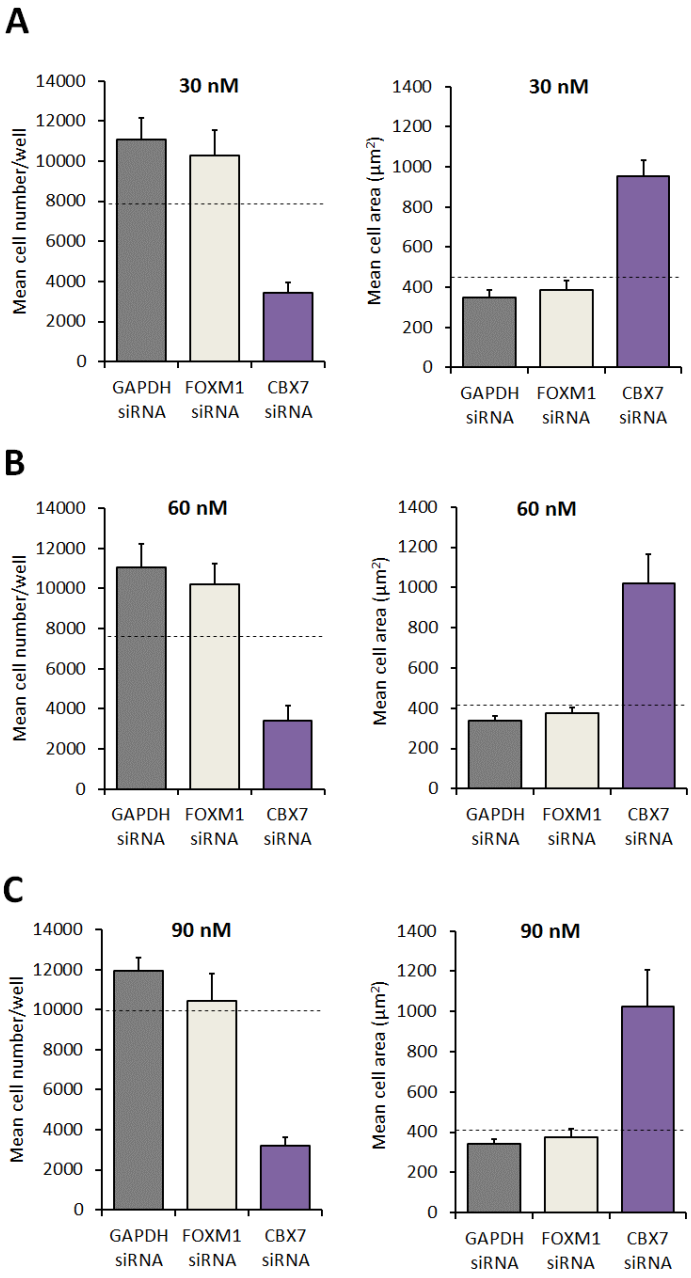

Figure 3.10: FOXM1 siRNA transfection of MDA-MB-468 cells. MDA-MB-468 cells were transfected with 30, 60 or 90 nM siRNA targeting FOXM1 together with control siRNA targeting GAPDH or CBX7 according to Section 2.3.2. Cells were fixed and stained with DAPI and Cell Mask according to Section 2.4. Cells were then imaged and quantified according to Section 2.5. **(A)** Mean cell number/well and mean cell area at 30 nM. **(B)** 60 nM **(C)** 90 nM. Bars denote mean +SD of a single representative experiment.

3.5 *Validation of 6-phosphogluconate dehydrogenase (PGD) siRNA knockdown in MDA-MB-468 cells*

As stated previously, of the 20 siRNAs to activate senescence within both p16-positive cancer cell lines, 11 targeted RPs and six of these were prioritised for further investigation (see Chapter

4). Of the remaining nine non-ribosomal hits, PGD was selected for further validation as Kaplan Meier analysis together with recent studies within the literature suggest PGD may be a poor prognostic marker in BLBC and implicate PGD in senescence evasion in the non-small cell lung adenocarcinoma cell line (H1975, p53 and p16 mutated) (Sukhatme and Chan, 2012, Chan et al., 2013). This work formed the basis of an MRes student research project and the data shown in Figure 3.11A-B was obtained by Daniel Yee (an MRes student in the Bishop Laboratory, May 2014-September 2014).

PGD is the second enzyme in the oxidative branch of the pentose phosphate pathway (PPP), sometimes referred to as the hexose monophosphate shunt. The oxidative PPP is a glucose metabolising pathway in which glucose-6-phosphate is converted to ribulose-5-phosphate (essential for nucleic acid synthesis) to produce nicotinamide adenine dinucleotide phosphate (NADPH) and CO_2 (reviewed in Stanton, 2012). It is well known that the PPP rate-limiting enzyme, glucose-6-phosphate dehydrogenase (G6PD), is often upregulated in cancer and that PPP activity is thought to be vital for the survival of hyper-proliferative cells (Boros et al., 1998, Tian et al., 1998). Importantly, the PPP has been found to be up-regulated in breast cancer metastases and Kaplan Meier analysis revealed that elevated PGD expression in BLBC is associated with a poor prognosis (HR=1.4, p=0.012, 10 year relapse free survival, N=580). More recently, it has also been shown that shRNA knockdown of PGD in H1975 cells resulted in a senescence-like phenotype together with reduced cell migration (Sukhatme and Chan, 2012, Chan et al., 2013).

In order to validate PGD siRNA knockdown at the protein level in MDA-MB-468 cells, the rabbit anti-PGD antibody was first examined via western blotting. MDA-MB-468 and HMEC cell lysates were probed for PGD according to Section 2.6. Western blot analysis revealed one clean band at approximately 45KDa in both cell lysates, confirming the specificity of the antibody (data not shown). Subsequently, MDA-MB-468 cells were reverse transfected in 6-well plate format with a pool of three siRNAs targeting PGD or each of these three PGD siRNAs individually, according to Section 2.3.5. After 48 hr, the cells were harvested for western blotting and the lysates were probed for PGD according to Section 2.6 (Figure 3.11A-B). After 48 hrs, all three PGD siRNAs together with the siRNA pool induced a significant reduction in PGD protein levels of more than 50%, validating each of the siRNAs used within the siRNA screens.

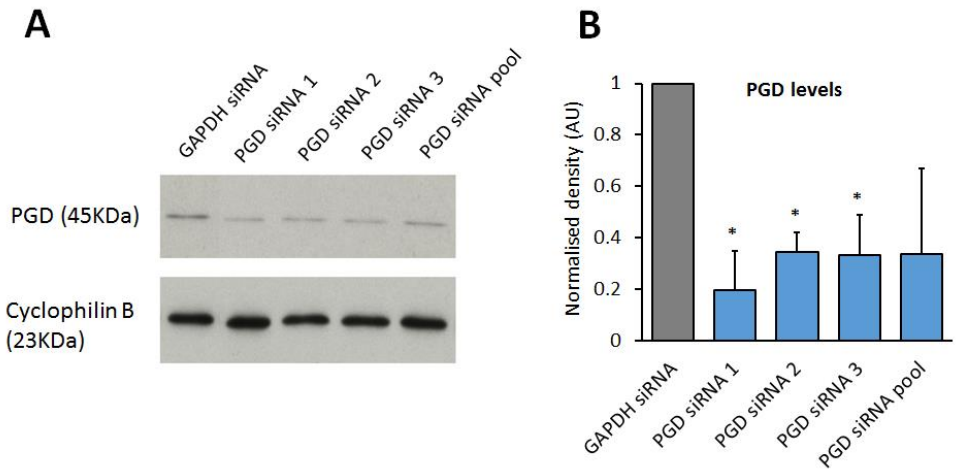

Figure 3.11: Validation of PGD siRNA knockdown in MDA-MB-468 cells. MDA-MB-468 cells were reverse transfected with three individual siRNAs or a 30 nM siRNA pool targeting PGD or 30 nM GAPDH siRNA according to Section 2.3.5. After 48 hrs cells, were lysed for western blotting and probed for PGD according to Section 2.6. **(A)** Representative western blots depicting PGD levels in MDA-MB-468 cells. Lysates were probed for rabbit anti-PGD and the rabbit anti-cyclophilin B antibody was used as a loading control. Antibody dilutions and conditions may be found in Section 2.6. **(B)** Densitometry analysis of PGD levels post siRNA transfection in MDA-MB-468s. Analysis was performed using ImageJ software according to Section 2.6.3. Bars denote mean density levels +SD normalised to GAPDH siRNA of two independent experiments. * = $p<0.05$. The data displayed within this figure was generated by Daniel Yee, MSc student within the Bishop laboratory.

3.6 *Discussion and future work*

3.6.1 *siRNA screening identified 20 siRNAs that activate senescence within two p16-positive cancer cell lines*

In summary, siRNA screening identified 20 siRNAs that activated senescence within two p16-positive cancer cell lines but did not affect the viability of normal HMECs. Strikingly, 11 of these 20 siRNAs targeted RPs (see Section 3.3.3) and a detailed discussion of the mammalian ribosome may be found within Chapter 1, Section 1.7. Of the 11 RPs identified here, six (RPL14, RPL18, RPL34, RPL35A, RPS3A and RPS7) were prioritised for further validation (see Chapter 4) and a discussion of each of these hits and their links with cancer may be found in Section 6.2. In addition, screening identified PGD as a potential senescence evader within p16-positive cancer and a discussion of PGD and its links with cancer and senescence induction may be found in Section 3.5. A brief summary of the current literature linking each of the remaining eight non-ribosomal senescence evaders identified within this thesis with cancer is outlined below.

Glutathione peroxidase 3 (GPX3) is expressed in a wide variety of normal tissues and functions to detoxify ROS and maintain ROS homeostasis (reviewed in Chen et al., 2011). Excessive ROS

levels are potentially cytotoxic and it is well established that elevated ROS plays a critical role in cancer initiation through chromosomal aberrations and point mutations in both oncogenes and tumour suppressor genes (reviewed in Waris and Ahsan, 2006). In addition, ROS can modulate gene expression via direct interaction with both proteins and RNA (reviewed in Chen et al., 2011). However, the exact effect of ROS imbalance on cancer cell survival remains unclear and altered expression of antioxidant enzymes in human cancers has not been widely documented. Interestingly, there is now evidence to suggest that GPX3 may function as a putative tumour suppressor gene that is often silenced in solid tumours. For example, a review of GPX3 expression across 63 cancer cell lines found that the GPX3 promotor was often hypermethylated and that GPX3 expression was down-regulated within many different human malignancies including bladder and head and neck cancers (Chen et al., 2011). In line with this finding, GPX3 has been found to be hypermethylated in prostate cancer (Yu et al., 2007) and oesophageal squamous cell carcinoma (He et al., 2011) and down-regulated in cervical cancer tissue (Zhang et al., 2014). Further, this down-regulation of GPX3 expression in cervical cancer was significantly associated with lymph node metastases and a reduced prognosis (Zhang et al., 2014). By contrast, Herault et al., 2012 showed that increased GPX3 expression correlated with an increased leukemic stem cell frequency (marker of poor prognosis in leukaemia) and a poor prognosis within acute myeloid leukaemia (AML), suggesting that GPX3 may represent a potential therapeutic drug target within AML. Lee et al., 2011 also found GPX3 to be overexpressed in clear cell type ovarian cancer (highly malignant disease subtype associated with a reduced overall survival) when compared with normal ovarian tissue and three additional ovarian cancer subtypes. Together these studies indicate that GPX3 may function in a tissue-specific manner and that in a subset of cancers (such as a 36% of breast cancers, according to the Human Protein Atlas database, available at: http://www.proteinatlas.org/cancer), where GPX3 is expressed, this potential senescence evader may act to protect cells from the cytotoxic effects of excessive ROS levels, enabling proliferation and senescence evasion. In addition, Kaplan Meier analysis indicated that elevated GPX3 expression may be associated with a reduced prognosis in BLBC (N=580, HR=1.23 and p=0.11, data not shown) suggesting GPX3 targeting may hold therapeutic potential within this disease subset.

SPAM1 (sometimes referred to as PH-20) is a hyaluronidase enzyme that functions to degrade hyaluronic acid (HA) located within the ECM of connective tissues. HA is a high molecular mass (HMM) glycosaminoglycan formed of 2,000-25,000 disaccharide units and is important for ECM maintenance (reviewed in Veiseh and Turley, 2011). High molecular mass HA (HMM-HA) is associated with healthy tissue, whereas low molecular mass HA (LMM-HA) (produced by

excessive hyaluronidase activity) is often associated with angiogenesis and tumour dissemination (Bouga et al., 2010). To date, there is no literature implicating SPAM1 activity in senescence evasion in cancer, however, there are multiple studies that have found SPAM1 to be overexpressed in a variety of human malignancies including laryngeal, colorectal and breast cancers (Godin et al., 2000, Bouga et al., 2010, Beech et al., 2002). Interestingly, Beech et al. found SPAM1 levels to be increased in tumours of African American women with metastatic breast cancer compared with Caucasian women with equivalent disease. This finding suggests SPAM1 expression and its role within metastatic breast cancer may differ depending on patient ethnicity. Importantly, increased SPAM1 expression appears to be associate with cancer progression and metastatic disease and multiple studies have shown SPAM1 elevation in secondary metastases compared with primary tumours (Goodin et al., 2000 and Beech et al., 2002). In line with these studies, Wang et al., 2004 found SPAM1 expression was elevated in breast tumours when compared to normal breast tissue and SPAM1 expression was identified in 83.3% of metastatic secondary tumours compared with just 58.4% of primary breast tumours, implicating SPAM1 in metastatic disease.

IL13RA1 is a subunit of the interleukin receptor 13 (IL13R) (important mediator of the inflammatory response) and is the primary interleukin 13 (IL13) binding site within the receptor. IL13 and its receptor have been found to be overexpressed in many human malignancies, including breast cancer (Kapp et al., 1999, Debinski et al., 1999, Srabovic et al., 2011). Further, Srabovici et al. noted that increased IL13 expression was associated with increased tumour size in patients with lymph node negative disease. There was no direct correlation, however, in patients with metastatic disease. Conversely, Formentini et al., 2012 showed elevated IL13R expression was associated with a reduced metastasis rate in patients with colorectal tumours. Furthermore, low IL13 levels were associated with a poorer prognosis in these patients, suggesting a tissue-specific role for IL13 signalling within cancer progression.

The topoisomerase enzyme, DNA topoisomerase II (TOP2) mediates the induction of DSBs in an ATP-dependent manner and plays an important role in regulating DNA topology and protecting it from harmful over-winding or under-winding during DNA replication and transcription (reviewed in Chen et al., 2012). Consequently, TOP2 enzymes are exploited by numerous highly effective chemotherapeutics such as Etoposide, Teniposide and Doxorubicin, often referred to as topoisomerase poisons (Osheroff, 1989). TOP2B is expressed in both proliferating and quiescent cells in almost all human tissues and, importantly, is not required for normal cell survival (Woessner et al., 1991, reviewed in Chen et al., 2012). Currently, there is no evidence implicating TOP2B in senescence evasion in cancer and the effect of TOP2B silencing in p16-

positive cancer is a question not yet addressed by the literature. It is possible that within a hyper-proliferative cancer setting, cells may become more heavily reliant upon TOP2B activity to meet the demands of enhanced transcription and DNA replication. Consequently, TOP2B silencing may activate senescence in a cancer-specific manner through disrupted DNA topology.

A literature search for the four remaining non-ribosomal hits: Coiled-coil domain containing 82 (CCDC82), DnaJ (Hsp40) homolog, subfamily C, member 5 gamma (DNAJC5G), Lysine-rich nucleolar protein 1 (KNOP1) and NHS-like 2 (NHSL2) revealed that the function of these proteins is largely unknown and, at present, there are no studies linking any of these candidates to carcinogenesis or senescence evasion.

In order to validate these non-ribosomal hits as novel senescence evaders within p16-positive BLBC cells, further validation experiments, such as those outlined in Chapter 4, ought to be conducted. It is important to note that initial selection of the 86 siRNAs tested within this Chapter was based on a genome-wide siRNA screen performed in HeLa cells that pre-dated this project. Although this strategy identified 20 siRNAs functional within both HeLa and MDA-MB-468 cells, an initial genome-wide based approach within two p16-positive BLBC cell lines such as MDA-MB-468 and BT549 cells (human breast carcinoma, $p16^{+/+}$, $p53^{R249S}$ mutated and RB-null) may have identified additional hits functional within a p16-positive BLBC setting.

3.6.2 *Deciphering the mechanism of senescence activation*

Immunofluorescence staining for p16 identified three siRNAs (targeting RPS18, RPLP2 and UBA52) that induced a significant increase in nuclear p16 protein levels upon senescence activation in HeLa cells (see Section 3.3.4). Subsequent immunofluorescence staining in MDA-MB-468 cells also demonstrated that the activation of senescence via RPS18 knockdown was accompanied by a significant increase in nuclear p16 protein levels and that siRNA targeting of many of the remaining RP hits (including the top six selected for further validation) induced a reproducible, although non-significant increase in nuclear p16 protein levels in these cells. Together, these results suggest that the activation of senescence via RP silencing may be mediated by p16. In addition, the HeLa cells used within this study were confirmed to be p53-negative (see Section 5.1.2) and MDA-MB-468 cells are known to contain the $p53^{R273H}$ gain-of-function mutation, severely reducing the likelihood of a p53-mediated senescence response in these cells. Given this, it is hypothesised that senescence activation following RP silencing in p16-positive cancer cells may be mediated by p16 re-sensitisation. The role of p16 within senescence initiation and maintenance following RP silencing is explored further within Chapter 5.

Recently, FOXM1 was identified as a critical phosphorylation target of CDK4/6/Cyclin D complexes (Anders et al., 2011) and it was hypothesised that in MDA-MB-468 cells CDK4/6/Cyclin D-mediated phosphorylation of FOXM1 may promote cell cycle progression and senescence evasion. Importantly, three potential FOXM1 transcriptional targets identified by the Lam laboratory were also found to be weak senescence evaders within the MDA-MB-468 cell line (see Section 3.4). With this in mind, it was proposed that senescence activation in the MDA-MB-468 cells may be mediated by p16-dependent FOXM1 inhibition. However, siRNA silencing of FOXM1 in MDA-MB-468 cells did not result in senescence induction, suggesting that FOXM1 is not a master regulator of senescence evasion within these cells and that senescence activation following RP silencing is unlikely to be mediated by a downregulation of FOXM1 transcriptional activity (see Section 3.4).

The most well characterised mechanism of p16-dependent senescence induction is via the p16/RB/E2F signalling axis (see Section 1.1.1). However, the MDA-MB-468 cell line is predicted to be RB-null, severely reducing the likelihood of a p16/RB/E2F mediated senescence response. Given this and the data discussed above, it is hypothesised that senescence activation following RP silencing may be mediated by an alternative p16-dependent signalling pathway and future work to explore the involvement of additional RB family members (p107 and p130) downstream of p16 is discussed in Chapter 6.

Chapter 4 **Validation of six ribosomal proteins as cancer-specific senescence evaders**

4.1 *Introduction*

4.1.1 *Chapter aims*

1. To investigate the patient relevance of the top 11 ribosomal hits identified within breast, lung, gastric and ovarian cancer using the Molecular Taxonomy of Breast Cancer International Consortium (METABRIC) and Kaplan Meier datasets.

2. To validate a subset of ribosomal hits as senescence evaders within p16-positive BLBC cells using three individual siRNAs targeting each candidate.

3. To determine whether siRNA knockdown of the ribosomal hits induces any effect on the proliferation or morphology of normal HMECs.

4. To further characterise the senescence phenotype and assess whether senescence induction is associated with elevated β-gal activity.

5. To investigate the long-term stability of the induced senescence phenotype.

4.2 *In silico analysis of the ribosome in breast cancer*

4.2.1 *Analysis of the METABRIC data set reveals extensive ribosomal dysregulation in BLBC*

Data from the siRNA screens implicates the cancer ribosome in senescence evasion and suggests that senescence can be activated in p16-positive cancer cells through the precise targeting of specific RPs (see Chapter 3). Importantly, growing evidence now points towards the cancer ribosome being severely disrupted, favouring the maintenance of a highly proliferative malignant state (see Section 1.7.5). For example, RPs have often been found to be overexpressed in a multitude of human cancers (reviewed in Ruggero and Pandolfi, 2003, de las Heras-Rubio et al., 2014), including breast, and key tumour suppressor genes, such as RB and p53, responsible for regulating ribosomal biosynthesis, are commonly mutated in cancer resulting in unchecked ribosomal assembly and activity (see Sections 1.7.4 and 1.7.5).

In order to investigate the degree of ribosomal dysregulation within BLBC, and, crucially, to ascertain the patient relevance of the ribosomal hits identified here, the publically available METABRIC dataset was mined for ribosomal transcript expression level changes. The METABRIC dataset compiles gene expression and prognostic data (such as tumour subtype and grade) for over 2,000 matched breast tumour samples. The average expression level for each of the ribosomal transcripts within the normal samples was compared to the level in each of the five PAM50 breast cancer subtypes. Expression levels were also assessed in the p16-high tumours (top 50% of p16-positive tumours) regardless of subtype and the results are displayed in Figure 4.1A.

This analysis revealed considerable dysregulation across the entire ribosome in each of the five breast cancer subsets, with many of the ribosomal transcripts (encoding both 40S and 60S components) up-regulated in the cancer setting. Strikingly, the ribosome appears to be the most disrupted in the Basal-like tumours and this pattern of dysregulation is mirrored in the p16-high tumours, unsurprisingly given the p16 status of the vast majority of BLBCs. Importantly, all 11 ribosomal hits identified by the siRNA screens were frequently upregulated in both the BLBC and p16-high subsets. This is highlighted by an example frequency distribution plot for one of the siRNA screen hits, RPL34 (Figure 4.1B).

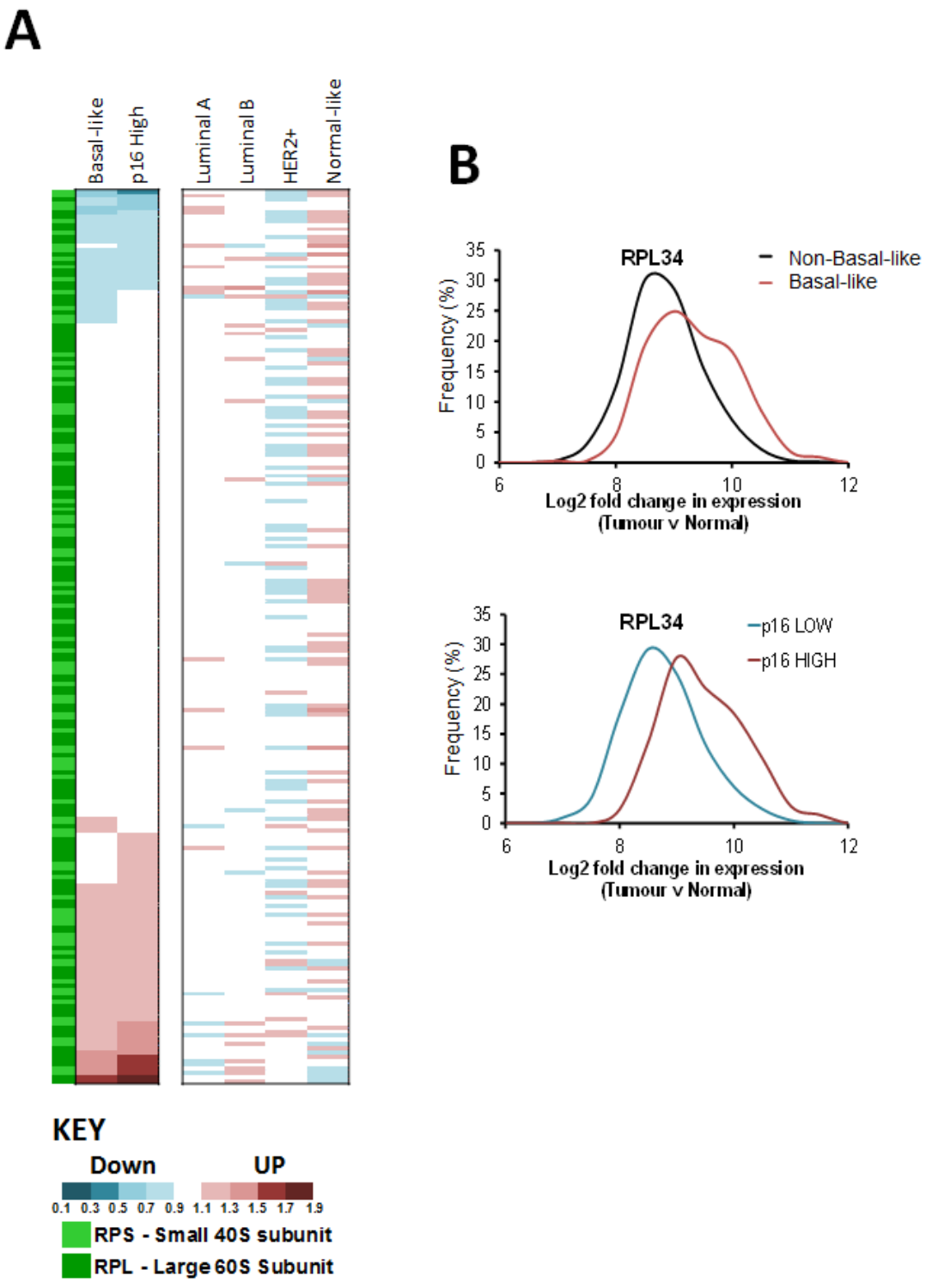

Figure 4.1: ***In silico*** **analysis of ribosomal transcript expression within breast cancer. (A)** Heatmap depicting dysregulated ribosomal transcript expression (Log2) within Basal-like tumours and p16-high tumours relative to the total METABRIC dataset. Expression levels for each of the ribosomal transcripts was also assessed in the Luminal A, Luminal B, HER2+ and Normal-like PAM50 subtypes. **(B)** Frequency distribution plots depicting Log2 fold changes in RPL34 expression within Basal-like versus Non-Basal-like tumours and p16-high tumours versus p16-low tumours.

4.2.2 *Analysis of the Kaplan Meier database reveals elevated expression of a subset of ribosomal transcripts is associated with a reduced prognosis in BLBC*

Next, the Kaplan Meier database was mined to ascertain whether the dysregulation in the expression of the RP hits observed within the METABRIC dataset influenced patient outcome (Kaplan Meier database found at: http://kmplot.com/analysis/). The Hazard Risk (HR) for elevated expression of each of the ribosomal hits was examined across all breast cancers and within four of the five PAM50 subtypes (Normal-like tumours are not annotated within the Kaplan Meier database). The data obtained for all available Affymetrix probes for each transcript is show in Figure 4.2A. For the pseudogenes RPL32P7 and RPL32P36, there were no probes available. Therefore, probes targeting RPL32 were analysed instead. Interestingly, elevated expression of a subset of the ribosomal hits resulted in a protective effect on prognosis within the Luminal A and Luminal B subsets, however, for many of the genes, this protective effect was lost within the Basal-like tumours (Figure 4.2A). Crucially, within the Basal-like tumours, elevated expression of six of the 11 ribosomal hits (RPL14, RPL18, RPL34, RPL35A, RPS3A and RPS7)) resulted in a poorer prognosis (indicated by at least one probe) therefore, these genes were prioritised for further investigation and will form the focus of all future work presented in this thesis (Figure 4.2B). These findings are in line with previous studies linking dysregulated ribosomal gene expression and cancer (reviewed in Ruggero and Pandolfi, 2003, de las Heras-Rubio et al., 2014) and provide important *in vivo* support for these ribosomal hits as potential therapeutic targets in BLBC cancer. Further, this data strengthens the rationale for further investigation into the therapeutic and prognostic utility of these hits in BLBC.

4.2.3 *Elevated expression of a subset of ribosomal transcripts is associated with a poor prognosis in lung and gastric cancer*

Given the data obtained for BLBC and the fact that RP dysregulation is a cancer hallmark observed across a wide array of human malignancies, it was hypothesised that elevated expression of a subset of the ribosomal hits may also predict a negative prognostic outcome in lung, gastric and ovarian cancers. The Kaplan Meier databases for these cancers were also mined in order to investigate the HR for elevated expression of the ribosomal candidates within other tumour types as described above (Figure 4.3A-B). As well as examining all lung cancer cases as a whole, cases where patients had previously smoked and cases where patients had never smoked were also analysed individually.

Strikingly, this analysis revealed that elevated expression of the ribosomal hits assessed is associated with a poor prognosis in lung cancer regardless of whether patients had previously smoked. The single exception to this is RPL14 (elevated expression is associated with a protective effect). The negative impact on patient survival is increased in non-smoking patients. Within this subtype, elevated RPL14 expression remains a predictor of a more favourable prognosis, however, importantly, elevated expression of four ribosomal hits (RPL34, RPL35A, RPS7 and RPL32) is associated with a stark, fourfold increased risk of death within ten years of diagnosis compared to a 20-50% increased risk in patients who had previously smoked (Figure 4.3A-B).

Together, this data suggests that, with the exception of RPL14, all ten of the ribosomal hits analysed here may act as novel prognostic biomarkers within lung cancer, with elevated expression a predictor of a negative patient outcome. Moreover, the potency of these potential biomarkers may be increased in non-smoking patients, where elevation of expression may predict an even greater risk of death. Further, this analysis has identified a novel molecular subgroup within non-smoking-associated lung cancer, characterised by high RP expression and a particularly poor patient outcome. It is possible that these tumours may exhibit a greater dependency on ribosomal dysregulation in order to maintain their malignant state. In addition, this data indicates that a subset of the ribosomal hits identified here may also be effective therapeutic targets within lung cancer and in particular, within non-smoking-associated cases. However, validation of these potential targets within lung cancer cells needs to be performed before further conclusions may be drawn.

This data mining exercise also revealed that elevated expression of six of the ribosomal hits (RPL14, RPL18, RPL35A, RPS7, RPLP2 and RPS18) is associated with a reduced prognosis in gastric cancer (Figure 4.3A-B). By contrast, assessment of HRs across the ovarian cancer dataset showed that elevated expression of each of the ribosomal hits within this cancer type had no impact on patient outcome (Figure 4.3A-B). This data highlights that despite having potential clinical relevance within breast, lung and gastric cancers, the RPs identified here are unlikely to hold any prognostic or therapeutic application within ovarian cancer. Together, the findings indicate an intrinsic difference between ovarian and the other cancer types examined here. The data suggests that tumours derived from differing tissues may exhibit varying degrees of ribosomal dysregulation and that ovarian tumours may not be as dependent upon RP upregulation for the maintenance of their malignant state as BLBC or non-smoking-associated lung cancer, for example.

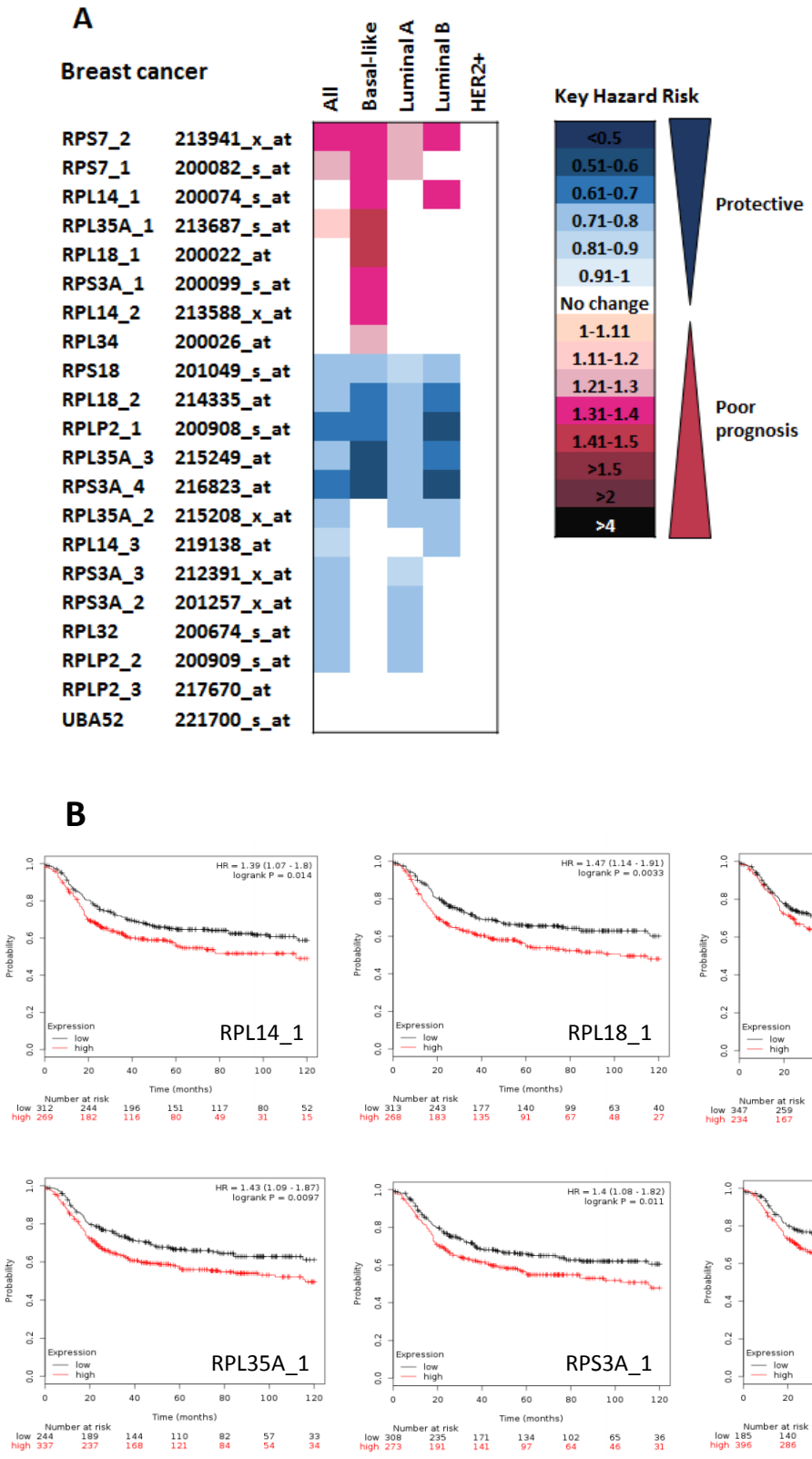

Figure 4.2: Analysis of HR for elevated expression of ten RPs in breast cancer. (A) Heatmap displaying the HR with a logrank p value <0.05 for ten ribosomal hits identified within the siRNA screens for All breast cancer cases (N=3,455), Basal-like (N=581), Luminal A (N=1,680), Luminal B (N=987) and HER2+ (N=207). Data shows 10 year relapse free survival generated by kmplot. Data was split by median expression levels. **(B)** Representative survival plots for the top six ribosomal hits in BLBC cases. Data shows 10 year relapse free survival generated by kmplot. Data was split by median expression levels.

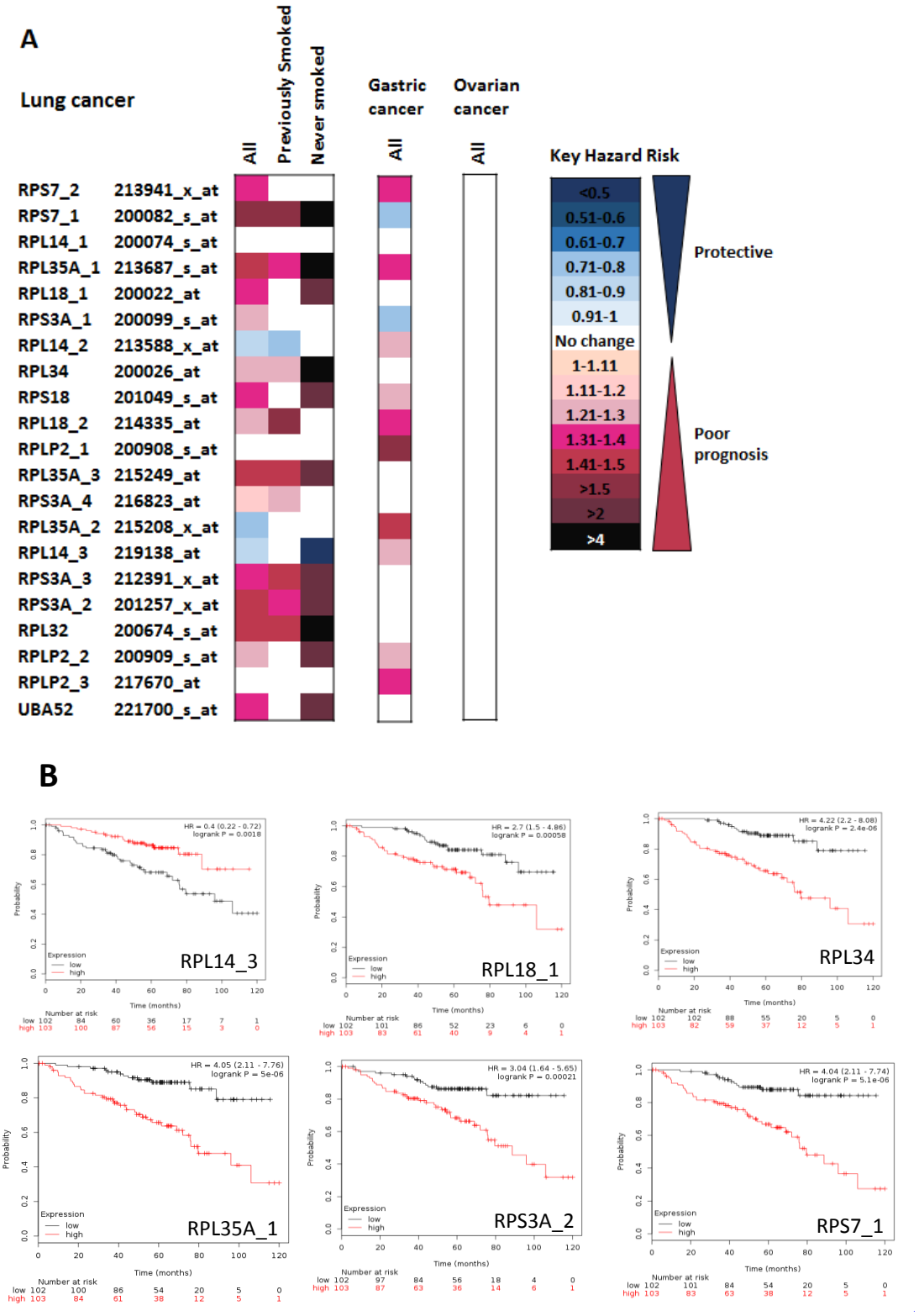

Figure 4.3: Analysis of HR for elevated expression of ten RPs in lung, gastric and ovarian cancer. (A) Heatmap displaying the HR with a logrank p value <0.05 for ten ribosomal hits identified within the siRNA screens for All (N=1,926), those who had previously smoked (N=821) and those who had never smoked (N=205) lung cancer cases, All gastric cancer cases (N=593) and All ovarian cancer cases (N=1,581). Data shows 10 year overall survival generated by kmplot. Data was split by median expression levels. **(B)** Representative survival plots for the top six ribosomal hits in lung cancer cases where patients had never smoked. Data shows 10 year overall survival generated by kmplot. Data was split by median expression levels.

4.2.4 *Analysis of the METABRIC data set reveals co-ordinated dysregulation of ribosomal transcripts in BLBC*

Analysis of the METABRIC dataset revealed considerable dysregulation across the ribosome in BLBC (Figure 4.1A) and analysis of the Kaplan Meir database showed that the elevated expression of a subset of six ribosomal hits was associated with a negative effect on prognosis in the disease subtype (Figure 4.2A-B). Given the structure of the ribosome and the fact that its regulation is finely tuned, it was hypothesised that transcriptional regulation is co-ordinately regulated across the ribosome and that the ribosome may be co-ordinately dysregulated in BLBC. For example, in an instance where one ribosomal transcript is elevated, it was predicted that all other ribosomal transcripts would also be increased. In order to ascertain whether the top six ribosomal hits were co-ordinately dysregulated within Basal-like tumours the expression level of each of the top six ribosomal transcripts was cross compared with each other within 329 Basal-like tumours using the METABRIC dataset. Example scatter plots depicting the correlation between two of the strongest RP hits (RPS3A and RPS7) (R^2=0.533) and RPS3A versus an additional 40S subunit protein (RPS5) (R^2=0.0811) are shown in Figure 4.4A-B. The R^2 coefficient for each cross comparison was calculated and are presented in the form of a heatmap. It was also established that in each case the correlation was positive (in Figure 4.4C).

By contrast with the initial hypothesis, this analysis revealed that the top six RP hits are not co-ordinately dysregulated in BLBC but instead fall into one of two distinct clusters (Figure 4.4D). For example, RPS3A and RPS7 together with (but to a lesser extent) RPL14 and RPL34 appear to be upregulated in BLBC together (Group 1, red) while RPL18 and RPL35A are co-ordinately dysregulated and form the second cluster (Group 2, dark green). Importantly, the expression of Group 1 versus Group 2 transcripts are poorly correlated suggesting that BLBCs may be subdivided into at least two novel molecular subtypes according to their ribosomal signature.

Next, this analysis was expanded to encompass the entire ribosome. The expression level of each of the top six RP hits was compared with the expression level of each of the remaining ribosomal transcripts as described above and R^2 coefficients were calculated and are displayed in the form of a heatmap (Figure 4.5 and Figure 4.6). Multiple probes were available for many of the transcripts and so a total of 222 probes were examined. This analysis revealed that the pattern of differential transcriptional regulation is conserved across the entire ribosome and the previously identified clusters (Group 1 and Group 2) were maintained. For example, a subset of 27 unique ribosomal transcripts (17 encoding 60S subunit proteins and ten encoding 40S subunit proteins) were co-ordinately dysregulated together with Group 1 members: RPL14, RPS3A and

RPS7 but were not co-regulated with RPL18 (Group 2) (Figure 4.5). In addition, a sub-cluster within Group 2 (Group 2b, light green) containing 21 unique probes (13 60S and eight 40S subunit proteins) was identified and transcripts here were co-ordinately regulated with RPL18 only (Figure 4.6). This analysis also revealed two additional clusters (Group 3 (orange) containing 8 transcripts (five 60S and three 40S subunit proteins) co-ordinately regulated with RPL14, RPL18, RPL34, RPL35A and RPS3A but not RPS7) and Group 4 containing those ribosomal transcripts that showed no co-ordinated regulation with any of the top six RP hits (see Appendix, Figure A.4).

This analysis showed that the ribosome as a whole is elevated in BLBC but appears to be dysregulated on a subunit basis. Further, this data suggests that there may not simply be more ribosomes in BLBC cells, instead, a specific subset of RP transcripts appear upregulated according to the tumour context raising the possibility that the cancer-associated ribosome is differentially dysregulated across the disease subtype as indicated by the five novel molecular subtypes identified. The data also suggests that by silencing one ribosomal component (such as RPS3A) there may be widespread effects on the remaining RPs within a given group. Furthermore, the impact of silencing RPS3A may be similar to the knockdown of additional Group 1 RPs (such as RPS7) but may differ to RPL18 (Group 2 component) silencing. In addition, this data also suggests that divergent pathways to senescence activation upon RP silencing may exist. For example, RPS3A silencing may activate an alternative pathway to senescence induction when compared to RPL18 knockdown (see Section 4.7 for further discussion).

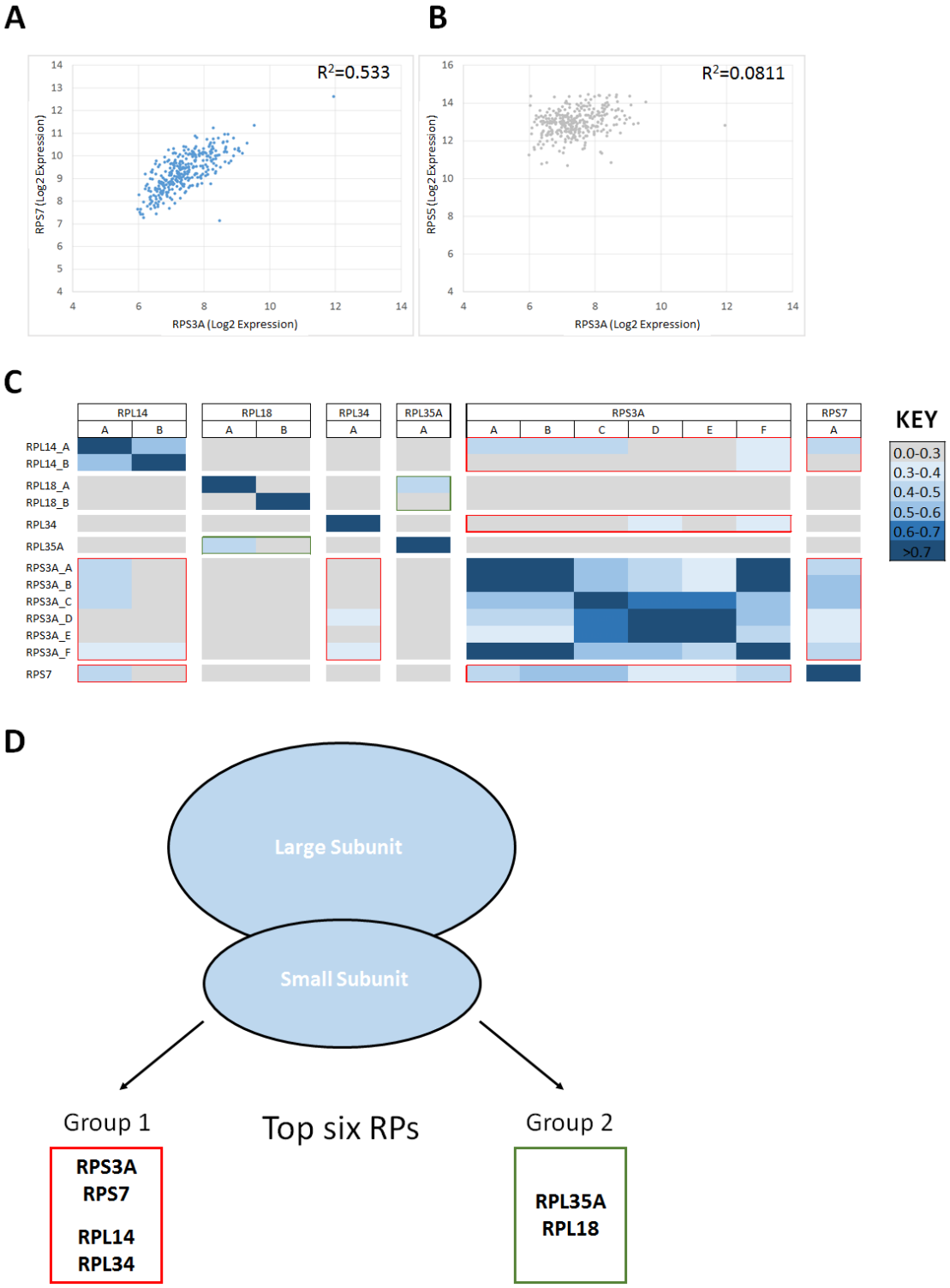

Figure 4.4: Assessment of the correlation of transcript levels between the top six RP hits within BLBC. **(A)** Scatter plot for RPS7 versus RPS3A transcript expression (Log2) within 329 Basal-like tumours. **(B)** Scatter plot for RPS5 versus RPS3A transcript expression (Log2) within 329 Basal-like tumours. R^2 coefficients are shown for **(A)** and **(B)**. **(C)** A heatmap depicting the R^2 coefficients for the cross comparison of each of the top six RP hits within 329 Basal-like tumours. In each case, the correlation was positive. The red and green boxes denote R^2 coefficients>0.3. R^2 coefficients were determined from the METABRIC dataset. **(D)** Cartoon to show the sub-categorisation of the top six RP hits according to their co-regulation within Basal-like tumours. The RP hits are divided into two groups. Group 1 contains RPS3A, RPS7, RPL14 and RPL34 (red) and Group 2 contains RPL35A and RPL18 (dark green).

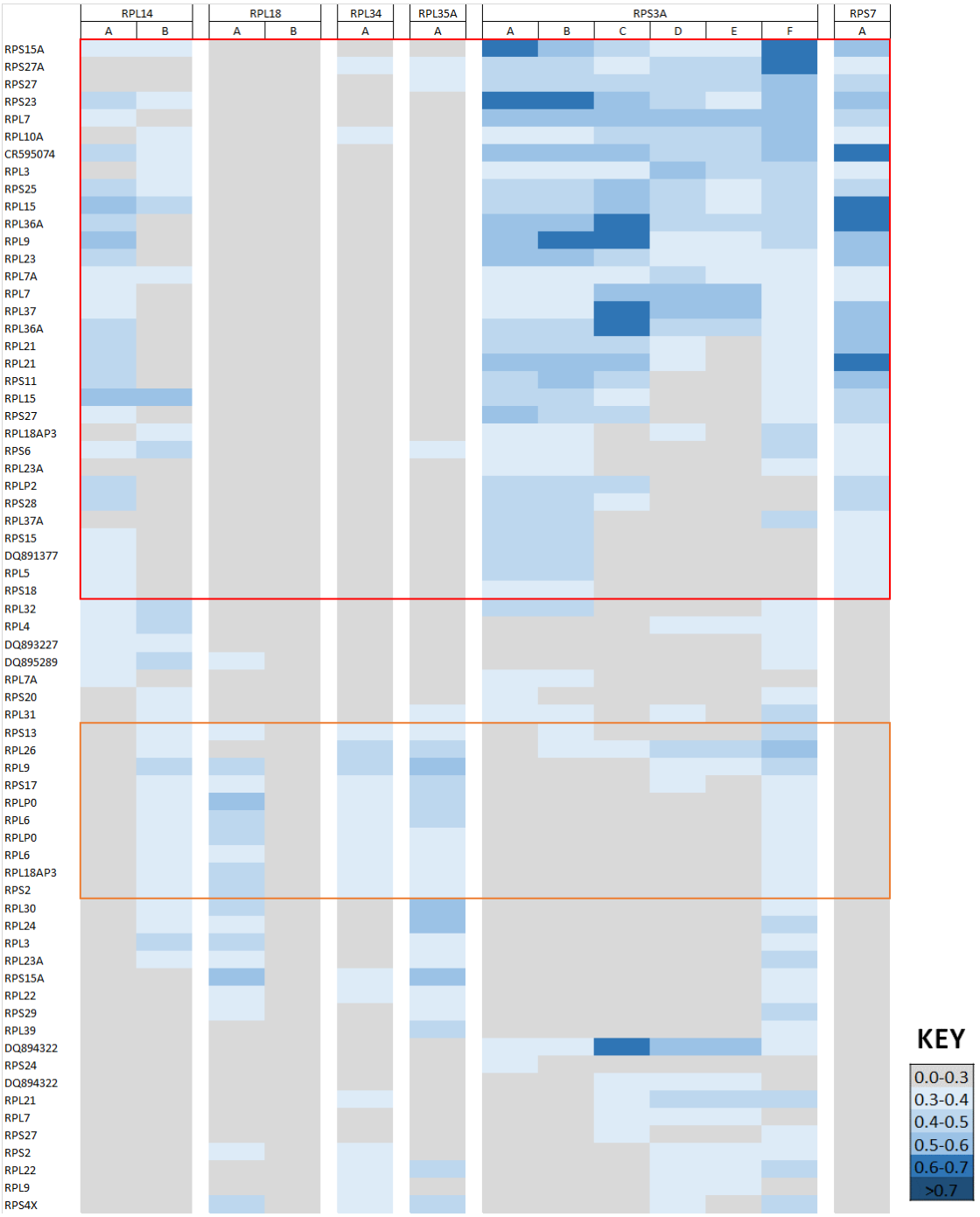

Figure 4.5: Assessment of the correlation of RP transcript levels within BLBC. A heatmap depicting the R^2 coefficients for the cross comparison of each of the top six RP hits with each of the RP transcripts within 329 Basal-like tumours. In each case, the correlation was positive. R^2 coefficients were determined from the METABRIC dataset. The red box highlights those transcripts that correlate with Group 1 RP transcripts (RPS3A, RPS7, RPL14 and RPL34). The orange box highlights those transcripts that correlate with RPL14, RPL18, RPL34, RPL35A and RPS3A (Group 3).

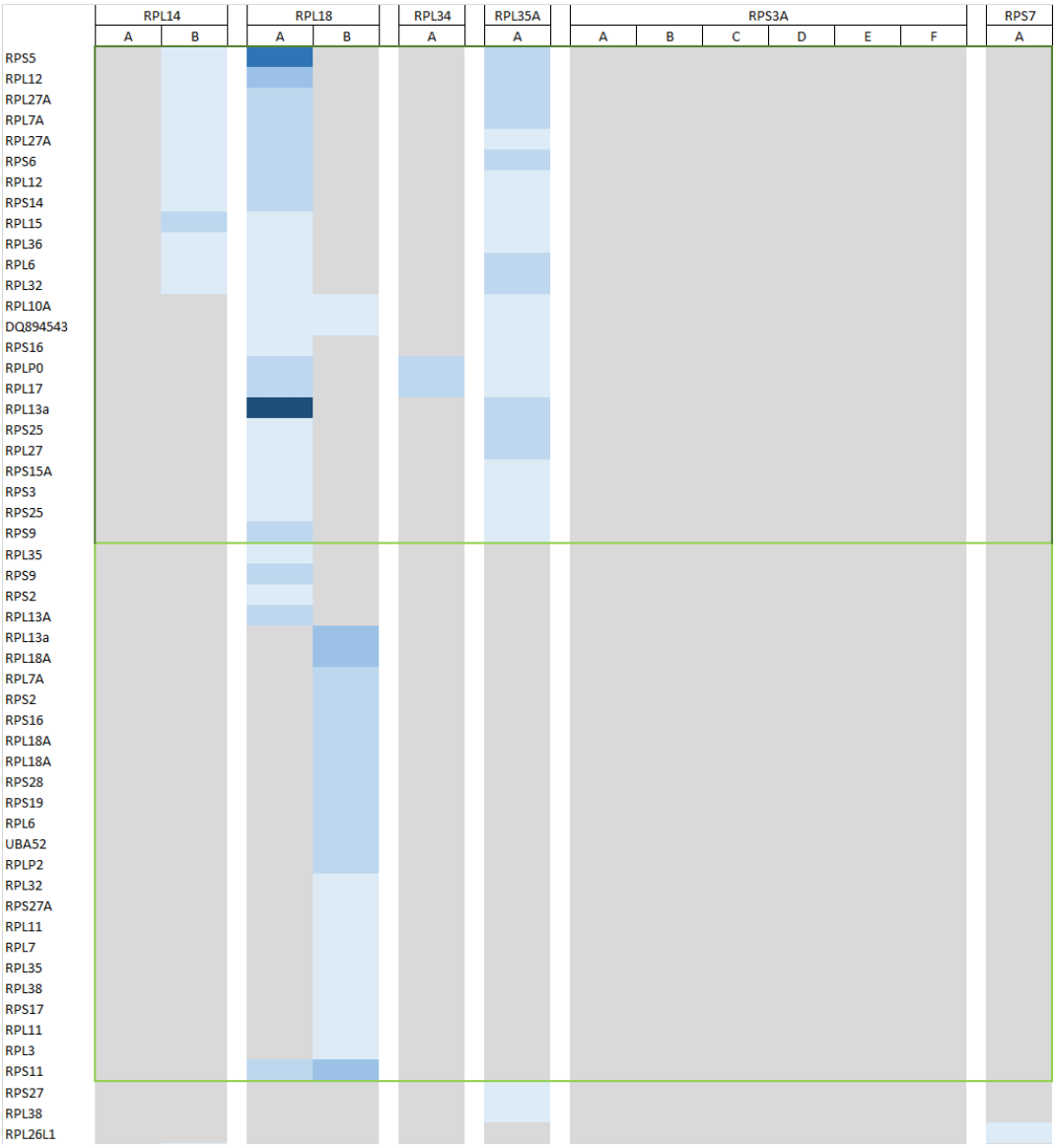

KEY

0.0-0.3
0.3-0.4
0.4-0.5
0.5-0.6
0.6-0.7
>0.7

Figure 4.6: Assessment of the correlation of RP transcript levels within BLBC (continued). A heatmap depicting the R^2 coefficients for the cross comparison of each of the top six RP hits with each of the RP transcripts within 329 Basal-like tumours. In each case, the correlation was positive. R^2 coefficients were determined from the METABRIC dataset. The dark green box highlights those transcripts that correlate with Group 2 RP transcripts (RPL18 and RPL35A). The light green box highlights those transcripts that correlate with RPL18 only (Group 2b).

4.3 *Phenotypic validation of six ribosomal hits in MDA-MB-468 cells*

4.3.1 *qRT-PCR analysis indicates mRNA knockdown of six ribosomal hits in MDA-MB-468s in response to siRNA transfection*

As described in Section 4.2, six RP hits (RPL14, RPL18, RPL34, RPL35A, RPS3A and RPS7) were selected for validation and further investigation.

An important post-screening validation step is to establish whether or not knockdown of specific transcripts is achieved following siRNA transfection. Therefore, to assess the level of siRNA silencing of the top six RP hits, MDA-MB-468 cells were reverse transfected with siRNA pools and gene expression level changes were assessed via qRT-PCR according to Section 2.7. Before gene expression levels of each of the RP transcripts could be investigated, an appropriate housekeeping gene was first identified. A panel of routinely used housekeeping genes (hypoxanthine phosphoribosyltransferase 1 (HPRT1), TATA box binding protein (TBP), cyclophilin A (PPIA) and cyclophilin B, PPIB) were selected for analysis on the basis that their relative gene expression levels did not change upon the induction of cellular senescence in HMECs (Bishop, unpublished). GAPDH was not included in this panel as GAPDH siRNA was used as a negative control within the siRNA transfections. The relative expression level of each of the housekeeping transcripts was assessed in MDA-MB-468 cells treated with 30 nM siRNA targeting GAPDH or RPS3A (Figure 4.7A). This analysis revealed HPRT1, TBP and PPIA expression remained relatively stable (less than 10% change in expression levels) upon senescence activation. Further N=2 analysis of HPRT1 relative expression in MDA-MB-468 cells 72 hr after GAPDH or RPS3A siRNA transfection confirmed HPRT1 mRNA levels remain stable (7.03% +/- 1.46% reduction in RPS3A siRNA sample compared to the GAPDH siRNA treated cells) upon senescence activation (data not shown). As such, HPRT1 was selected to be used for normalisation within all future qRT-PCR analysis (see Section 2.7.4 for further details on qRT-PCR data analysis).

Examination of RP expression levels following siRNA transfection in MDA-MB-468 cells showed that each siRNA pool reduced its corresponding target gene expression by at least 43% when compared to the GAPDH siRNA control (Figure 4.7B). Crucially, this data indicates that at least one siRNA within each siRNA pool is functional against its specific ribosomal target gene. In addition the siRNA pools targeting either RPS3A or RPS7 gave rise to the greatest level of gene expression knockdown (64% and 76.6%, respectively) and were also found to be among the strongest inducers of senescence within the previously performed siRNA screens. This data

indicates that senescence induction following RP siRNA silencing is likely to be a direct result of specific ribosomal gene knockdown rather than the result of an OTE.

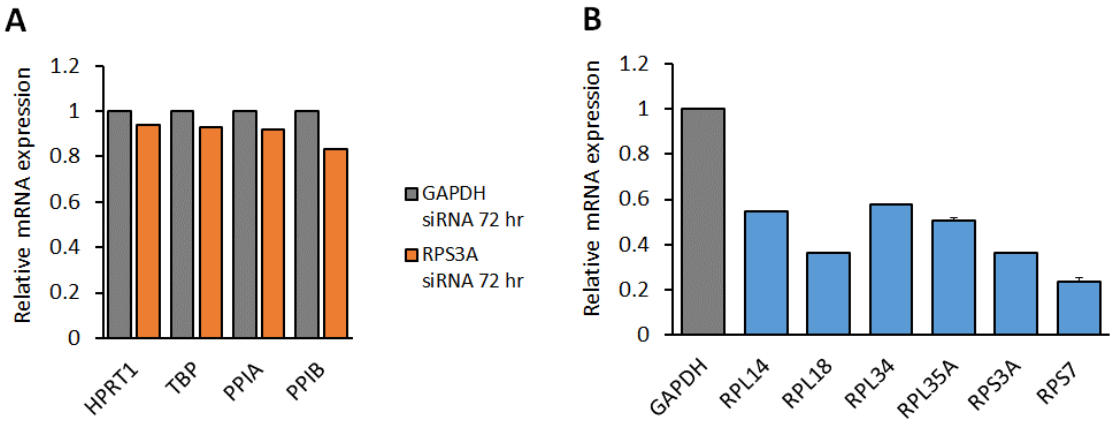

Figure 4.7: Relative mRNA expression levels in MDA-MB-468 cells. (A) MDA-MB-468 cells were reverse transfected with 30 nM siRNA targeting GAPDH or RPS3A according to Section 2.3.2. After 72 hr cells were harvested for RNA extraction, and cDNA conversion and qRT-PCR was performed according to Section 2.7. CT values were normalised to the PPIA standard curve and mRNA expression levels were normalised to GAPDH siRNA. Bars denote relative mRNA expression from a single experiment containing one technical repeat. **(B)** MDA-MB-468 cells were reverse transfected with 30 nM siRNA pools targeting each of the top six ribosomal hits or GAPDH siRNA according to Section 2.3.2. After 72 hr cells were harvested for RNA extraction, and cDNA conversion and qRT-PCR was performed according to Section 2.7. CT values were normalised to the HPRT1 standard curve and mRNA expression levels were normalised to GAPDH siRNA. Bars denote mean mRNA expression levels +SD within a single experiment containing two technical repeats.

4.3.2 *Phenotypic validation of six ribosomal hits in MDA-MB-468 cells*

Once it was confirmed that siRNA knockdown of each of the top six ribosomal hits had been achieved, the siRNA pools were de-convoluted and the three individual siRNAs targeting each ribosomal candidate were validated phenotypically in the MDA-MB-468 cells. MDA-MB-468 cells were reverse transfected with three individual siRNAs targeting each of the top six ribosomal hits and senescence induction was assessed phenotypically according to Section 2.3.2. Multiparameter analysis was also performed in order to ascertain whether or not each of the three individual siRNAs directed against the same ribosomal transcript induced a similar senescence phenotype with shared morphological characteristics.

This analysis revealed that siRNA pools targeting RPL14, RPL18, RPL35A and RPS3A each contained three functional siRNAs, while the pool targeting RPS7 contained two functional siRNAs and just one functional siRNA was identified for RPL34. (Figure 4.8A-C). Multiparameter analysis showed that the individual siRNAs targeting the same RP transcript induced a senescence phenotype with similar phenotypic characteristics, and helps to control for OTEs. For example, it is highly unlikely that an OTE generated by three unique siRNAs (targeting the

same RP transcript) could induce a similar phenotype characterised by eight individual parameters. Interestingly, the majority of the siRNAs tested may be grouped together within Category 6 and is in line with the previous screening data, where the RP siRNAs induced similar phenotypic changes to nuclear and cellular morphology (see Section 3.3.3). However, in contrast with the siRNA screens, this validation exercise showed that RP silencing by each of the functional siRNAs (excluding RPL35A 3) resulted in a significant increase in the number of cellular protrusions (Z scores=6.6, 10.2, 5.7, 9.6, 4.8 and 5.2 for RPL14, RPL18, RPL34, RPL35A, RPS3A and RPS7, respectively). Within the siRNA screens, silencing of RPL18, RPL35A, RPS3A and RPS7 did induce a small, non-significant increase in cellular protrusions (Z scores=0.7, 0.6, 0.7 and 0.4, respectively) and it is proposed that the small-scale nature of the validation experiments has allowed this subtle phenotypic change to be accentuated and better detected.

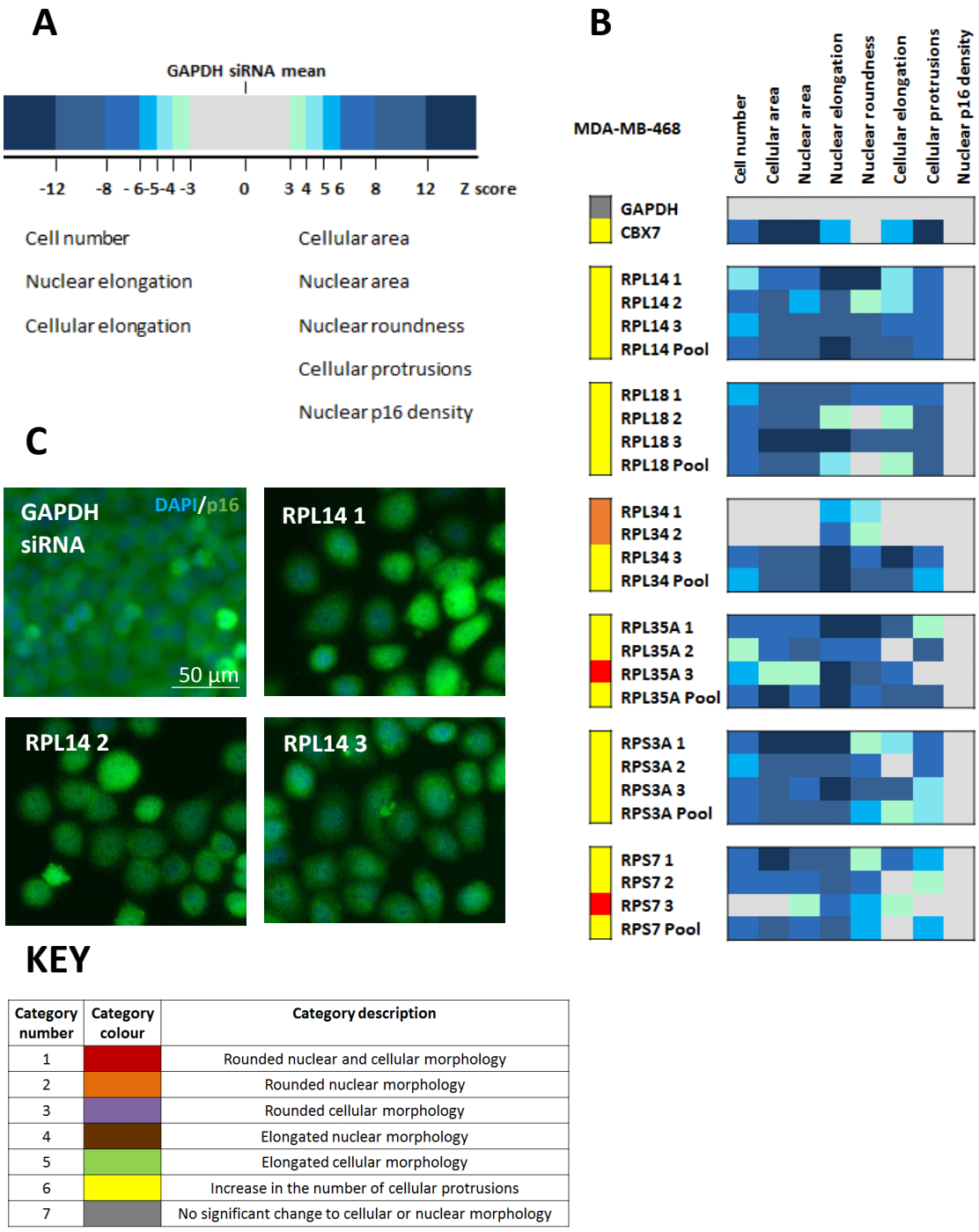

Category number	Category colour	Category description
1		Rounded nuclear and cellular morphology
2		Rounded nuclear morphology
3		Rounded cellular morphology
4		Elongated nuclear morphology
5		Elongated cellular morphology
6		Increase in the number of cellular protrusions
7		No significant change to cellular or nuclear morphology

Figure 4.8: Phenotypic validation of the top six ribosomal hits in MDA-MB-468 cells. (A) Scale bar depicting the number of Z scores that correspond to the colours within the heatmap and the directionality of the quantified senescence-associated changes. **(B)** Heatmap depicting the mean Z score for each of the senescence-associated parameters selected for quantification. Data is from two independent experiments. MDA-MB-468 cells were reverse transfected with 30 nM of three individual siRNAs together with a siRNA pool targeting each of the top six RP hits as well as control siRNAs targeting GAPDH or CBX7 according to Section 2.3.2. After 5 days, cells were fixed, stained and multiparameter analysis was performed according to Section 2.5. **(C)**. Representative immunofluorescence images of MDA-MB-468 cells treated with either GAPDH siRNA or three individual siRNAs targeting RPL14. DAPI (blue), p16 (green). Size bar denotes 50 µm.

4.3.3 *Confirmation of RPS3A and RPS7 protein knockdown via western blotting analysis*

Once siRNA knockdown of the top six RP hits had been confirmed via qRT-PCR and individual siRNAs targeting each of the ribosomal hits had been validated phenotypically, protein knockdown following siRNA knockdown of two of the top six RP hits (RPS3A and RPS7) was assessed via western blotting. MDA-MB-468 cells were reverse transfected with siRNA targeting either GAPDH, RPS3A or RPS7 according to Section 2.3.5. After 5 days, the cells were harvested and cell lysates were probed for RPS3A and RPS7 according to Section 2.6. For both antibodies, western blot analysis revealed one clean band at the appropriate height (approximately 30KDa for RPS3A and approximately 22KDa for RPS7) within the GAPDH siRNA treated lysates (Figure 4.9A). Importantly, quantification, performed according to Section 2.6.3, revealed a 56.67% (+/- 28.37%) reduction in RPS3A levels upon transfection with RPS3A siRNA and a 70.2% (+/- 15.26%) reduction in RPS7 levels upon RPS7 siRNA transfection relative to the GAPDH siRNA control (Figure 4.9B). Together with the qRT-PCR and phenotypic data, this analysis indicates that the siRNA pools targeting RPS3A and RPS7 are specific for their target genes of interest and are able to induce RP knockdown in MDA-MB-468 cells 5 days post transfection.

Interestingly, this data also showed that siRNA knockdown of RPS3A resulted in a statistically significant 79.56% (+/- 12.53%) reduction in RPS7 levels ($p=0.0108$) and silencing of RPS7 resulted in a 23.87% (+/- 27.61%) reduction in RPS3A protein levels (although not statistically significant, $p=0.1776$), indicating a potential degree of interplay may exist between these two RPs (Figure 4.9A-B). This finding is in line with the METABRIC data presented previously (Figure 4.4A), which shows the expression of RPS3A is co-ordinately dysregulated ($R^2=0.533$) with RPS7 within BLBC. Further, this finding suggests that by silencing one RP there may be a knock-on effect for other members of the ribosome that may eventually leave the 'cancer ribosome' unable to translate the proteins required to maintain a highly proliferative phenotype. Given that the p value generated for RPS3A protein levels following RPS7 siRNA knockdown is greater than 0.05, these experiments ought to be repeated with an improved level of transfection efficiency and at a range of time points to attempt to achieve statistically significant knockdown at the protein level. This potential interplay is explored further in Section 4.7.

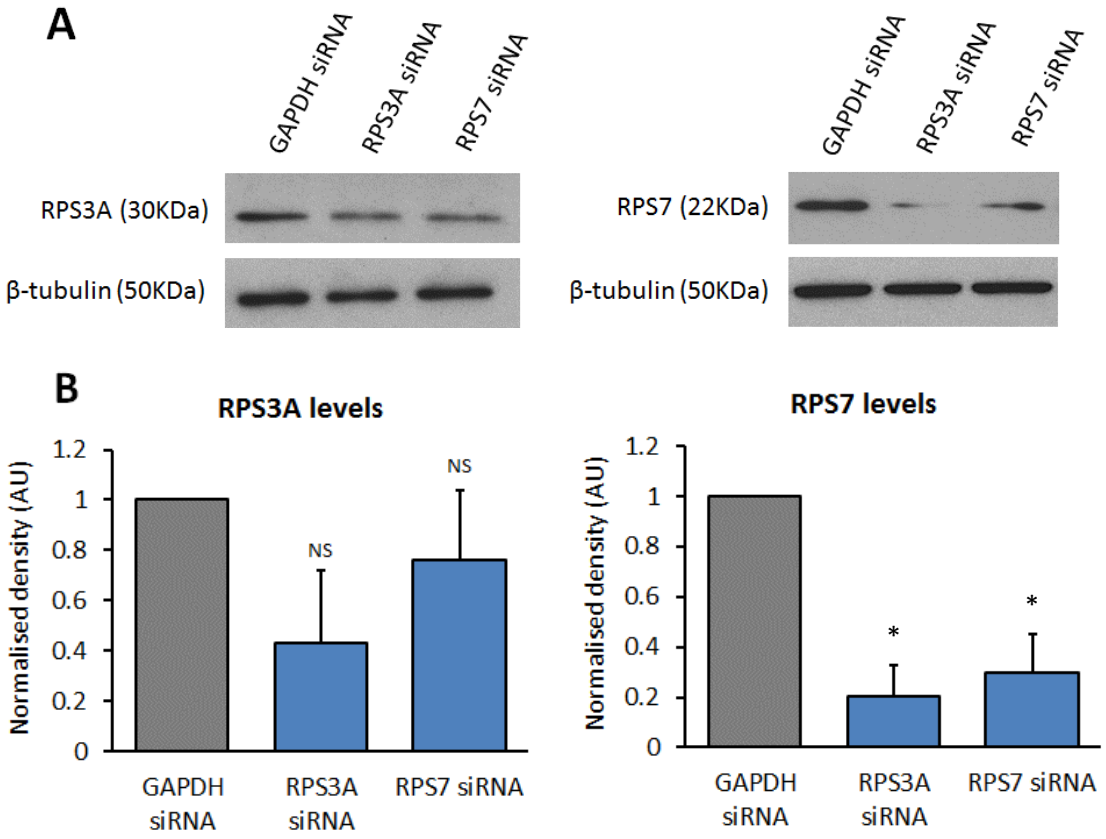

Figure 4.9: Western blot analysis of RPS3A and RPS7 levels post siRNA transfection in MDA-MB-468 cells. (A) Representative western blots depicting RPS3A and RPS7 levels in MDA-MB-468 cells. Cells were reverse transfected with 30 nM siRNA targeting either GAPDH, RPS3A or RPS7 according to Section 2.3.5 and cell lysates were then harvested for western blotting according to Section 2.6. Lysates were probed for either rabbit anti-RPS3A or mouse anti-RPS7 and the mouse anti-β-tubulin antibody was used as a loading control. Antibody dilutions and conditions may be found in Section 2.6. **(B)** Densitometry analysis of RPS3A and RPS7 levels post siRNA transfection in MDA-MB-468s. Analysis was performed using ImageJ software according to Section 2.6.3. Bars denote mean density levels +SD normalised to GAPDH siRNA of two independent experiments. * = $p<0.05$.

4.4 *siRNA knockdown of six RP hits does not induce senescence in normal HMECs*

In order for the RP hits to remain potential cancer-specific drug targets for BLBC, it is vital that their manipulation does not impact the viability of normal cells. Importantly, the original 86 candidates identified for siRNA knockdown within the initial validation screens (see Chapter 3) were selected on the basis that knockdown of these candidates in HMECs did not induce any significant changes to proliferation or cellular morphology (N=1, Bishop et al., 2010). As such, it was hypothesised that siRNA knockdown of these hits in HMECs, as part of a small-scale validation experiment, would not result in any significant impact on proliferation or morphology.

In order to test this, HMECs were reverse transfected with three individual siRNAs, together with a siRNA pool targeting each of the top six RP hits as well as control siRNAs targeting PPIB (siGLO) or CBX7. The transfection step was performed by Dr. Cleo Bishop according to Section 2.3.4, and all subsequent steps were performed by Madeleine Moore. After 5 days, the cells were fixed, stained and imaged according to Sections 2.4 and 2.5. Multiparameter analysis was subsequently performed in order to detect any possible changes in as many senescence-associated parameters as possible.

The positive control siRNA targeting CBX7 induced a premature senescence phenotype characterised by significant shifts in multiple senescence-associated parameters such as a reduction in proliferation, an increase in nuclear p16 protein levels and an increase in cellular and nuclear area (Figure 4.10A). Crucially, none of the ribosomal siRNAs tested induced a significant reduction in proliferation or increase in cell area indicating that, unlike the HeLa and MDA-MB-468 cells, normal HMECs are able to tolerate siRNA silencing of these specific RPs and that their knockdown does not result in senescence induction (Figure 4.10B). However, although RP silencing did not result in any changes to nuclear morphology, this analysis did reveal a significant increase in nuclear area (commonly 3-4 Z scores greater than the siGLO mean), often associated with senescence induction. It is important to note that this increase was less pronounced than that induced by CBX7 siRNA (11.77 Z scores greater than the siGLO mean) and was significantly smaller than the increase observed in MDA-MB-468 cells, where RP silencing induced an increase in nuclear area of 7-9 Z scores above the GAPDH siRNA mean (See Section 4.3.2). In addition, preliminary p16 immunofluorescence staining (N=1) suggested that four RP siRNAs (RPL34 1, 2 and 3 and RPL35A 2) increased nuclear p16 protein levels by 3-4 Z scores above the siGLO mean. Once again, this increase was not as pronounced as that induced by CBX7 silencing (Z score=5.1 above the siGLO mean) but does indicate that RPL34 and RPL35A may be less cancer-specific therapeutic targets.

Together, this data suggests that, unlike within the cancer setting, silencing of certain RPs in normal HMECs does not affect proliferation or cell survival but instead, may result in an increase in nuclear size and for RPL34 and RP35A, an increase in nuclear p16 protein levels. In summary, these findings offer promising support for at least four (RPL14, RPL18, RPS3A and RPS7) of the six ribosomal candidates as potential cancer-specific therapeutic targets in BLBC. However, further investigation into the impact and duration of increased nuclear area and nuclear p16 protein levels on the cell population ought to be conducted. For example, inducible shRNA constructs for each of the top six RP hits could be generated and used to stably silencing the RPs

in HMECs. By employing this strategy, longer-term studies could be conducted and would enable the effects of RP silencing in normal cells to be investigated further.

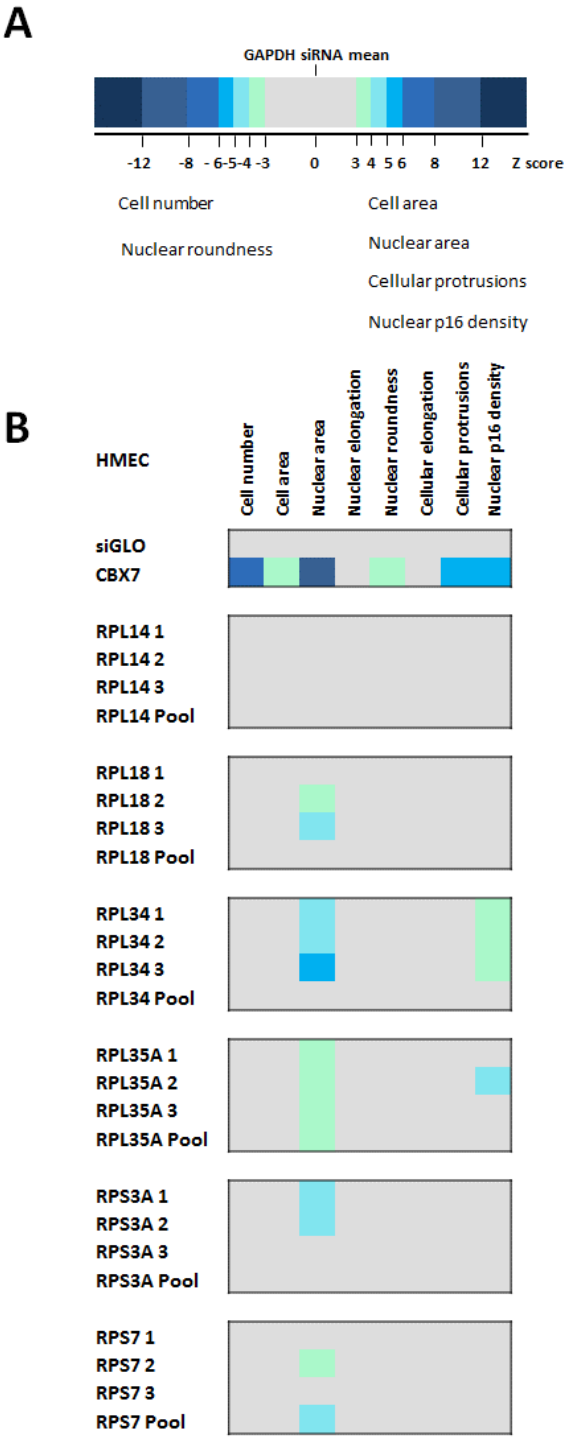

Figure 4.10: siRNA knockdown of the top six ribosomal hits in HMECs. (A) Scale bar depicting the number of Z scores that correspond to the colours within the heatmap and the directionality of the quantified senescence-associated changes induced by CBX7 siRNA. **(B)** Heatmap depicting the mean Z score for each of the senescence-associated parameters selected for quantification. The parameters were selected as senescence induction in HeLa and MDA-MB-468 cells was characterised by significant shifts in each of these measures. For each morphological measure data is from two independent experiments, each containing three technical repeats. Nuclear p16 density is from one single experiment. HMECs were reverse transfected with 30 nM of three individual siRNAs together with a siRNA pool targeting each of the top six RP hits as well as control siRNAs targeting PPIB (siGLO) or CBX7 according to Section 2.3.4. After 5 days, cells were fixed, stained and multiparameter analysis was performed according to Sections 2.4 and 2.5. The siRNA transfection step was performed by Dr. Cleo Bishop.

4.5 *Senescence induction is not associated with increased β-galactosidase activity*

In order to further characterise the senescence phenotype, an additional senescence-associated marker was assessed. β-gal staining was selected for investigation as increased β-gal enzymatic activity is a well-established marker of classical senescence in normal cells (see Section 1.2.3). Further, it is known that siRNA knockdown of CBX7 in normal HMECs triggers the induction of senescence accompanied by increased β-gal activity (Bishop, unpublished). In addition, data presented within this thesis implicates CBX7 as a potent senescence evader within MDA-MB-468 cells and its knockdown induces a senescence response phenotypically similar to that triggered by RP siRNA silencing (see Chapter 3). As such, it was hypothesised that the induction of senescence via both CBX7 and RP knockdown would be accompanied by elevated β-gal enzymatic activity. In order to test this, an appropriate incubation time point for assessing β-gal activity in MDA-MB-468 cells was first optimised. Proliferating MDA-MB-468 cells were seeded in 384-well plate format and after 5 days, cells were fixed and stained for β-gal activity according to Section 2.8. Cells were imaged every 2 hr over an 8 hr time course and at 24 hr post fixation. After 8 hr the majority of the culture stained positive for β-gal activity and, as predicted, at the 24 hr time point, 100% of the culture was β-gal-positive (data not shown). Given this, an imaging window of 4-6 hr (where proliferating MDA-MB-468 cells have minimal detectable β-gal activity) was identified. Subsequently, MDA-MB-468 cells were reverse transfected with 30 nM siRNA targeting each of the top six RPs, GAPDH or CBX7 and after 5 days, the cells were fixed and stained for β-gal activity according to Section 2.8. Cells were imaged at 4 and 6 hr post fixation and there were no observed differences between these two time points. As such, representative images from the 6 hr time point only are shown (Figure 4.11).

Interestingly, this analysis showed that, unlike classical senescence, the 'cancer-associated' senescence phenotype induced via either CBX7 or RP silencing in MDA-MB-468 cells is not characterised by any increase in β-gal activity (Figure 4.11). Further, this data is in line with literature that has shown that immortalised cultures often express high β-gal levels (Severino et al., 2000). High baseline levels of β-gal activity within these cells during proliferation may prevent any further increase in expression upon senescence induction and offers an explanation as to why levels have been found to not increase here. Additionally, it is important to note that increased β-gal staining is not a fail-safe senescence biomarker. For example, Dankort et al., 2007 showed that OIS cells in mice expressing mutant $BRAF^{V600E}$ were negative for increase β-gal activity (see Section 1.5.1).

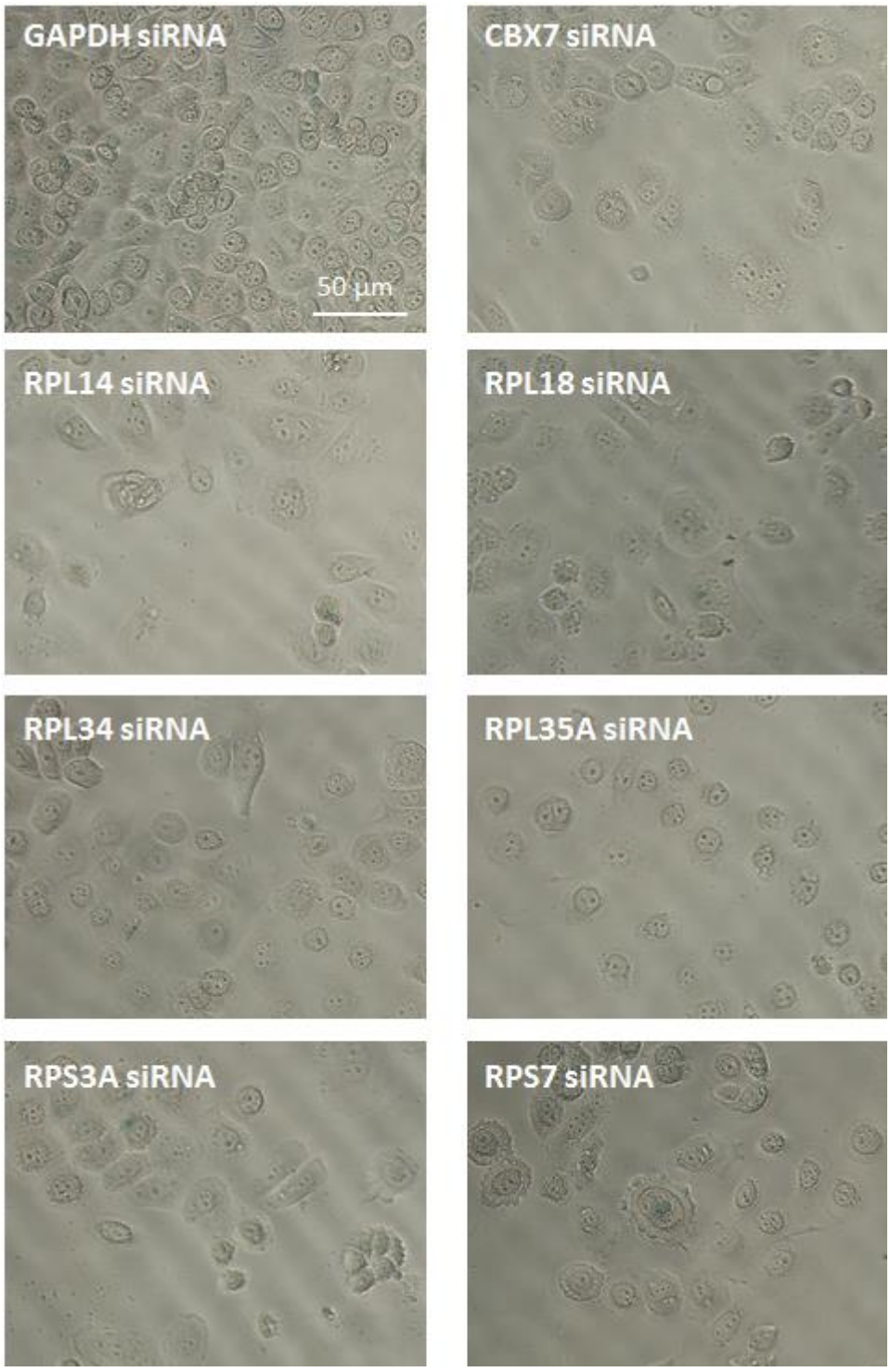

Figure 4.11: MDA-MB-468 cells stained for β-gal enzymatic activity. MDA-MB-468 cells were reverse transfected with 30 nM siRNA targeting GAPDH, CBX7 or each of the top six ribosomal hits according to Section 2.3.2. After 5 days, cells were fixed and stained for β-gal activity according to Section 2.8 and cells were imaged using a light microscope at 20X magnification. Size bar denotes 50 µm. Images were taken at 6 hr after fixation and are representative of two independent experiments, each performed in triplicate.

4.6 *RP siRNA silencing induces a stable senescence phenotype*

Senescence is characterised by a stable cell cycle arrest. As such, the long-term stability of the senescence phenotype following RP silencing was explored. MDA-MB-468 cells were reverse transfected with 30 nM siRNA targeting GAPDH, PLK1 or each of the top six RP hits and after 16 days cells were fixed and cell numbers were quantified according to Section 2.5. The data generated was then compared to a previously performed siRNA screen where MDA-MB-468 cells were fixed and quantified after 5 days (Figure 4.12A). This analysis revealed that by day 16, cell numbers following RP silencing were more than 30 times lower than the value calculated for the GAPDH siRNA, indicating potent cell cycle arrest. Further, for RPL35A, RPS3A and RPS7 siRNA, there was no statistically significant difference between the cell numbers quantified at the 5 or 16 day time points, indicating that senescence induction following RPL35A, RPS3A or RPS7 knockdown is stable for at least 16 days.

However, closer scrutiny of the data revealed that for each of the RP siRNAs there was a subtle increase in cell number from the 5 day to the 16 day time point, indicating a small degree of proliferation had occurred during the longer time course experiment. Furthermore, this increase was statistically significant for siRNAs targeting RPL14, RPL18 and RPL34, suggesting senescence induced by silencing of these three RPs may be less stable than the phenotype following RPL35A, RPS3A or RPS7 knockdown. Importantly, detailed examination of the images acquired at day 16 indicated that, following RP silencing, the majority of the culture was stably arrested while a small subset of cells appeared proliferative in clusters and may have been driving the slight increases in cell number quantified at day 16 (Figure 4.12B). Given this, it was hypothesised that this localised proliferation following RP knockdown may be due to insufficient transcript knockdown in a subpopulation of cells. Previous experiments performed in the Bishop laboratory have shown that by increasing p16 siRNA dose, greater transcript knockdown may be achieved in HMECs (data not shown). As such, MDA-MB-468 cells were transfected with 30-90 nM siRNA targeting GAPDH, PLK1 and each of the top six RP hits and cell numbers were quantified at day 16. Data generated was then compared to a previously performed siRNA screen as described above (N=1, Figure 4.12C-D). Interestingly, this analysis showed that increased RP siRNA did not act to reduce the small degree of cellular proliferation observed during the longer time course experiments and suggests that insufficient transcript knockdown does not drive senescence escape in these cells.

A more likely explanation for this observed localised proliferation following RP silencing is a less than 100% transfection efficiency. MDA-MB-468 cells are highly proliferative and if left

untransfected, a single cell could potentially continue to proliferate, diluting the senescent culture and result in isolated areas of highly proliferative cells. The level of cell death induced by the PLK1 siRNA after 5 days (88.65% +/- 13.40%) indicates the transfection efficiency is high but is unlikely to 100%. Interestingly, there is also an increase (although statistically insignificant) in total cell numbers from the 5 to the 16 day time point following PLK1 siRNA, further indicating a less than 100% transfection efficiency. A second dose of RP siRNA at day 5, following an initial reverse transfection with RP siRNA may boost the transfection efficiency and result in a stably arrested culture. Alternatively, an inducible shRNA construct for each of the RP hits would enable the stability of the senescence phenotype to be better investigated and evade the issues discussed here, commonly associated with siRNA transfection. Further investigation into the stability of the senescence phenotype and the rate of senescence bypass *in vivo* would hold important clinical relevance and may help to establish a therapeutic window for the administration of secondary senolytic therapies. A third possibility is that a subpopulation of the MDA-MB-468 culture may be resistant to RP knockdown. Combination siRNA knockdowns of multiple RPs may circumvent any potential resistance and result in a stably arrested culture.

In addition to a stable growth arrest, senescent cells commonly increase in size over time. With this in mind, MDA-MB-468 cells were reverse transfected with 30 nM siRNA targeting GAPDH, PLK1 or each of the top six RP hits and after 16 days cells were stained with Cell Mask and cell area was quantified according to Section 2.5. The data generated was then compared to a previously performed siRNA screen where MDA-MB-468 cells were fixed and quantified after 5 days (Figure 4.13A-B). It should be noted that, this Cell Mask staining was only performed once and ought to be repeated. However, this preliminary data indicated that cells transfected with siRNA targeting RPS3A or RPS7 may increase in size over time, indicative of a stable cell cycle arrest. Together, these long-term studies have allowed the top six RP hits to be sub-classified into ‘weak’ less stable inducers of senescence (RPL14, RPL18, RPL34 and to a lesser extent, RPL35A) and ‘strong’ more stable hits (RPS3A and RPS7).

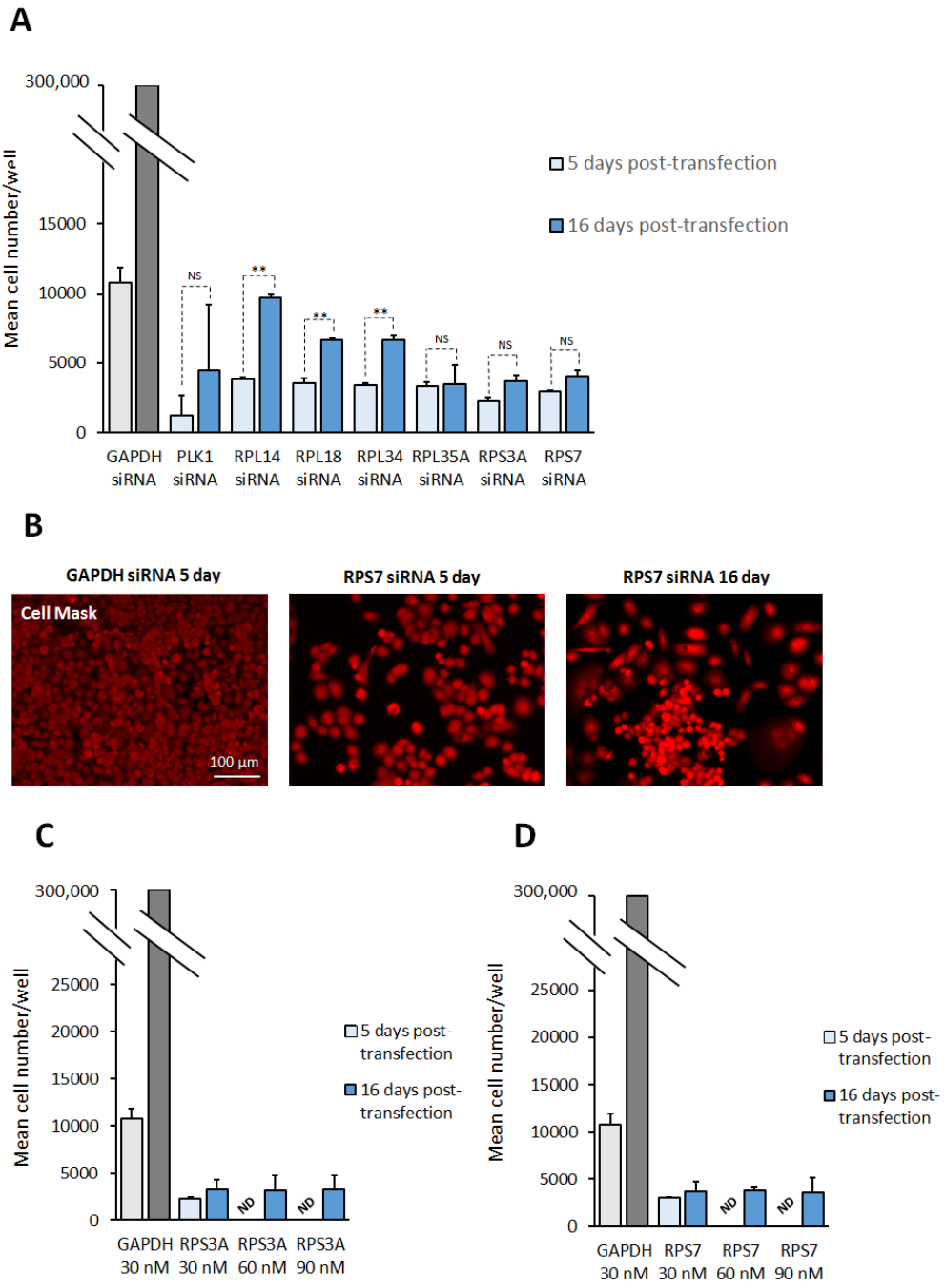

Figure 4.12: Analysis of the long-term stability of the senescence phenotype following RP siRNA transfection. MDA-MB-468 cells were reverse transfected with 30 nM siRNA targeting GAPDH, PLK1 or each of the top six RP hits according to Section 2.3.2 and after 5 or 16 days cells were fixed and cell numbers were quantified according to Sections 2.4 and 2.5. Cell numbers in GAPDH siRNA treated wells could not be quantified as the wells were completely overgrown. Instead, day 16 cell number for the GAPDH siRNA control was calculated based on known population doubling times. **(A)** Mean cell numbers/well at 5 or 16 days post 30 nM siRNA transfection. Bars denote mean +SD of two independent experiments, each performed in triplicate. ** = $p<0.01$. **(B)** Representative images of MDA-MB-468 cells transfected with 30 nM GAPDH or RPS7 siRNA fixed and stained with Cell Mask at either 5 or 16 days post transfection. Images are at 10X magnification, size bar denotes 100 µm. Cell Mask staining was performed once. **(C-D)** Mean cell number/well at 5 or 16 days post siRNA transfection. MDA-MB-468 cells were transfected with 30, 60 or 90 nM siRNA. 5 day transfections at 60 or 90 nM were not performed (indicated by 'ND' on the bar charts). Bars denote mean +SD of a single experiment performed in triplicate.

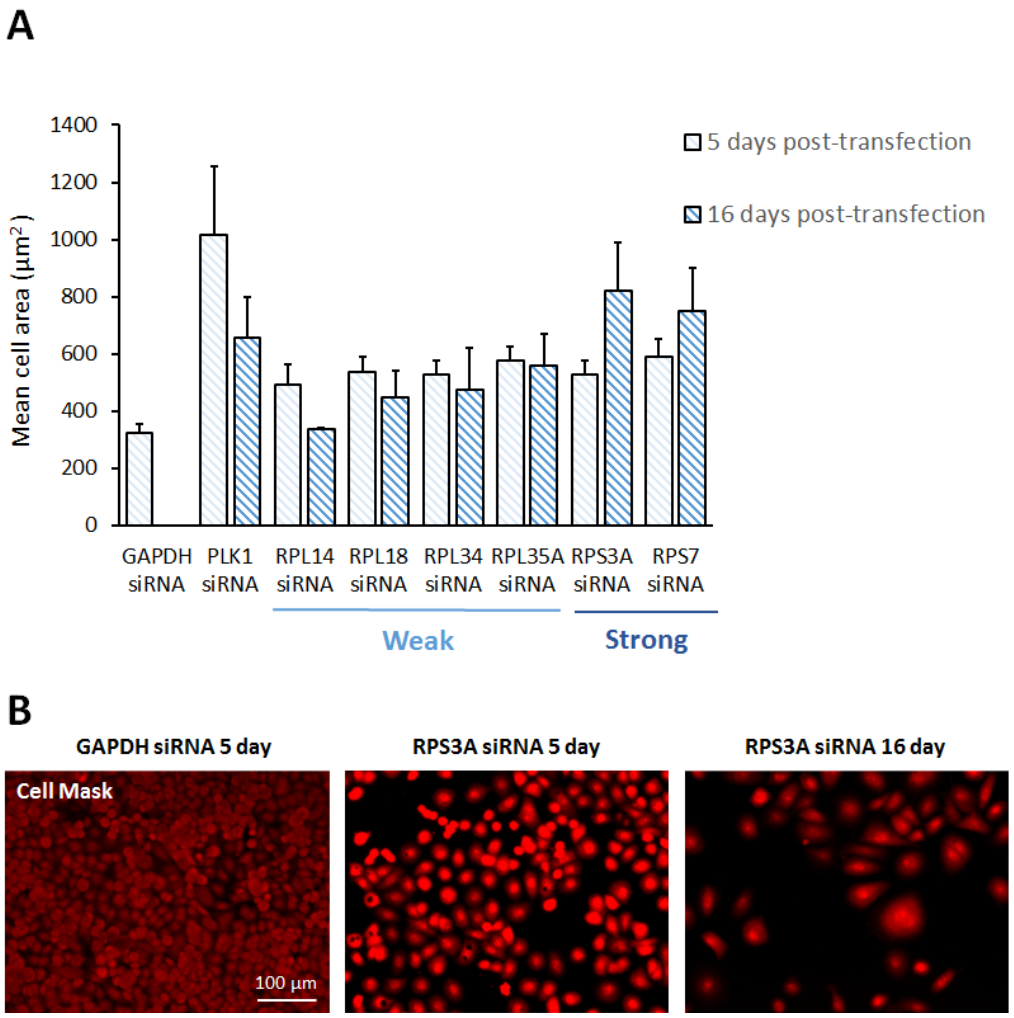

Figure 4.13: Analysis of cell area at 5 or 16 days following RP siRNA silencing in MDA-MB-468 cells. (A) MDA-MB-468 cells were reverse transfected with 30 nM siRNA targeting GAPDH, PLK1 or each of the top six RP hits according to Section 2.3.2 and after 5 or 16 days cells were fixed and cell area was quantified according to Sections 2.4 and 2.5. Cell area in GAPDH siRNA treated wells could not be quantified as the wells were completely overgrown. Bars denote mean cell area +SD of a single experiment performed in triplicate. **(B)** Representative images of MDA-MB-468 cells transfected with 30 nM GAPDH or RPS3A siRNA fixed and stained with Cell Mask at either 5 or 16 days post siRNA transfection. Images are at 10X magnification, size bar denotes 100 µm. Cell Mask staining was performed once.

4.7 *Discussion and Future work*

Within this Chapter the clinical relevance of the top RP hits was investigated using the METABRIC dataset and the Kaplan Meier database for breast, lung, gastric and ovarian cancer (see Section 4.2). Following this analysis, six RPs were prioritised for further validation (see Section 4.3) and testing in normal HMECs offered support for at least four (RPL14, RPL18, RPS3A and RPS7) of the six ribosomal candidates as potential cancer-specific therapeutic targets in BLBC (see Section 4.4). In addition, long-term studies showed that silencing of at least three of the top six RP hits (RPL35A, RPS3A and RPS7) induced a stable growth arrest associated with a slight increase in

cell area over time (for siRNA targeting RPS3A and RPS7). Together these studies have enabled the sub-classification of the top six RPs and have identified RPS3A and RPS7 as the strongest hits. Further discussion of the *in silico* data presented within this Chapter is outlined in Sections 4.7.1 - 4.7.3 and the wider role of each of the top six RPs within cancer is discussed more thoroughly in Chapter 6.

4.7.1 *In silico analysis of the Kaplan Meier database identified six novel potential biomarkers in BLBC*

Analysis of the Kaplan Meier database showed that elevated expression of six RP hits was associated with a poor prognosis in BLBC and suggests that these RPs may represent novel prognostic biomarkers in BLBC (see Section 4.2.2). A tissue microarray (TMA) whereby tumour protein levels of each of the top six RP hits are cross compared with patient information (including p16 status, tumour grade and response to therapy) may support the *in silico* findings presented here and help to further validate these top six RP hits as effective prognostic biomarkers in BLBC. This strategy is disused in more detail in Chapter 6.

Additionally, this analysis also indicated that elevated expression of a subset of the RPs identified may predict a poor prognosis in lung and gastric cancer. Future *in vitro* validation (such as those experiments described in Section 4.3) of these RP candidates in lung and gastric cancer cells lines may provide evidence for these hits as potential therapeutic targets in lung and gastric cancer. Importantly, no correlation between RP expression and prognosis was observed for ovarian cancer indicating that ribosomal dysregulation in cancer may hold an element of tissue-specificity and that the RP identified here are unlikely to be of any prognostic value in ovarian cancer. Given this, Kaplan Meier analysis of all remaining RPs within the breast, lung, gastric and ovarian datasets is a logical next step and may identify additional predictors of disease outcome within these human malignancies.

4.7.2 *In silico analysis of the METABRIC dataset revealed five ribosomal gene signatures in BLBC*

In silico analysis of the METABRIC dataset demonstrated that components of the ribosome are co-ordinately dysregulated on a subunit basis in BLBC and that the disease subtype may be sub-classified into at least five novel molecular clusters (Figure 4.14) according to a tumour's ribosomal signature (see Section 4.2.4). As discussed in Section 4.7.3, this analysis suggests that the silencing of a single RP may impact the expression of additional RPs within the same cluster and that siRNA knockdown of each of the top six RPs may result in differing ribosomal expression

signatures. Future work aiming to explore this potential interplay between specific ribosomal components is discussed in Section 4.7.3.

Disease stratification within a clinical setting based on a tumour's ribosomal expression signature may enable sophisticated personalisation of novel pro-senescent therapies resulting in improved patient outcomes. In addition, profiling the ribosomal signature in BLBC may also be a useful prognostic tool. Stratification of the METABRIC dataset based on the ribosomal expression signature and subsequent analysis of the patient data (tumour grade, p16 expression status, response to therapy) associated with each of the newly identified molecular clusters will help to assess the impact of a particular ribosomal signature on patient prognosis.

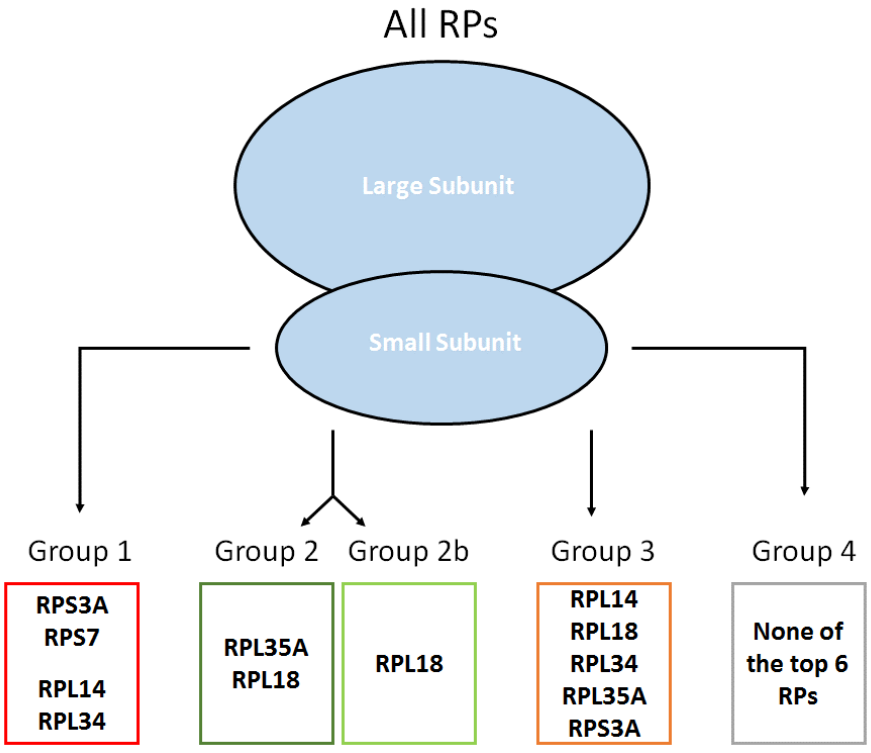

Figure 4.14: Schematic depicting each of the five ribosomal clusters identified within 329 Basal-like tumours following analysis of the METABRIC dataset.

4.7.3 *Western blot analysis revealed a novel interplay between the senescence evaders, RPS3A and RPS7 upon senescence induction*

Interestingly, western blot analysis (presented in Section 4.3.3) clearly demonstrated that a degree of interplay exists between two of the strongest RP hits (RPS3A and RPS7) upon senescence activation. For example, siRNA knockdown of RPS3A in MDA-MB-468 cells resulted in a statistically significant reduction in RPS7 protein levels and, in turn, a modest decrease

(23.87%, +/- 27.61%) in RPS3A protein levels was observed following RPS7 knockdown and senescence induction. Importantly, this data is in line with the METABRIC data presented in Section 4.2.4 that showed RPS3A and RP7 gene expression is co-ordinately dysregulated in BLBC and suggests that silencing of a single RP may impact the expression of multiple other ribosomal components. Given the western blotting data discussed here and the findings from the METABRIC dataset that showed RPS3A is co-ordinately dysregulated with multiple other RPs in BLBC, gene expression analysis was performed for each of the top six RP hits following RPS3A knockdown in order to assess whether these *in silico* findings could be replicated *in vitro*. MDA-MB-468 cells were reverse transfected with siRNA targeting GAPDH or RPS3A and relative mRNA expression levels of each of the top six RP hits was assessed via qRT-PCR (Figure 4.15). Importantly, this analysis was performed only once and needs to be repeated and experiments using individual siRNAs should also be performed. Interestingly, and in line with data presented previously, this preliminary data suggests that a degree of interplay exists between RPS3A and four of the top six RP hits. For example, RPS3A silencing resulted in a 30.62% (+/- 4.19%) decrease in RPS7 mRNA expression together with a 15.4% (+/- 2.52%), 13.35% (+/- 1.15%) and 16.99% (+/- 4.3%) decrease in RPL14, RPL34 and RPL35A expression, respectively. Excitingly, RPS3A silencing did not result in a decrease in RPL18 expression levels suggesting that (unlike RPS3A, RPS7, RPL14, RPL34 and RPL35A) these two senescence evaders do not share any reciprocal interplay. Together, these findings further support the METABRIC data presented in Section 4.2.4 and strengthens the case for differential regulation across the ribosome.

A PCR array whereby the gene expression level of every RP component is assessed following siRNA RP silencing would enable this potential RP interplay to be explored in greater detail and would allow further investigation into the impact of senescence activation on the ribosome as a whole. Following siRNA silencing of each of the top six RP hits in MDA-MB-468 cells, the RT² Profiler™ PCR Array System could be used profile the expression of 86 RPs and establish the ribosome's expression signature upon senescence activation. Crucially, this analysis may validate the *in silico* findings discussed in Section 4.2.4 and may unify or subdivide the top six RP hits depending on their ribosomal profiles generated upon senescence activation. In addition, profiling the senescent ribosome may also help to decipher the mechanism of senescence induction following RP silencing in p16-positive cancer and may reveal additional senescence evaders and potential drug targets in BLBC.

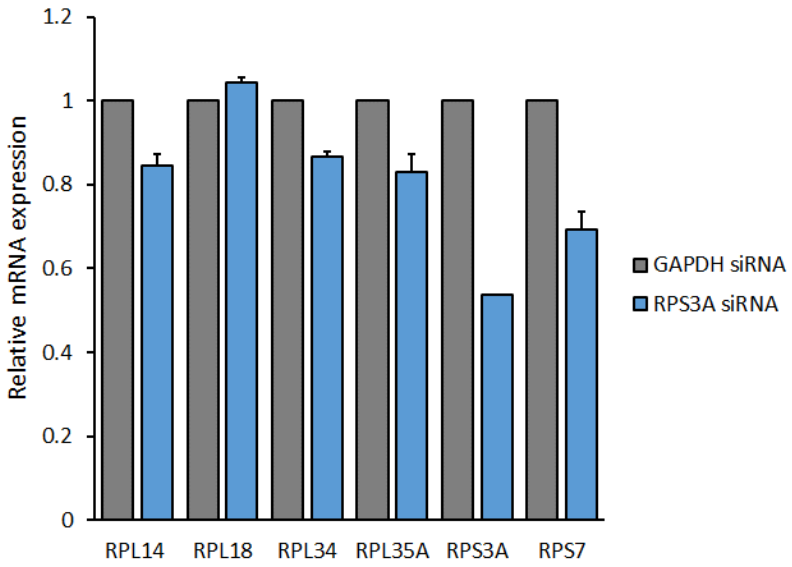

Figure 4.15: Relative mRNA expression levels in MDA-MB-468 cells. MDA-MB-468 cells were reverse transfected with 30 nM siRNA targeting GAPDH or RPS3A according to Section 2.3.5. After 5 days, cells were harvested for RNA extraction and cDNA conversion and qRT-PCR analysis was performed according to Section 2.7. CT values were normalised to the HPRT standard curve and mRNA expression levels were normalised to GAPDH siRNA. Bars denote relative mRNA expression from a single experiment containing two technical repeats.

Chapter 5

Investigating the mechanism of senescence induction following RP silencing in p16+ cancer cells

5.1 *Introduction*

5.1.1 *Chapter aims*

1. To confirm the protein status of three key senescence mediators (p53, p16 and p21) within the HeLa, MDA-MB-468 and MDA-MB-231 cell lines, used throughout this thesis.

2. To investigate the role of p53, p16 and p21 in senescence initiation following RP silencing in MDA-MB-468 cells.

3. To further probe the role of p16 expression in senescence initiation following RP silencing using the p16-null BLBC cell line, MDA-MB-231.

4. To investigate the impacts of RP silencing and senescence activation on the nucleolus (site for ribosomal assembly) in both normal HMECs and in MDA-MB-468 cells.

5.1.2 *Western blotting to demonstrate the p53, p16 and p21 status in HeLa, MDA-MB-468 and MDA-MB-231 cells*

Before conducting studies to investigate the mechanism of senescence activation following RP silencing, first the status of three key senescence mediators was determined in each of the cancer cell lines used throughout this thesis. HeLa, MDA-MB-468 and MDA-MB-231 (p16-null BLBC cell line) cells were harvested and cell lysates were probed for p16, p53 and p21 according to Section 2.6 (Figure 5.1). Importantly, each of the antibodies generated a single clean band at the appropriate height, validating the use of these antibodies for future immunofluorescence staining (uncropped blots may be found in the Appendix, Figure A.1A-C). This analysis confirmed the p16 positivity of the HeLa and MDA-MB-468 cell lines and, as predicted, the MDA-MB-231 cell line was established as p16-null. In addition, the MDA-MB-468 and 231 cell lines were confirmed as p53-positive, whilst the HeLa cell line was found to be negative for p53 protein expression. This finding may be explained by the activity of the viral oncogene, E6, which functions to drive p53 protein degradation via MDM2 upregulation and is commonly expressed by HeLa cells (see Section 1.6.1). Interestingly, all of the cell lines probed were positive for p21.

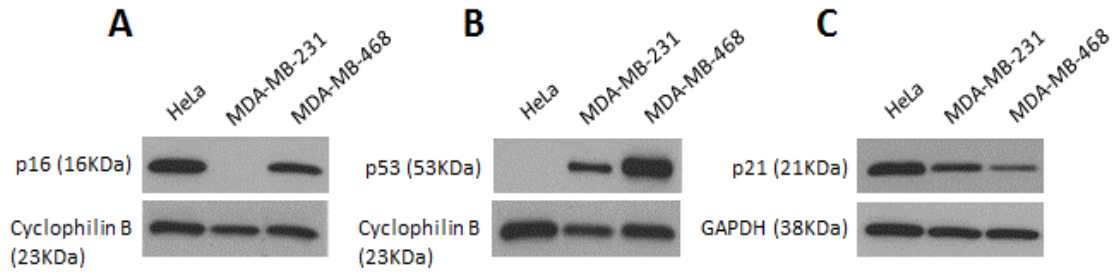

Figure 5.1: Western blot analysis of p16, p53 and p21 levels in HeLa, MDA-MB-231 and MDA-MB-468 cells. Representative western blots depicting **(A)** p16, **(B)** p53 and **(C)** p21 levels in HeLa, MDA-MB-231 and MDA-MB-468 cells. Cell lysates were harvested for western blotting according to Section 2.6. Lysates were probed for mouse anti-p16, rabbit anti-p53 and rabbit anti-p21. Rabbit anti-Cyclophilin B or rabbit anti-GAPDH were used as loading controls. Antibody dilutions and conditions may be found in Section 2.6.

5.2 *Senescence activation in MDA-MB-468 cells is independent of increased nuclear p53 protein levels*

5.2.1 *Senescence induction in MDA-MB-468 is not associated with a significant increase in nuclear p53 protein levels*

The tumour suppressor protein, p53 is a well-established mediator of telomere-associated senescence and has also been implicated in the induction of OIS in mice (see Section 1.5). The stabilisation of p53 has been associated with nucleolar-mediated senescence induction and a

key paper by Fumagalli et al., 2009 demonstrated that the knockdown of specific RPs in A549 cells (p16-null, p53 WT) results in senescence induction together with p53 stabilisation (see Section 1.7.6). Given this, it was hypothesised that senescence activation following RP silencing in MDA-MB-468 cells may be associated with a significant increase in nuclear p53 protein levels and that p53 stabilisation may mediate senescence activation in this context. In order to assess this, the rabbit anti-p53 antibody was first validated via western blotting and optimised for immunofluorescence staining (Appendix, Figure A.1B). Subsequently, MDA-MB-468 cells were reverse transfected with GAPDH siRNA or three individual siRNAs together with a siRNA pool targeting each of the top six ribosomal hits according to Section 2.3.2. Cells were then fixed and stained with DAPI, rabbit anti-p53 and donkey anti-rabbit Alexa Fluor-546 conjugated antibody and nuclear p53 protein levels were quantified according to Section 2.5 (Figure 5.2).

In contrast with the study conducted by Fumagalli et al. this analysis showed that senescence induction in MDA-MB-468 cells via specific RP silencing is not associated with a significant increase in nuclear p53 protein levels. In addition, plates from the original HeLa screen (p53-negative) that were subsequently re-stained for p53 revealed that senescence induction within these cells occurs in the absence of p53 activation (data not shown). Together, this data suggests that within a p16-positive cancer setting, RP silencing results in senescence induction in the absence of significant nuclear p53 stabilisation or activation and that senescence initiation in this context may be mediated via a p53-independent mechanism.

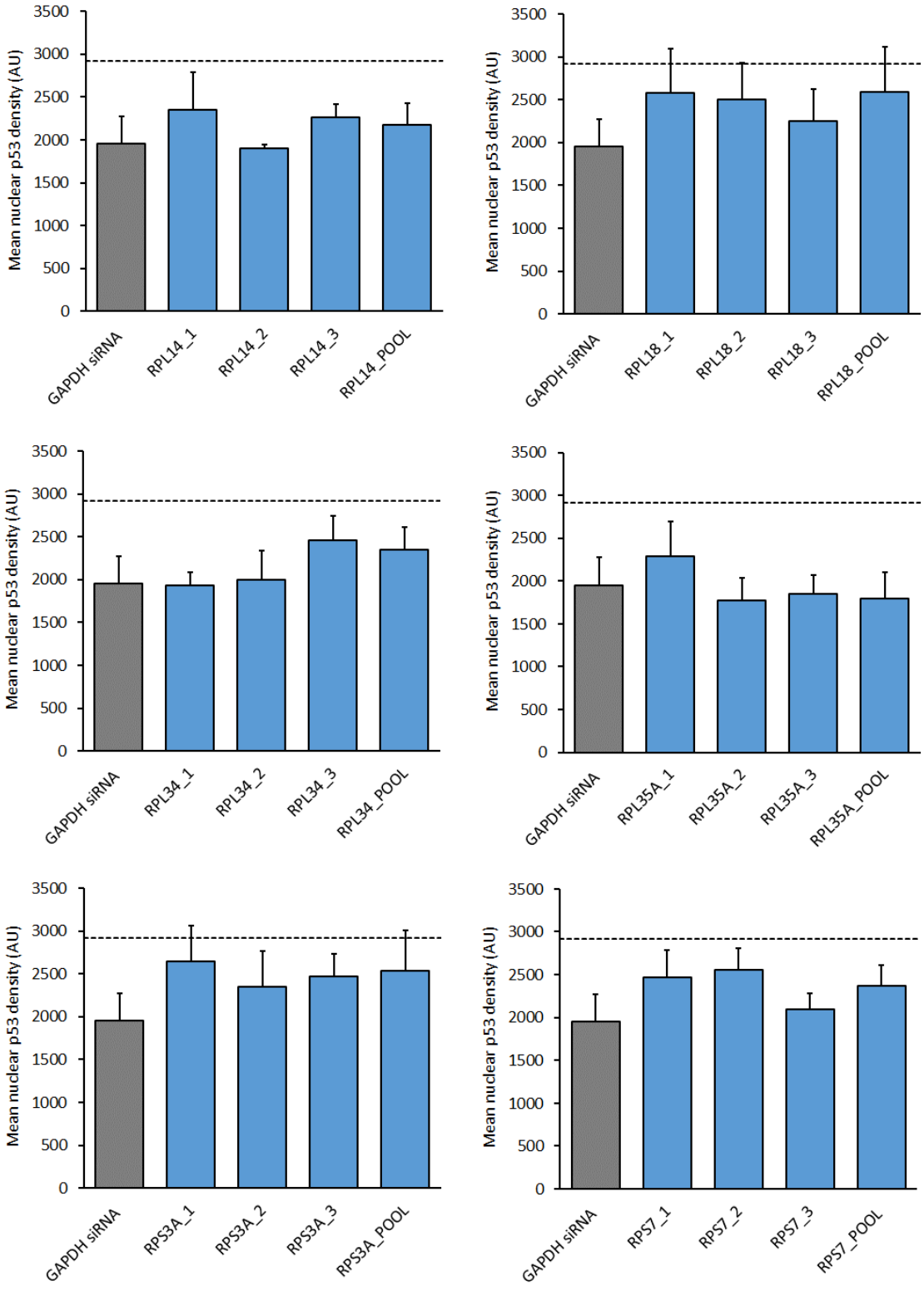

Figure 5.2: Nuclear p53 density levels following RP siRNA transfection of MDA-MB-468 cells. MDA-MB-468 cells were reverse transfected with 30 nM of three individual siRNAs together with a siRNA pool targeting each of the top six RP hits as well as control siRNA targeting GAPDH according to Section 2.3.2. After 5 days, cells were fixed and stained with DAPI, rabbit anti-p53 and donkey Alexa Fluor-546 conjugated anti-rabbit and nuclear p53 density levels were calculated according to Sections 2.4 and 2.5. Bars denote mean +SD of two independent experiments each containing three technical repeats. Dotted line denotes significance threshold at three Z scores above the GAPDH mean.

5.3 *Investigating the role of p16 and p21 in senescence initiation*

5.3.1 *Senescence activation in MDA-MB-468 cells is associated with p16 nuclear translocation*

Given the data presented in the previous Section which suggests senescence activation in a p16-positive context may be independent of p53 stabilisation, it was hypothesised that senescence induction following RP silencing in MDA-MB-468 cells may be mediated by a re-sensitisation to endogenous p16 signalling. The original MDA-MB-468 screening plates were stained with mouse anti-p16 antibody and p16 protein levels were quantified according to Sections 2.4 and 2.5 (see Chapter 3, Section 3.3.4). In addition, MDA-MB-468 validation plates (cells transfected with three individual siRNAs targeting each of the top six RP hits) were also stained for p16 according to Section 2.4 (see Chapter 4, Section 4.3.2). Together, these studies indicated that senescence activation via knockdown of each of the top six RP hits or CBX7 silencing was not associated with a significant increase in total p16 protein levels (data not shown) and this finding was subsequently confirmed via western blotting for two of the strongest RP hits, RPS3A and RPS7 (Figure 5.3A-B).

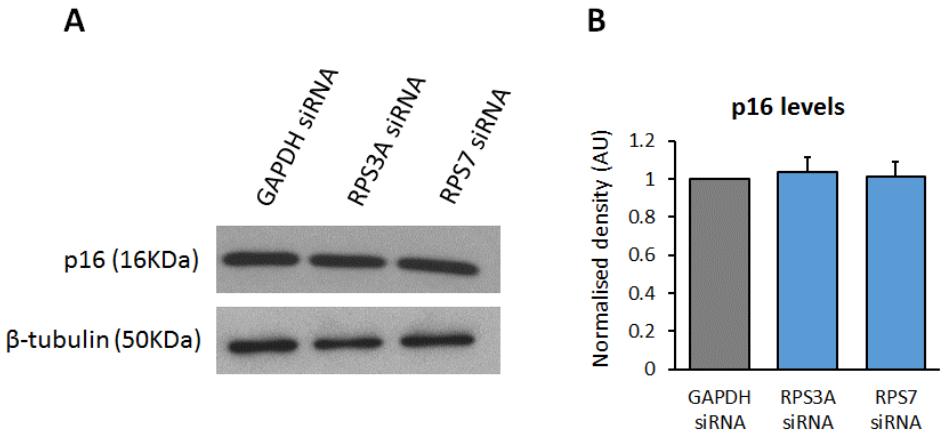

Figure 5.3: Western blot analysis of p16 levels post siRNA transfection in MDA-MB-468 cells. (A) Representative western blot analysis of p16 levels in MDA-MB-468 cells reverse transfected with 30 nM GAPDH siRNA, RPS3A siRNA pool or RPS7 siRNA pool (see Section 2.3.2). Cell lysates were then harvested for western blotting and lysates were probed for mouse anti-p16 according to Section 2.6. Mouse anti-β-tubulin was used as a loading control. Antibody dilutions and conditions may be found in Section 2.6 . **(B)** Densitometry analysis of p16 levels post siRNA transfection in MDA-MB-468s. Analysis was performed using ImageJ software. Bars denote mean density levels +SD normalised to GAPDH siRNA of two independent experiments.

However, re-examination of the images acquired indicated that senescence activation appears to be associated with an increase in nuclear p16 protein levels. Importantly, quantitation of nuclear p16 protein levels within the original MDA-MB-468 screens revealed that senescence induction via RPS18 silencing was associated with a significant increase in nuclear p16 protein

levels (Chapter 3, Section 3.3.4) whilst knockdown of the top six RPs was associated with a non-significant but reproducible increase in nuclear p16 protein levels (data not shown).

Given the data discussed above, it was hypothesised that senescence activation via knockdown of the top six RPs is associated with no overall change to total p16 protein levels but instead, may be associated with a translocation of p16 from the cytoplasm into the nucleus. In order to assess this, MDA-MB-468 cells were reverse transfected with GAPDH siRNA, CBX7 siRNA or siRNA pools targeting each of the top six RP hits and cells were stained with mouse anti-p16 according to Section 2.4. Nuclear and cytoplasmic p16 protein levels were quantified and the p16 nuclear/cytoplasmic ratio was generated on a cell by cell basis according to Section 2.5 (Figure 5.4A-B).

Interestingly, this analysis revealed that the induction of senescence via CBX7 siRNA resulted in a small reduction in cytoplasmic p16 protein levels together with an increase in nuclear p16 protein levels. Further, the p16 nuclear/cytoplasmic ratio was significantly increased when compared to the GAPDH siRNA control, indicating a translocation of p16 protein from the cytoplasm to the nucleus upon senescence induction. Crucially, silencing of two of the strongest senescence evaders, RPS3A and RPS7, also resulted in a decrease in cytoplasmic p16 levels together with an increase in nuclear p16 protein levels and a statistically significant increase in the p16 nuclear/cytoplasmic ratio, indicating a translocation of p16 protein from the cytoplasm to the nucleus. It is proposed that this translocation event may enable a re-sensitisation to p16 signalling upon RP silencing and that senescence initiation and/or maintenance may be dependent on the presence of WT p16 protein within the nucleus. However, further work must be performed in order to investigate the kinetics of this translocation event and to establish whether or not senescence initiation and/or maintenance is dependent on nuclear p16 abundance.

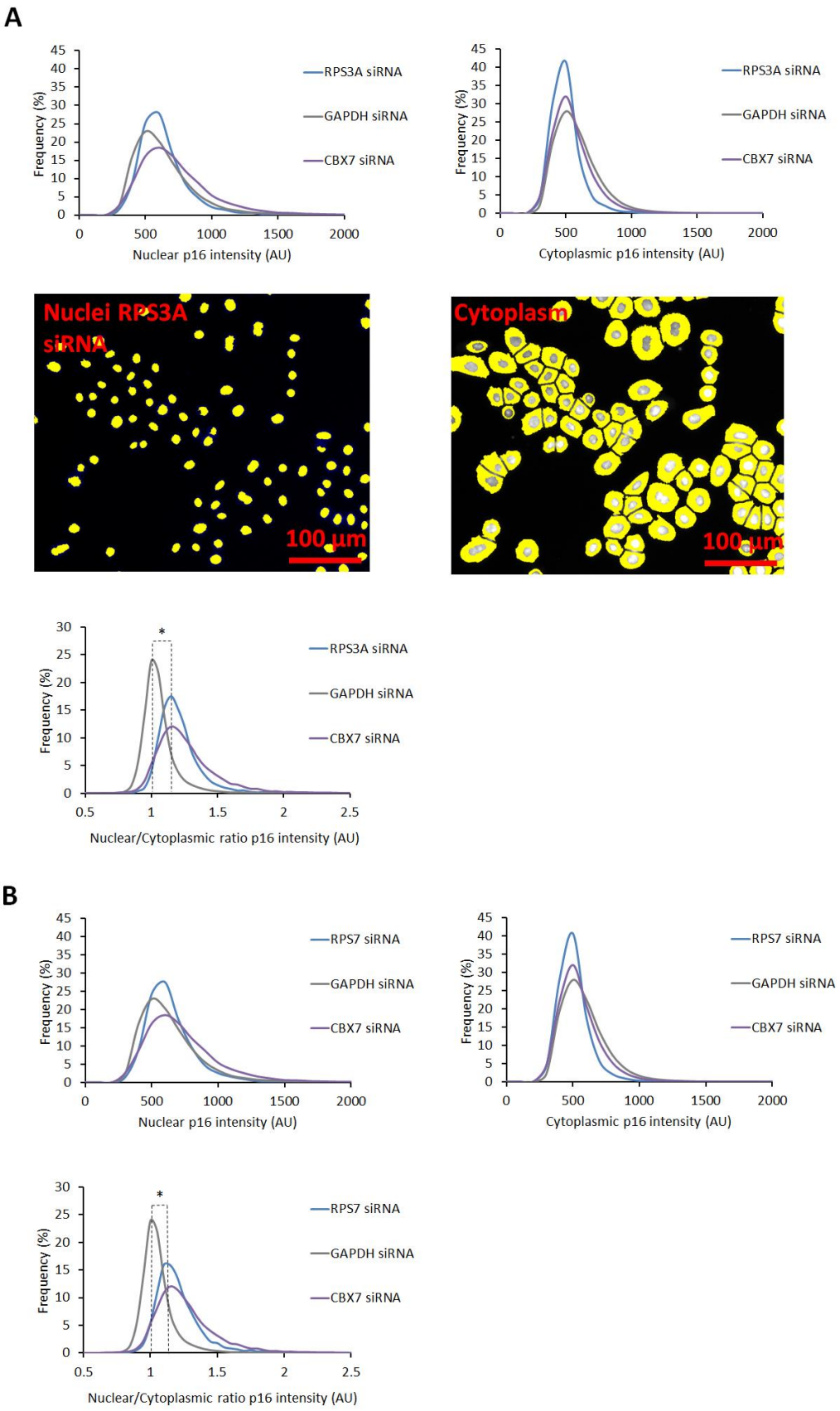

Figure 5.4: Nuclear and cytoplasmic p16 protein levels in MDA-MB-468 cells after RPS3A or RPS7 siRNA transfection. Representative frequency distribution plots of nuclear or cytoplasmic p16 protein levels together with a frequency distribution plot for the p16 Nuclear/Cytoplasmic ratio for MDA-MB-468 cells

transfected with siRNA targeting GAPDH, CBX7 and **(A)** RPS3A or **(B)** RPS7**.** Cells were reverse transfected with 30 nM siRNA and were fixed and stained with DAPI, Cell Mask, mouse anti-p16 and Alexa Fluor-488 conjugated anti-mouse and nuclear and cytoplasmic p16 protein levels were quantified according to Sections 2.4 and 2.5. Two independent experiments, each containing three technical repeats, were performed. Representative immunofluorescence images depict MDA-MB-468 cells transfected with 30 nM RPS3A siRNA and stained with Cell Mask together with the nuclear or cytoplasmic segmentation overlay. Images are at 10X magnification, size bar denotes 100 µm. * = p<0.05.

5.3.2 *Senescence initiation is dependent on p16 expression*

The data presented previously within this Chapter suggests that senescence activation in p16-positive cancer cells following RP silencing may be independent of p53 activation (HeLa screening, p53-negative) or stabilisation (MDA-MB-468s, $p53^{+/+}$) and is associated with a nuclear translocation of p16 protein. As such, it was hypothesised that senescence initiation may be dependent on p16 expression and, in contrast to Fumagalli et al., 2009, RP silencing in a p16-positive cancer setting may result in senescence induction mediated by p16 signalling.

In order to investigate this, double transfections were performed. MDA-MB-468 cells were simultaneously reverse transfected with 30 nM siRNA targeting p16 (previously validated, see Chapter 3, Section 3.2.2), together with siRNA pools targeting each of the top six RP hits according to Section 2.3.2 (Figure 5.5A-B). Given the potency of the senescence induction previously achieved with 30 nM RP siRNA (see Chapter 4, Section 4.3.2), a range of RP siRNA doses (0.3-30 nM) was used in order to maximise the possibility of senescence rescue. GAPDH siRNA at 30 nM or 60 nM was used as a negative control. Importantly, 60 nM GAPDH siRNA was well tolerated and there was no significant difference in proliferation or cellular morphology between the two doses. After 5 days, cells were fixed and stained with DAPI and Cell Mask and cell number and area were quantified according to Sections 2.4 and 2.5.

Interestingly, the combination of 30 nM p16 siRNA and 30 nM RP siRNA was not sufficient to fully rescue senescence induction, suggesting that senescence initiation may still be triggered in the absence of p16. However, double transfection of 30 nM p16 siRNA with 3 nM siRNA targeting RPL34 and RPL35A resulted in a significant (RPL34 p=0.0287, RPL35A p=0.007) rescue of cellular proliferation together with a reduction in cell area compared with 3 nM RP siRNA alone (RPL34 p=0.035, RPL35A p=0.055) (Figure 5.5A-B). In addition, for each of the remaining RP hits, p16 silencing resulted in a partial (non-significant) rescue of the senescence phenotype. Importantly, senescence activation following 30 nM or 3 nM RP siRNA transfection was comparable and there was no significant difference in cell number or cell area generated by each of the two doses. Together, this data indicates that senescence rescue may be achieved via p16 silencing and that p16 signalling may mediate senescence initiation following RP siRNA knockdown in these cells.

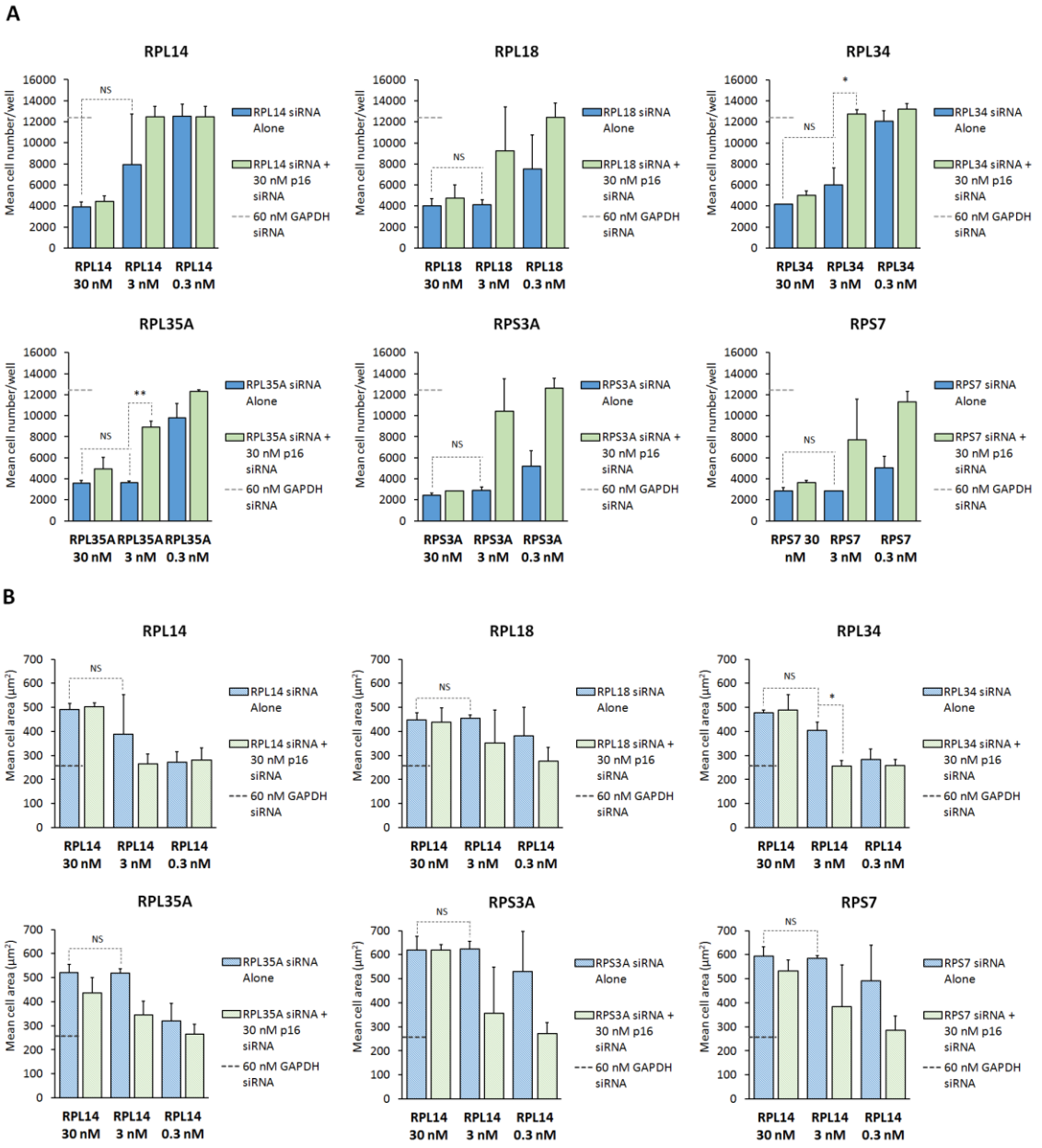

Figure 5.5: MDA-MB-468 cells reverse transfected with 0.3 nM, 3 nM or 30 nM RP siRNA +/- 30 nM p16 siRNA. MDA-MB-468 cells were reverse transfected with 30 nM or 60 nM GAPDH siRNA or 0.3, 3 or 30 nM siRNA pools targeting each of the top six RP hits alone and in combination with 30 nM p16 siRNA according to Section 2.3.2. After 5 days, cells were fixed and stained with DAPI and Cell Mask and cell number and cell area were quantified according to Sections 2.4 and 2.5. Bars denote **(A)** mean cell number or **(B)** mean cell area +SD of two independent experiments each containing three technical repeats. * = p<0.05, ** = p<0.01.

Although the combination of 30 nM p16 siRNA and 3 nM RP siRNA achieved a significant rescue for two of the top six RP hits, 30 nM p16 siRNA did not restore cell numbers or cell area to that of the GAPDH siRNA control for the remaining hits. This may be due to a variety of factors such as the potency of the p16 siRNA, the abundancy of the p16 transcript and protein, the half-life of the p16 protein and the kinetics of the experimental setup (simultaneous siRNA transfection).

As such, it was hypothesised that by increasing the p16 siRNA dose from 30 nM to 60 nM, thereby potentially increasing the level of p16 knockdown, a greater rescue of the senescence phenotype may be achieved.

In order to investigate this, MDA-MB-468 cells were reverse transfected with 60 nM p16 siRNA together with a pool of three siRNAs (total concentration 3 nM) targeting each of the top RP hits according to Section 2.3.2 (N=1). After 5 days, cells were fixed and stained with DAPI and Cell Mask and multiparameter analysis was performed according to Sections 2.4 and 2.5 (Figure 5.6A-C). Multiparameter analysis revealed that (with the exception of RPS7) p16 silencing fully rescued the senescence phenotype and restored cell numbers and all other senescence-associated parameters to match those generated by GAPDH siRNA. A partial senescence rescue was achieved in the case of RPS7. This is most likely due to the kinetics of the experimental setup and the highly rapid nature of RPS7 siRNA-mediated senescence induction. In order to circumvent this issue, often associated with simultaneous siRNA transfection, an inducible p16 shRNA construct could be used to stably silence p16 in MDA-MB-468 cells. Subsequent RP siRNA transfection within a p16 shRNA context would better determine whether or not p16 expression is required for senescence initiation (see Section 5.6 for further discussion).

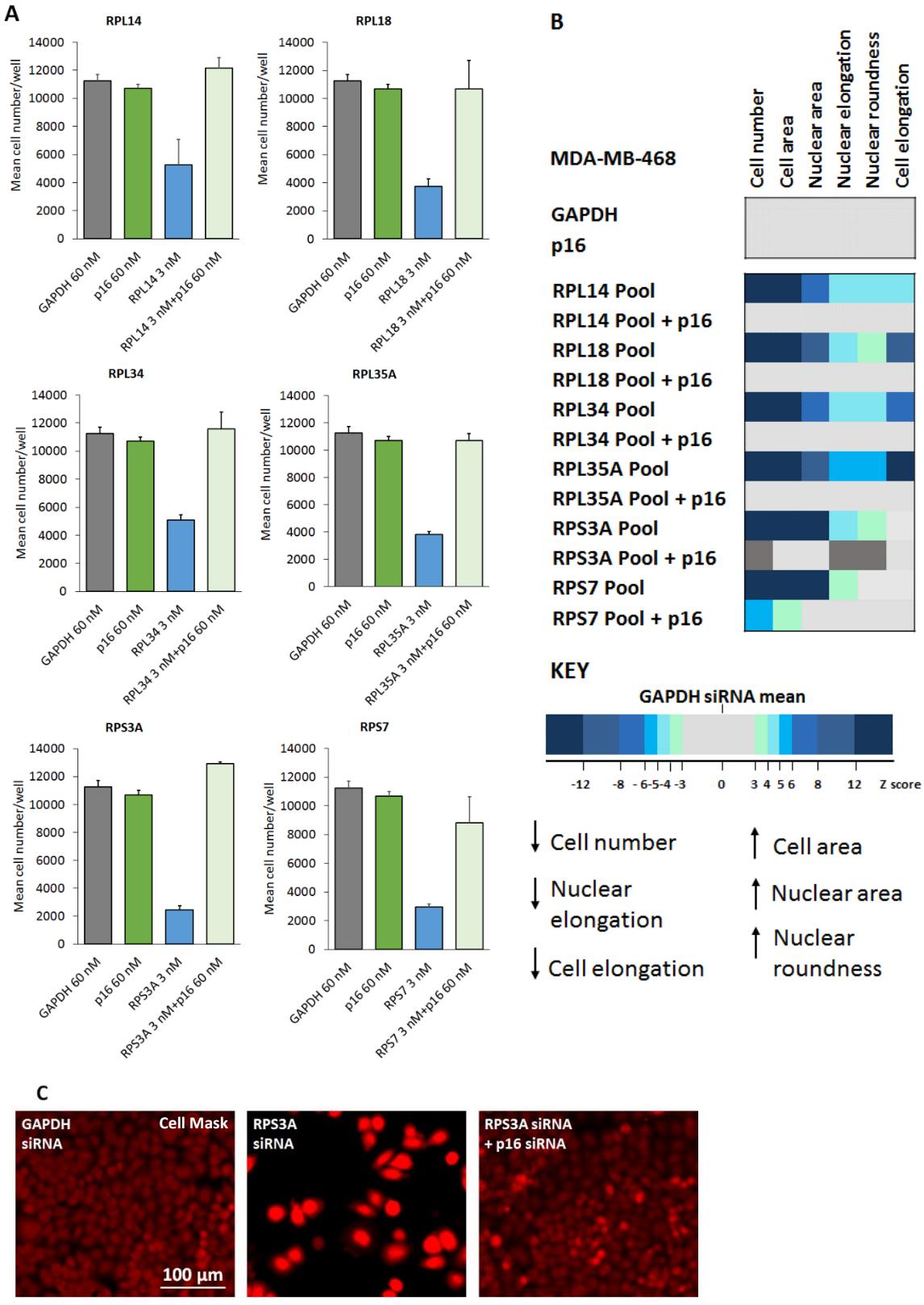

Figure 5.6: MDA-MB-468 cells reverse transfected with 3 nM RP siRNA and 60 nM p16 siRNA. MDA-MB-468 cells were reverse transfected with 60 nM control siRNAs targeting GAPDH or p16 as well as 3 nM siRNA pools targeting each of the top six RP hits +/- 60 nM p16 siRNA according to Section 2.3.2. After 5 days, cells were fixed and stained with DAPI and Cell Mask and multiparameter analysis was performed according to Sections 2.4 and 2.5. **(A)** Mean cell number. Bars denote mean +SD of a single experiment containing three technical repeats. **(B)** Heatmap depicting the mean Z score for each of the senescence-

associated parameters selected for quantification. The scale bar shows the number of Z scores that correspond to the colours within the heatmap and the directionality of the quantified senescence-associated changes. Dark grey indicates a significant change in the opposite direction to that expected and is associated with a proliferative phenotype. **(C)** Representative immunofluorescence images of MDA-MB-468 cells transfected with 60 nM GAPDH siRNA, 3 nM RPS3A siRNA pool or 3 nM RPS3A siRNA pool and 60 nM p16 siRNA and stained with Cell Mask. Images are at 10X magnification and size bar denotes 100 µm.

Taken together, these findings suggest that senescence activation is associated with nuclear translocation of p16 and that initiation of the phenotype is dependent on p16 expression. As such, it is hypothesised that p16 is a crucial mediator of senescence activation and that RP silencing may drive p16 nuclear translocation, enabling a re-sensitisation to p16 signalling and senescence initiation and/or maintenance (Figure 5.7). However, this experiment needs to be repeated and further work must be performed in order to establish whether p16 nuclear translocation is a driver or simply, a consequence of senescence initiation and/or maintenance within these cells (see Section 5.6 for further discussion).

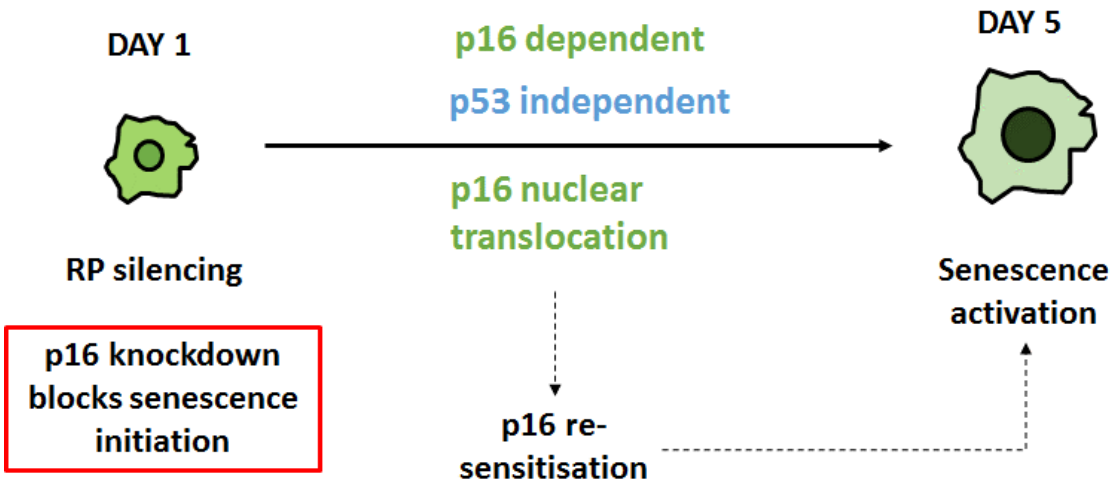

Figure 5.7: Schematic summarising the proposed route to senescence initiation in MDA-MB-468 cells. Data presented above has shown that RP silencing results in senescence activation in MDA-MB-468 cells and that senescence initation in these cells requires p16 expression. Further, it has also been demonstrated that senescence activation is not associated with a significant increase in nuclear p53 protein levels or a change in total p16 protein levels. As such it is hypothesised that senescence initiation is independent of p53 signalling but instead, may require p16 nuclear translocation and re-sensitisation. Solid lines are supported by *in vitro* evidence and dashed lines denote a hypothesis.

5.3.3 *Senescence activation is associated with a potent decrease in nuclear and cytoplasmic p21 protein levels*

Given the p21 (key senescence-mediator downstream of p53, see Section 1.1.1) protein status of the MDA-MB-468 cell line (Figure 5.1), it was hypothesised that RP silencing may trigger p21 stabilisation and re-sensitisation in a p53-independent manner and that, in addition to p16, p21 may function to mediate senescence initiation and/or maintenance in these cells. In order to investigate this, the rabbit anti-p21 antibody was first validated and optimised for immunofluorescence staining (Appendix, Figure A.1C). Subsequently, MDA-MB-468 cells were reverse transfected with GAPDH siRNA or a pool of three siRNAs targeting each of the top six RP hits according to Section 2.3.2. After 5 days, cells were then fixed and stained with DAPI, Cell Mask, rabbit anti-p21 and donkey Alexa Fluor-488 conjugated anti-rabbit and nuclear and cytoplasmic p21 protein levels were quantified according to Sections 2.4 and 2.5 (Figure 5.8A-C).

Unexpectedly, this analysis revealed a non-significant decrease in both nuclear and cytoplasmic p21 protein levels in response to siRNA knockdown of each of the top six RPs and senescence activation in MDA-MB-468 cells. Additionally, this decrease in p21 protein levels was subsequently validated via western blotting for two of the strongest senescence evaders, RPS3A and RPS7 (Figure 5.9A-B). This analysis indicated that at 5 days post-transfection, senescence activation resulted in a 65% (+/- 2.3%) and a 54% (+/- 33.5%) reduction in total p21 protein levels following RPS3A and RPS7 silencing, respectively. Crucially, given the decrease in p21 protein levels associated with the establishment of senescence, it is highly unlikely that p21 expression or protein activity is required for the maintenance of the senescence phenotype in this context, although further work ought to be conducted to investigate this.

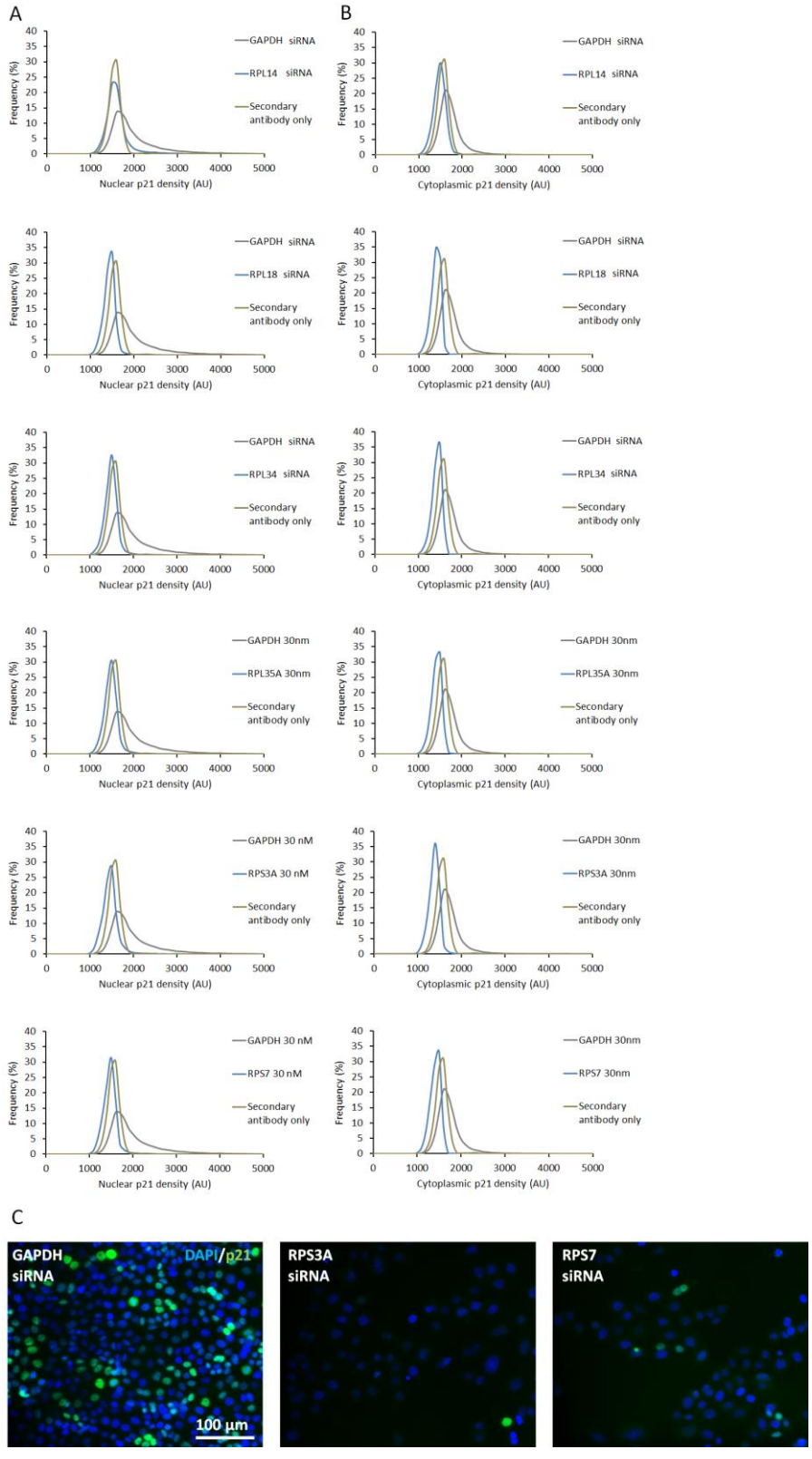

Figure 5.8: Nuclear and cytoplasmic p21 protein levels in MDA-MB-468 cells following RP silencing. Representative frequency distribution plots of **(A)** nuclear or **(B)** cytoplasmic p21 protein levels for MDA-MB-468 cells transfected with 30 nM siRNA targeting GAPDH or each of the top six RP hits. Cells were reverse transfected with 30 nM siRNA and were fixed and stained with DAPI, rabbit anti-p21 and Alexa Fluor-488 conjugated anti-rabbit and nuclear and cytoplasmic p21 protein levels were quantified according to Sections 2.4 and 2.5. Two independent experiments, each containing three technical repeats, were performed. Statistical analysis revealed none of the shifts in p21 protein levels to be statistically

significant. **(C)** Representative immunofluorescence images of MDA-MB-468 cells transfected with 30 nM GAPDH siRNA or 30 nM siRNA pool targeting RPS3A or RPS7 and stained for DAPI (blue) and p21 (green). Images are at 10X magnification and size bar denotes 100 µm.

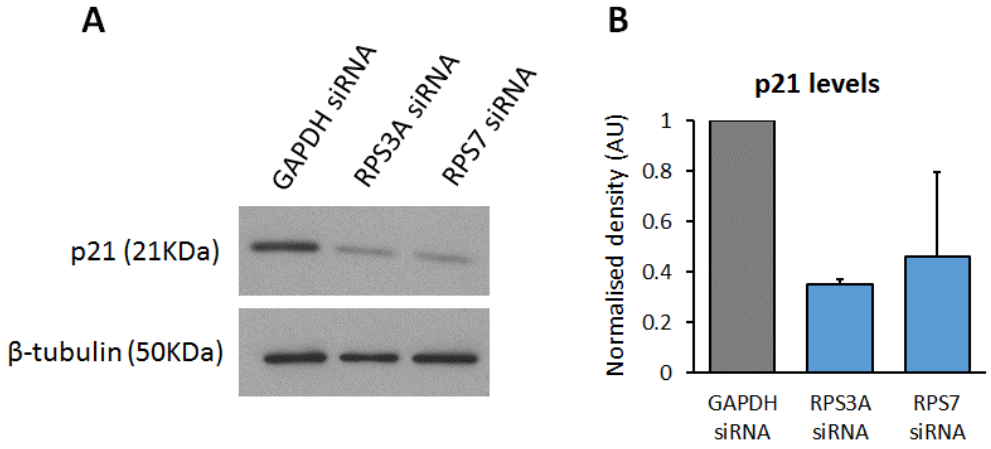

Figure 5.9: Western blot analysis of p21 levels post siRNA transfection in MDA-MB-468 cells. (A) Representative western blot analysis of p21 levels in MDA-MB-468 cells transfected with GAPDH, RPS3A or RPS7 siRNA. Cells were reverse transfected with 30 nM GAPDH siRNA or siRNA pools targeting RPS3A or RPS7 according to Section 2.3.5. Cell lysates were then harvested for western blotting and lysates were probed for rabbit anti-p21 according to Section 2.6. Mouse anti-β-tubulin was used as a loading control. Antibody dilutions and conditions may be found in Section 2.6. **(B)** Densitometry analysis of p21 levels post siRNA transfection in MDA-MB-468s. Analysis was performed using ImageJ software. Bars denote mean density levels +SD normalised to GAPDH siRNA of two independent experiments. Statistical analysis showed the decreases in p21 protein levels to be non-significant.

5.3.4 *Senescence initiation is dependent on p21 expression*

The data presented above demonstrates that senescence establishment via RP silencing is associated with a dramatic reduction in both nuclear and cytoplasmic p21 levels, reducing the likelihood of p21 involvement in senescence maintenance. However, the role of p21 signalling in senescence initiation has yet to be deciphered. It is proposed that, in addition to p16, p21 expression may also be required for the initiation of senescence following RP silencing and may be subsequently degraded as the phenotype is established.

In order to investigate this, siRNA targeting p21 was first validated via immunofluorescence staining using a previously validated rabbit anti-p21 antibody (data not shown). Subsequently, double transfections were performed and MDA-MB-468 cells were simultaneously reverse transfected with 30 nM siRNA targeting p21 together with a pool of three siRNAs (30 nM final concentration) targeting each of the top six RP hits according to Section 2.3.2. GAPDH siRNA was used as a negative control and cells were also transfected with 30 nM p21 siRNA alone. Importantly, transfection with p21 siRNA did not result in a significant increase in cell number when compared to the GAPDH control indicating that proliferating MDA-MB-468 cells are non-

responsive to p21 signalling. After 5 days, cells were fixed and stained with DAPI and cell number was quantified according to Sections 2.4 and 2.5 (Figure 5.10A-B). Interestingly, knockdown of each of the RPs (excluding RPL18, where statistical analysis could not be performed) in combination with p21 silencing resulted in a significant rescue of cellular proliferation, implicating p21 signalling in senescence initiation (Figure 5.10A-B). With this in mind, it is proposed that both p16 and p21 expression are required for senescence initiation following RP silencing and that p21 protein degradation may be a consequence of senescence establishment. However, the exact mechanism by which p21 and p16 may interact and function to mediate senescence induction is still yet to be deciphered. The findings presented so far within this Chapter are summarised in the schematic below (Figure 5.11).

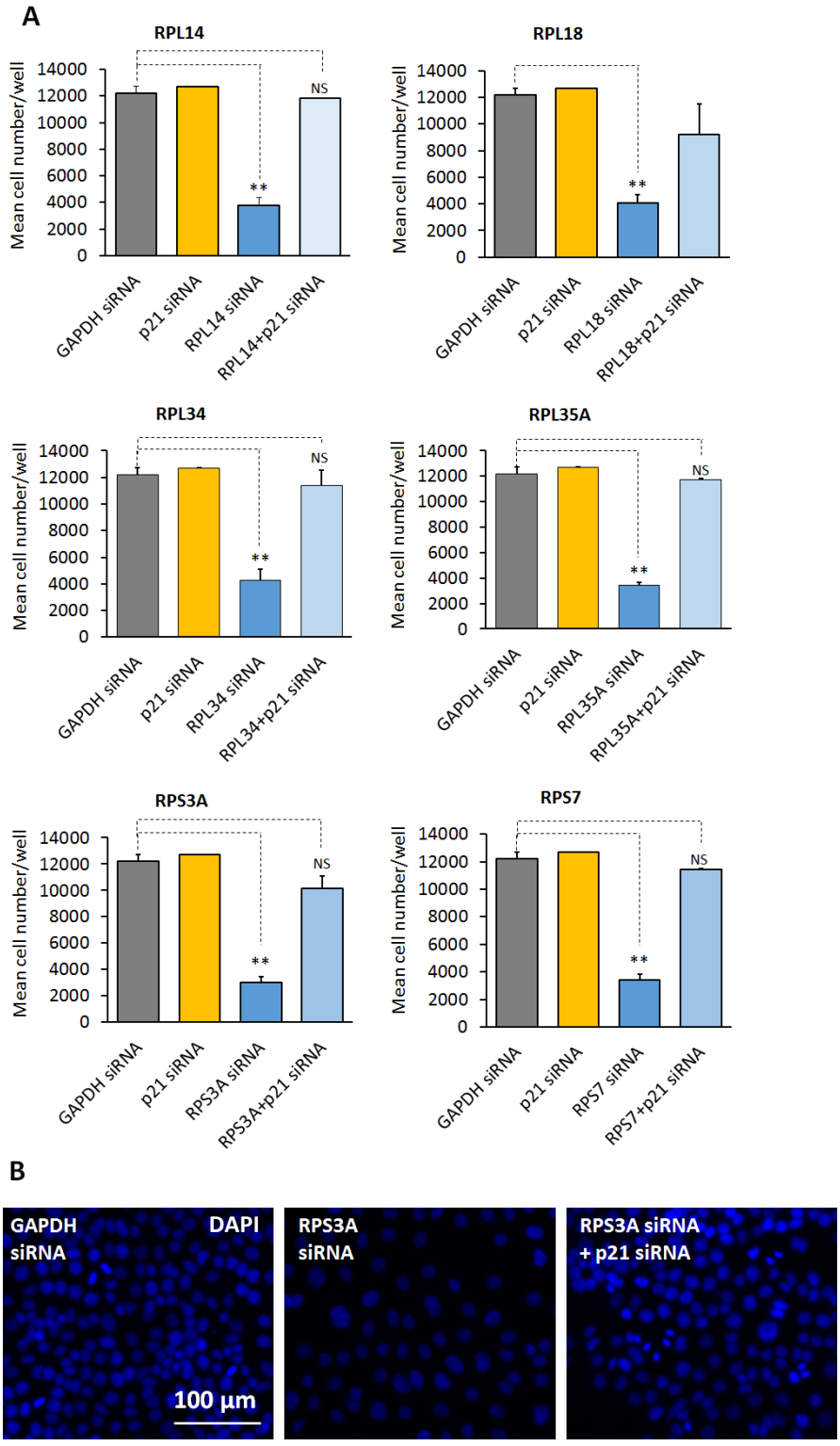

Figure 5.10: MDA-MB-468 cells reverse transfected with 30 nM RP siRNA +/- 30 nM p21 siRNA. MDA-MB-468 cells were reverse transfected with 60 nM control siRNAs targeting GAPDH or p21 as well as 30 nM siRNA pools targeting each of the top six RP hits +/- 30 nM p21 siRNA according to Section 2.3.2. After 5 days, cells were fixed and stained with DAPI and nuclei number was quantified according to Sections 2.4 and 2.5. **(A)** Bars denote mean cell number +SD of two independent experiments each containing three technical repeats. ** = $p<0.01$. Statistical analysis was not performed on RPL18+p21 siRNA as this dataset failed the F-test. **(B)** Representative immunofluorescence images of MDA-MB-468 cells transfected with GAPDH siRNA, RPS3A siRNA or RPS3A siRNA and p21 siRNA and stained with DAPI. Images are at 10X magnification and size bar denotes 100 µm.

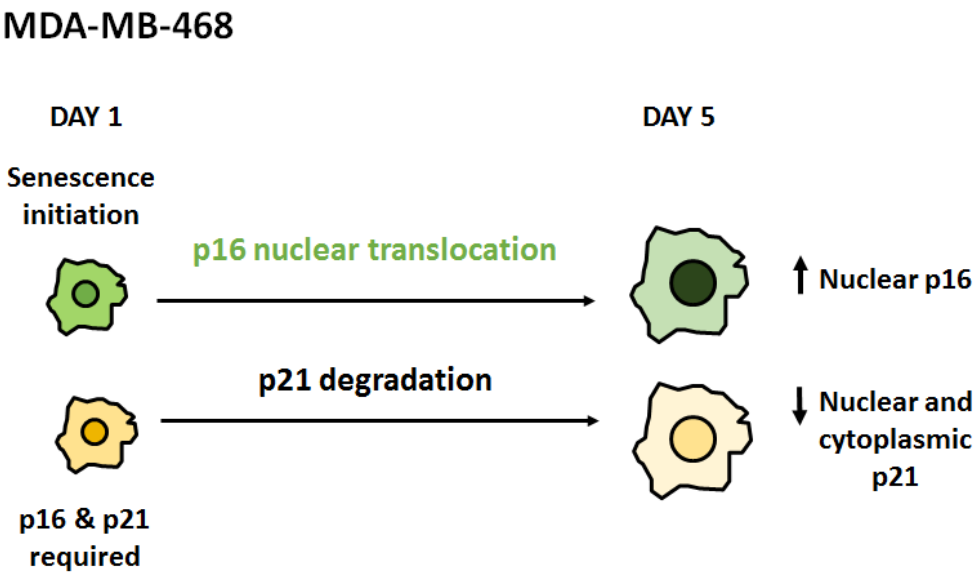

Figure 5.11: Cartoon summarising the role of p16 and p21 during senescence initiation and establishment following RP siRNA knockdown in MDA-MB-468 cells. *In vitro* experiments presented within this Chapter suggest that both p16 and p21 are required for senescence initiation (Day 1) in MDA-MB-468 cells and that by Day 5 (senescence establishment) p16 has translocated to the nucleus while nuclear and cytoplasmic p21 protein levels are reduced.

It is important to note that the order of events following RP silencing in MDA-MB-468 cells has not yet been fully deciphered. However, given the data presented above, it is hypothesised that RP silencing may trigger p21 re-sensitisation and p16 nuclear translocation resulting in p16-resensitisation, p21 degradation and senescence initiation (Figure 5.12A). Alternatively, it is also possible that p21 degradation may occur as an early event during senescence initiation and drive p16 nuclear translocation and senescence establishment (Figure 5.12B). In this instance, p16 nuclear translocation may function solely to mediate senescence maintenance. However, given the data that suggests p21 is required for initiation of the senescence phenotype, the hypothesis outlined in Figure 5.12A is thought to be the most likely. Time course experiments to investigate the kinetics of p16 nuclear translocation and p21 degradation following RP silencing ought to be performed in order to fully elucidate the role of p16 and p21 in senescence initiation and maintenance and to assess a possible interplay between these two key proteins. Further future work proposals may be found in Section 5.6.

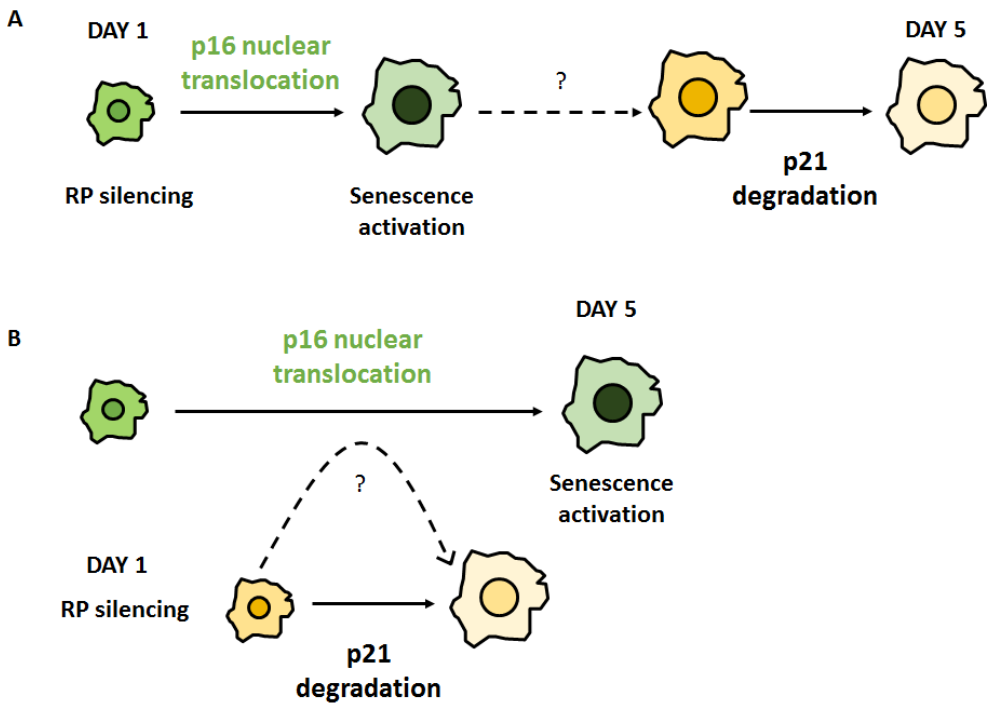

Figure 5.12: Cartoon depicting two possible mechanisms for p16 and p21 interaction following RP silencing in MDA-MB-468 cells. (A) RP silencing may trigger p16 to translocate to the nucleus, mediating senescence activation and subsequent p21 protein degradation. **(B)** RP silencing may first result in p21 protein degradation which, in turn, results in p16 nuclear translocation and senescence activation.

5.4 *Ribosomal silencing in MDA-MB-231 cells results in cell death not senescence*

5.4.1 *RP silencing in MDA-MB-231 cells is associated with a decrease in nuclear p21 protein levels*

A second BLBC model (MDA-MB-231 cell line) was selected in order to further examine the role of tumour suppressors, p16 and p21, in senescence initiation following RP silencing. First, MDA-MB-231 cells were confirmed to be p16-null, $p53^{+/+}$ and $p21^{+/+}$ via western blotting (see Figure 5.1). Given the data presented previously within this Chapter which implicates p16 expression in senescence initiation in MDA-MB-468 cells, it was hypothesised that RP silencing in MDA-MB-231 cells (p16-null setting) would not result in senescence activation, further supporting the requirement for p16 in senescence initiation. In order to test this, siRNA transfection of MDA-MB-231s was optimised according to Section 2.2 (data not shown) and MDA-MB-231 cells were subsequently reverse transfected with GAPDH siRNA or a pool of three siRNAs targeting each of the top six RP hits. After 5 days, cells were fixed and stained with DAPI and cell numbers were quantified according to Sections 2.4 and 2.5 (Figure 5.17A-B).

Unexpectedly, silencing of each of the top six RP hits within MDA-MB-231 cells resulted in a decrease in cell number, suggestive of a highly potent reduction in cell proliferation. The tumour suppressor, p21 is an important repressor of the cell cycle (see Section 1.1.1). As such, it was hypothesised that, in the absence of p16, the reduction in cellular proliferation following RP silencing in MDA-MB-231 cells may be p21-dependent and may also be associated with an increase in nuclear p21 protein levels. In order to investigate this, MDA-MB-231 cells were reverse transfected with siRNA pools targeting each of the top six RP hits or control siRNAs targeting GAPDH or p21, and were stained for p21 protein levels (Figure 5.13). Interestingly, RP knockdown was not associated with nuclear p21 stabilisation. Instead, knockdown of small ribosomal subunit proteins, RPS3A and RPS7, resulted in no change to nuclear p21 protein levels whilst, silencing of RPL14, RPL18, RPL34 and RPL35A induced a reproducible reduction in nuclear p21 protein levels. In the absence of p16 expression or p21 nuclear stabilisation, it was proposed that an alternative phenotype, such as apoptosis, may be driving the observed reduction in cell number in response to RP silencing in these cells.

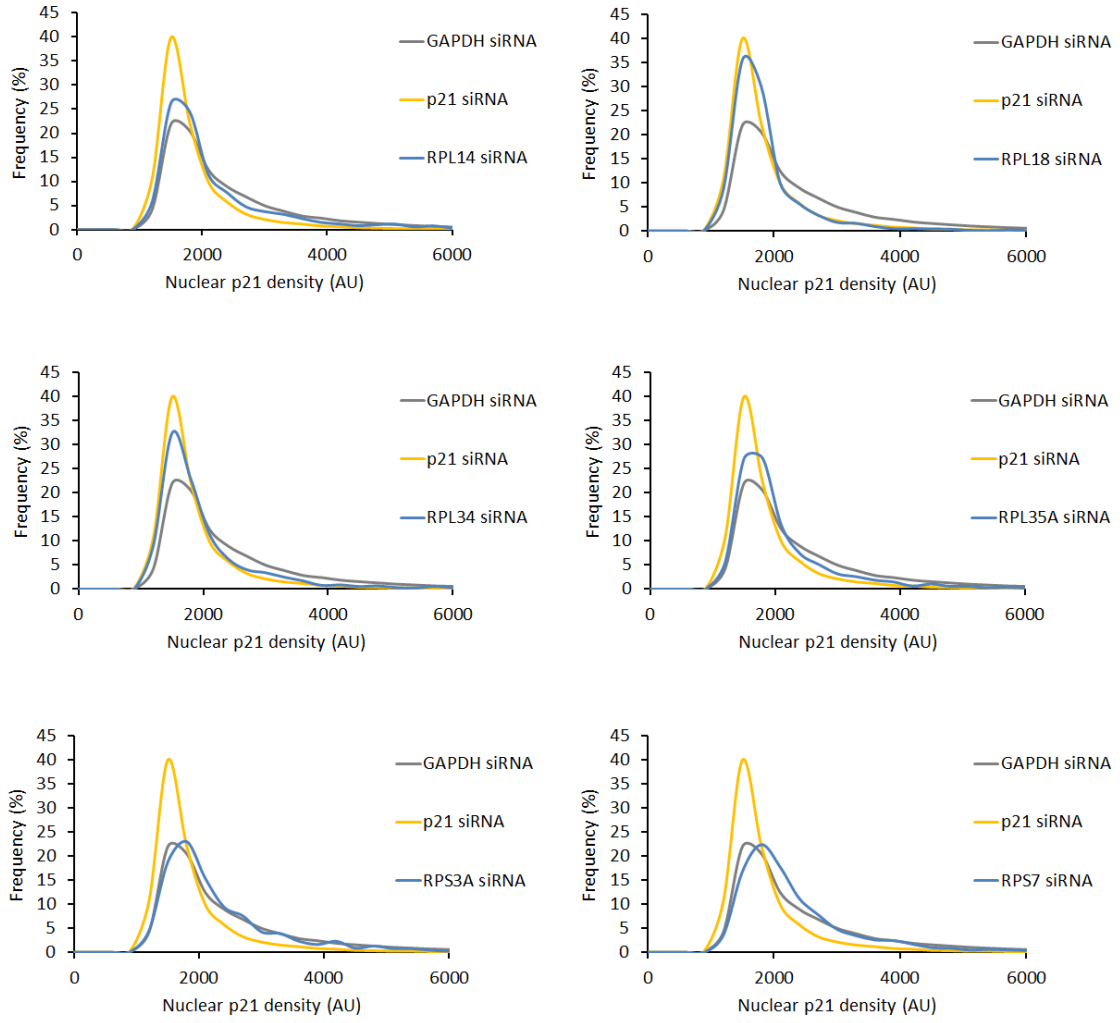

Figure 5.13: Nuclear p21 protein levels in MDA-MB-231 cells following RP silencing. Representative frequency distribution plots of nuclear p21 protein levels for MDA-MB-231 cells transfected with 30 nM siRNA targeting GAPDH, p21 or each of the top six RP hits. After 5 days, cells were fixed and stained with DAPI, rabbit anti-p21 and Alexa Fluor-488 conjugated anti-rabbit and nuclear p21 protein levels were quantified according to Sections 2.4 and 2.5. Two independent experiments, each containing three technical repeats, were performed. Statistical analysis revealed none of the shifts in p21 protein levels to be statistically significant.

5.4.2 *RP silencing induces a 'death-like' phenotype in MDA-MB-231 cells*

Closer examination of immunofluorescence and bright field images following siRNA transfection revealed that RP silencing may activate a 'death-like' phenotype rather than senescence initiation in MDA-MB-231 cells (Figure 5.14 and Figure 5.15). For example, at five or even eight days post-transfection, the majority of the culture appeared to be dying in response to RP knockdown. Furthermore, preliminary quantitation of key senescence-associated parameters such as nuclear and cellular area following RP silencing, revealed that knockdown of two of the strongest senescence evaders, RPS7 and RPS3A (identified within MDA-MB-468 cells), was

associated with a reduction in nuclear and cellular area, characteristic of cell death (data not shown). Interestingly, preliminary data also suggests that CBX7 siRNA (positive control for senescence induction in MDA-MB-468 cells) induces senescence in MDA-MB-231s (Figure 5.15), indicating that senescence activation in this cellular context is possible. Further, the data indicates that, in addition to p16, CBX7 functions to repress other downstream targets that may be critical for senescence activation in the MDA-MB-231 cells. Intriguingly, in contrast to RP silencing, CBX7 silencing in MDA-MB-231s was associated with an increase in nuclear p21 protein levels (Appendix, Figure A.5), indicating that p21 nuclear stabilisation may mediate senescence activation in response to CBX7 silencing, in the absence of p16 expression.

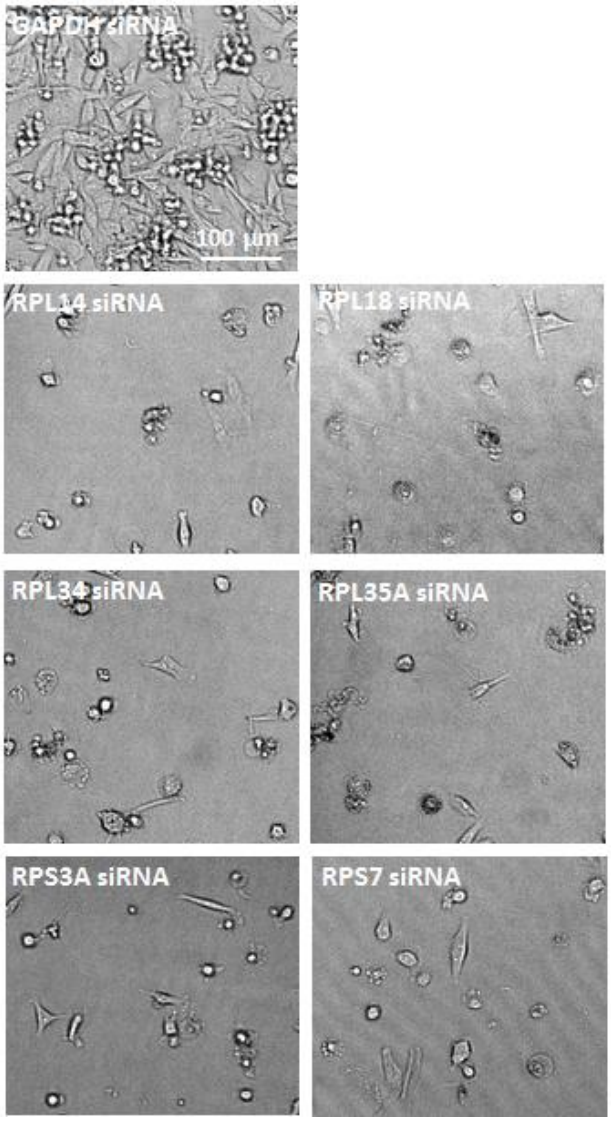

Figure 5.14: Representative bright field images depicting MDA-MB-231 cells transfected with each of the top six RP siRNAs together with GAPDH siRNA. MDA-MB-231 cells were reverse transfected according to Section 2.3.2 with 30 nM siRNA targeting GAPDH or 30 nM siRNA pools targeting each of the top six RPs. Cells were imaged at Day 8 using the IN Cell 1000 automated microscope. Images are at 10X magnification and are taken from a single experiment containing three technical repeats. Size bar denotes 100 µm.

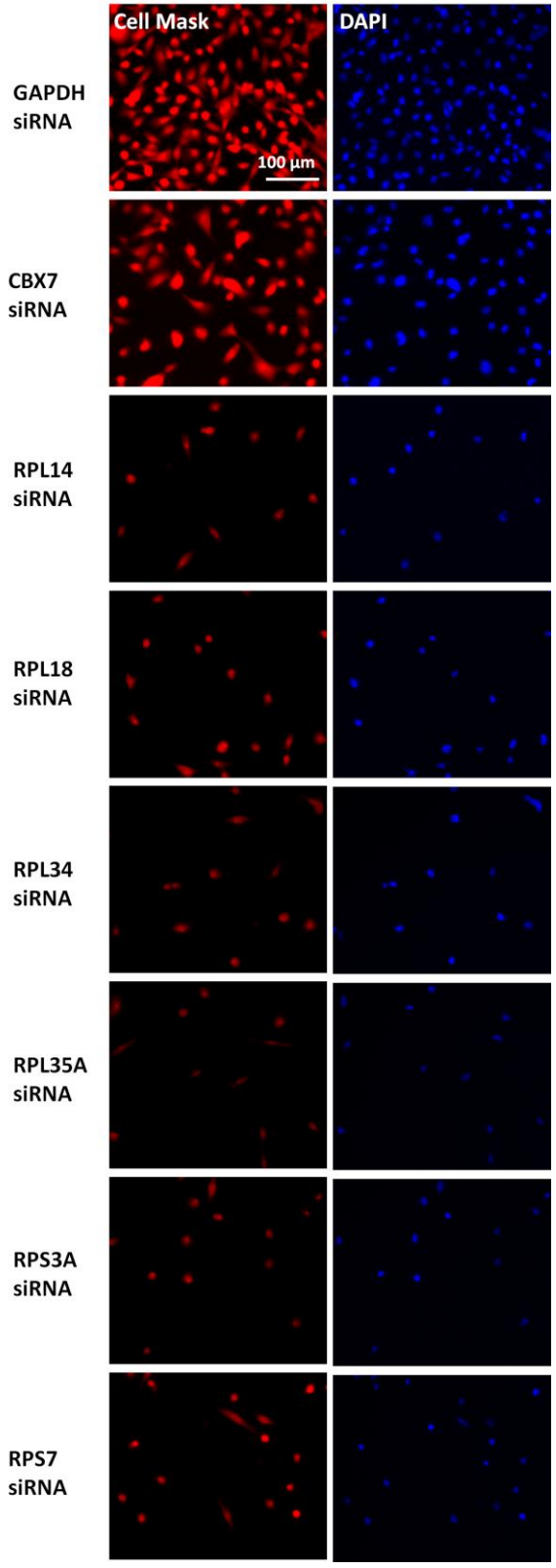

Figure 5.15: Representative immunofluorescence images of MDA-MB-231 cells transfected with each of the top six RP siRNAs together with control siRNAs targeting GAPDH and CBX7. MDA-MB-231 cells were reverse transfected according to Section 2.3.2 with 30 nM siRNA targeting GAPDH, CBX7 or 30 nM siRNA pools targeting each of the top six RPs. After 5 days, cells were fixed and stained with DAPI (blue) and Cell Mask (red) and imaged according to Sections 2.4 and 2.5. Images are at 10X magnification and size bar denotes 100 µm.

In order to assess whether RP silencing in MDA-MB-231 cells resulted in cell death, a direct cell death assay using the nucleic acid stain, SYTOX was performed. SYTOX is a live-cell stain that is only able to penetrate cells with compromised plasma membranes. As such, SYTOX staining can be used to indicate dead or dying cells within a culture. First, the SYTOX dose and incubation time was optimised within MDA-MB-231 cells using PLK1 siRNA as a positive control for cell death (data not shown). Subsequently, MDA-MB-231 cells were reverse transfected with GAPDH, PLK1 or CBX7 control siRNAs as well as pools of three siRNAs targeting each of the top six RP hits, according to Section 2.3.3. After 6 days, live cells were stained with SYTOX and Hoechst (nuclear stain) and were imaged according to Sections 2.9 and 2.5. The percentage of SYTOX-positive nuclei was then calculated in order to indicate the level of cell death within the culture (Figure 5.16A-B).

Strikingly, this analysis revealed that siRNA silencing of each of the top six RP hits induced an increase in the number of SYTOX-positive nuclei when compared to the GAPDH or CBX7 siRNA controls. Moreover, knockdown of the strongest senescence evaders (RPS3A and RPS7, identified within the MDA-MB-468 screens) induced the highest level of toxicity in the MDA-MB-231 cells (RPS3A=42.09% +/- 13.47% and RPS7=43.36% +/- 11.25% SYTOX positive nuclei). Taken together, these preliminary findings suggest that, in contrast to MDA-MB-468 cells, within a p16-null context, RP silencing may induce a death-like phenotype accompanied by a decrease in nuclear p21 protein levels.

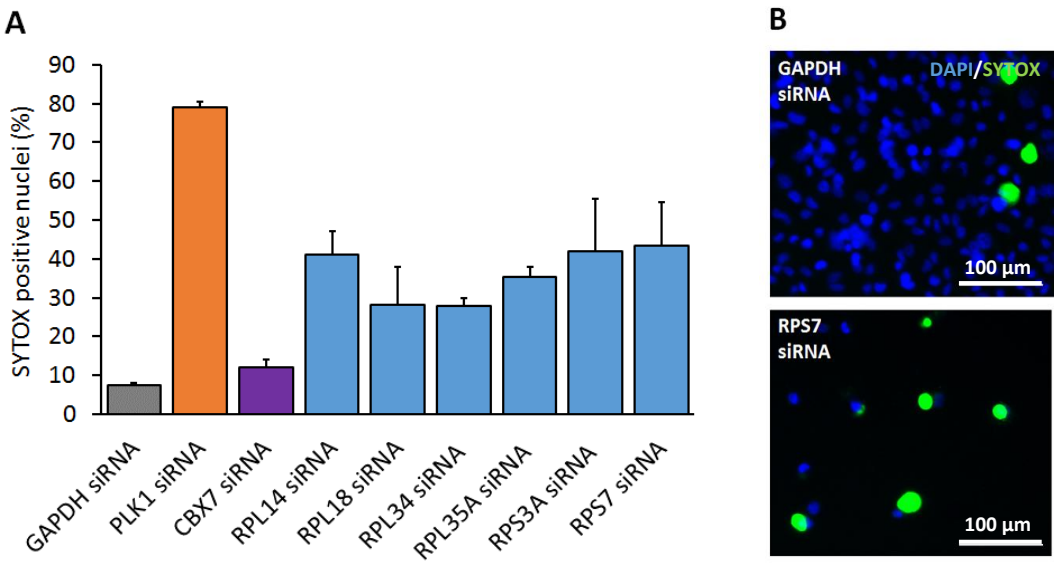

Figure 5.16: Percentage of SYTOX-positive nuclei in MDA-MB-231 cells transfected with RP siRNA. MDA-MB-231 cells were reverse transfected with 30 nM control siRNAs targeting GAPDH, PLK1 or CBX7 together with 30 nM siRNA pools targeting each of the top six RP hits according to Section 2.3.3. After 6 days, cells were incubated with SYTOX and Hoechst for 2.5 hr and were imaged accoring to Sections 2.9 and 2.5. **(A)** Bars denote mean percentage of SYTOX-positive nuclei +SD within a single experiment

containing three technical repeats. **(B)** Representative immunofluorescence images of MDA-MB-231 cells transfected with 30 nM GAPDH siRNA or RPS7 siRNA and stained with Hoechst (blue) and SYTOX (green). Images are at 10X magnification and size bar denotes 100 µm.

5.4.3 *Initiation of cell death in MDA-MB-231s following RP silencing is dependent on p21 expression*

In order to investigate whether p21 is required for the initiation of the death-like phenotype in MDA-MB-231 cells following RP silencing, MDA-MB-231 cells were simultaneously reverse transfected with 30 nM siRNA targeting p21 together with a pool of three siRNAs targeting each of the top six RP hits, according to Section 2.3.3. Doses of 3 or 30 nM RP siRNA were used in order to maximise the possibility of phenotypic rescue. GAPDH siRNA was used as a negative control and cells were also transfected with 30 nM p21 siRNA alone. Importantly, transfection with p21 siRNA did not result in a significant increase in cell number when compared to the GAPDH control indicating that proliferating MDA-MB-231s are non-responsive to p21 signalling. CBX7 siRNA was used as a positive control for senescence induction and PKL1 siRNA was used as an indicator of transfection efficiency. After 5 days, cells were fixed and stained with DAPI and cell number was quantified according to Sections 2.4 and 2.5 (Figure 5.17A-B).

Interestingly, p21 silencing partially rescued the 'death-like' phenotype induced by each of the top six RP siRNAs. Of note, the inter-experimental variability within the 'rescued' conditions was particularly high for the most potent siRNAs, RPS3A and RPS7, indicating p21 knockdown was insufficient to reproducibly rescue the 'death-like' phenotype here. Increasing the concentration of p21 siRNA to 60 nM in future experiments may result in a more reproducible rescue for each of the six RP hits. Together, this data suggests that p21 expression is required to initiate a full cytotoxic response following RP silencing in MDA-MB-231 cells (Figure 5.18A), however, the role that p21 plays in the activation of cell death in this context is yet to be deciphered.

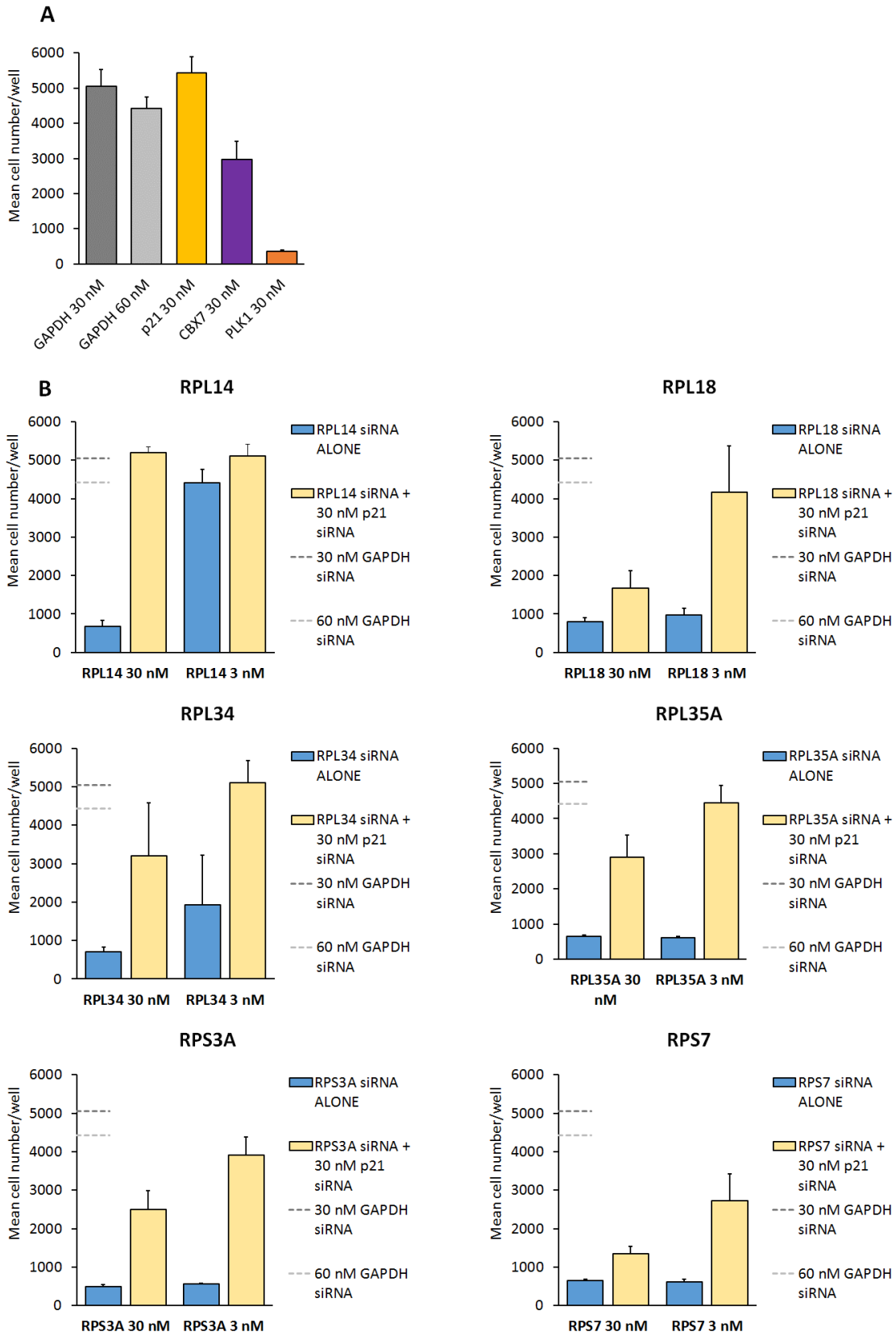

Figure 5.17: MDA-MB-231 cells reverse transfected with 3 or 30 nM RP siRNA and 30 nM p21 siRNA. MDA-MB-231 cells were reverse transfected with **(A)** control siRNAs **(B)** or 3 or 30 nM siRNA pools targeting each of the top six RP hits +/- 30 nM p21 siRNA according to Section 2.3.3. After 5 days, cells were fixed and stained with DAPI and cell number was quantified according to Sections 2.4 and 2.5. Bars denote mean cell number +SD of a single representative experiment containing three technical repeats.

p21 is a CDK inhibitor that functions to repress CDK1/2 activity (see Section 1.1.1). As such, p21 plays an instrumental role in regulating cell cycle progression and there is now a wealth of evidence implicating p21 within senescence initiation. In addition to this, studies have also demonstrated that p21 may also mediate apoptosis via a specific C-terminus cleavage event (Schreiber et al., 1999, Levkau et al., 1998) (Figure 5.18B). Importantly, Levkau et al., 1998 showed that apoptotic HUVECs (human umbilical vein endothelial cells) were negative for full length p21 protein but contained a truncated form of the protein (approximately 14KDa). It was proposed that this truncated form is generated via a specific cleavage event within the C-terminus of p21 protein, mediated by caspase 3, apoptosis-related cysteine peptidase (CPP32) caspase enzyme. Further, the authors also demonstrated that upon cleavage, truncated p21 exits the nucleus due to the loss of its nuclear localisation sequence, present with the C-terminus. This mechanism of p21 C-terminal cleavage and nuclear exit has been shown to drive apoptosis activation, possibly via enhanced CDK2 activity and reduced p21-mediated DNA repair (Levkau et al., 1998). In support of this, mutated p21, resistant to C-terminal cleavage, was protective against apoptosis in HUVEC cells in response to growth factor deprivation. Therefore, this data reveals a mechanism by which p21 is able to mediate apoptosis activation in response to cellular stress. With this in mind, it is hypothesised that in MDA-MB-231 cells, RP silencing may trigger a specific C-terminal cleavage event within native p21 protein, resulting in cytoplasmic translocation of truncated p21 and apoptosis activation.

This work by Levkau et al. supports our hypothesis presented herein. For example, data presented within this Chapter has shown that activation of a death-like phenotype following RP silencing in MDA-MB-231 cells is partially dependent on p21 expression and is associated with a subtle reduction in full length nuclear p21 protein levels. The epitope for the rabbit anti-p21 antibody, used within this thesis to detect nuclear full length p21 levels, sits within the cleaved C-terminal region of the native p21 protein. As such, this antibody is only able to detect full length p21 and is unable to detect the truncated form of the protein. Immunofluorescence staining with this antibody presented here (Figure 5.13) demonstrated that RP silencing in MDA-MB-231s resulted in a slight reduction in full length nuclear p21 protein levels and it is hypothesised that this reduction could be due to p21 C-terminal cleavage. Further immunofluorescence staining, using a second p21 antibody with an epitope located within the protein's N-terminus, would determine whether or not truncated p21 is translocated to the cytoplasm upon RP silencing in these cells. In addition, western blot analysis using an N-terminal binding anti-p21 antibody would also help to determine whether or not p21 is cleaved in response to RP silencing. Truncated p21 (14KDa) would run slightly below full length p21 protein

on a western blot and two bands may be detectable if the cleavage event has occurred. Further experiments, such as immunofluorescence staining for CPP32 caspase enzyme, would also help determine whether apoptosis is activated in response to RP silencing in the absence of p16 expression (see Section 5.6 for further discussion).

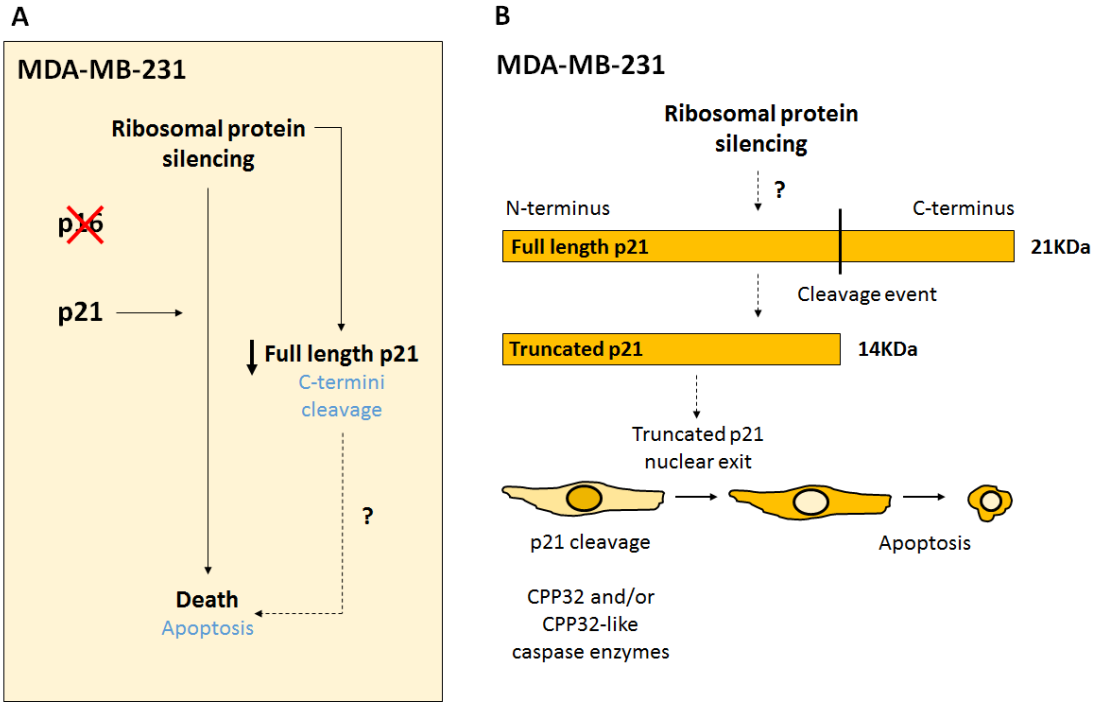

Figure 5.18: Schematic summarising the proposed mechanism of cell death in MDA-MB-231 cells following RP silencing. (A) Schematic summarising the findings presented within this Chapter. Solid lines are supported by *in vitro* data and dashed lines denote a hypothesis. **(B)** It is hypothesised that RP silencing in MDA-MB-231 cells may trigger p21 C-terminal cleavage, followed by truncated p21 nuclear exit and apoptosis activation.

5.4.4 *RP silencing and senescence induction in MDA-MB-468 cells is not associated with C-terminal p21 cleavage*

Previous data presented above showed that in MDA-MB-468 cells (p16-positive), RP silencing resulted in senescence induction accompanied by a reduction in full length p21 protein levels. As such, it was hypothesised that RP silencing in MDA-MB-468 cells does not result in p21 C-terminal cleavage and apoptosis activation, but instead, induces senescence together with full length p21 protein degradation. In order to investigate this, MDA-MB-468 cells were reverse transfected with GAPDH siRNA or pools of three siRNA targeting either RPS3A or RPS7 (two of the strongest senescence evaders) according to Section 2.3.2. After 5 days, cells were harvested and cell lysates were probed for p21 using an N-terminal binding mouse anti-p21 antibody

according to Section 2.6 (Figure 5.19A-B)**.** If p21 protein had been cleaved within its C-terminus, in response to RPS3A or RPS7 silencing, a band running at approximately 14KDa would be visible on the western blot. Interestingly, this analysis revealed just one single band at approximately 21KDa for each of the cell lysates, indicating p21 protein is not cleaved in response to RPS3A or RPS7 silencing in MDA-MB-468 cells. Further, this analysis also showed that full length p21 protein levels are reduced in response to RP silencing (RPS3A=37.6% +/- 7.16% and RPS7=61.87% +/- 30.32%) and is in line with the data presented previously within this Chapter. Taken together, these studies indicate that in MDA-MB-468 cells, RP silencing and senescence induction is not accompanied by p21 C-terminal cleavage, instead, senescence activation is associated with nuclear and cytoplasmic p21 protein degradation. However, the mechanism by which RP silencing drives p21 protein degradation is not yet clear.

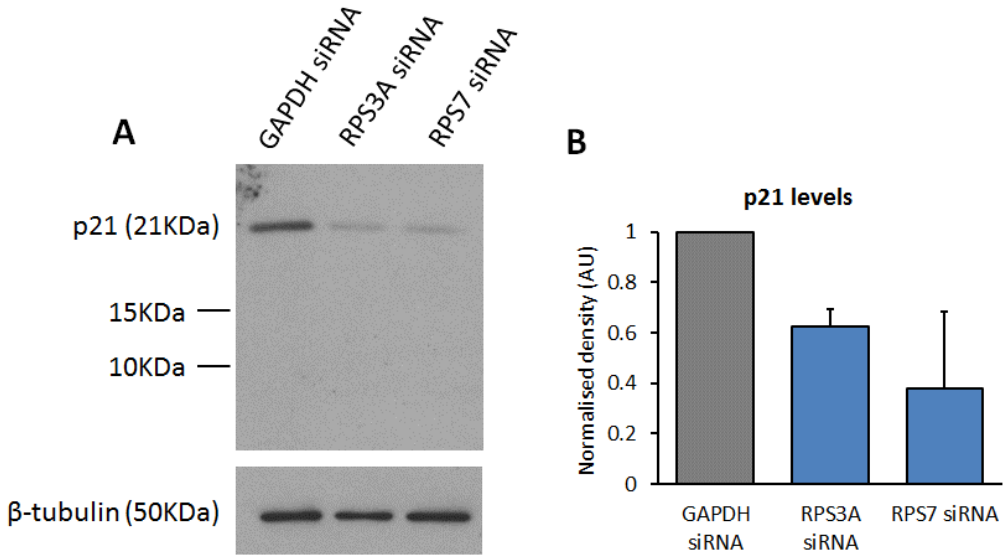

Figure 5.19: Western blot analysis of p21 levels post siRNA transfection in MDA-MB-468 cells. (A) Representative western blot analysis of p21 levels in MDA-MB-468 cells transfected with 30 nM GAPDH, RPS3A or RPS7 siRNA. Cells were reverse transfected with 30 nM GAPDH siRNA or siRNA pools targeting RPS3A or RPS7 according to Section 2.3.5. Cell lysates were then harvested for western blotting and lysates were probed for mouse anti-p21 according to Section 2.6. Mouse anti-β-tubulin was used as a loading control. Antibody dilutions and conditions may be found in Section 2.6. **(B)** Densitometry analysis of p21 levels post siRNA transfection in MDA-MB-468s. Analysis was performed using ImageJ software. Bars denote mean density levels +SD normalised to GAPDH siRNA of two independent experiments. Statistical analysis showed the decreases in p21 protein levels to be non-significant.

5.5 *Senescence induction in MDA-MB-468 cells is associated with dramatic changes to nucleoli number and morphology*

5.5.1 *Actinomycin D treatment induces cytotoxicity and nucleoli disruption in MDA-MB-468 cells*

The nucleolus is the site for ribosomal assembly and is known to function as a 'stress sensor' co-ordinating the induction of p53-mediated senescence in normal cells (see Section 1.7.6). Furthermore, the nucleolus is a dynamic structure that disassembles and reassembles in accordance with rRNA transcription and nucleoli number and morphology is often used to indicate the rate of ribosomal biosynthesis within a cell (see Section 1.7.5). In addition, recent studies have shown that nucleoli morphology is altered upon senescence induction and arrested cells are associated with a single enlarged nucleoli (Ugrinova et al., 2007). As such, it is hypothesised that senescence induction following RP silencing in MDA-MB-468 cells may be accompanied by disrupted ribosomal biosynthesis together with dramatic alterations to nucleoli morphology and number.

NCL (key structural nucleolar protein also involved in rRNA synthesis, see Section 1.7.4) immunofluorescence staining is an established approach for examining nucleolar morphology *in vitro*. Importantly, nucleoli disruption driven by low doses of agents such as Actinomycin D (Pol I inhibitor) is associated with senescence induction (Montanaro et al., 2007). In addition, genome-wide siRNA screening revealed that knockdown of NCL resulted in senescence induction in normal HMECs (Bishop et al., 2010). As such, it was further hypothesised that those siRNAs that are able to activate senescence independently of nucleolus disruption may target the most cancer-specific senescence evaders and that those ribosomal siRNAs capable of nucleolus disruption in normal HMECs would not represent suitable therapeutic targets. Consequently, examination of nucleoli morphology following senescence activation may enable the top six RP hits to be sub-categorised into two subgroups (nucleoli disruptors and non-nucleoli disruptors) and may highlight those most cancer-specific hits for further validation.

Analysis of the METABRIC data set revealed that BLBCs and p16-positive breast cancers, regardless of subtype, are enriched for increased NCL expression (Figure 5.20A). In addition, Kaplan Meier analysis revealed that this elevated expression is also associated with a poor prognosis in breast cancer (where all intrinsic subtypes are considered within a single category, HR=1.18, p=0.0054). Elevated NCL expression is also associated with a reduced prognosis in BLBCs (HR=1.09, p=0.51), however this effect was not statistically significant (Figure 5.20B).

Consequently, NCL immunofluorescence staining was selected as a means of examining nucleoli morphology following senescence initiation in MDA-MB-468 cells.

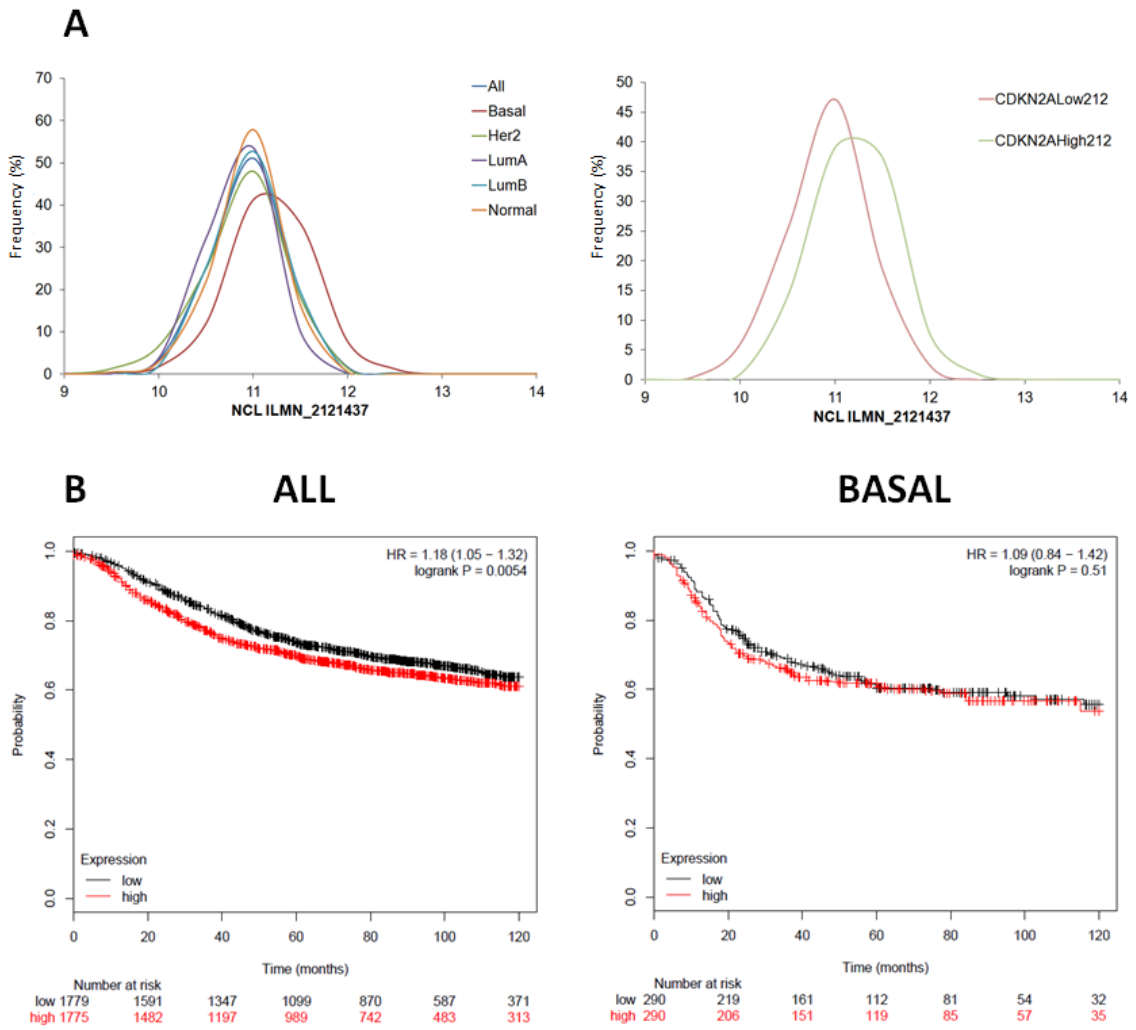

Figure 5.20: *In silico* analysis of NCL transcript expression in breast cancer. (A) Frequency distribution plots depicting log2 fold changes in NCL expression (NCL ILMN_2121437) within each of the PAM50 breast cancer subtypes (left) and within p16-high tumours versus p16-low tumours (right, CDKN2AHigh212 and CDKN2ALow212 respectively). **(B)** Representative survival plots for NCL within all breast cancer cases (N=3,554) (left) and within Basal-like tumours only (N=580) (right). Data shows 10 year relapse free survival generated by kmplot. Data was split by median expression levels.

Before the nucleoli morphology of senescent MDA-MB-468 cells could be examined, a rabbit anti-NCL antibody was first optimised for immunofluorescence staining (data not shown). Actinomycin D treatment (known inducer of nucleoli disruption and senescence) was selected as a positive control for nucleoli disruption and was used to profile nucleoli disruption in MDA-MB-468 cells. Following optimisation (data not shown), proliferating MDA-MB-468 cells were treated with 10 µg/mL Actinomycin D or DMSO only for 8 hours before being fixed and stained with DAPI, rabbit anti-nucleolin and donkey Alexa Fluor-546 conjugated anti-rabbit according to Sections 2.10 and 2.4. Cells were then imaged and cell number was quantified according to

Section 2.5 (Figure 5.21A-B). In line with the literature, this analysis demonstrated that Actinomycin D drug treatment of MDA-MB-468 cells resulted in diffuse nuclear NCL immunofluorescence staining, characteristic of potent nucleoli disruption. Further, this observed nucleoli disruption was associated with a small reduction in cell proliferation, indicating possible cytotoxicity or senescence induction.

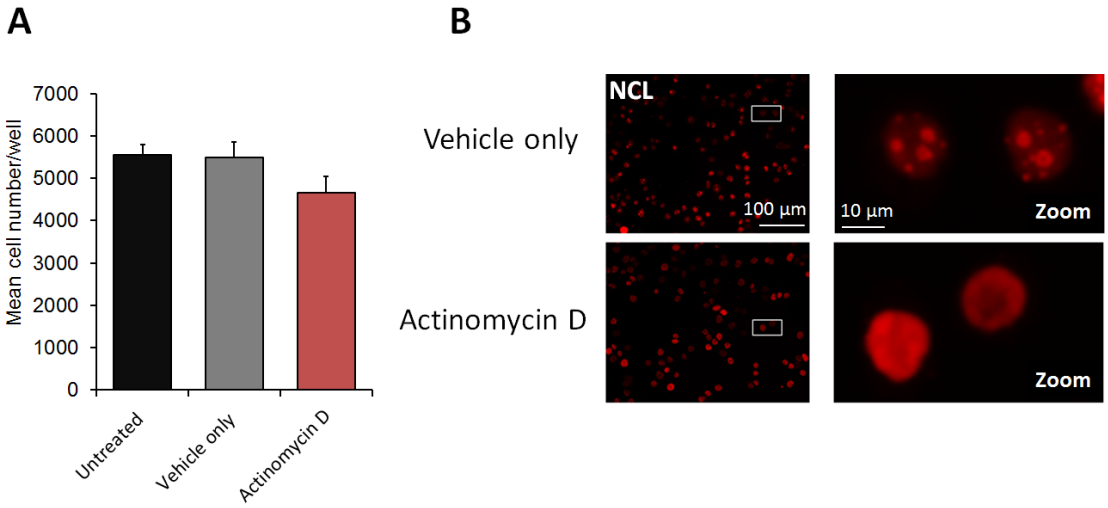

Figure 5.21: Cell number and nucleoli morphology of MDA-MB-468 cells treated with Actinomycin D. MDA-MB-468 cells were incubated with DMSO only or 10 µg/mL Actinomycin D for 8 hours before being fixed and stained with DAPI, rabbit anti-nucleolin and donkey Alexa Fluor-546 conjugated anti-rabbit according to Sections 2.10 and 2.4. Cells were then imaged and cell number was quantified according to Section 2.5. **(A)** Bars denote mean cell number +SD of a single representative experiment containing six technical repeats. **(B)** Representative immunofluorescence images of MDA-MB-468 cells treated with either DMSO (vehicle only) or 10 µg/mL Actinomycin D and stained for NCL. Images are at 20X magnification. Size bar denotes 100 µm on original image and 10 µm on digital zoom.

5.5.2 *Premature senescence activation is associated with dramatic changes to nucleoli morphology in HMECs*

Before the nucleoli were examined within the cancer setting, nucleoli morphology was examined within both proliferating, senescent, and prematurely senescent HMECs with the aim of profiling the senescence-associated nucleoli signature in these contexts. It was hypothesised that senescent HMECs (irrespective of the trigger), would be associated with nucleoli alterations characteristic of cell cycle arrest, i.e. a single enlarged nucleoli (Ugrinova et al., 2007). In order to investigate this, HMECs were transfected with either siGLO (negative control), p16 or CBX7 (positive control for premature senescence activation) siRNA according to Section 2.3.4. Transfection were performed by Dr. Cleo Bishop. After 5 days, cells were fixed and stained for NCL and p16 and nucleoli number and morphology were quantified according to Sections 2.4 and 2.5 (Figure 5.22A-B).

Interestingly, this quantitation demonstrated that proliferative HMECs treated with p16 siRNA ('young' highly proliferative population) were characterised by rounded, highly uniform nucleoli. Wells treated with siGLO siRNA contained a mixed population of proliferative and cellular senescent cells, characterised by high p16 protein expression levels and an enlarged nuclear and cellular area. In line with the literature, the majority of these cellular senescent cells (Figure 5.22A, second panel) contained a single enlarged rounded nucleoli, characteristic of cell cycle arrest. However, perhaps most striking was the nucleoli phenotype observed upon CBX7 silencing. In contrast with highly proliferative and cellular senescent cells, prematurely arrested HMECs were associated with an extremely irregular nucleoli signature, characterised by significant increases in nucleoli number, area and elongation.

Together, this data established the 'nucleoli signature' within both proliferating, cellular senescent and prematurely senescent HMECs. These findings strongly suggest that alterations to nucleoli morphology may be used to identify senescence activation in normal cells and unlike current markers, may also be able to distinguish between different subtypes of senescence induction. Further, given the highly irregular nucleoli morphology associated with CBX7 silencing, it is possible that, in contrast to cellular senescence, premature senescence induction (such as OIS) may be associated with perturbed nucleolar function and disrupted ribosomal biosynthesis. Examination of the nucleoli morphology upon cellular senescence, replicative senescence and OIS activation in these cells would help to investigate this.

5.5.3 *RP silencing in HMECs is not associated with significant changes to nucleoli morphology*

Previously presented data demonstrated that RP siRNA knockdown in HMECs does not result in senescence activation (see Section 4.4). In parallel, it was therefore hypothesised that RP silencing in HMECs would not result in any significant changes to nucleoli number or morphology. In order to investigate this, HMECs were also transfected with three individual siRNAs as well as a siRNA pool targeting each of the top six RP hits and were stained for NCL according to Section 2.4 (Figure 5.22C). Interestingly, siRNA knockdown of each of the top six RP hits in HMECs did not result in any significant change to nucleoli number or morphology, suggesting that specific RP silencing in these cells is not sufficient to induce significant ribosomal biosynthesis disruption or nucleoli dysfunction. Further, this data also suggests that in normal cells, altered nucleoli morphology may be a senescence-specific marker and not simply a direct consequence of RP silencing.

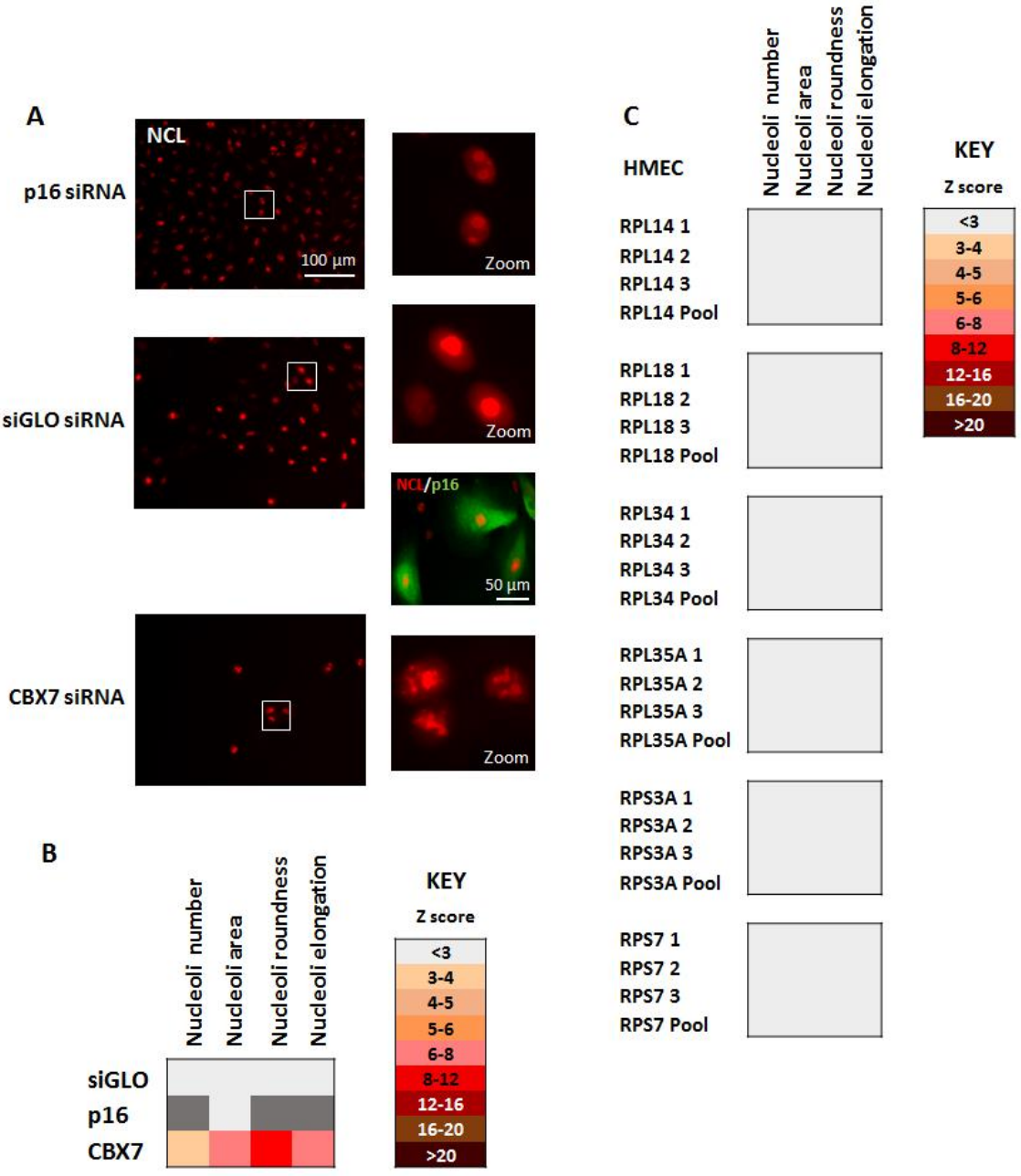

Figure 5.22: Nucleoli morphology in proliferating, cellular senescent and prematurely senescent HMECs. Normal primary HMECs were reverse transfected with 30 nM siRNA targeting p16, PPIB (siGLO) or CBX7 as well as three individual siRNAs and a siRNA pool targeting each of the top six RPs accoring to Section 2.3.4. After 5 days, cells were fixed and stained with DAPI, rabbit anti-NCL and donkey Alexa Fluor-546 conjugated anti-rabbit according to Section 2.4. Nuclei were then imaged and nucleoli morphology was quantified according to Section 2.5. Transfections were performed by Dr Cleo Bishop. **(A)** Representative immunofluorescence images and digitally zoomed images of HMECs transfected with either p16, siGLO or CBX7 siRNA and stained for NCL (red) and p16 (green). Images are at 20X magnification. Size bar denotes 100 or 50 µm. **(B)** Heatmap depicting mean Z scores for nucleoli number/cell, nucleoli area, roundness and elongation. p16 siRNA resulted in a highly proliferative phenotype characterised by a decrease in nucleoli number, size and elongation together with an increase in nucleoli roundness. These changes are denoted by dark grey boxes. CBX7 siRNA-induced senescence was associated with an increase in nucleoli number, size and elongation together with a reduction in nucleoli roundness. **(C)** Heatmap depicting nucleoli morphology in HMECs transfected with 30 nM siRNA targeting each of the top six RP hits.

5.5.4 *Senescence induction in MDA-MB-468 cells following RP silencing is associated with dramatic changes to nucleoli morphology*

As stated earlier in Section 5.5.1, it was hypothesised that in MDA-MB-468s, senescence activation may be associated with dramatic alterations to nucleoli morphology, similar to those observed during premature senescence induction in normal cells and indicative of disrupted ribosomal biosynthesis. Further, those siRNAs that induce senescence in the absence of complete nucleoli disruption may target the most cancer-specific senescence evaders and will be prioritised for further validation. In order to examine the nucleoli morphology upon senescence induction in MDA-MB-468 cells, cells were reverse transfected with three individual siRNAs together with a siRNA pool targeting each of the top six RP hits as well as control siRNAs targeting GAPDH or CBX7 according to Section 2.3.2. After 5 days, cells were fixed and stained with DAPI, rabbit anti-NCL and donkey Alexa Fluor-546 conjugated anti-rabbit and nucleoli number and morphology was quantified according to Sections 2.4 and 2.5 (Figure 5.23A-B).

This analysis revealed that senescence activation following RP silencing was not associated with complete nucleoli disruption but was associated with dramatic changes to nucleoli number and morphology. Importantly, each of the siRNAs tested (with the exception of RPL34 1 and RPL34 2, previously found to be non-functional, see Section, 4.3.2) induced a significant increase in nucleoli number and elongation together with a significant decrease in nucleoli roundness. Strikingly, this irregular senescence-associated nucleoli phenotype was also observed in MDA-MB-468 cells transfected with CBX7 siRNA and was reminiscent of the nucleoli signature observed in prematurely senescent HMECs. As such, it is proposed that cancer-associated senescence following RP silencing may resemble a premature senescence phenotype as opposed to a replicative or a cellular senescence state.

Together, these studies suggest that specific changes to nucleoli morphology may be used to define senescence induction both in normal epithelial cells and in cancer cells. Examination and quantification of nucleoli morphology in p16-positive BLBC cells *in vivo* may be a useful prognostic tool when assessing responses to pro-senescence therapy. In support of this, recent literature has also shown that an enlarged and irregular nucleoli phenotype is associated with a poor prognosis in breast cancer (Derenzini et al., 2009). With this in mind, it is proposed that examination of nucleoli morphology in combination with p16, RP and NCL protein expression data in BLBC may enable the identification of novel molecular subtypes and more effective personalised treatment regimes (see Section 5.6 for further discussion).

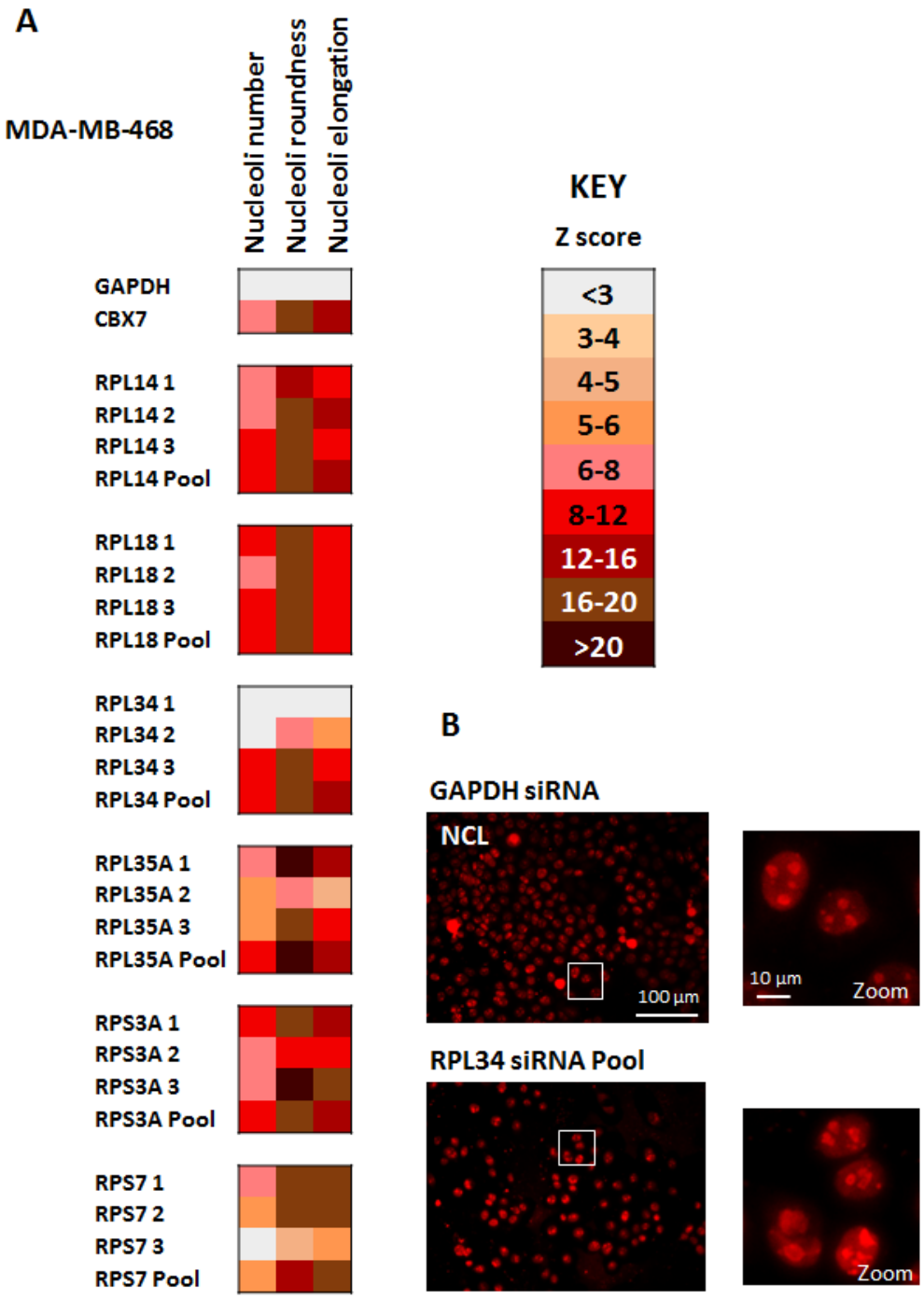

Figure 5.23: Nucleoli morphology in MDA-MB-468 cells transfected with siRNA targeting each of the top six RP hits. MDA-MB-468 cells were reverse transfected with 30 nM control siRNA targeting GAPDH or CBX7 as well as three individual siRNAs and a siRNA pool targeting each of the top six RP hits according to Section 2.3.2. After 5 days, cells were fixed and stained with DAPI, rabbit anti-NCL and donkey Alexa Fluor-546 conjugated anti-rabbit according to Section 2.4. Cells were then imaged and nucleoli morphology was quantified according to Section 2.5. **(A)** Heatmap depicting mean Z scores for nucleoli number/cell, nucleoli roundness and elongation from two independent experiments, each containing three technical repeats. Senescence was associated with an increase in nucleoli number and elongation together with a reduction in nucleoli roundness. **(B)** Representative immunofluorescence images and digitally zoomed images of MDA-MB-468 cells transfected with either 30 nM GAPDH siRNA or RPL34 siRNA pool and stained for NCL. Images are at 20X magnification. Size bar denotes 100 µm on original images and 10 µm on zoomed images.

5.6 *Discussion and future work*

5.6.1 *RP siRNA silencing in MDA-MB-468 cells is associated with p16 nuclear translocation and p21 degradation*

In summary, the data presented within this Chapter has attempted to decipher the mechanism by which RP silencing drives senescence activation in p16-positive BLBC cells. In contrast to the study performed by Fumagalli et al., 2009, data in Section 5.2 demonstrated that senescence initiation in MDA-MB-468 or HeLa cells is not associated with significant p53 stabilisation or activation, suggesting that in a p16-positive context, senescence activation, following RP silencing may be independent of p53 signalling. Crucially, senescence initiation in MDA-MB-468 cells was found to be dependent on p16 and p21 expression and it is proposed that RP silencing drives p16 and p21 re-sensitisation via a novel mechanism, not yet fully resolved. In order to fully elucidate the role of tumour suppressors p53, p16 and p21 in senescence initiation and maintenance in p16-positive BLBC cells, inducible shRNA constructs for p53, p16 and p21 ought to be generated. RP siRNA transfection within a MDA-MB-468 p53, p16 or p21 shRNA context would better determine whether or not each of these proteins are required for senescence initiation in the cellular model of p16-positive BLBC.

Senescence activation was associated with p16 nuclear translocation and it is hypothesised that this may be mediated by p21 signalling. RP silencing +/- p21 shRNA in MDA-MB-468 cells followed by western blotting analysis for p16 within both the nuclear and cytoplasmic cellular fractions would further test whether RP silencing induces p16 nuclear translocation in a p21 dependent manner. In addition, immunofluorescence staining for p16 followed by confocal microscopy analysis following RP silencing +/- p21 shRNA in MDA-MB-468 cells would also help to further validate the findings presented within Section 5.3.1.

Senescence activation in MDA-MB-468 cells was also found to be associated with potent p21 degradation. Given the role of p21 within senescence initiation in these cells, it is hypothesised that p21 is degraded as a consequence of senescence induction and may be a consequence of p16 nuclear translocation. As such, it is proposed that a potential novel interplay may exist between p16 and p21 that may be critical for senescence initiation and maintenance following RP silencing in p16-positive cancer cells. A time course experiment where nuclear and cytoplasmic p21 and p16 protein levels are quantified via western blotting at 24 hour time points for 5 days following RP silencing would determine whether or not p21 degradation is a driver or a consequence of p16 nuclear translocation and senescence activation. In addition, RP silencing

+/- p16 or p21 shRNA followed by p21 and p16 immunofluorescence staining would help determine whether an interplay between these two senescence mediators exists in MDA-MB-468 cells following RP silencing.

Additionally, inducible shRNA constructs for each of the top six RPs would also help to determine the role of p53, p16 and p21 within senescence maintenance. For example, given the potent p21 degradation following senescence induction in MDA-MB-468 cells, it is hypothesised that p16 is required for the maintenance of the senescence phenotype. In order to test this, senescence ought to be stably induced in MDA-MB-468 cells via shRNA RP silencing. Following this, p16 siRNA transfection of senescent MDA-MB-468 cells would determine whether or not senescence maintenance is mediated by p16.

5.6.2 *RP siRNA knockdown induces a 'death-like' phenotype in MDA-MB-231 cells*

In contrast to the studies conducted in the p16-positive cell line, MDA-MB-468, data presented within Section 5.4 shows that RP silencing in MDA-MB-231 cells (p16-null) induces a 'death-like' phenotype as opposed to senescence activation. As such, it is hypothesised that RP silencing in BLBC cancer cells activates a 'cell fate decision fork' with the outcome determined by p16 status. For example, where p16 is expressed, RP silencing activates senescence in a p16 and p21 dependent manner accompanied by p21 degradation and p16 nuclear translocation. However in a p16-null setting, it is hypothesised that RP silencing induces apoptosis mediated by specific C-terminal p21 cleavage (Figure 5.24). Interestingly, RP and p16 silencing in MDA-MB-468 cells did not result in cell death. Instead the senescence phenotype was rescued (Figure 5.6A-C) suggesting that, in these cells, p21 may be mutated and resistant to C-terminal cleavage preventing apoptosis activation following RP silencing. Sequencing of the p21 gene in MDA-MB-468 cells would help to validate this hypothesis.

As discussed in Section 5.4.3, RP silencing in MDA-MB-231 cells followed by immunofluorescence staining and western blot analysis using an N-terminal binding anti-p21 antibody would help to determine whether p21 is cleaved and translocated to the cytoplasm in response to RP silencing in these cells. Additionally, the SYTOX death assay ought to be repeated in the MDA-MB-231 and 468 cells following RP silencing in order confirm a cytotoxic response in activated only in the absence of p16 expression. Further experiments, such as immunofluorescence staining for CPP32 caspase enzyme, or a Terminal deoxynucleotidyl transferase dUTP nick end labelling (TUNEL) assay would also help determine whether apoptosis is activated in response to RP silencing in the absence of p16 expression.

The suggestion that RP silencing in cancer cells may elicit differing cellular responses depending upon p16 status has significant clinical implications when considering RP silencing as a potential pro-senescence anti-cancer therapy for BLBC. For example, it is predicted that RP silencing in p16-positive tumours would result in senescence induction. In these cases senolytics or immune system-boosting agents may also be required in order to fully clear the senescent cancer cells and prevent disease relapse. Alternatively, given the data presented in Section 5.4, it is also predicted that RP silencing in p16-negative BLBC tumours would also be an effective therapeutic strategy. In this context, it is possible that RP silencing would activate apoptosis within the tumour and that a secondary senolytic therapy would not be required.

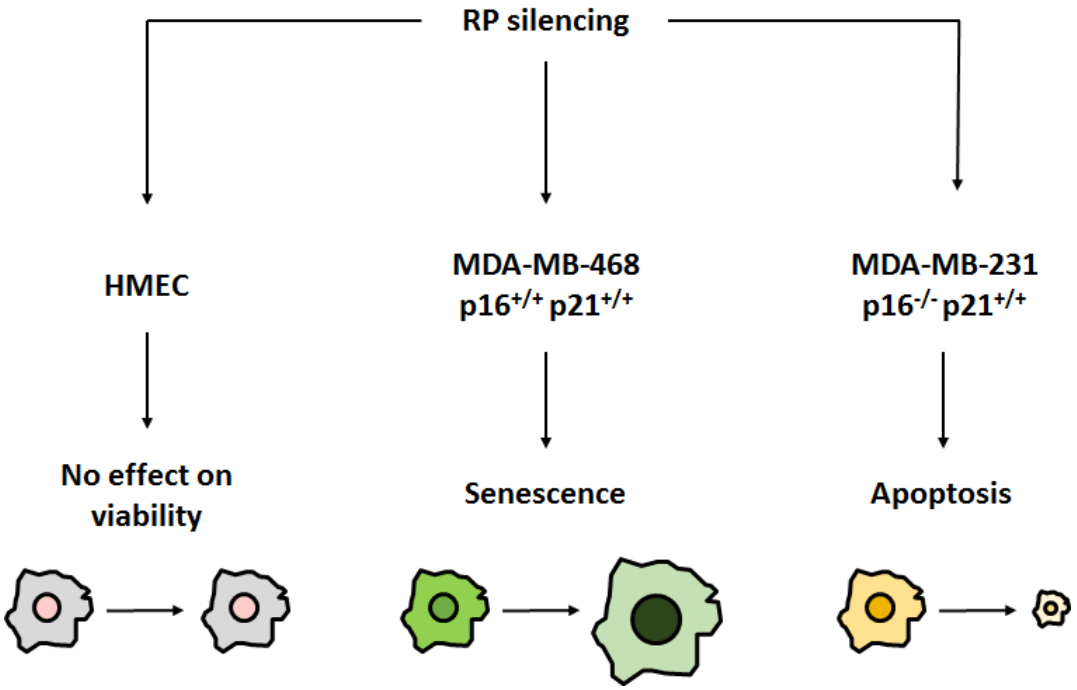

Figure 5.24: Schematic summarising the differential responses to RP silencing within HMECs, MDA-MB-468 and MDA-MB-231 cells. Data presented within this thesis has shown that RP silencing is well tolerated within HMECs. However, within the cancer setting, RP silencing induces a 'decision fork' whereby senescence or a 'cell death-like' phenotype is activated.

5.6.3 *Senescence activation was associated with dramatic alterations to nucleoli morphology*

In addition to the data discussed above, studies presented within this Chapter also aimed to investigate the impact of senescence activation on the nucleolus in both HMECs and MDA-MB-468 cells. In summary, dramatic changes to nucleoli morphology were associated with senescence induction in normal HMECs and, unlike current markers, nucleoli morphology may be used to distinguish between different subtypes of senescence initiation. Importantly, RP silencing in HMECs did not induce significant alterations to nucleoli number or morphology

suggesting that silencing of the top six RP hits in these cells does not result in significant ribosomal biosynthesis disruption or nucleoli dysfunction. Further, examination of the nucleolus within p16-positive BLBC may be a useful prognostic tool when assessing response to pro-senescence therapies.

Chapter 6
Discussion

6.1 *RP silencing induces a cancer-specific senescence response in p16-positive BLBC cells*

6.1.1 *RP silencing has previously been shown to activate senescence in A549 cells*

In summary, data presented within this thesis has identified six novel senescence evaders within two p16-positive cancer cell lines, including the BLBC cell line, MDA-MB-468. Knockdown of these hits in MDA-MB-468 cells resulted in senescence activation and long-term experiments revealed RPS3A and RPS7 siRNA as the strongest and most stable inducers of senescence. In order to further validate the top six RPs as senescence evaders in p16-positive BLBC cells, analysis of RP silencing ought to be expanded to encompass additional p16-positive BLBC cell lines such as BT549 cells (human breast carcinoma, $p16^{+/+}$ $p53^{R249S}$ mutated and RB-null) and HCC1937 (human ductal carcinoma, $p16^{+/+}$ $p53^{R306STOP}$ mutated and RB mutated, in frame deletion). It may also be interesting to explore the effects of RP silencing within non-malignant hTERT immortalised HMECs (p53 WT). This analysis may help pinpoint the cellular context along the road to carcinogenesis where specific RP silencing is no longer tolerated.

Fumagalli et al., 2009 demonstrated that siRNA knockdown of the 40S RP, RPS6 resulted in senescence induction in A549 cells (lung adenocarcinoma cell line, p16-null, p53 WT) characterised by decreased BrdU integration and an accumulation of cells in G1. Here, Fumagalli et al. presented data in line with an earlier study by Volarević et al., 2000 who showed that conditional deletion of the RPS6 gene in mice resulted in reduced Cyclin E and CDK2 (crucial for S phase progression) mRNA and protein expression within extracted liver samples. Together, these studies provide good evidence for senescence activation within cancer cells following RP silencing both *in vitro* and *in vivo*.

It should be noted that the mechanism by which senescence is activated following RPS6 knockdown (as outlined by Fumagalli et al.) differs substantially to that elucidated within this thesis. Fumagalli et al. showed that senescence activation, following RPS6 siRNA knockdown, was accompanied by an increase in both p53 and p21 protein levels as well as an increase in RPL11 translation. Free RPL11 was found to interact with MDM2 and it is proposed that RPL11 may inhibit MDM2 activity, driving p53 stabilisation and senescence induction following RPS6 knockdown. p53 and p21 induction was impaired following RPL11 siRNA knockdown and senescence activation was rescued by p53 siRNA, demonstrating the p53-dependency of the phenotype in this cellular context. Interestingly, siRNA knockdown of RPS6 in MDA-MB-468 cells resulted in potent senescence induction with a subtle (non-significant) increase in nuclear p16

protein levels (data not shown) suggesting RPS6 may also activate senescence in the absence of functional p53 in a p16-positive cancer setting. By contrast, immunofluorescence staining and western blot analysis presented in Sections 5.2 and 5.3.3 showed that senescence activation in MDA-MB-468 cells following knockdown of each of the top six RPs was not accompanied by a significant increase in nuclear p53 or p21 protein levels, but instead, was associated with p21 protein degradation. Further, siRNA rescue experiments presented in Chapter 5 showed that both p16 and p21 were required for senescence initiation in MDA-MB-468 cells following RP knockdown and that, crucially, senescence activation was associated with a translocation of p16 to the nucleus following RPS3A and RPS7 silencing (see Section 5.3). Unlike A549 cells, MDA-MB-468 cells are known to contain the $p53^{R273H}$ gain-of-function mutation, severely reducing the likelihood of a p53-mediated senescence response in these cells. Therefore, it is hypothesised that in a p16-positive, p53-mutated cancer setting, RP silencing may initiate a re-sensitisation to p16 signalling and elicit a p16-dependent senescence response, independent of p53 signalling.

6.1.2 *Exploring the mechanism of senescence downstream of p16*

The mechanism by which RP silencing is able to drive a p16-mediated senescence response in cancer is an exciting question not yet addressed within the literature. In a normal cellular context, p16 functions to block the CDK4/6/Cyclin D-mediated phosphorylation of RB family members, RB, p130 and p107, resulting in cell cycle arrest (see Section 1.1). MDA-MB-468 cells are known to be RB-null, however, studies have shown that the additional RB family members, p130 and p107 may also mediate senescence activation in BLBC cells (Bazarov et al., 2012). Given this, it is hypothesised that following RP silencing in MDA-MB-468 cells, p16 may function to inhibit the phosphorylation of RB family members, p130 and p107, resulting in E2F-mediated transcriptional repression and senescence activation. In order to test this, future work ought to investigate whether senescence activation following RP silencing, is dependent on the activity of hypo-phosphorylated p130 or p107. First, the RB, p130 and p107 status of the MDA-MB-468 cells used within this project ought to be confirmed via western blotting. Subsequently, the phosphorylation status of p130 and p107 should be ascertained before and after RP silencing in MDA-MB-468 cells via western blotting. An increase in the level of hypo-phosphorylated p130 or p107 following RP silencing would implicate the p16/p130/p107/E2F signalling axis in senescence activation in a p16-positive cancer setting. In addition, siRNA knockdown of the top six RPs, together with p130 or p107 silencing, in MDA-MB-468 cells would also help to determine the role (and relative contribution) of hypo-phosphorylated p130 or p107 in senescence activation.

6.1.3 *siRNA screening has identified six potential cancer-specific therapeutic targets*

Kaplan Meier analysis showed that elevated expression of RPS6, RPS23 or RPL7A (also identified as potential senescence evaders in A549 cells by Fumagalli et al.) is associated with a poor prognosis in lung cancer (RPS6 HR=1.36, p=0.0000038, RPS23 HR=1.33, p=0.000014 and RPL7A HR=1.41 p=0.00000012, N=1,926, data not shown) however, by contrast, elevated expression of these RPs in breast cancer (when Luminal A, Luminal B, HER2-enriched and Basal-like tumours are considered together) is associated with a favourable prognosis (RPS6 HR=0.7, p=0.0000000012, RPS23 HR=0.77, p=0.0014 and RPL7A HR=0.84, p=0.0023, N=1,660, data not shown) highlighting a potential tissue-dependent role for these RPs. Despite the fact that elevated expression of RPS6, RPS23 and RPL7A is associated with a poor prognosis in lung cancer, these three RPs are unlikely to represent cancer-specific therapeutic targets. Crucially, the effect of RPS6, RPS23 and RPL7A silencing within normal cells was not explored by Fumagalli et al., however, genome-wide siRNA screening performed within the Bishop laboratory showed that knockdown of RPS6, RPS23 and RPL7A in normal, HMECs resulted in senescence activation (Bishop et al., 2010). By contrast, work presented within this thesis has identified six novel cancer-specific senescence evaders functional within two p16-positive cancer cell lines. Importantly, siRNA knockdown of these top six RPs did not affect the viability or nucleoli signature of normal HMECs. Therefore, unlike the RPs identified within the literature, knockdown of the top six RPs identified here appears to be well-tolerated in normal cells and these RPs may represent novel cancer-specific drug targets for future pro-senescence therapies.

6.1.4 *RP silencing induces a differential response depending on the cellular context*

The data presented in Section 5.4 demonstrated that RP silencing in MDA-MB-231 cells (p16-null, $p53^{R280K}$ gain-of-function mutation) resulted in cell death and contrasts with the findings obtained by Fumagalli et al. who showed RPS6 silencing in a p16-null cancer cell line (A549) resulted in senescence activation. Given this, it is hypothesised that RP silencing may drive a cancer cell to reach a 'decision fork' whereby the cellular context may determine cell fate. Following RP silencing, senescence may be activated via the activity of either p53 or p16, potentially dependent on the tissue type (lung versus breast) and the p16 and p53 mutational status. However, where neither WT p16 nor p53 are functional (as is the case for MDA-MB-231 cells), RP silencing may activate apoptosis via p21 C-terminal cleavage (see Section 5.4.2). In order to investigate this hypothesis further, siRNAs targeting each of the 82 RPs should to be tested within a panel of BLBC cell lines including BT549 cells (human breast carcinoma, $p16^{+/+}$ $p53^{R249S}$ mutated and RB-null), HCC1937 (human ductal carcinoma, $p16^{+/+}$ $p53^{R306STOP}$ mutated

and RB mutated, in frame deletion), DU-4475 cells (human breast carcinoma cell line, p53 WT, methylated INK4a), and MDA-MB-231 cells (p16-null, $p53^{R280K}$ gain-of-function mutation) and senescence or apoptosis induction together with p16, p53 and p21 activation ought to be established. This approach may sub-categorise the RPs based on the route by which their silencing activates senescence and may identify both p53 and p16-dependent mechanisms of senescence induction.

6.1.5 *Future work to further profile the senescence phenotype following RP silencing*

Interestingly, a recent study by Teng et al., 2013 showed that siRNA silencing of the 60S RPs, RPL5 and RPL11 in MRC5 cells (primary human lung fibroblasts) impaired cellular proliferation in the absence of p53 activation or cell cycle arrest. By contrast, preliminary cell cycle profile analysis performed here (N=1, data not shown) suggested that RPS3A and RPS7 silencing in MDA-MB-468 cells is associated an accumulation of cells in G1. Further, data presented within this thesis demonstrated that RPS3A and RPS7 silencing in MDA-MB-468 cells is associated with nuclear p16 translocation and a stable cell cycle arrest, indicative of senescence induction rather than simply a slowing of cell cycle progression (see Sections 5.3.1 and 4.6, respectively). RP silencing in MDA-MB-468 cells followed by flow cytometry analysis and cell cycle profile analysis would better determine whether or not knockdown of the top six RP hits identified here results in a true G1 cell cycle arrest. Inducible shRNA constructs for each of the top six RP hits could be generated and used to stably silencing the RPs in MDA-MB-468 cells. Cells could then be fixed and stained with a DNA-binding dye such as propidium iodide or 7-aminoactinomycin-D and cell cycle analysis could be performed before and after RP silencing.

To further profile the senescence phenotype, additional biomarkers of senescence induction ought to be examined. For example, immunofluorescence staining for H3K9 methyl marks and PML nuclear bodies at 5 days and 16 days post-RP silencing in MDA-MB-468 cells may help to determine the presence of SAHF following RP knockdown. Examination of the nucleoli morphology revealed that the nucleoli signature of senescent MDA-MB-468 cells was similar to that displayed by senescent HMECs treated with CBX7 siRNA (see Section 5.5). Given this, it is hypothesised that the senescence phenotype generated via RP silencing in p16-positive cancer cells may resemble a protective/premature senescence response triggered in normal cells. In order to further investigate this, RNA-sequencing (RNA-seq) could be performed on proliferating and senescent MDA-MB-468 cells following knockdown of CBX7 or each of the top six RPs. The data generated could then be compared to RNA-seq performed on proliferating, prematurely senescent HMECs (following CBX7 knockdown), and HMECs that have undergone normal cellular

senescence. Subsequent pathway analysis may provide further mechanistic insight into the routes to senescence activation in p16-positive BLBC cells and may also help to determine whether or not the cancer RNA expression profile (following RP silencing) resembles a premature or more 'normal-like' senescence signature. The data generated could then be cross-compared with additional publically available senescence RNA-seq datasets, such as those generated for OIS, UV-irradiated or replicative senescent cells. This approach may also help to determine whether the cancer RNA expression profile (following RP silencing) resembles a premature (OIS/DNA-damaged induced) or more a more classical replicative senescence signature. Alternatively, this analysis may also reveal a novel senescence activation pathway, unique to the cancer setting. In addition, this strategy may enable further sub-categorisation of the top six RP hits according to their senescence-associated expression signatures and may also identify additional potential therapeutic targets (downregulated upon senescence induction) in p16-positive BLBC, downstream of RP silencing. The clinical relevance of these additional downstream hits within BLBC could then be explored using the METABRIC dataset.

The senescence-associated methylome within fibroblasts and HMECs is now well-established (Cruickshanks et al., 2013, Lowe et al., 2015). Analysis of the senescence-associated methylome in MDA-MB-468 cells following RP silencing using an Illumina 450K array would enable profiling of the methylome dynamics upon senescence initiation within a cancer cell, and the identification of differentially methylated positions and their location within the genome. The data generated here could be cross-compared with the RNA-seq data (outlined above), the methylome profiles associated with both proliferating and senescent HMECs (Lowe et al., 2015) and the cancer-associated Illumina 450K array data available within TCGA database. This strategy may help to further stratify the top six RP hits according to their methylome profiles and determine whether or not the cancer methylome (following RP silencing) resembles a premature or more a more 'normal-like' cellular senescent signature.

Together, these studies will further characterise the senescence phenotype following RP silencing in p16-positive BLBC and may help to elucidate the exact mechanism by which siRNA knockdown of specific RPs results in p16 nuclear translocation, p21 degradation and senescence activation in MDA-MB-468 cells.

6.2 *The ribosome is severely disrupted in cancer and may drive cancer cell survival and senescence evasion*

6.2.1 *The ribosome is often disrupted in cancer*

Analysis of the current literature and data mining of the Human Protein Atlas database revealed that the top six RPs identified by siRNA screening are highly expressed within a wide array of human malignancies, including breast and cervical cancer (see Figure 6.1). Further, analysis of the METABRIC dataset (see Section 4.2.1) also showed that the ribosome is severely disrupted in BLBC and each of the top six RPs are overexpressed in both BLBC and p16-high tumours. However, at present, the exact role of each of the top six RPs in cancer initiation or senescence evasion is unknown. The key studies linking RP overexpression with cancer initiation and survival are summarised below.

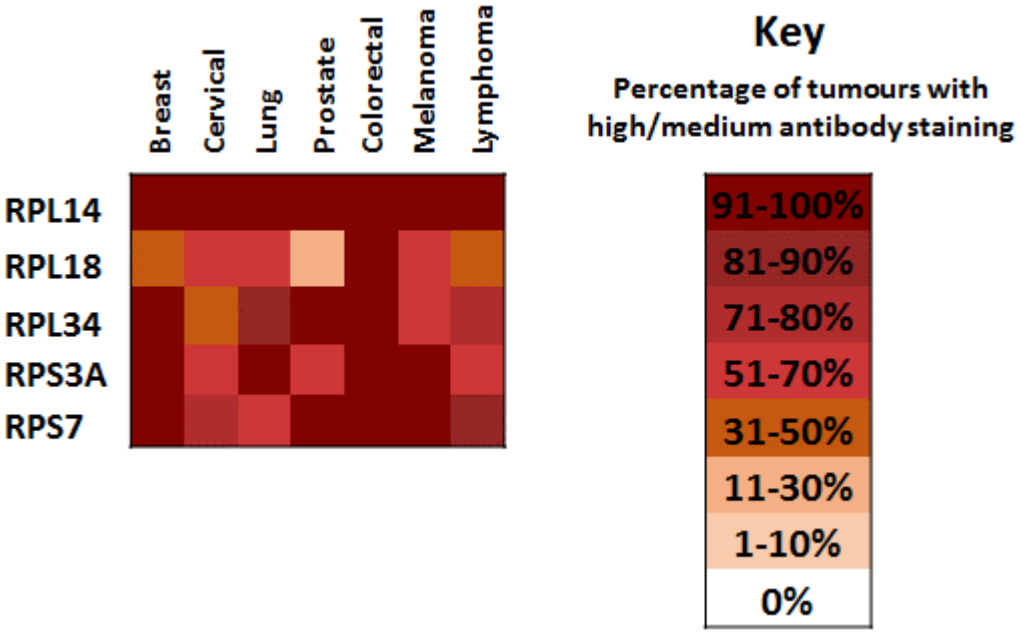

Figure 6.1: Heatmap summarising the level of antibody staining for the top six RP hits within breast and cervical cancer as well as five of the most common cancers in the UK. Data was taken from the Human Protein Atlas database (available at: http://www.proteinatlas.org/cancer). Data for RPL35A was not available. CRUK cancer incidence statistics were used to select the five most common malignancies in the UK (excluding breast cancer) for analysis.

Numerous studies have found RPS3A to be overexpressed in a wide variety of malignancies including squamous cell lung carcinoma and simian immunodeficiency virus-associated monkey lymphoma, (Slizhikova et al., 2005, Tarantul et al., 2000). In addition, Goodin and Rutherford, 2002 found that RPS3A expression was inversely correlated with cellular differentiation in prostate cancer and that RPS3A expression was highest in undifferentiated prostate cancer cells.

Further, cellular transformation of human and rodent cells is often associated with increased RPS3A expression and monoallelic disruption of the gene encoding RPS3A has been found to cause a loss of the transformed phenotype in v-fos-transformed Rat-I fibroblasts (Kho et al., 1996). In addition, Kho et al. showed that RPS3A levels were highest in synchronised human fibroblasts undergoing DNA synthesis, suggesting elevated RPS3A expression is required for S phase progression. Interestingly, RPS3A has been found to be up-regulated upon Epstein-Barr virus (EBV)-induced transformation of B-cells and has been identified as a binding partner of EBV encoded nuclear antigen (EBNA-5). It is proposed that EBNA-5 may facilitate B-cell transformation via direct binding to RPS3A, resulting in disrupted cell cycle control (Kashuba et al., 2005). In addition, RPS3A has also been found to be overexpressed in Hepatitis B virus (HBV)-induced hepatocellular carcinoma when compared with normal tissue and is implicated in the initiation of HBV-induced hepatocellular carcinoma (Lim et al., 2011).

In line with the findings presented within this thesis, Armakolas et al., 2012 found RPS7 to be overexpressed in blood samples taken from 88 primary breast cancer patients when compared to samples taken from matched healthy controls. Elevated RPS7 expression was also proposed as a prognostic biomarker within the HER2+ breast cancer subtype (Armakolas et al., 2012). In addition, RPS7 missense mutations have been identified in 50-60% of patients with the cancer susceptibility syndrome, Diamond Blackfan anaemia (reviewed in Farrar and Dahl, 2011). There is also evidence to suggest that elevated RPS7 levels may contribute to the initiation and progression of human malignancy. For example, treatment of a human hepatoma cell line with hepatic growth factor (HGF) resulted in c-Myc induction as well as upregulated RPS7 expression. This suggests RPS7 may be a novel c-Myc target gene, whose overexpression contributes to carcinogenesis (Hunecke et al., 2012). Contradictory to the data previously discussed, shRNA silencing of RPS7 in epithelial ovarian cancer cells resulted in enhanced proliferation and cell cycle progression together with an increase in ovarian cancer cell invasion and migration (Wang et al., 2013) suggesting that, unlike in BLBC, RPS7 may not be a suitable therapeutic target in ovarian cancer.

RPL14 is highly expressed in almost all human malignancies including breast and cervical cancer (Figure 6.1). However, by contrast, multiple studies have also reported RPL14 LOH in cancer (including squamous cell carcinoma of the head and neck and squamous cell oesophageal cancer) (Shriver et al., 1998, Huang et al., 2006, He et al., 2008), suggesting that in some tissue types RPL14 may perform a tumour suppressive function and is lost during the early stages of cancer development. This data is also in line with the Kaplan Meier data presented in Section

4.2.3 that shows elevated RPL14 expression is associated with a poor prognosis in BLBC and gastric cancer but is protective in lung cancer.

Currently, there is very little literature linking RPL18 or RPL34 to cancer, however, analysis of the Protein Atlas database revealed both RPL18 and RPL34 to be expressed in most human malignancies, including breast and cervical cancer (Figure 6.1).

Interestingly, RPL35A has also been implicated in the cancer susceptibility syndrome, Diamond Blackfan anaemia and RPL35A silencing within a leukemic cell line used to model Diamond Blackfan anaemia resulted in reduced cellular proliferation together with a reduction in 60S ribosomal subunit biogenesis (Farrar et al., 2008). In addition, RPL35A expression has been found to be elevated in human osteosarcoma cell lines compared with normal osteoblasts (Olstad et al., 2003) and increased expression has also been associated with malignant brain tumour formation (Kroes et al., 2000). Importantly, Lopez et al., 2002 showed that RPL35A overexpression in Jurkat cells (immortalised T-lymphocytes) was associated with resistance to UV irradiation and doxorubicin resistance. Interestingly, this resistance to cytotoxic therapies was not associated with enhanced expression of P-glycoprotein (drug efflux pump) or elevated expression of anti-apoptotic factors. These findings suggest that RPL35A may protect cancer cells from cytotoxic damage and, in doing so, mediate senescence evasion in cancer.

The exact mechanism by which the ribosome is grossly dysregulated in cancer is an important question not yet fully addressed within the literature and future work ought to investigate the key transcription factors, miRNAs or epigenetic events responsible for regulating RP expression. It is highly likely that these regulatory mechanisms are disrupted in p16-positive BLBC and perhaps dysregulation within these key pathways may represent early diagnostic biomarkers within this disease subset.

6.2.2 *Does RP silencing and senescence activation alter the cancer translatome?*

Given the level of RP dysregulation associated with BLBC (See Section 4.2) and numerous other human malignancies (see previous Section), it is hypothesised that the cancer ribosome may have an altered composition compared to non-malignant cells and may direct the translation of cancer-promoting transcripts. Importantly, a recent study by Zhang et al., 2015 demonstrated that the cancer ribosome is highly dynamic and may adopt an alternative composition in response to cellular stress such as heat shock. Here, Zhang et al. showed that in response to an elevation in temperature, an alternative cytosolic form of MRPL18 was translated and integrated into the 80S ribosome in HeLa cells. The authors then went on to show that cytosolic MRPL18 expression facilitated the translation of Heat shock Protein 70 (Hsp70) in MEFs and proposes

that perhaps 'specialised ribosomes' are required for the selective translation of a subset of transcripts in response to cellular stress. With this in mind, it is hypothesised that the highly dysregulated cancer ribosome may favour the translation of cancer-promoting transcripts and may mediate senescence evasion and cancer cell survival. Data presented within this thesis suggests that RP silencing in MDA-MB-468 cells induces significant ribosomal biosynthesis dysfunction, reflected by the dramatic alterations to nucleoli number and morphology observed upon senescence activation (see Section 5.5). Furthermore, *in silico* and *in vitro* data presented within Sections 4.2.4 and 4.3.3, respectively, suggests that specific RP silencing may influence the expression of multiple RPs and may alter the cancer-associated 'ribosomal profile', resulting in ribosomes with an altered composition and translational preference. As such, it is hypothesised that knockdown of each of the top six RPs in MDA-MB-468 cells may result in key alterations to the cancer-associated translatome, enabling p16-resensitsation and subsequent senescence activation. Importantly, data presented in Section 4.4 showed that siRNA knockdown of each of the top RP hits did not induce senescence in normal HMECs suggesting that in normal cells, the ribosomal profile may be less vulnerable to the loss of these RPs. However, genome-wide siRNA screening also revealed that most RPs, including RPS6, are essential for both cancer and normal cell proliferation, suggesting that there may be a varied degree of redundancy across the ribosome in normal cells.

In order to confirm that the ribosomes are still intact in cancer cells following RP silencing, TEM could be used to image the ribosomes of MDA-MB-468 cells before and after siRNA knockdown of CBX7 and each of the top six RP hits. In addition, Ribosomal-Sequencing, of both proliferating and senescent MDA-MB-468 cells (following silencing of CBX7 or each of the top six RPs) will enable changes to the translatome upon senescence activation to be explored and may reveal mechanistic insight into the route of p16 re-sensitisation following RP silencing in p16-positive BLBC cells. The data generated here may unite or subcategorise the top six RP hits and may also identify additional potential therapeutic targets downstream of RP silencing. For example, following further validation, those transcripts whose translation is severely reduced upon senescence induction may represent effective drug targets in p16-positive BLBC. Further, the expression level of each of these newly identified transcripts could be assessed in cancer using both the METABRIC and TCGA databases. Those transcripts that are highly expressed in cancer may represent the most suitable therapeutic targets and ought to be prioritised for further validation.

Further experiments, such as protein labelling with radioactive [35S] methionine of both proliferating and senescent MDA-MB-468 cells, would help determine the effect of senescence

activation following RP silencing on global translation levels. In addition, polysome profiling and quantification of rRNAs and their precursors via qRT-PCR within both proliferating and senescent MDA-MB-468s would help elucidate the impact of specific RP silencing on ribosomal biogenesis.

6.3 *The top six RP hits may represent novel therapeutic targets in p16-positive BLBC*

6.3.1 *Can the ribosome be targeted in cancer?*

Analysis of the METABRIC data set (presented in Section 4.2) revealed that the ribosome is severely dysregulated in BLBC and that elevated expression of each of the top six RPs in BLBC is associated with a poor prognosis. In line with this, *in vitro* data presented here has shown that siRNA knockdown of each of the top six RPs resulted in potent senescence activation in MDA-MB-468 cells, in a cancer-specific manner. In addition, RP silencing in MDA-MB-231 cells (p16-null) resulted in cell death. Together, these findings suggest that these RP hits may represent novel drug targets for future pro-senescence therapies in p16-positive BLBC and that targeting these hits in p16-null BLBCs may also be therapeutically favourable. Crucially, the near atomic structure of the human 80S ribosome was recently published and all potential ligand-blinding domains present within the structure have been identified (Khatter et al., 2015). These recent findings may enable future structure-guided *in silico* drug design and allow the cancer ribosome to be targeted by novel small molecule drugs designed to inhibit or replace specific RPs. This is an exciting prospect and one that may revolutionise the personalised treatment of BLBC.

6.3.2 *Future work to validate the top six RP hits as novel therapeutic targets in BLBC*

In order to further validate the top six RP hits as effective therapeutic targets in BLBC, breast cancer patient derived xenografts (p16-null, $p16^{+/+}$ $p21^{+/+}$ or $p16^{+/+}$ p21-null background) containing an inducible shRNA construct targeting each of the top six RP hits could to be implanted into immunodeficient mice. Tumour size, metastasis and life expectancy could then be assessed +/- RP silencing. Crucially, this strategy would enable the therapeutic effectiveness of RP silencing to be assessed *in vivo* and may rank the top six RP candidates according to their therapeutic activity.

At present, it is difficult to estimate the long-term consequences of pro-senescence therapies, such as RP silencing, and it is proposed that following initial senescence activation, senescent cancer cells ought to be rapidly eliminated as part of a two-step therapeutic approach (see Section 1.6.4 for further details). There is now mounting evidence to suggest that components of the SASP are able to trigger the clearance of senescent cells *in vivo* following stimulation of

the immune system (see Section 1.5.3). In addition, Acosta et al., 2013 demonstrated that the SASP may also function to activate senescence in neighbouring cells and promote tumour suppression in surrounding cells vulnerable to transformation. Importantly, it has not yet been established whether or not senescence activation following RP silencing in cancer is associated with a SASP. In order to explore the nature of the SASP associated with RP silencing, a cytokine array could be performed on both proliferating and senescent MDA-MB-468 cells following siRNA knockdown of each of the top six RPs or CBX7. A cytokine array would enable the SASP to be profiled and may indicate whether or not RP silencing *in vivo* is likely to harness the immune system for senescent cell clearance. In addition, conditioned medium experiments where medium taken from senescent MDA-MB-468 cells is applied to proliferating MDA-MB-468 cells and HMECs together with a Transwell assay where senescent MDA-MB-468 cells are co-cultured with proliferating MDA-MB-468 cells and HMECs would assess the paracrine nature of the SASP following RP silencing and may indicate the likely effects of senescent cancer cells on surrounding cancer cells and normal tissues. Together, these experiments may indicate the potential effectiveness of secondary therapies such as immuno-boosting agents following RP silencing and may help to establish a therapeutic window for senescence cell clearance *in vivo*.

As well as immune-boosting agents, it is hypothesised that senolytic agents may also be required as a secondary therapy in order to successfully eliminate senescent cancer cells *in vivo* (see Section 1.6.4). In order to identify those agents capable of selectively targeting senescent cells following RP silencing, inducible shRNA MDA-MB-468 lines for each of the six RP hits ought to be established and a compound screen using these cells +/- shRNA induction as well as proliferating HMECs could be performed. This strategy may identify novel selective senolytic agents that may represent an effective secondary therapy in p16-positive BLBC following RP silencing. These agents could then be tested within the patient derived xenograft models described previously in order to assess their effectiveness *in vivo*.

6.4 *Nucleoli morphology together with the top six RPs may act as novel prognostic biomarkers in p16-positive BLBC*

BLBC is highly heterogeneous and remains the most clinically challenging subtype due to the lack of effective targeted therapies (see Section 1.8). Further stratification of this disease subset and the identification of novel molecular subtypes may drive the development of effective targeted agents and may enable a more sophisticated personalised therapeutic approach. Importantly, analysis of the Kaplan Meier database revealed that elevated expression of each of the top six RPs is associated with a poor prognosis in BLBC suggesting that these ribosomal hits

may represent novel prognostic biomarkers in this disease subset (see Section 4.2.2). In addition, Derenzini et al., 2009 showed that an enlarged and irregular nucleoli is associated with a poor prognosis in breast cancer. In order to assess whether the Kaplan Meier expression data may be replicated at the protein level and to assess the clinical relevance of the top six RPs as potential prognostic biomarkers in BLBC a TMA utilising the METABRIC dataset could be performed. Protein levels of each of the top six RPs together with p16 and the nucleoli signature could be examined within each of the tumour samples. This information could then be cross-compared with known patient data including p53 status, tumour subtype, tumour grade, lymph node status, response to therapy and survival. This strategy may validate the top six RP hits identified here as novel prognostic biomarkers within BLBC and may enable further stratification of this highly heterogeneous disease subtype within the clinic. Routine profiling of the ribosomal signature together with p16 status and nucleoli morphology within BLBC may revolutionise the treatment of BLBC patients and allow the personalised application of novel pro-senescence therapies.

References

ACOSTA, J. C., BANITO, A., WUESTEFELD, T., GEORGILIS, A., JANICH, P., MORTON, J. P., ATHINEOS, D., KANG, T.-W., LASITSCHKA, F., ANDRULIS, M., PASCUAL, G., MORRIS, K. J., KHAN, S., JIN, H., DHARMALINGAM, G., SNIJDERS, A. P., CARROLL, T., CAPPER, D., PRITCHARD, C., INMAN, G. J., LONGERICH, T., SANSOM, O. J., AZNAR BENITAH, S., ZENDER, L. & GIL, J. 2013. A complex secretory program orchestrated by the inflammasome controls paracrine senescence. *Nature Cell Biology,* 15**,** 978-U221.

ACOSTA, J. C. & GIL, J. 2012. Senescence: a new weapon for cancer therapy. *Trends in Cell Biology,* 22**,** 211-219.

AGUILO, F., ZHOU, M.-M. & WALSH, M. J. 2011. Long Noncoding RNA, Polycomb, and the Ghosts Haunting INK4b-ARF-INK4a Expression. *Cancer Research,* 71**,** 5365-5369.

AHMAD, Y., BOISVERT, F.-M., GREGOR, P., COBLEY, A. & LAMOND, A. I. 2009. NOPdb: Nucleolar Proteome Database-2008 update. *Nucleic Acids Research,* 37**,** D181-D184.

ALCORTA, D. A., XIONG, Y., PHELPS, D., HANNON, G., BEACH, D. & BARRETT, J. C. 1996. Involvement of the cyclin-dependent kinase inhibitor p16 (INK4a) in replicative senescence of normal human fibroblasts. *Proceedings of the National Academy of Sciences of the United States of America,* 93**,** 13742-13747.

ANDERS, L., KE, N., HYDBRING, P., CHOI, Y. J., WIDLUND, H. R., CHICK, J. M., ZHAI, H., VIDAL, M., GYGI, S. P., BRAUN, P. & SICINSKI, P. 2011. A Systematic Screen for CDK4/6 Substrates Links FOXM1 Phosphorylation to Senescence Suppression in Cancer Cells. *Cancer Cell,* 20**,** 620-634.

ANDERSEN, J. S., LYON, C. E., FOX, A. H., LEUNG, A. K. L., LAM, Y. W., STEEN, H., MANN, M. & LAMOND, A. I. 2002. Directed proteomic analysis of the human nucleolus. *Current Biology,* 12**,** 1-11.

ARCHAMBAULT, V., LEPINE, G. & KACHANER, D. 2015. Understanding the Polo Kinase machine. *Oncogene,* 34**,** 4799-4807.

ARMAKOLAS, A., STATHOPOULOS, G. P., NEZOS, A., THEOS, A., STATHAKI, M. & KOUTSILIERIS, M. 2012. Subdivision of molecularly-classified groups by new gene signatures in breast cancer patients. *Oncology Reports,* 28**,** 2255-2263.

ARNOLD, C. R., WOLF, J., BRUNNER, S., HERNDLER-BRANDSTETTER, D. & GRUBECK-LOEBENSTEIN, B. 2011. Gain and Loss of T Cell Subsets in Old Age-Age-Related Reshaping of the T Cell Repertoire. *Journal of Clinical Immunology,* 31**,** 137-146.

ASGHAR, U., WITKIEWICZ, A. K., TURNER, N. C. & KNUDSEN, E. S. 2015. The history and future of targeting cyclin-dependent kinases in cancer therapy. *Nature Reviews Drug Discovery,* 14**,** 130-146.

BABIANO, R. & DE LA CRUZ, J. 2010. Ribosomal protein L35 is required for 27SB pre-rRNA processing in Saccharomyces cerevisiae. *Nucleic Acids Research,* 38**,** 5177-5192.

BADVE, S., DABBS, D. J., SCHNITT, S. J., BAEHNER, F. L., DECKER, T., EUSEBI, V., FOX, S. B., ICHIHARA, S., JACQUEMIER, J., LAKHANI, S. R., PALACIOS, J., RAKHA, E. A., RICHARDSON, A. L., SCHMITT, F. C., TAN, P.-H., TSE, G. M., WEIGELT, B., ELLIS, I. O. & REIS-FILHO, J. S. 2011. Basal-like and triple-negative breast cancers: a critical review with an emphasis on the implications for pathologists and oncologists. *Modern Pathology,* 24**,** 157-167.

BAIRD, R. D. & CALDAS, C. 2013. Genetic heterogeneity in breast cancer: the road to personalized medicine? *Bmc Medicine,* 11.

BAKER, D. J., WIJSHAKE, T., TCHKONIA, T., LEBRASSEUR, N. K., CHILDS, B. G., VAN DE SLUIS, B., KIRKLAND, J. L. & VAN DEURSEN, J. M. 2011. Clearance of p16(Ink4a)-positive senescent cells delays ageing-associated disorders. *Nature,* 479**,** 232-U112.

BALDIN, V., LUKAS, J., MARCOTE, M. J., PAGANO, M. & DRAETTA, G. 1993. CYCLIN D1 IS A NUCLEAR-PROTEIN REQUIRED FOR CELL-CYCLE PROGRESSION IN G(1). *Genes & Development,* 7**,** 812-821.

BAN, N., BECKMANN, R., CATE, J. H. D., DINMAN, J. D., DRAGON, F., ELLIS, S. R., LAFONTAINE, D. L. J., LINDAHL, L., LILJAS, A., LIPTON, J. M., MCALEAR, M. A., MOORE, P. B., NOLLER, H. F., ORTEGA, J., PANSE, V. G., RAMAKRISHNAN, V., SPAHN, C. M. T., STEITZ, T. A., TCHORZEWSKI, M., TOLLERVEY, D., WARREN, A. J., WILLIAMSON, J. R., WILSON, D., YONATH, A. & YUSUPOV, M. 2014. A new system for naming ribosomal proteins. *Current Opinion in Structural Biology,* 24**,** 165-169.

BAO, B., WANG, Z., ALI, S., KONG, D., BANERJEE, S., AHMAD, A., LI, Y., AZMI, A. S., MIELE, L. & SARKAR, F. H. 2011. Over-Expression of FoxM1 Leads to Epithelial-Mesenchymal Transition and Cancer Stem Cell Phenotype in Pancreatic Cancer Cells. *Journal of Cellular Biochemistry,* 112**,** 2296-2306.

BAZAROV, A. V., LEE, W. J., BAZAROV, I., BOSIRE, M., HINES, W. C., STANKOVICH, B., CHICAS, A., LOWE, S. W. & YASWEN, P. 2012. The specific role of pRb in p16(INK4A)-mediated arrest of normal and malignant human breast cells. *Cell Cycle,* 11**,** 1008-1013.

BEECH, D. J., MADAN, A. K. & DENG, N. 2002. Expression of PH-20 in normal and neoplastic breast tissue. *Journal of Surgical Research,* 103**,** 203-207.

BEKTAS, N., TEN HAAF, A., VEECK, J., WILD, P. J., LUESCHER-FIRZLAFF, J., HARTMANN, A., KNUECHEL, R. & DAHL, E. 2008. Tight correlation between expression of the Forkhead transcription factor FOXM1 and HER2 in human breast cancer. *Bmc Cancer,* 8.

BELLA, L., ZONA, S., DE MORAES, G. N. & LAM, E. W. F. 2014. FOXM1: A key oncofoetal transcription factor in health and disease. *Seminars in Cancer Biology,* 29**,** 32-39.

BERKOVICH, E., LAMED, Y. & GINSBERG, D. 2003. E2F and Ras synergize in transcriptionally activating p14ARF expression. *Cell cycle (Georgetown, Tex.),* 2**,** 127-33.

BETZ, B. L., STROBECK, M. W., REISMAN, D. N., KNUDSEN, E. S. & WEISSMAN, B. E. 2002. Re-expression of hSNF5/INI1/BAF47 in pediatric tumor cells leads to G(1) arrest associated with induction of p16ink4a and activation of RB. *Oncogene,* 21**,** 5193-5203.

BISHOP, C. L., BERGIN, A.-M. H., FESSART, D., BORGDORFF, V., HATZIMASOURA, E., GARBE, J. C., STAMPFER, M. R., KOH, J. & BEACH, D. H. 2010. Primary Cilium-Dependent and -Independent Hedgehog Signaling Inhibits p16(INK4A). *Molecular Cell,* 40**,** 533-547.

BOLTE, C., ZHANG, Y., YORK, A., KALIN, T. V., SCHULTZ, J. E. J., MOLKENTIN, J. D. & KALINICHENKO, V. V. 2012. Postnatal Ablation of Foxm1 from Cardiomyocytes Causes Late Onset Cardiac Hypertrophy and Fibrosis without Exacerbating Pressure Overload-Induced Cardiac Remodeling. *Plos One,* 7.

BORASCHI, D. & ITALIANI, P. 2014. Immunosenescence and vaccine failure in the elderly: Strategies for improving response. *Immunology Letters,* 162**,** 346-353.

BOROS, L. G., BRANDES, J. L., YUSUF, F. I., CASCANTE, M., WILLIAMS, R. D. & SCHIRMER, W. J. 1998. Inhibition of the oxidative and nonoxidative pentose phosphate pathways by somatostatin: a possible mechanism of antitumor action. *Medical Hypotheses,* 50**,** 501-506.

BOUGA, H., TSOUROS, I., BOUNIAS, D., KYRIAKOPOULOU, D., STAVROPOULOS, M. S., PAPAGEORGAKOPOULOU, N., THEOCHARIS, D. A. & VYNIOS, D. H. 2010. Involvement of hyaluronidases in colorectal cancer. *Bmc Cancer,* 10.

BOULON, S., WESTMAN, B. J., HUTTEN, S., BOISVERT, F.-M. & LAMOND, A. I. 2010. The Nucleolus under Stress. *Molecular Cell,* 40**,** 216-227.

BOUTROS, M. & AHRINGER, J. 2008. The art and design of genetic screens: RNA interference. *Nature Reviews Genetics,* 9**,** 554-566.

BRACKEN, A. P., KLEINE-KOHLBRECHER, D., DIETRICH, N., PASINI, D., GARGIULO, G., BEEKMAN, C., THEILGAARD-MONCH, K., MINUCCI, S., PORSE, B. T., MARINE, J.-C., HANSEN, K. H. & HELIN, K. 2007. The Polycomb group proteins bind throughout the INK4A-ARF locus and are disassociated in senescent cells. *Genes & Development,* 21**,** 525-530.

BRAIG, M., LEE, S., LODDENKEMPER, C., RUDOLPH, C., PETERS, A., SCHLEGELBERGER, B., STEIN, H., DORKEN, B., JENUWEIN, T. & SCHMITT, C. A. 2005. Oncogene-induced senescence as an initial barrier in lymphoma development. *Nature,* 436**,** 660-665.

BREHM, A., MISKA, E. A., MCCANCE, D. J., REID, J. L., BANNISTER, A. J. & KOUZARIDES, T. 1998. Retinoblastoma protein recruits histone deacetylase to repress transcription. *Nature,* 391**,** 597-601.

BRENNER, A. J., STAMPFER, M. R. & ALDAZ, C. M. 1998. Increased p16 expression with first senescence arrest in human mammary epithelial cells and extended growth capacity with p16 inactivation. *Oncogene,* 17**,** 199-205.

BROWN, D. D. & GURDON, J. B. 1964. ABSENCE OF RIBOSOMAL RNA SYNTHESIS IN THE ANUCLEOLATE MUTANT OF XENOPUS LAEVIS. *Proceedings of the National Academy of Sciences,* 51**,** 139-146.

BRUUNSGAARD, H. & PEDERSEN, B. K. 2003. Age-related inflammatory cytokines and disease. *Immunology and Allergy Clinics of North America,* 23**,** 15-+.

BURCHETT, K. M., YAN, Y. & OUELLETTE, M. M. 2014. Telomerase Inhibitor Imetelstat (GRN163L) Limits the Lifespan of Human Pancreatic Cancer Cells. *Plos One,* 9.

BUTT, A. J., SERGIO, C. M., INMAN, C. K., ANDERSON, L. R., MCNEIL, C. M., RUSSELL, A. J., NOUSCH, M., PREISS, T., BIANKIN, A. V., SUTHERLAND, R. L. & MUSGROVE, E. A. 2008. The estrogen and c-Myc target gene HSPC111 is over-expressed in breast cancer and associated with poor patient outcome. *Breast Cancer Research,* 10.

BYWATER, M. J., POORTINGA, G., SANIJ, E., HEIN, N., PECK, A., CULLINANE, C., WALL, M., CLUSE, L., DRYGIN, D., ANDERES, K., HUSER, N., PROFFITT, C., BLIESATH, J., HADDACH, M., SCHWAEBE, M. K., RYCKMAN, D. M., RICE, W. G., SCHMITT, C., LOWE, S. W., JOHNSTONE, R. W., PEARSON, R. B., MCARTHUR, G. A. & HANNAN, R. D. 2012. Inhibition of RNA Polymerase I as a Therapeutic Strategy to Promote Cancer-Specific Activation of p53. *Cancer Cell,* 22**,** 51-65.

CAMPISI, J. 2005. Senescent cells, tumor suppression, and organismal aging: Good citizens, bad neighbors. *Cell,* 120**,** 513-522.

CAMPISI, J. 2011. Cellular senescence: putting the paradoxes in perspective. *Current Opinion in Genetics & Development,* 21**,** 107-112.

CAMPISI, J. & DI FAGAGNA, F. D. A. 2007. Cellular senescence: when bad things happen to good cells. *Nature Reviews Molecular Cell Biology,* 8**,** 729-740.

CANCER RESEARCH UK. 2014. *Breast cancer* [Online]. Available: http://www.cancerresearchuk.org/cancer-help/type/breast-cancer/ [Accessed 23/03/2014 2014].

CAREY, L. A., DEES, E. C., SAWYER, L., GATTI, L., MOORE, D. T., COLLICHIO, F., OLLILA, D. W., SARTOR, C. I., GRAHAM, M. L. & PEROU, C. M. 2007. The triple negative paradox: Primary tumor chemosensitivity of breast cancer subtypes. *Clinical Cancer Research,* 13**,** 2329-2334.

CAVANAUGH, A. H., HEMPEL, W. M., TAYLOR, L. J., ROGALSKY, V., TODOROV, G. & ROTHBLUM, L. I. 1995. ACTIVITY OF RNA-POLYMERASE-I TRANSCRIPTION FACTOR UBF BLOCKED BY RB GENE-PRODUCT. *Nature,* 374**,** 177-180.

CHAN, B., VANDERLAAN, P. A. & SUKHATME, V. P. 2013. 6-Phosphogluconate dehydrogenase regulates tumor cell migration in vitro by regulating receptor tyrosine kinase c-Met. *Biochemical and Biophysical Research Communications,* 439**,** 247-251.

CHEN, B., RAO, X., HOUSE, M. G., NEPHEW, K. P., CULLEN, K. J. & GUO, Z. 2011. GPx3 promoter hypermethylation is a frequent event in human cancer and is associated with tumorigenesis and chemotherapy response. *Cancer Letters,* 309**,** 37-45.

CHEN, D., SHAN, J., ZHU, W.-G., QIN, J. & GU, W. 2010. Transcription-independent ARF regulation in oncogenic stress-mediated p53 responses. *Nature,* 464**,** 624-U193.

CHEN, D., ZHANG, Z., LI, M., WANG, W., LI, Y., RAYBURN, E. R., HILL, D. L., WANG, H. & ZHANG, R. 2007. Ribosomal protein S7 as a novel modulator of p53-MDM2 interaction: binding to MDM2, stabilization of p53 protein, and activation of p53 function. *Oncogene,* 26**,** 5029-5037.

CHEN, Q., FISCHER, A., REAGAN, J. D., YAN, L. J. & AMES, B. N. 1995. OXIDATIVE DNA-DAMAGE AND SENESCENCE OF HUMAN-DIPLOID FIBROBLAST CELLS. *Proceedings of the National Academy of Sciences of the United States of America,* 92**,** 4337-4341.

CHEN, W., QIU, J. & SHEN, Y. M. 2012. Topoisomerase IIalpha, rather than IIbeta, is a promising target in development of anti-cancer drugs. *Drug discoveries & therapeutics,* 6**,** 230-7.

CHEN, Z. B., TROTMAN, L. C., SHAFFER, D., LIN, H. K., DOTAN, Z. A., NIKI, M., KOUTCHER, J. A., SCHER, H. I., LUDWIG, T., GERALD, W., CORDON-CARDO, C. & PANDOLFI, P. P. 2005. Crucial role of p53-dependent cellular senescence in suppression of Pten-deficient tumorigenesis. *Nature,* 436**,** 725-730.

CHEN, Z. J. & PIKAARD, C. S. 1997. Epigenetic silencing of RNA polymerase I transcription: a role for DNA methylation and histone modification in nucleolar dominance. *Genes & Development,* 11**,** 2124-2136.

COLLADO, M., GIL, J., EFEYAN, A., GUERRA, C., SCHUHMACHER, A. J., BARRADAS, M., BENGURIA, A., ZABALLOS, A., FLORES, J. M., BARBACID, M., BEACH, D. & SERRANO, M. 2005. Tumour biology - Senescence in premalignant tumours. *Nature,* 436**,** 642-642.

COUDREUSE, D. & NURSE, P. 2010. Driving the cell cycle with a minimal CDK control network. *Nature,* 468**,** 1074-U474.

CRUICKSHANKS, H. A., MCBRYAN, T., NELSON, D. M., VANDERKRAATS, N. D., SHAH, P. P., VAN TUYN, J., RAI, T. S., BROCK, C., DONAHUE, G., DUNICAN, D. S., DROTAR, M. E., MEEHAN, R. R., EDWARDS, J. R., BERGER, S. L. & ADAMS, P. D. 2013. Senescent cells harbour features of the cancer epigenome. *Nature Cell Biology,* 15**,** 1495-+.

CURTIS, C., SHAH, S. P., CHIN, S.-F., TURASHVILI, G., RUEDA, O. M., DUNNING, M. J., SPEED, D., LYNCH, A. G., SAMARAJIWA, S., YUAN, Y., GRAEF, S., HA, G., HAFFARI, G., BASHASHATI, A., RUSSELL, R., MCKINNEY, S., LANGEROD, A., GREEN, A., PROVENZANO, E., WISHART, G., PINDER, S., WATSON, P., MARKOWETZ, F., MURPHY, L., ELLIS, I., PURUSHOTHAM, A., BORRESEN-DALE, A.-L., BRENTON, J. D., TAVARE, S., CALDAS, C., APARICIO, S. & GRP, M. 2012. The genomic and transcriptomic architecture of 2,000 breast tumours reveals novel subgroups. *Nature,* 486**,** 346-352.

D'ADDA DI FAGAGNA, F., REAPER, P. M., CLAY-FARRACE, L., FIEGLER, H., CARR, P., VON ZGLINICKI, T., SARETZKI, G., CARTER, N. P. & JACKSON, S. P. 2003. A DNA damage checkpoint response in telomere-initiated senescence. *Nature,* 426**,** 194-8.

DALTON, S. 1992. CELL-CYCLE REGULATION OF THE HUMAN CDC2 GENE. *Embo Journal,* 11**,** 1797-1804.

DANKORT, D., FILENOVA, E., COLLADO, M., SERRANO, M., JONES, K. & MCMAHON, M. 2007. A new mouse model to explore the initiation, progression, and therapy of BRAF(V600E)-induced lung tumors. *Genes & Development,* 21**,** 379-384.

DE LAS HERAS-RUBIO, A., PERUCHO, L., PACIUCCI, R., VILARDELL, J. & LLEONART, M. E. 2014. Ribosomal proteins as novel players in tumorigenesis. *Cancer and Metastasis Reviews,* 33**,** 115-141.

DEBINSKI, W., GIBO, D. M., HULET, S. W., CONNOR, J. R. & GILLESPIE, G. Y. 1999. Receptor for interleukin 13 is a marker and therapeutic target for human high-grade gliomas. *Clinical Cancer Research,* 5**,** 985-990.

DEMARIA, M., OHTANI, N., YOUSSEF, S. A., RODIER, F., TOUSSAINT, W., MITCHELL, J. R., LABERGE, R.-M., VIJG, J., VAN STEEG, H., DOLLE, M. E. T., HOEIJMAKERS, J. H. J., DE BRUIN, A., HARA, E. & CAMPISI, J. 2014. An Essential Role for Senescent Cells in Optimal Wound Healing through Secretion of PDGF-AA. *Developmental Cell,* 31**,** 722-733.

DENG, W., GOWEN, B. G., ZHANG, L., WANG, L., LAU, S., IANNELLO, A., XU, J., ROVIS, T. L., XIONG, N. & RAULET, D. H. 2015. A shed NKG2D ligand that promotes natural killer cell activation and tumor rejection. *Science,* 348**,** 136-139.

DERENZINI, M., MONTANARO, L. & TRERE, D. 2009. What the nucleolus says to a tumour pathologist. *Histopathology,* 54**,** 753-762.

DERENZINI, M., TRERE, D., PESSION, A., GOVONI, M., SIRRI, V. & CHIECO, P. 2000. Nucleolar size indicates the rapidity of cell proliferation in cancer tissues. *Journal of Pathology,* 191**,** 181-186.

DIEP, C., CHARLES, N., BLAKE GILKS, C., KALLOGER, S., ARGENTA, P. & LANGE, C. A. 2013. Progesterone receptors induce FOXO1-dependent senescence in ovarian cancer cells. *Cell Cycle,* 12**,** 1433-1449.

DILEONARDO, A., LINKE, S. P., CLARKIN, K. & WAHL, G. M. 1994. DNA-DAMAGE TRIGGERS A PROLONGED P53-DEPENDENT G(1) ARREST AND LONG-TERM INDUCTION OF CIP1 IN NORMAL HUMAN FIBROBLASTS. *Genes & Development,* 8**,** 2540-2551.

DIMRI, G. P., LEE, X. H., BASILE, G., ACOSTA, M., SCOTT, C., ROSKELLEY, C., MEDRANO, E. E., LINSKENS, M., RUBELJ, I., PEREIRASMITH, O., PEACOCKE, M. & CAMPISI, J. 1995. A BIOMARKER THAT IDENTIFIES SENESCENT HUMAN-CELLS IN CULTURE AND IN AGING SKIN IN-VIVO. *Proceedings of the National Academy of Sciences of the United States of America,* 92**,** 9363-9367.

DOERR, J. R., YU, Y., MILANOVIC, M., BEUSTER, G., ZASADA, C., DAEBRITZ, J. H. M., LISEC, J., LENZE, D., GERHARDT, A., SCHLEICHER, K., KRATZAT, S., PURFUERST, B., WALENTA, S., MUELLER-KLIESER, W., GRAELER, M., HUMMEL, M., KELLER, U., BUCK, A. K., DOERKEN, B., WILLMITZER, L., REIMANN, M., KEMPA, S., LEE, S. & SCHMITT, C. A. 2013. Synthetic lethal metabolic targeting of cellular senescence in cancer therapy. *Nature,* 501**,** 421-+.

DOHERTY, L., SHEEN, M. R., VLACHOS, A., CHOESMEL, V., O'DONOHUE, M.-F., CLINTON, C., SCHNEIDER, H. E., SIEFF, C. A., NEWBURGER, P. E., BALL, S. E., NIEWIADOMSKA, E., MATYSIAK, M., GLADER, B., ARCECI, R. J., FARRAR, J. E., ATSIDAFTOS, E., LIPTON, J. M., GLEIZES, P.-E. & GAZDA, H. T. 2010. Ribosomal Protein Genes RPS10 and RPS26 Are Commonly Mutated in Diamond-Blackfan Anemia. *American Journal of Human Genetics,* 86**,** 222-228.

DRAGON, F., GALLAGHER, J. E. G., COMPAGNONE-POST, P. A., MITCHELL, B. M., PORWANCHER, K. A., WEHNER, K. A., WORMSLEY, S., SETTLAGE, R. E., SHABANOWITZ, J., OSHEIM, Y., BEYER, A. L., HUNT, D. F. & BASERGA, S. J. 2002. A large nucleolar U3 ribonucleoprotein required for 18S ribosomal RNA biogenesis. *Nature,* 417**,** 967-970.

DRYGIN, D., LIN, A., BLIESATH, J., HO, C. B., O'BRIEN, S. E., PROFFITT, C., OMORI, M., HADDACH, M., SCHWAEBE, M. K., SIDDIQUI-JAIN, A., STREINER, N., QUIN, J. E., SANIJ, E., BYWATER, M. J., HANNAN, R. D., RYCKMAN, D., ANDERES, K. & RICE, W. G. 2011. Targeting RNA Polymerase I with an Oral Small Molecule CX-5461 Inhibits Ribosomal RNA Synthesis and Solid Tumor Growth. *Cancer Research,* 71**,** 1418-1430.

DRYGIN, D., SIDDIQUI-JAIN, A., O'BRIEN, S., SCHWAEBE, M., LIN, A., BLIESATH, J., HO, C. B., PROFFITT, C., TRENT, K., WHITTEN, J. P., LIM, J. K. C., VON HOFF, D., ANDERES, K. & RICE, W. G. 2009. Anticancer Activity of CX-3543: A Direct Inhibitor of rRNA Biogenesis. *Cancer Research,* 69**,** 7653-7661.

DYSON, N. 1998. The regulation of E2F by pRB-family proteins. *Genes & Development,* 12**,** 2245-2262.

ELDEIRY, W. S., TOKINO, T., VELCULESCU, V. E., LEVY, D. B., PARSONS, R., TRENT, J. M., LIN, D., MERCER, W. E., KINZLER, K. W. & VOGELSTEIN, B. 1993. WAF1, A POTENTIAL MEDIATOR OF P53 TUMOR SUPPRESSION. *Cell,* 75**,** 817-825.

FALSCHLEHNER, C., STEINBRINK, S., ERDMANN, G. & BOUTROS, M. 2010. High-throughput RNAi screening to dissect cellular pathways: A how-to guide. *Biotechnology Journal,* 5**,** 368-376.

FARRAR, J. E. & DAHL, N. 2011. Untangling the Phenotypic Heterogeneity of Diamond Blackfan Anemia. *Seminars in Hematology,* 48**,** 124-135.

FARRAR, J. E., NATER, M., CAYWOOD, E., MCDEVITT, M. A., KOWALSKI, J., TAKEMOTO, C. M., TALBOT, C. C., JR., MELTZER, P., ESPOSITO, D., BEGGS, A. H., SCHNEIDER, H. E., GRABOWSKA, A., BALL, S. E., NIEWIADOMSKA, E., SIEFF, C. A., VLACHOS, A., ATSIDAFTOS, E., ELLIS, S. R., LIPTON, J. M., GAZDA, H. T. & ARECI, R. J. 2008. Abnormalities of the large ribosomal subunit protein, Rp135a, in Diamond-Blackfan anemia. *Blood,* 112**,** 1582-1592.

FATICA, A., CRONSHAW, A. D., DLAKIC, M. & TOLLERVEY, D. 2002. Ssf1p prevents premature processing of an early pre-60S ribosomal particle. *Molecular Cell,* 9**,** 341-351.

FATICA, A. & TOLLERVEY, D. 2002. Making ribosomes. *Current Opinion in Cell Biology,* 14**,** 313-318.

FERREIRA-CERCA, S., POELL, G., KUEHN, H., NEUEDER, A., JAKOB, S., TSCHOCHNER, H. & MILKEREIT, P. 2007. Analysis of the in vivo assembly pathway of eukaryotic 40S ribosomal proteins. *Molecular Cell,* 28**,** 446-457.

FERREIRA-CERCA, S., POLL, G., GLEIZES, P. E., TSCHOCHNER, H. & MILKEREIT, P. 2005. Roles of eukaryotic ribosomal proteins in maturation and transport of pre-18S rRNA and ribosome function. *Molecular Cell,* 20**,** 263-275.

FIGUEROA-MAGALHÃES, M. C., JELOVAC, D., CONNOLLY, R. M. & WOLFF, A. C. 2014. Treatment of HER2-positive breast cancer. *The Breast,* 23**,** 128-136.

FINN, R. S., DERING, J., CONKLIN, D., KALOUS, O., COHEN, D. J., DESAI, A. J., GINTHER, C., ATEFI, M., CHEN, I., FOWST, C., LOS, G. & SLAMON, D. J. 2009. PD 0332991, a selective cyclin D kinase 4/6 inhibitor, preferentially inhibits proliferation of luminal estrogen receptor-positive human breast cancer cell lines in vitro. *Breast Cancer Research,* 11.

FIRE, A., XU, S. Q., MONTGOMERY, M. K., KOSTAS, S. A., DRIVER, S. E. & MELLO, C. C. 1998. Potent and specific genetic interference by double-stranded RNA in Caenorhabditis elegans. *Nature,* 391**,** 806-811.

FORMENTINI, A., BRAUN, P., FRICKE, H., LINK, K.-H., HENNE-BRUNS, D. & KORNMANN, M. 2012. Expression of interleukin-4 and interleukin-13 and their receptors in colorectal cancer. *International Journal of Colorectal Disease,* 27**,** 1369-1376.

FREUND, A., LABERGE, R.-M., DEMARIA, M. & CAMPISI, J. 2012. Lamin B1 loss is a senescence-associated biomarker. *Molecular Biology of the Cell,* 23**,** 2066-2075.

FREUND, A., ORJALO, A. V., DESPREZ, P.-Y. & CAMPISI, J. 2010. Inflammatory networks during cellular senescence: causes and consequences. *Trends in Molecular Medicine,* 16**,** 238-246.

FROMONT-RACINE, M., SENGER, B., SAVEANU, C. & FASIOLO, F. 2003. Ribosome assembly in eukaryotes. *Gene,* 313**,** 17-42.

FUMAGALLI, S., DI CARA, A., NEB-GULATI, A., NATT, F., SCHWEMBERGER, S., HALL, J., BABCOCK, G. F., BERNARDI, R., PANDOLFI, P. P. & THOMAS, G. 2009. Absence of nucleolar disruption after impairment of 40s ribosome biogenesis reveals an rpL11-translation-dependent mechanism of p53 induction. *Nature Cell Biology,* 11**,** 501-U350.

GADAL, O., STRAUSS, D., KESSL, J., TRUMPOWER, B., TOLLERVEY, D. & HURT, E. 2001. Nuclear export of 60S ribosomal subunits depends on Xpo1p and requires a nuclear export sequence-containing factor, Nmd3p that associates with the large subunit protein Rpl10p. *Molecular and Cellular Biology,* 21**,** 3405-3415.

GAGNON, A. M., CHABOT, J., PARDASANI, D. & SORISKY, A. 1998. Extracellular matrix induced by TGF beta impairs insulin signal transduction in 3T3-L1 preadipose cells. *Journal of Cellular Physiology,* 175**,** 370-378.

GIL, J., BERNARD, D., MARTINEZ, D. & BEACH, D. 2004. Polycomb CBX7 has a unifying role in cellular lifespan. *Nature Cell Biology,* 6**,** 67-U19.

GIL, J. & PETERS, G. 2006. Regulation of the INK4b-ARF-INK4a tumour suppressor locus: all for one or one for all. *Nature Reviews Molecular Cell Biology,* 7**,** 667-677.

GODIN, D. A., FITZPATRICK, P. C., SCANDURRO, A. B., BELAFSKY, P. C., WOODWORTH, B. A., AMEDEE, R. G., BEECH, D. J. & BECKMAN, B. S. 2000. PH-20 - A novel tumor marker for laryngeal cancer. *Archives of Otolaryngology-Head & Neck Surgery,* 126**,** 402-404.

GOMEZ-ROMAN, N., FELTON-EDKINS, Z. A., KENNETH, N. S., GOODFELLOW, S. J., ATHINEOS, D., ZHANG, J. X., RAMSBOTTOM, B. A., INNES, F., KANTIDAKIS, T., KERR, E. R., BRODIE, J., GRANDORI, C. & WHITE, R. J. 2006. Activation by c-Myc of transcription by RNA polymerases I, II and III. *In:* ROBERTS, S. G. E., WEINZIERL, R. O. J. & WHITE, R. J. (eds.) *Transcription.*

GONZALEZ, L., GHADAOUIA, S., MARTINEZ, A. & RODIER, F. 2015. Premature aging/senescence in cancer cells facing therapy: good or bad? *Biogerontology***,** 1-17.

GOODIN, J. L. & RUTHERFORD, C. L. 2002. Characterization of human ribosomal S3a gene expression during adenosine 3 ': 5 ' cyclic monophosphate induced neuroendocrine differentiation of LNCaP cells - Regulation of S3a gene expression in LNCaP. *Molecular Biology Reports,* 29**,** 301-316.

GRANDI, P., RYBIN, V., BASSLER, J., PETFALSKI, E., STRAUSS, D., MARZIOCH, M., SCHAFER, T., KUSTER, B., TSCHOCHNER, H., TOLLERVEY, D., GAVIN, A. C. & HURT, E. 2002. 90S pre-ribosomes include the 35S pre-rRNA, the U3 snoRNP, and 40S subunit processing factors but predominantly lack 60S synthesis factors. *Molecular Cell,* 10**,** 105-115.

GRANNEMAN, S. & TOLLERVEY, D. 2007. Building ribosomes: Even more expensive than expected? *Current Biology,* 17**,** R415-R417.

GRAY-SCHOPFER, V. C., CHEONG, S. C., CHONG, H., CHOW, J., MOSS, T., ABDEL-MALEK, Z. A., MARAIS, R., WYNFORD-THOMAS, D. & BENNETT, D. C. 2006. Cellular senescence in naevi and immortalisation in melanoma: a role for p16? *British Journal of Cancer,* 95**,** 496-505.

GREASLEY, P. J., BONNARD, C. & AMATI, B. 2000. Myc induces the nucleolin and BN51 genes: possible implications in ribosome biogenesis. *Nucleic Acids Research,* 28**,** 446-453.

GREEN, M. D., FRANCIS, P. A., GEBSKI, V., HARVEY, V., KARAPETIS, C., CHAN, A., SNYDER, R., FONG, A., BASSER, R., FORBES, J. F. & AUSTRALIAN NEW ZEALAND BREAST, C. 2009. Gefitinib treatment in hormone-resistant and hormone receptor-negative advanced breast cancer. *Annals of Oncology,* 20**,** 1813-1817.

GRIFFITH, J. D., COMEAU, L., ROSENFIELD, S., STANSEL, R. M., BIANCHI, A., MOSS, H. & DE LANGE, T. 1999. Mammalian telomeres end in a large duplex loop. *Cell,* 97**,** 503-514.

GRUMMT, I., SMITH, V. A. & GRUMMT, F. 1976. AMINO-ACID STARVATION AFFECTS INITIATION FREQUENCY OF NUCLEOLAR RNA-POLYMERASE. *Cell,* 7**,** 439-445.

HA, L., ICHIKAWA, T., ANVER, M., DICKINS, R., LOWE, S., SHARPLESS, N. E., KRIMPENFORT, P., DEPINHO, R. A., BENNETT, D. C., SVIDERSKAYA, E. V. & MERLINO, G. 2007. ARF functions as a melanoma tumor suppressor by inducing p53-independent senescence. *Proceedings of the National Academy of Sciences of the United States of America,* 104**,** 10968-10973.

HAN, Z. Y., WEI, W. Y., DUNAWAY, S., DARNOWSKI, J. W., CALABRESI, P., SEDIVY, J., HENDRICKSON, E. A., BALAN, K. V., PANTAZIS, P. & WYCHE, J. H. 2002. Role of p21 in apoptosis and senescence of human colon cancer cells treated with camptothecin. *Journal of Biological Chemistry,* 277**,** 17154-17160.

HANAHAN, D. & WEINBERG, R. A. 2011. Hallmarks of Cancer: The Next Generation. *Cell,* 144**,** 646-674.

HARASHIMA, H., DISSMEYER, N. & SCHNITTGER, A. 2013. Cell cycle control across the eukaryotic kingdom. *Trends in Cell Biology,* 23**,** 345-356.

HARBECK, N., SOTLAR, K., WUERSTLEIN, R. & DOISNEAU-SIXOU, S. 2014. Molecular and protein markers for clinical decision making in breast cancer: Today and tomorrow. *Cancer Treatment Reviews,* 40**,** 434-444.

HARDING, E. 2015. Palbociclib for hormone receptor-positive breast cancer. *The Lancet Oncology,* 16**,** e318.

HARLEY, C. B., FUTCHER, A. B. & GREIDER, C. W. 1990. TELOMERES SHORTEN DURING AGING OF HUMAN FIBROBLASTS. *Nature,* 345**,** 458-460.

HAYAKAWA, Y. & SMYTH, M. J. 2006. NKG2D and cytotoxic effector function in tumor immune surveillance. *Seminars in Immunology,* 18**,** 176-185.

HAYFLICK, L. 1965. THE LIMITED IN VITRO LIFETIME OF HUMAN DIPLOID CELL STRAINS. *Experimental cell research,* 37**,** 614-36.

HAYFLICK, L. & MOORHEAD, P. S. 1961. The serial cultivation of human diploid cell strains. *Experimental cell research,* 25**,** 585-621.

HE, S., GUO, G.-M., LIU, F.-X., HUANG, X.-P., XU, X., CAI, Y., HAN, Y.-L., ZHAN, Q.-M., WU, M., DONG, J.-T., WANG, G.-Q. & WANG, M.-R. 2008. Molecular analysis in combination with iodine staining may contribute to the risk prediction of esophageal squamous cell carcinoma. *Journal of Cancer Research and Clinical Oncology,* 134**,** 307-315.

HE, Y., WANG, Y., LI, P., ZHU, S., WANG, J. & ZHANG, S. 2011. Identification of GPX3 Epigenetically Silenced by CpG Methylation in Human Esophageal Squamous Cell Carcinoma. *Digestive Diseases and Sciences,* 56**,** 681-688.

HELIN, K., HARLOW, E. & FATTAEY, A. 1993. INHIBITION OF E2F-1 TRANSACTIVATION BY DIRECT BINDING OF THE RETINOBLASTOMA PROTEIN. *Molecular and Cellular Biology,* 13**,** 6501-6508.

HEMANN, M. T., STRONG, M. A., HAO, L. Y. & GREIDER, C. W. 2001. The shortest telomere, not average telomere length, is critical for cell viability and chromosome stability. *Cell,* 107**,** 67-77.

HERAULT, O., HOPE, K. J., DENEAULT, E., MAYOTTE, N., CHAGRAOUI, J., WILHELM, B. T., CELLOT, S., SAUVAGEAU, M., ANDRADE-NAVARRO, M. A., HEBERT, J. & SAUVAGEAU, G. 2012. A role for GPx3 in activity of normal and leukemia stem cells. *Journal of Experimental Medicine,* 209**,** 895-901.

HERBIG, U., JOBLING, W. A., CHEN, B. P. C., CHEN, D. J. & SEDIVY, J. M. 2004. Telomere shortening triggers senescence of human cells through a pathway involving ATM, p53, and p21(CIP1), but not p16(INK4a). *Molecular Cell,* 14**,** 501-513.

HERSCHKOWITZ, J. I., HE, X., FAN, C. & PEROU, C. M. 2008. The functional loss of the retinoblastoma tumour suppressor is a common event in basal-like and luminal B breast carcinomas. *Breast Cancer Research,* 10.

HIEBERT, S. W., CHELLAPPAN, S. P., HOROWITZ, J. M. & NEVINS, J. R. 1992. THE INTERACTION OF RB WITH E2F COINCIDES WITH AN INHIBITION OF THE TRANSCRIPTIONAL ACTIVITY OF E2F. *Genes & Development,* 6**,** 177-185.

HOLST, C. R., NUOVO, G. J., ESTELLER, M., CHEW, K., BAYLIN, S. B., HERMAN, J. G. & TLSTY, T. D. 2003. Methylation of p16(INK4a) promoters occurs in vivo in histologically normal human mammary epithelia. *Cancer Research,* 63**,** 1596-1601.

HUANG, C., QIU, Z., WANG, L., PENG, Z., JIA, Z., LOGSDON, C. D., LE, X., WEI, D., HUANG, S. & XIE, K. 2012. A Novel FoxM1-Caveolin Signaling Pathway Promotes Pancreatic Cancer Invasion and Metastasis. *Cancer Research,* 72**,** 655-665.

HUANG, X. P., ZHAO, C. X., LI, Q. J., CAI, Y., LIU, F. X., HU, H., XU, X., HAN, Y. L., WU, M., ZHAN, Q. M. & WANG, M. R. 2006. Alteration of RPL14 in squamous cell carcinomas and preneoplastic lesions of the esophagus. *Gene,* 366**,** 161-168.

HUI, R., MACMILLAN, R. D., KENNY, F. S., MUSGROVE, E. A., BLAMEY, R. W., NICHOLSON, R. I., ROBERTSON, J. F. R. & SUTHERLAND, R. L. 2000. INK4a gene expression and

methylation in primary breast cancer: Overexpression of p16(INK4a) messenger RNA is a marker of poor prognosis. *Clinical Cancer Research,* 6**,** 2777-2787.

HUNECKE, D., SPANEL, R., LAENGER, F., NAM, S. W. & BORLAK, J. 2012. MYC-regulated genes involved in liver cell dysplasia identified in a transgenic model of liver cancer. *Journal of Pathology,* 228**,** 520-533.

HUNT, T. 2002. Protein synthesis, proteolysis, and cell cycle transitions. *Bioscience Reports,* 22**,** 465-486.

HUSCHTSCHA, L. I., NOBLE, J. R., NEUMANN, A. A., MOY, E. L., BARRY, P., MELKI, J. R., CLARK, S. J. & REDDEL, R. R. 1998. Loss of p16(INK4) expression by methylation is associated with lifespan extension of human mammary epithelial cells. *Cancer Research,* 58**,** 3508-3512.

ILIN, A. A., MALYGIN, A. A. & KARPOVA, G. G. 2011. Ribosomal protein S18e as a putative molecular staple for the 18S rRNA 3 '-major domain core. *Biochimica Et Biophysica Acta-Proteins and Proteomics,* 1814**,** 505-512.

JACOBS, J. J. L. & DE LANGE, T. 2004. Significant role for p16(INK4a) in p53-independent telomere-directed senescence. *Current Biology,* 14**,** 2302-2308.

JACOBS, J. J. L., KIEBOOM, K., MARINO, S., DEPINHO, R. A. & VAN LOHUIZEN, M. 1999. The oncogene and Polycomb-group gene bmi-1 regulates cell proliferation and senescence through the ink4a locus. *Nature,* 397**,** 164-168.

JECK, W. R., SIEBOLD, A. P. & SHARPLESS, N. E. 2012. Review: a meta-analysis of GWAS and age-associated diseases. *Aging Cell,* 11**,** 727-731.

JELINSKY, S. A. & SAMSON, L. D. 1999. Global response of Saccharomyces cerevisiae to an alkylating agent. *Proceedings of the National Academy of Sciences of the United States of America,* 96**,** 1486-1491.

JUN, J.-I. & LAU, L. F. 2010. The matricellular protein CCN1 induces fibroblast senescence and restricts fibrosis in cutaneous wound healing (vol 12, pg 676, 2010). *Nature Cell Biology,* 12**,** 1249-1249.

KANG, T.-W., YEVSA, T., WOLLER, N., HOENICKE, L., WUESTEFELD, T., DAUCH, D., HOHMEYER, A., GEREKE, M., RUDALSKA, R., POTAPOVA, A., IKEN, M., VUCUR, M., WEISS, S., HEIKENWALDER, M., KHAN, S., GIL, J., BRUDER, D., MANNS, M., SCHIRMACHER, P., TACKE, F., OTT, M., LUEDDE, T., LONGERICH, T., KUBICKA, S. & ZENDER, L. 2011. Senescence surveillance of pre-malignant hepatocytes limits liver cancer development. *Nature,* 479**,** 547-551.

KAPP, U., YEH, W. C., PATTERSON, B., ELIA, A. J., KAGI, D., HO, A., HESSEL, A., TIPSWORD, M., WILLIAMS, A., MIRTSOS, C., ITIE, A., MOYLE, M. & MAK, T. W. 1999. Interleukin 13 is secreted by and stimulates the growth of Hodgkin and Reed-Sternberg cells. *Journal of Experimental Medicine,* 189**,** 1939-1945.

KASHUBA, E., YURCHENKO, M., SZIRAK, K., STAHL, J., KLEIN, G. & SZEKELY, L. 2005. Epstein-Barr virus-encoded EBNA-5 binds to Epstein-Barr virus-induced Fte1/S3a protein. *Experimental Cell Research,* 303**,** 47-55.

KHATTER, H., MYASNIKOV, A. G., NATCHIAR, S. K. & KLAHOLZ, B. P. 2015. Structure of the human 80S ribosome. *Nature,* 520**,** 640-U338.

KHO, C. J., WANG, Y. & ZARBL, H. 1996. Effect of decreased fte-1 gene expression on protein synthesis, cell growth, and transformation. *Cell Growth & Differentiation,* 7**,** 1157-1166.

KIRKWOOD, T. B. L. & AUSTAD, S. N. 2000. Why do we age? *Nature,* 408**,** 233-238.

KITTANEH, M., MONTERO, A. J. & GLUCK, S. 2013. Molecular profiling for breast cancer: a comprehensive review. *Biomarkers in cancer,* 5**,** 61-70.

KLEIN, J. & GRUMMT, I. 1999. Cell cycle-dependent regulation of RNA polymerase I transcription: The nucleolar transcription factor UBF is inactive in mitosis and early

G(1). *Proceedings of the National Academy of Sciences of the United States of America,* 96**,** 6096-6101.

KNUDSEN, E. S. & WANG, J. Y. J. 1997. Dual mechanisms for the inhibition of E2F binding to RB by cyclin-dependent kinase-mediated RB phosphorylation. *Molecular and Cellular Biology,* 17**,** 5771-5783.

KOBERNA, K., MALINSKY, J., PLISS, A., MASATA, M., VECEROVA, J., FIALOVA, M., BEDNAR, J. & RASKA, I. 2002. Ribosomal genes in focus: new transcripts label the dense fibrillar components and form clusters indicative of "Christmas trees" in situ. *Journal of Cell Biology,* 157**,** 743-748.

KOBOLDT, D. C., FULTON, R. S., MCLELLAN, M. D., SCHMIDT, H., KALICKI-VEIZER, J., MCMICHAEL, J. F., FULTON, L. L., DOOLING, D. J., DING, L., MARDIS, E. R., WILSON, R. K., ALLY, A., BALASUNDARAM, M., BUTTERFIELD, Y. S. N., CARLSEN, R., CARTER, C., CHU, A., CHUAH, E., CHUN, H.-J. E., COOPE, R. J. N., DHALLA, N., GUIN, R., HIRST, C., HIRST, M., HOLT, R. A., LEE, D., LI, H. I., MAYO, M., MOORE, R. A., MUNGALL, A. J., PLEASANCE, E., ROBERTSON, A. G., SCHEIN, J. E., SHAFIEI, A., SIPAHIMALANI, P., SLOBODAN, J. R., STOLL, D., TAM, A., THIESSEN, N., VARHOL, R. J., WYE, N., ZENG, T., ZHAO, Y., BIROL, I., JONES, S. J. M., MARRA, M. A., CHERNIACK, A. D., SAKSENA, G., ONOFRIO, R. C., PHO, N. H., CARTER, S. L., SCHUMACHER, S. E., TABAK, B., HERNANDEZ, B., GENTRY, J., HUY, N., CRENSHAW, A., ARDLIE, K., BEROUKHIM, R., WINCKLER, W., GETZ, G., GABRIEL, S. B., MEYERSON, M., CHIN, L., PARK, P. J., KUCHERLAPATI, R., HOADLEY, K. A., AUMAN, J. T., FAN, C., TURMAN, Y. J., SHI, Y., LI, L., TOPAL, M. D., HE, X., CHAO, H.-H., PRAT, A., SILVA, G. O., IGLESIA, M. D., ZHAO, W., USARY, J., BERG, J. S., ADAMS, M., BOOKER, J., WU, J., GULABANI, A., BODENHEIMER, T., HOYLE, A. P., SIMONS, J. V., SOLOWAY, M. G., MOSE, L. E., JEFFERYS, S. R., BALU, S., PARKER, J. S., HAYES, D. N., PEROU, C. M., MALIK, S., MAHURKAR, S., SHEN, H., WEISENBERGER, D. J., TRICHE, T., JR., et al. 2012. Comprehensive molecular portraits of human breast tumours. *Nature,* 490**,** 61-70.

KRIMPENFORT, P., IJPENBERG, A., SONG, J.-Y., VAN DER VALK, M., NAWIJN, M., ZEVENHOVEN, J. & BERNS, A. 2007. p15(Ink4b) is a critical tumour suppressor in the absence of p16(Ink4a). *Nature,* 448**,** 943-U11.

KRIZHANOVSKY, V., YON, M., DICKINS, R. A., HEARN, S., SIMON, J., MIETHING, C., YEE, H., ZENDER, L. & LOWE, S. W. 2008. Senescence of activated stellate cells limits liver fibrosis. *Cell,* 134**,** 657-667.

KROES, R. A., JASTROW, A., MCLONE, M. G., YAMAMOTO, H., COLLEY, P., KERSEY, D. S., YONG, V. W., MKRDICHIAN, E., CERULLO, L., LEESTMA, J. & MOSKAL, J. R. 2000. The identification of novel therapeutic targets for the treatment of malignant brain tumors. *Cancer Letters,* 156**,** 191-198.

KRTOLICA, A., PARRINELLO, S., LOCKETT, S., DESPREZ, P. Y. & CAMPISI, J. 2001. Senescent fibroblasts promote epithelial cell growth and tumorigenesis: A link between cancer and aging. *Proceedings of the National Academy of Sciences of the United States of America,* 98**,** 12072-12077.

KUILMAN, T. & PEEPER, D. S. 2009. Senescence-messaging secretome: SMS-ing cellular stress. *Nature Reviews Cancer,* 9**,** 81-94.

KWOK, J. M. M., PECK, B., MONTEIRO, L. J., SCHWENEN, H. D. C., MILLOUR, J., COOMBES, R. C., MYATT, S. S. & LAM, E. W. F. 2010. FOXM1 Confers Acquired Cisplatin Resistance in Breast Cancer Cells. *Molecular Cancer Research,* 8**,** 24-34.

LAFONTAINE, D. L. J. 2015. Noncoding RNAs in eukaryotic ribosome biogenesis and function. *Nature Structural & Molecular Biology,* 22**,** 11-19.

LAM, E. W. F., BROSENS, J. J., GOMES, A. R. & KOO, C.-Y. 2013. Forkhead box proteins: tuning forks for transcriptional harmony. *Nature Reviews Cancer,* 13**,** 482-495.

LAM, Y. W. & TRINKLE-MULCAHY, L. 2015. New insights into nucleolar structure and function. *F1000prime reports,* 7**,** 48-48.

LANIER, L. L. 2005. NK cell recognition. *Annual Review of Immunology.*

LEARY, D. J. & HUANG, S. 2001. Regulation of ribosome biogenesis within the nucleolus. *Febs Letters,* 509**,** 145-150.

LEE, H. J., DO, J. H., BAE, S., YANG, S., ZHANG, X., LEE, A., CHOI, Y. J., PARK, D. C. & AHN, W. S. 2011. Immunohistochemical evidence for the over-expression of Glutathione peroxidase 3 in clear cell type ovarian adenocarcinoma. *Medical Oncology,* 28**,** S522-S527.

LEVKAU, B., KOYAMA, H., RAINES, E. W., CLURMAN, B. E., HERREN, B., ORTH, K., ROBERTS, J. M. & ROSS, R. 1998. Cleavage of p21(Cip1/Waf1) and p27(Kip1) mediates apoptosis in endothelial cells through activation of Cdk2: Role of a caspase cascade. *Molecular Cell,* 1**,** 553-563.

LEWIS, J. D. & TOLLERVEY, D. 2000. Like attracts like: Getting RNA processing together in the nucleus. *Science,* 288**,** 1385-1389.

LI, S. K. M., SMITH, D. K., LEUNG, W. Y., CHEUNG, A. M. S., LAM, E. W. F., DIMRI, G. P. & YAO, K.-M. 2008. FoxM1c counteracts oxidative stress-induced senescence and stimulates Bmi-1 expression. *Journal of Biological Chemistry,* 283**,** 16545-16553.

LIM, K.-H., KIM, K.-H., IL CHOI, S., PARK, E.-S., PARK, S. H., RYU, K., PARK, Y. K., KWON, S. Y., YANG, S.-I., LEE, H. C., SUNG, I.-K. & SEONG, B. L. 2011. RPS3a Over-Expressed in HBV-Associated Hepatocellular Carcinoma Enhances the HBx-Induced NF-kappa B Signaling via Its Novel Chaperoning Function. *Plos One,* 6.

LIN, A. W., BARRADAS, M., STONE, J. C., VAN AELST, L., SERRANO, M. & LOWE, S. W. 1998. Premature senescence involving p53 and p16 is activated in response to constitutive MEK/MAPK mitogenic signaling. *Genes & Development,* 12**,** 3008-3019.

LIN, N. U., CLAUS, E., SOHL, J., RAZZAK, A. R., ARNAOUT, A. & WINER, E. P. 2008. Sites of Distant Recurrence and Clinical Outcomes in Patients With Metastatic Triple-negative Breast Cancer High Incidence of Central Nervous System Metastases. *Cancer,* 113**,** 2638-2645.

LIU, D. & HORNSBY, P. J. 2007. Senescent human fibroblasts increase the early growth of xenograft tumors via matrix metalloproteinase secretion. *Cancer Research,* 67**,** 3117-3126.

LIU, G., SUN, Y., JI, P., LI, X., COGDELL, D., YANG, D., KERRIGAN, B. C. P., SHMULEVICH, I., CHEN, K., SOOD, A. K., XUE, F. & ZHANG, W. 2014. MiR-506 suppresses proliferation and induces senescence by directly targeting the CDK4/6-FOXM1 axis in ovarian cancer. *Journal of Pathology,* 233**,** 308-318.

LIU, H., FERGUSSON, M. M., CASTILHO, R. M., LIU, J., CAO, L., CHEN, J., MALIDE, D., ROVIRA, I. I., SCHIMEL, D., KUO, C. J., GUTKIND, J. S., HWANG, P. M. & FINKEL, T. 2007. Augmented Wnt signaling in a mammalian model of accelerated aging. *Science,* 317**,** 803-806.

LLANOS, S., CLARK, P. A., ROWE, J. & PETERS, G. 2001. Stabilization of p53 by p14(ARF) without relocation of MDM2 to the nucleolus. *Nature Cell Biology,* 3**,** 445-452.

LOERCHER, A. E., TANK, E. M. H., DELSTON, R. B. & HARBOUR, J. W. 2005. MITF links differentiation with cell cycle arrest in melanocytes by transcriptional activation of INK4A. *Journal of Cell Biology,* 168**,** 35-40.

LOPEZ, C. D., MARTINOVSKY, G. & NAUMOVSKI, L. 2002. Inhibition of cell death by ribosomal protein L35a. *Cancer Letters,* 180**,** 195-202.

LOWE, R., OVERHOFF, M. G., RAMAGOPALANL, S. V., GARBE, J. C., KOH, J., STAMPFER, M. R., BEACH, D. H., RAKYAN, V. K. & BISHOP, C. L. 2015. The senescent methylome and its relationship with cancer, ageing and germline genetic variation in humans. *Genome Biology,* 16.

MARTENS, U. M., CHAVEZ, E. A., POON, S. S. S., SCHMOOR, C. & LANDSDORP, P. M. 2000. Accumulation of short telomeres in human fibroblasts prior to replicative senescence. *Experimental cell research,* 256**,** 291-299.

MAYER, E. L. 2015. Targeting Breast Cancer with CDK Inhibitors. *Current Oncology Reports,* 17.

MICHALOGLOU, C., VREDEVELD, L. C. W., SOENGAS, M. S., DENOYELLE, C., KUILMAN, T., VAN DER HORST, C., MAJOOR, D. M., SHAY, J. W., MOOI, W. J. & PEEPER, D. S. 2005. BRAF(E600)-associated senescence-like cell cycle arrest of human naevi. *Nature,* 436**,** 720-724.

MILLER, O. L. & BEATTY, B. R. 1969. Visualization of Nucleolar Genes. *Science,* 164**,** 955-957.

MINAMINO, T., MIYAUCHI, H., YOSHIDA, T., ISHIDA, Y., YOSHIDA, H. & KOMURO, I. 2002. Endothelial cell senescence in human atherosclerosis - Role of telomere in endothelial dysfunction. *Circulation,* 105**,** 1541-1544.

MINCIONE, G., ESPOSITO, D. L., DI MARCANTONIO, M. C., PICCIRELLI, A., CAMA, A. & COLLETTA, G. 2003. TGF-beta 1 modulation of IGF-I signaling pathway in rat thyroid epithelial cells. *Experimental cell research,* 287**,** 411-423.

MONTANARO, L., MAZZINI, G., BARBIERI, S., VICI, M., NARDI-PANTOLI, A., GOVONI, M., DONATI, G., TRERE, D. & DERENZINI, M. 2007. Different effects of ribosome biogenesis inhibition on cell proliferation in retinoblastoma protein- and p53-deficient and proficient human osteosarcoma cell lines. *Cell Proliferation,* 40**,** 532-549.

MUNOZ-ESPIN, D., CANAMERO, M., MARAVER, A., GOMEZ-LOPEZ, G., CONTRERAS, J., MURILLO-CUESTA, S., RODRIGUEZ-BAEZA, A., VARELA-NIETO, I., RUBERTE, J., COLLADO, M. & SERRANO, M. 2013. Programmed Cell Senescence during Mammalian Embryonic Development. *Cell,* 155**,** 1104-1118.

MUNOZ-ESPIN, D. & SERRANO, M. 2014. Cellular senescence: from physiology to pathology. *Nature Reviews Molecular Cell Biology,* 15**,** 482-+.

MUNRO, J., BARR, N. I., IRELAND, H., MORRISON, V. & PARKINSON, E. K. 2004. Histone deacetylase inhibitors induce a senescence-like state in human cells by a p16-dependent mechanism that is independent of a mitotic clock. *Experimental cell research,* 295**,** 525-538.

NARITA, M., NUNEZ, S., HEARD, E., LIN, A. W., HEARN, S. A., SPECTOR, D. L., HANNON, G. J. & LOWE, S. W. 2003. Rb-mediated heterochromatin formation and silencing of E2F target genes during cellular senescence. *Cell,* 113**,** 703-716.

NELSON, G., WORDSWORTH, J., WANG, C. F., JURK, D., LAWLESS, C., MARTIN-RUIZ, C. & VON ZGLINICKI, T. 2012. A senescent cell bystander effect: senescence-induced senescence. *Aging Cell,* 11**,** 345-349.

NESS, K. K., ARMSTRONG, G. T., KUNDU, M., WILSON, C. L., TCHKONIA, T. & KIRKLAND, J. L. 2015. Frailty in Childhood Cancer Survivors. *Cancer,* 121**,** 1540-1547.

NISSAN, T. A., BASSLER, J., PETFALSKI, E., TOLLERVEY, D. & HURT, E. 2002. 60S pre-ribosome formation viewed from assembly in the nucleolus until export to the cytoplasm. *Embo Journal,* 21**,** 5539-5547.

NURSE, P. M. 2002. Cyclin dependent kinases and cell cycle control. *Bioscience Reports,* 22**,** 487-499.

O'HAGAN, D. T., OTT, G. S., DE GREGORIO, E. & SEUBERT, A. 2013. The mechanism of action of MF59 - An innately attractive adjuvant formulation (vol 30, pg 4341, 2012). *Vaccine,* 31**,** 1877-1877.

OFIR-ROSENFELD, Y., BOGGS, K., MICHAEL, D., KASTAN, M. B. & OREN, M. 2008. Mdm2 Regulates p53 mRNA Translation through Inhibitory Interactions with Ribosomal Protein L26. *Molecular Cell,* 32**,** 180-189.

OHTANI, K., DEGREGORI, J. & NEVINS, J. R. 1995. Regulation of the cyclin E gene by transcription factor E2F1. *Proceedings of the National Academy of Sciences of the United States of America,* 92**,** 12146-12150.

OLSTAD, O. K., GAUTVIK, V. T., REPPE, S., RIAN, E., JEMTLAND, R., OHLSSON, C., BRULAND, O. S. & GAUTVIK, K. M. 2003. Molecular heterogeneity in human osteosarcoma demonstrated by enriched mRNAs isolated by directional tag PCR subtraction cloning. *Anticancer Research,* 23**,** 2201-2216.

ORTEGA, S., MALUMBRES, M. & BARBACID, M. 2002. Cyclin D-dependent kinases, INK4 inhibitors and cancer. *Biochimica Et Biophysica Acta-Reviews on Cancer,* 1602**,** 73-87.

OSHEROFF, N. 1989. EFFECT OF ANTINEOPLASTIC AGENTS ON THE DNA CLEAVAGE RELIGATION REACTION OF EUKARYOTIC TOPOISOMERASE-II - INHIBITION OF DNA RELIGATION BY ETOPOSIDE. *Biochemistry,* 28**,** 6157-6160.

PAN, Q., VAN DER LAAN, L. J. W., JANSSEN, H. L. A. & PEPPELENBOSCH, M. P. 2012. A dynamic perspective of RNAi library development. *Trends in Biotechnology,* 30**,** 206-215.

PARKER, J. S., MULLINS, M., CHEANG, M. C. U., LEUNG, S., VODUC, D., VICKERY, T., DAVIES, S., FAURON, C., HE, X., HU, Z., QUACKENBUSH, J. F., STIJLEMAN, I. J., PALAZZO, J., MARRON, J. S., NOBEL, A. B., MARDIS, E., NIELSEN, T. O., ELLIS, M. J., PEROU, C. M. & BERNARD, P. S. 2009. Supervised Risk Predictor of Breast Cancer Based on Intrinsic Subtypes. *Journal of Clinical Oncology,* 27**,** 1160-1167.

PARO, R. & HOGNESS, D. S. 1991. THE POLYCOMB PROTEIN SHARES A HOMOLOGOUS DOMAIN WITH A HETEROCHROMATIN-ASSOCIATED PROTEIN OF DROSOPHILA. *Proceedings of the National Academy of Sciences of the United States of America,* 88**,** 263-267.

PARRINELLO, S., SAMPER, E., KRTOLICA, A., GOLDSTEIN, J., MELOV, S. & CAMPISI, J. 2003. Oxygen sensitivity severely limits the replicative lifespan of murine fibroblasts. *Nature Cell Biology,* 5**,** 741-747.

PASSEGUE, E. & WAGNER, E. F. 2000. JunB suppresses cell proliferation by transcriptional activation of p16(INK4a) expression. *Embo Journal,* 19**,** 2969-2979.

PEDERSON, T. 2011. The Nucleolus. *Cold Spring Harbor Perspectives in Biology,* 3.

PEROU, C. M., SORLIE, T., EISEN, M. B., VAN DE RIJN, M., JEFFREY, S. S., REES, C. A., POLLACK, J. R., ROSS, D. T., JOHNSEN, H., AKSLEN, L. A., FLUGE, O., PERGAMENSCHIKOV, A., WILLIAMS, C., ZHU, S. X., LONNING, P. E., BORRESEN-DALE, A. L., BROWN, P. O. & BOTSTEIN, D. 2000. Molecular portraits of human breast tumours. *Nature,* 406**,** 747-752.

PLANTA, R. J., BROWN, A. J. P., CADAHIA, J. L., CERDAN, M. E., DE JONGE, M., GENT, M. E., HAYES, A., KOLEN, C., LOMBARDIA, L. J., SEFTON, M., OLIVER, S. G., THEVELEIN, J., TOURNU, H., VAN DELFT, Y. J., VERBART, D. J. & WINDERICKX, J. 1999. Transcript analysis of 250 novel yeast genes from chromosome XIV. *Yeast,* 15**,** 329-350.

POLYAK, K., LEE, M. H., ERDJUMENTBROMAGE, H., KOFF, A., ROBERTS, J. M., TEMPST, P. & MASSAGUE, J. 1994. CLONING OF P27(KIP1), A CYCLIN-DEPENDENT KINASE INHIBITOR AND A POTENTIAL MEDIATOR OF EXTRACELLULAR ANTIMITOGENIC SIGNALS. *Cell,* 78**,** 59-66.

PRADHAN, A. D., MANSON, J. E., RIFAI, N., BURING, J. E. & RIDKER, P. M. 2001. C-reactive protein, interleukin 6, and risk of developing type 2 diabetes mellitus. *Jama-Journal of the American Medical Association,* 286**,** 327-334.

PRAT, A., PARKER, J. S., KARGINOVA, O., FAN, C., LIVASY, C., HERSCHKOWITZ, J. I., HE, X. & PEROU, C. M. 2010. Phenotypic and molecular characterization of the claudin-low intrinsic subtype of breast cancer. *Breast Cancer Research,* 12.

PRIEUR, A. & PEEPER, D. S. 2008. Cellular senescence in vivo: a barrier to tumorigenesis. *Current Opinion in Cell Biology,* 20**,** 150-155.

QUIN, J. E., DEVLIN, J. R., CAMERON, D., HANNAN, K. M., PEARSON, R. B. & HANNAN, R. D. 2014. Targeting the nucleolus for cancer intervention. *Biochimica Et Biophysica Acta-Molecular Basis of Disease,* 1842**,** 802-816.

RAMAKRISHNAN, V. 2011. The Eukaryotic Ribosome. *Science,* 331**,** 681-682.

RAMIREZ, R. D., MORALES, C. P., HERBERT, B. S., ROHDE, J. M., PASSONS, C., SHAY, J. W. & WRIGHT, W. E. 2001. Putative telomere-independent mechanisms of replicative aging reflect inadequate growth conditions. *Genes & Development,* 15**,** 398-403.

RODIER, F. & CAMPISI, J. 2011. Four faces of cellular senescence. *Journal of Cell Biology,* 192**,** 547-556.

RUGGERO, D. 2012. Revisiting the Nucleolus: From Marker to Dynamic Integrator of Cancer Signaling. *Science Signaling,* 5.

RUGGERO, D. & PANDOLFI, P. P. 2003. Does the ribosome translate cancer? *Nature Reviews Cancer,* 3**,** 179-192.

SAGIV, A., BIRAN, A., YON, M., SIMON, J., LOWE, S. W. & KRIZHANOVSKY, V. 2013. Granule exocytosis mediates immune surveillance of senescent cells. *Oncogene,* 32**,** 1971-1977.

SAGIV, A. & KRIZHANOVSKY, V. 2013. Immunosurveillance of senescent cells: the bright side of the senescence program. *Biogerontology,* 14**,** 617-628.

SANOFF, H. K., DEAL, A. M., KRISHNAMURTHY, J., TORRICE, C., DILLON, P., SORRENTINO, J., IBRAHIM, J. G., JOLLY, T. A., WILLIAMS, G., CAREY, L. A., DROBISH, A., GORDON, B.-B., ALSTON, S., HURRIA, A., KLEINHANS, K., RUDOLPH, K. L., SHARPLESS, N. E. & MUSS, H. B. 2014. Effect of Cytotoxic Chemotherapy on Markers of Molecular Age in Patients With Breast Cancer. *Jnci-Journal of the National Cancer Institute,* 106.

SCHAFER, T., STRAUSS, D., PETFALSKI, E., TOLLERVEY, D. & HURT, E. 2003. The path from nucleolar 90S to cytoplasmic 40S pre-ribosomes. *Embo Journal,* 22**,** 1370-1380.

SCHERL, A., COUTE, Y., DEON, C., CALLE, A., KINDBEITER, K., SANCHEZ, J. C., GRECO, A., HOCHSTRASSER, D. & DIAZ, J. J. 2002. Functional proteomic analysis of human nucleolus. *Molecular Biology of the Cell,* 13**,** 4100-4109.

SCHETTER, A. J., HEEGAARD, N. H. H. & HARRIS, C. C. 2010. Inflammation and cancer: interweaving microRNA, free radical, cytokine and p53 pathways. *Carcinogenesis,* 31**,** 37-49.

SCHREIBER, M., MULLER, W. J., SINGH, G. & GRAHAM, F. L. 1999. Comparison of the effectiveness of adenovirus vectors expressing cyclin kinase inhibitors p16(INK4A), p18(INK4C), p19(INK4D), p21(WAF1/CIP1) and p27(KIP1) in inducing cell cycle arrest, apoptosis and inhibition of tumorigenicity. *Oncogene,* 18**,** 1663-1676.

SCHULZE, A., ZERFASS, K., SPITKOVSKY, D., MIDDENDORP, S., BERGES, J., HELIN, K., JANSENDURR, P. & HENGLEIN, B. 1995. CELL-CYCLE REGULATION OF THE CYCLIN-A GENE PROMOTER IS MEDIATED BY A VARIANT E2F SITE. *Proceedings of the National Academy of Sciences of the United States of America,* 92**,** 11264-11268.

SCHWARZ, J. K., DEVOTO, S. H., SMITH, E. J., CHELLAPPAN, S. P., JAKOI, L. & NEVINS, J. R. 1993. INTERACTIONS OF THE P107 AND RB PROTEINS WITH E2F DURING THE CELL-PROLIFERATION RESPONSE. *Embo Journal,* 12**,** 1013-1020.

SEMERAD, C. L., LIU, F. L., GREGORY, A. D., STUMPF, K. & LINK, D. C. 2002. G-CSF is an essential regulator of neutrophil trafficking from the bone marrow to the blood. *Immunity,* 17**,** 413-423.

SEMERAD, C. L., POURSINE-LAURENT, J., LIU, F. L. & LINK, D. C. 1999. A role for G-CSF receptor signaling in the regulation of hematopoietic cell function but not lineage commitment or differentiation. *Immunity,* 11**,** 153-161.

SERRANO, M., HANNON, G. J. & BEACH, D. 1993. A NEW REGULATORY MOTIF IN CELL-CYCLE CONTROL CAUSING SPECIFIC-INHIBITION OF CYCLIN-D/CDK4. *Nature,* 366**,** 704-707.

SERRANO, M., LIN, A. W., MCCURRACH, M. E., BEACH, D. & LOWE, S. W. 1997. Oncogenic ras provokes premature cell senescence associated with accumulation of p53 and p16(INK4a). *Cell,* 88**,** 593-602.

SEVERINO, J., ALLEN, R. G., BALIN, S., BALIN, A. & CRISTOFALO, V. J. 2000. Is beta-galactosidase staining a marker of senescence in vitro and in vivo? *Experimental Cell Research,* 257**,** 162-171.

SHERR, C. J. & ROBERTS, J. M. 1999. CDK inhibitors: positive and negative regulators of G(1)-phase progression. *Genes & Development,* 13**,** 1501-1512.

SHRIVER, S. P., SHRIVER, M. D., TIRPAK, D. L., BLOCH, L. M., HUNT, J. D., FERRELL, R. E. & SIEGFRIED, J. M. 1998. Trinucleotide repeat length variation in the human ribosomal protein L14 gene (RPL14): localization to 3p21.3 and loss of heterozygosity in lung and oral cancers. *Mutation Research-Genomics,* 406**,** 9-23.

SIKORA, E., ARENDT, T., BENNETT, M. & NARITA, M. 2011. Impact of cellular senescence signature on ageing research. *Ageing Research Reviews,* 10**,** 146-152.

SLIZHIKOVA, D. K., VINOGRADOVA, T. V. & SVERDLOV, E. D. 2005. The, NOLA2 and RPS3A genes as highly informative markers of human squamous cell lung cancer. *Bioorganicheskaya Khimiya,* 31**,** 195-199.

SORLIE, T., PEROU, C. M., TIBSHIRANI, R., AAS, T., GEISLER, S., JOHNSEN, H., HASTIE, T., EISEN, M. B., VAN DE RIJN, M., JEFFREY, S. S., THORSEN, T., QUIST, H., MATESE, J. C., BROWN, P. O., BOTSTEIN, D., LONNING, P. E. & BORRESEN-DALE, A. L. 2001. Gene expression patterns of breast carcinomas distinguish tumor subclasses with clinical implications. *Proceedings of the National Academy of Sciences of the United States of America,* 98**,** 10869-10874.

SRABOVIC, N., MUJAGIC, Z., MUJANOVIC-MUSTEDANAGIC, J., MUMINOVIC, Z., SOFTIC, A. & BEGIC, L. 2011. Interleukin 13 expression in the primary breast cancer tumour tissue. *Biochemia Medica,* 21**,** 131-138.

STANTON, R. C. 2012. Glucose-6-phosphate dehydrogenase, NADPH, and cell survival. *Iubmb Life,* 64**,** 362-369.

STORER, M., MAS, A., ROBERT-MORENO, A., PECORARO, M., ORTELLS, M. C., DI GIACOMO, V., YOSEF, R., PILPEL, N., KRIZHANOVSKY, V., SHARPE, J. & KEYES, W. M. 2013. Senescence Is a Developmental Mechanism that Contributes to Embryonic Growth and Patterning. *Cell,* 155**,** 1119-1130.

STOTT, F. J., BATES, S., JAMES, M. C., MCCONNELL, B. B., STARBORG, M., BROOKES, S., PALMERO, I., RYAN, K., HARA, E., VOUSDEN, K. H. & PETERS, G. 1998. The alternative product from the human CDKN2A locus, p14(ARF), participates in a regulatory feedback loop with p53 and MDM2. *Embo Journal,* 17**,** 5001-5014.

STREZOSKA, Z., PESTOV, D. G. & LAU, L. F. 2000. Bop1 is a mouse WD40 repeat nucleolar protein involved in 28S and 5.8S rRNA processing and 60S ribosome biogenesis. *Molecular and Cellular Biology,* 20**,** 5516-5528.

SUKHATME, V. P. & CHAN, B. 2012. Glycolytic cancer cells lacking 6-phosphogluconate dehydrogenase metabolize glucose to induce senescence. *Febs Letters,* 586**,** 2389-2395.

TAFFOREAU, L., ZORBAS, C., LANGHENDRIES, J.-L., MULLINEUX, S.-T., STAMATOPOULOU, V., MULLIER, R., WACHEU, L. & LAFONTAINE, D. L. J. 2013. The Complexity of Human Ribosome Biogenesis Revealed by Systematic Nucleolar Screening of Pre-rRNA Processing Factors. *Molecular Cell,* 51**,** 539-551.

TAKAI, H., SMOGORZEWSKA, A. & DE LANGE, T. 2003. DNA damage foci at dysfunctional telomeres. *Current Biology,* 13**,** 1549-1556.

TAO, J., XU, X.-S., SONG, Y.-Z., QU, K., WU, Q.-F., WANG, R.-T., MENG, F.-D., WEI, J.-C., DONG, S.-B., ZHANG, Y.-L., TAI, M.-H., DONG, Y.-F., WANG, L. & LIU, C. 2014. Down-regulation of FoxM1 inhibits viability and invasion of gallbladder carcinoma cells, partially dependent on inducement of cellular senescence. *World Journal of Gastroenterology,* 20**,** 9497-9505.

TARANTUL, V. Z., NIKOLAEV, A. I., MARTYNENKO, A., HANNIG, H., HUNSMANN, G. & BODEMER, W. 2000. Differential gene expression in B-Cell non-Hodgkin's lymphoma of SIV-infected monkey. *Aids Research and Human Retroviruses,* 16**,** 173-179.

TCHKONIA, T., ZHU, Y., VAN DEURSEN, J., CAMPISI, J. & KIRKLAND, J. L. 2013. Cellular senescence and the senescent secretory phenotype: therapeutic opportunities. *Journal of Clinical Investigation,* 123**,** 966-972.

TE POELE, R. H., OKOROKOV, A. L., JARDINE, L., CUMMINGS, J. & JOEL, S. P. 2002. DNA damage is able to induce senescence in tumor cells in vitro and in vivo. *Cancer Research,* 62**,** 1876-1883.

TENG, T., MERCER, C. A., HEXLEY, P., THOMAS, G. & FUMAGALLI, S. 2013. Loss of Tumor Suppressor RPL5/RPL11 Does Not Induce Cell Cycle Arrest but Impedes Proliferation Due to Reduced Ribosome Content and Translation Capacity. *Molecular and Cellular Biology,* 33**,** 4660-4671.

TIAN, W. N., BRAUNSTEIN, L. D., PANG, J. D., STUHLMEIER, K. M., XI, Q. C., TIAN, X. N. & STANTON, R. C. 1998. Importance of glucose-6-phosphate dehydrogenase activity for cell growth. *Journal of Biological Chemistry,* 273**,** 10609-10617.

TOFT, D. J. & CRYNS, V. L. 2011. Minireview: Basal-Like Breast Cancer: From Molecular Profiles to Targeted Therapies. *Molecular Endocrinology,* 25**,** 199-211.

TRAPMAN, J., RETEL, J. & PLANTA, R. J. 1975. RIBOSOMAL PRECURSOR PARTICLES FROM YEAST. *Experimental Cell Research,* 90**,** 95-104.

TSCHOCHNER, H. & HURT, E. 2003. Pre-ribosomes on the road from the nucleolus to the cytoplasm. *Trends in Cell Biology,* 13**,** 255-263.

TSUNO, A., MIYOSHI, K., TSUJII, R., MIYAKAWA, T. & MIZUTA, K. 2000. RRS1, a conserved essential gene, encodes a novel regulatory protein required for ribosome biogenesis in Saccharomyces cerevisiae. *Molecular and Cellular Biology,* 20**,** 2066-2074.

UDEM, S. A. & WARNER, J. R. 1972. RIBOSOMAL-RNA SYNTHESIS IN SACCHAROMYCES-CEREVISIAE. *Journal of Molecular Biology,* 65**,** 227-&.

UGRINOVA, I., MONIER, K., IVALDI, C., THIRY, M., STORCK, S., MONGELARD, F. & BOUVET, P. 2007. Inactivation of nucleolin leads to nucleolar disruption, cell cycle arrest and defects in centrosome duplication. *Bmc Molecular Biology,* 8.

VAN DEURSEN, J. M. 2014. The role of senescent cells in ageing. *Nature,* 509**,** 439-446.

VAN SLUIS, M. & MCSTAY, B. 2014. Ribosome biogenesis: Achilles heel of cancer? *Genes & cancer,* 5**,** 152-3.

VANROBAYS, E., GLEIZES, P. E., BOUSQUET-ANTONELLI, C., NOAILLAC-DEPEYRE, J., CAIZERGUES-FERRER, M. & GELUGNE, J. P. 2001. Processing of 20S pre-rRNA to 18S ribosomal RNA in yeast requires Rrp10p, an essential non-ribosomal cytoplasmic protein. *Embo Journal,* 20**,** 4204-4213.

VEISEH, M. & TURLEY, E. A. 2011. Hyaluronan metabolism in remodeling extracellular matrix: probes for imaging and therapy of breast cancer. *Integrative Biology,* 3**,** 304-315.

VENKATARAMAN, S., ALIMOVA, I., BALAKRISHNAN, I., HARRIS, P., BIRKS, D. K., GRIESINGER, A., AMANI, V., CRISTIANO, B., REMKE, M., TAYLOR, M. D., HANDLER, M., FOREMAN, N. K. & VIBHAKAR, R. 2014. Inhibition of BRD4 attenuates tumor cell self-renewal and suppresses stem cell signaling in MYC driven medulloblastoma. *Oncotarget,* 5**,** 2355-2371.

VOIT, R., SCHAFER, K. & GRUMMT, I. 1997. Mechanism of repression of RNA polymerase I transcription by the retinoblastoma protein. *Molecular and Cellular Biology,* 17**,** 4230-4237.

VOLAREVIĆ, S., STEWART, M. J., LEDERMANN, B., ZILBERMAN, F., TERRACCIANO, L., MONTINI, E., GROMPE, M., KOZMA, S. C. & THOMAS, G. 2000. Proliferation, But Not Growth, Blocked by Conditional Deletion of 40S Ribosomal Protein S6. *Science,* 288**,** 2045-2047.

WANG, C., JURK, D., MADDICK, M., NELSON, G., MARTIN-RUIZ, C. & VON ZGLINICKI, T. 2009. DNA damage response and cellular senescence in tissues of aging mice. *Aging Cell,* 8**,** 311-323.

WANG, L.-P., XU, X.-M., NING, H.-Y., YANG, S.-M., CHEN, J.-G., YU, J.-Y., DING, H.-Y., UNDERHILL, C. B. & ZHANG, L.-R. 2004. Expression of PH20 in primary and metastatic breast cancer and its pathological significance. *Zhonghua bing li xue za zhi Chinese journal of pathology,* 33**,** 320-3.

WANG, Z., BANERJEE, S., KONG, D., LI, Y. & SARKAR, F. H. 2007. Down-regulation of Forkhead Box M1 transcription factor leads to the inhibition of invasion and angiogenesis of pancreatic cancer cells. *Cancer Research,* 67**,** 8293-8300.

WANG, Z., HOU, J., LU, L., QI, Z., SUN, J., GAO, W., MENG, J., WANG, Y., SUN, H., GU, H., XIN, Y., GUO, X. & YANG, G. 2013. Small Ribosomal Protein Subunit S7 Suppresses Ovarian Tumorigenesis through Regulation of the PI3K/AKT and MAPK Pathways. *Plos One,* 8.

WARIS, G. & AHSAN, H. 2006. Reactive oxygen species: role in the development of cancer and various chronic conditions. *Journal of carcinogenesis,* 5**,** 14-14.

WARNER, J. R. 1999. The economics of ribosome biosynthesis in yeast. *Trends in Biochemical Sciences,* 24**,** 437-440.

WEHNER, K. A., GALLAGHER, J. E. G. & BASERGA, S. J. 2002. Components of an interdependent unit within the SSU processome regulate and mediate its activity. *Molecular and Cellular Biology,* 22**,** 7258-7267.

WEILAND, T., LAMPE, J., ESSMANN, F., VENTURELLI, S., BERGER, A., BOSSOW, S., BERCHTOLD, S., SCHULZE-OSTHOFF, K., LAUER, U. M. & BITZER, M. 2014. Enhanced killing of therapy-induced senescent tumor cells by oncolytic measles vaccine viruses. *International Journal of Cancer,* 134**,** 235-243.

WELLS, S. I., FRANCIS, D. A., KARPOVA, A. Y., DOWHANICK, J. J., END, J. D. B., BENSON, J. D. & HOWLEY, P. M. 2000. Papillomavirus E2 induces senescence in HPV-positive cells via pRB- and p21(CIP)-dependent pathways. *Embo Journal,* 19**,** 5762-5771.

WESTBROOK, L., MANUVAKHOVA, M., KERN, F. G., ESTES, N. R., II, RAMANATHAN, H. N. & THOTTASSERY, J. V. 2007. Cks1 regulates cdk1 expression: A novel role during mitotic entry in breast cancer cells. *Cancer Research,* 67**,** 11393-11401.

WOESSNER, R. D., MATTERN, M. R., MIRABELLI, C. K., JOHNSON, R. K. & DRAKE, F. H. 1991. PROLIFERATION-DEPENDENT AND CELL CYCLE-DEPENDENT DIFFERENCES IN EXPRESSION OF THE 170-KILODALTON AND 180-KILODALTON FORMS OF TOPOISOMERASE-II IN NIH-3T3 CELLS. *Cell Growth & Differentiation,* 2**,** 209-214.

XUE, W., ZENDER, L., MIETHING, C., DICKINS, R. A., HERNANDO, E., KRIZHANOVSKY, V., CORDON-CARDO, C. & LOWE, S. W. 2007. Senescence and tumour clearance is triggered by p53 restoration in murine liver carcinomas. *Nature,* 445**,** 656-660.

YE, H. G., HOLTERMAN, A. X., YOO, K. W., FRANKS, R. R. & COSTA, R. H. 1999. Premature expression of the winged helix transcription factor HFH-11B in regenerating mouse liver accelerates hepatocyte entry into S phase. *Molecular and Cellular Biology,* 19**,** 8570-8580.

YE, H. G., KELLY, T. F., SAMADANI, U., LIM, L., RUBIO, S., OVERDIER, D. G., ROEBUCK, K. A. & COSTA, R. H. 1997. Hepatocyte nuclear factor 3/fork head homolog 11 is expressed in proliferating epithelial and mesenchymal cells of embryonic and adult tissues. *Molecular and Cellular Biology,* 17**,** 1626-1641.

YIM, E.-K. & PARK, J.-S. 2005. The role of HPV E6 and E7 oncoproteins in HPV-associated cervical carcinogenesis. *Cancer research and treatment : official journal of Korean Cancer Association,* 37**,** 319-24.

YU, Y. P., YU, G., TSENG, G., CIEPLY, K., NELSON, J., DEFRANCES, M., ZARNEGAR, R., MICHALOPOULOS, G. & LUO, J.-H. 2007. Glutathione peroxidase 3, deleted or methylated in prostate cancer, suppresses prostate cancer growth and metastasis. *Cancer Research,* 67**,** 8043-8050.

YUN, M. H., DAVAAPIL, H. & BROCKES, J. P. 2015. Recurrent turnover of senescent cells during regeneration of a complex structure. *eLife,* 4.

ZENG, J., WANG, L., LI, Q., LI, W., BJORKHOLM, M., JIA, J. & XU, D. 2009. FoxM1 is up-regulated in gastric cancer and its inhibition leads to cellular senescence, partially dependent on p27(kip1). *Journal of Pathology,* 218**,** 419-427.

ZHAI, W. G. & COMAI, L. 2000. Repression of RNA polymerase I transcription by the tumor suppressor p53. *Molecular and Cellular Biology,* 20**,** 5930-5938.

ZHANG, S., TENG, H., DING, Q., FAN, J., SHI, W., ZHOU, Y. & ZHANG, C. 2013. FoxM1 Involvement in Astrocyte Proliferation after Spinal Cord Injury in Rats. *Journal of Molecular Neuroscience,* 51**,** 170-179.

ZHANG, X., GAO, X., COOTS, R. A., CONN, C. S., LIU, B. & QIAN, S.-B. 2015. Translational control of the cytosolic stress response by mitochondrial ribosomal protein L18. *Nature Structural & Molecular Biology,* 22**,** 404-U80.

ZHANG, X., ZHENG, Z., SHEN, Y., KIM, H., JIN, R., LI, R., LEE, D. Y., ROH, M. R. & YANG, S. 2014. Downregulation of glutathione peroxidase 3 is associated with lymph node metastasis and prognosis in cervical cancer. *Oncology Reports,* 31**,** 2587-2592.

ZHU, J. Y., WOODS, D., MCMAHON, M. & BISHOP, J. M. 1998. Senescence of human fibroblasts induced by oncogenic Raf. *Genes & Development,* 12**,** 2997-3007.

ZHU, Y., TCHKONIA, T., PIRTSKHALAVA, T., GOWER, A. C., DING, H., GIORGADZE, N., PALMER, A. K., IKENO, Y., HUBBARD, G. B., LENBURG, M., O'HARA, S. P., LARUSSO, N. F., MILLER, J. D., ROOS, C. M., VERZOSA, G. C., LEBRASSEUR, N. K., WREN, J. D., FARR, J. N., KHOSLA, S., STOUT, M. B., MCGOWAN, S. J., FUHRMANN-STROISSNIGG, H., GURKAR, A. U., ZHAO, J., COLANGELO, D., DORRONSORO, A., LING, Y. Y., BARGHOUTHY, A. S., NAVARRO, D. C., SANO, T., ROBBINS, P. D., NIEDERNHOFER, L. J. & KIRKLAND, J. L. 2015. The Achilles' heel of senescent cells: from transcriptome to senolytic drugs. *Aging Cell,* 14**,** 644-658.

Appendix

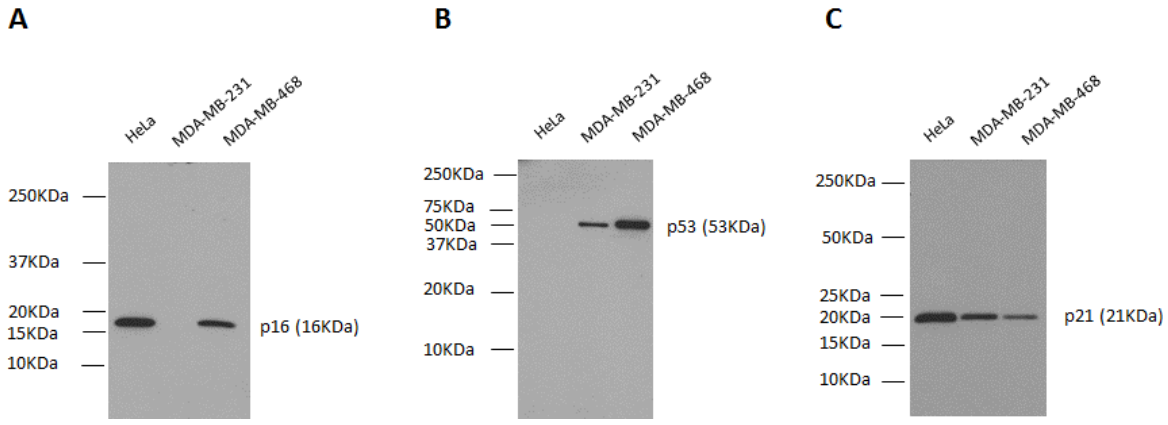

Figure A.1: Uncropped western blots of p16, p53 and p21 in HeLa, MDA-MB-231 and MDA-MB-468 cells. Cell lysates were probed for mouse anti-p16, rabbit anti-p53 and rabbit anti-p21 according to Section 2.6. **(A)** p16 **(B)** p53 **(C)** p21.

Gene Symbol	Full Gene Name	Gene ID
ZMIZ2	zinc finger, MIZ-type containing 2	83637
ALPP	alkaline phosphatase, placental (Regan isozyme)	250
ANKRD7	ankyrin repeat domain 7	56311
BBX	bobby sox homolog (Drosophila)	56987
BRMS1L	breast cancer metastasis-suppressor 1-like	84312
FAM120A	family with sequence similarity 120A	23196
CSNK1G1	casein kinase 1, gamma 1	53944
DDX6	DEAD (Asp-Glu-Ala-Asp) box polypeptide 6	1656
DLX5	distal-less homeo box 5	1749
DLX6	distal-less homeo box 6	1750
DNAJC5G	DnaJ (Hsp40) homolog, subfamily C, member 5 gamma	285126
DNM1	dynamin 1	1759
C19orf73	chromosome 19 open reading frame 73	55150
CCDC82	coiled-coil domain containing 82	79780
C11orf44	chromosome 11 open reading frame 44	283171
FSIP2	fibrous sheath interacting protein 2	401024
MLST8	MTOR associated protein, LST8 homolog	64223
GEMIN6	gem (nuclear organelle) associated protein 6	79833
GPX3	glutathione peroxidase 3 (plasma)	2878
GRM8	glutamate receptor, metabotropic 8	2918
IL13RA1	interleukin 13 receptor, alpha 1	3597
CWC22	CWC22 spliceosome-associated protein	57703
MFHAS1	malignant fibrous histiocytoma amplified sequence 1	9258
IGSF21	immunoglobin superfamily, member 21	84966
GLIDR	glioblastoma down-regulated RNA	389741
DENND6B	DENN/MADD domain containing 6B	414918
MKNK2	MAP kinase interacting serine/threonine kinase 2	2872

MRPL13	mitochondrial ribosomal protein L13	28998
MRPS24	mitochondrial ribosomal protein S24	64951
NAB2	NGFI-A binding protein 2 (EGR1 binding protein 2)	4665
NFKBIA	nuclear factor of kappa light polypeptide gene enhancer in B-cells inhibitor, alpha	4792
NR1I2	nuclear receptor subfamily 1, group I, member 2	8856
NUDT14	nudix (nucleoside diphosphate linked moiety X)-type motif 14	256281
OC200226	-	200226
EMC10	ER membrane protein complex subunit 10	284361
NHSL2	NHS-like 2	340527
MSGN1	mesogenin 1	343930
RPL32P7	ribosomal protein L32 pseudogene 7	391560
RPL32P36	ribosomal protein L32 pseudogene 36	392447
KNOP1	lysine-rich nucleolar protein 1	400506
DUOXA2	dual oxidase maturation factor 2	405753
DUOXA1	dual oxidase maturation factor 1	90527
CYB5RL	cytochrome b5 reductase-like	606495
OPLAH	5-oxoprolinase (ATP-hydrolysing)	26873
OR4K5	olfactory receptor, family 4, subfamily K, member 5	79317
OR6C76	olfactory receptor, family 6, subfamily C, member 76	390326
PBRM1	polybromo 1	55193
PDZRN4	PDZ domain containing RING finger 4	29951
PGD	6-phosphogluconate dehydrogenase	5226
PRLR	prolactin receptor	5618
PTK6	PTK6 protein tyrosine kinase 6	5753
PYM	within bgcn homolog (Drosophila)	84305
RAD21	RAD21 homolog (S. pombe)	5885
RNF17	ring finger protein 17	56163
RPL14	ribosomal protein L14	9045
RPL18	ribosomal protein L18	6141
RPL34	ribosomal protein L34	6164
RPL35A	ribosomal protein L35a	6165
RPLP2	ribosomal protein, large P2	6181
RPS18	ribosomal protein S18	6222
RPS3A	ribosomal protein S3A	6189
RPS7	ribosomal protein S7	6201
RTCD1	RNA terminal phosphate cyclase domain 1	8634
RUFY2	RUN and FYVE domain containing 2	55680
SLC38A1	solute carrier family 38, member 1	81539
SMO	smoothened homolog (Drosophila)	6608
SOCS6	suppressor of cytokine signaling 6	9306
SPAM1	sperm adhesion molecule 1 (PH-20 hyaluronidase, zona pellucida binding)	6677
SPATS1	spermatogenesis associated, serine-rich 1	221409

SPTA1	spectrin, alpha, erythrocytic 1 (elliptocytosis 2)	6708
SRP54	signal recognition particle 54kDa	6729
SRPK1	SFRS protein kinase 1	6732
STXBP5	syntaxin binding protein 5 (tomosyn)	134957
TRAPPC9	trafficking protein particle complex 9	83696
TCEB1	transcription elongation factor B (SIII), polypeptide 1 (15kDa, elongin C)	6921
TCTEL1	t-complex-associated-testis-expressed 1-like 1	6993
TOP2B	topoisomerase (DNA) II beta 180kDa	7155
TTBK2	tau tubulin kinase 2	146057
U2AF1L3	U2(RNU2) small nuclear RNA auxiliary factor 1-like 3	199746
UBA52	ubiquitin A-52 residue ribosomal protein fusion product 1	7311
UNC93B1	unc-93 homolog B1 (C. elegans)	81622
CEACAM20	carcinoembryonic antigen-related cell adhesion molecule 20	125931
VRK1	vaccinia related kinase 1	7443
WFDC8	WAP four-disulfide core domain 8	90199
YAP	YY1 associated protein 1	55249
ZMYM1	zinc finger, MYM domain containing 1	79830

Figure A.2: List of 86 genes targeted within the HeLa siRNA screens.

Gene Symbol	**Full Gene Name**	**Gene ID**
ALPP	alkaline phosphatase, placental (Regan isozyme)	250
FAM120A	family with sequence similarity 120A	23196
CCDC82	coiled-coil domain containing 82	79780
CWC22	CWC22 spliceosome-associated protein	57703
CYB5RL	cytochrome b5 reductase-like	606495
DDX6	DEAD (Asp-Glu-Ala-Asp) box polypeptide 6	1656
DENND6B	DENN/MADD domain containing 6B	414918
DLX5	distal-less homeo box 5	1749
DLX6	distal-less homeo box 6	1750
DNAJC5G	DnaJ (Hsp40) homolog, subfamily C, member 5 gamma	285126
DUOXA1	dual oxidase maturation factor 1	90527
DUOXA2	dual oxidase maturation factor 2	405753
FSIP2	fibrous sheath interacting protein 2	401024
GEMIN6	gem (nuclear organelle) associated protein 6	79833
GPX3	glutathione peroxidase 3 (plasma)	2878
GRM8	glutamate receptor, metabotropic 8	2918
IL13RA1	interleukin 13 receptor, alpha 1	3597
KNOP1	lysine-rich nucleolar protein 1	400506
MFHAS1	malignant fibrous histiocytoma amplified sequence 1	9258

MRPL10	mitochondrial ribosomal protein L10	124995
MRPL13	mitochondrial ribosomal protein L13	28998
MRPL30	mitochondrial ribosomal protein L30	51263
MRPL41	mitochondrial ribosomal protein L41	64975
MRPL55	mitochondrial ribosomal protein L55	128308
MRPS24	mitochondrial ribosomal protein S24	64951
MRPS27	mitochondrial ribosomal protein S27	23107
MRPS31	mitochondrial ribosomal protein S31	10240
MRPS6	mitochondrial ribosomal protein S6	64968
NFKBIA	nuclear factor of kappa light polypeptide gene enhancer in B-cells inhibitor, alpha	4792
NHSL2	NHS-like 2	340527
NR1I2	nuclear receptor subfamily 1, group I, member 2	8856
OR4K5	olfactory receptor, family 4, subfamily K, member 5	79317
PBRM1	polybromo 1	55193
PGD	6-phosphogluconate dehydrogenase	5226
PRLR	prolactin receptor	5618
RPL14	ribosomal protein L14	9045
RPL18	ribosomal protein L18	6141
RPL32P36	ribosomal protein L32 pseudogene 36	392447
RPL32P7	ribosomal protein L32 pseudogene 7	391560
RPL34	ribosomal protein L34	6164
RPL35A	ribosomal protein L35a	6165
RPLP2	ribosomal protein, large P2	6181
RPS18	ribosomal protein S18	6222
RPS3A	ribosomal protein S3A	6189
RPS7	ribosomal protein S7	6201
SPAM1	sperm adhesion molecule 1 (PH-20 hyaluronidase, zona pellucida binding)	6677
SPATS1	spermatogenesis associated, serine-rich 1	221409
TCTEL1	t-complex-associated-testis-expressed 1-like 1	6993
TOP2B	topoisomerase (DNA) II beta 180kDa	7155
U2AF1L3	U2(RNU2) small nuclear RNA auxiliary factor 1-like 3	199746
UBA52	ubiquitin A-52 residue ribosomal protein fusion product 1	7311
UNC93B1	unc-93 homolog B1 (C. elegans)	81622
CEACAM20	carcinoembryonic antigen-related cell adhesion molecule 20	125931
WFDC8	WAP four-disulfide core domain 8	90199
YAP	YY1 associated protein 1	55249
ZMIZ2	zinc finger, MIZ-type containing 2	83637
ZMYM1	zinc finger, MYM domain containing 1	79830

Figure A.3: List of 57 genes targeted within the MDA-MB-468 siRNA screens.

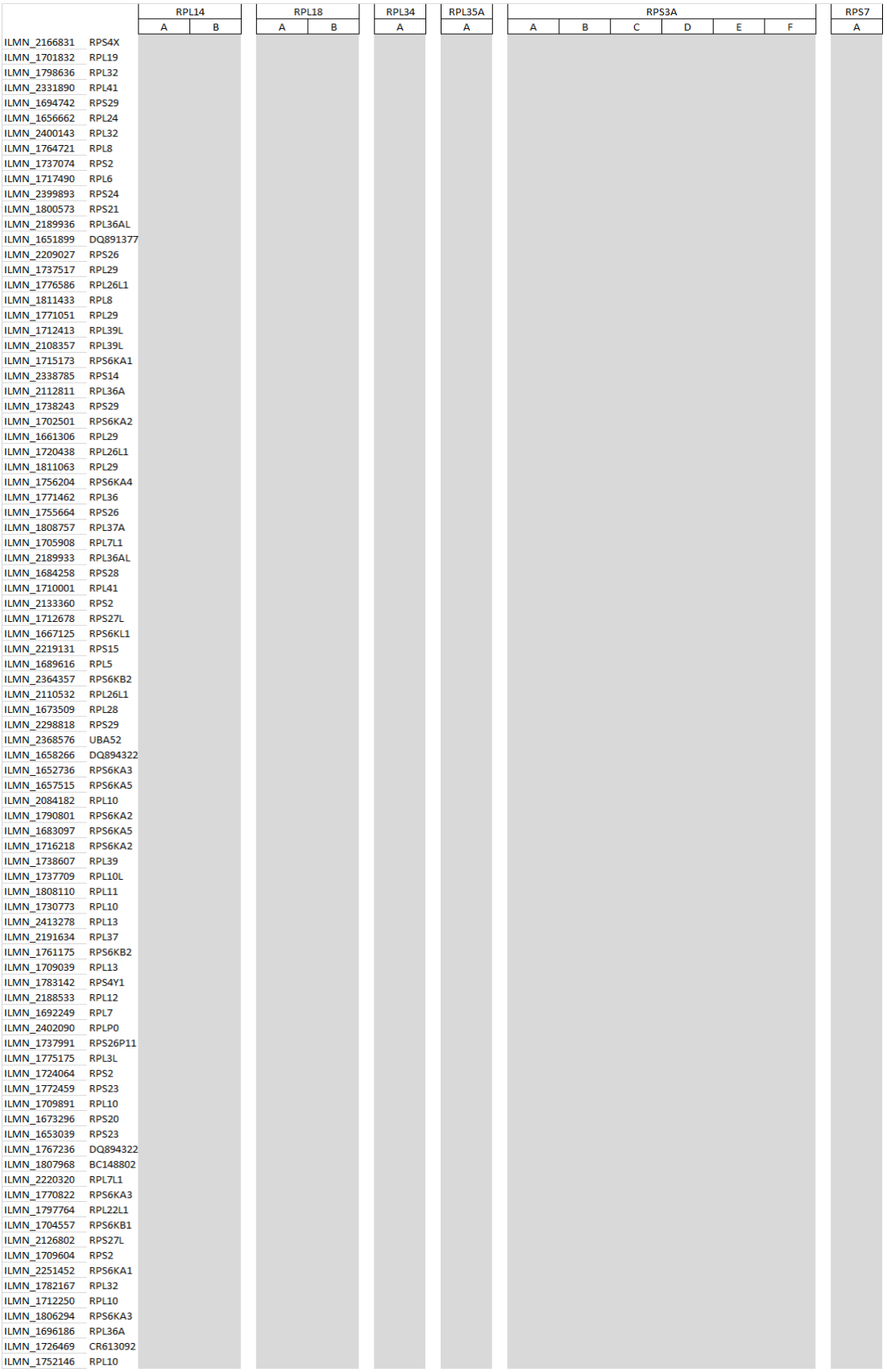

Figure A.4: Heatmap depicting those RP transcripts with no correlation with the top six RP hits in BLBC cases within the METABRIC dataset.

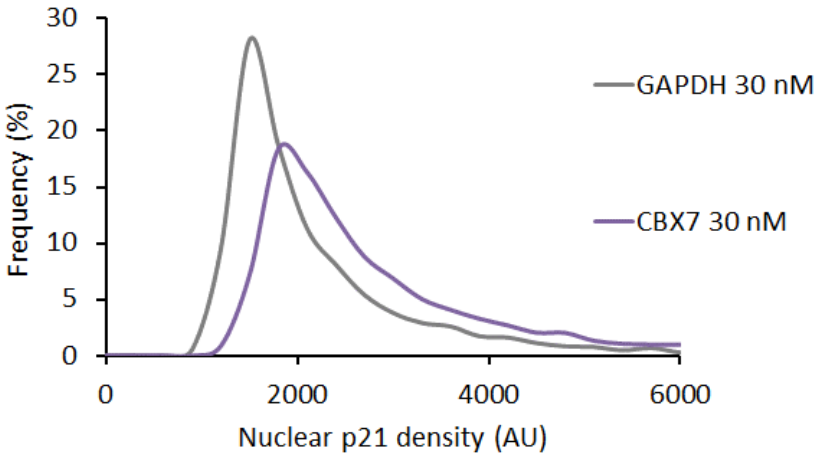

Figure A.5: Nuclear p21 protein levels in MDA-MB-231 cells following CBX7 silencing. Cells were reverse transfected wit 30 nM siRNA targeting GAPDH or CBX7 according to Section 2.3.3 and were fixed and stained with DAPI, rabbit anti-p21 and Alexa Fluor-488 conjugated anti-rabbit according to Section 2.4. Nuclear p21 protein levels were quantified according to Section 2.5. The frequency distribution is from a single experiment containing three technical repeats.